

**Study of Spectral Beam Combination  
Techniques for High Power, Pulsed Dye  
Laser Applications**

*By*

**PARAMJIT RANA**

**Enrolment No: PHYS01201404017**

**Bhabha Atomic Research Centre, Mumbai**

*A thesis submitted to the*

*Board of Studies in Physical Sciences*

*In partial fulfillment of requirements*

*for the Degree of*

**DOCTOR OF PHILOSOPHY**

*of*

**HOMI BHABHA NATIONAL INSTITUTE**



**December, 2019**

# Homi Bhabha National Institute

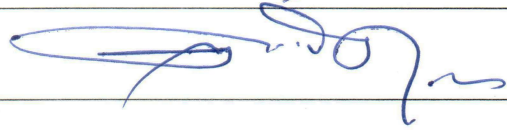
## Recommendations of the Viva Voce Committee

As members of the Viva Voce Committee, we certify that we have read the dissertation prepared by **Sh. Paramjit Rana** entitled " **Study of Spectral Beam Combination Techniques for High Power, Pulsed Dye Laser Applications**" and recommend that it may be accepted as fulfilling the thesis requirement for the award of Degree of Doctor of Philosophy.

Chairman – Prof. S.G. Nakhate



Guide / Convener – Dr .V.S. Rawat



Co-guide -

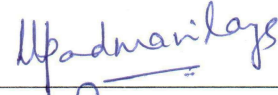
Examiner - Prof. Hirdyesh Mishra, BHU Varanasi



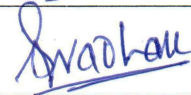
Member 1- Prof. S.K. Dixit, RRCAT Indore



Member 2- Prof. Padma Nilaya



Member 3- Prof. S. Pradhan



Technology Adviser – Dr. Jaya Mukherjee



Final approval and acceptance of this thesis is contingent upon the candidate's submission of the final copies of the thesis to HBNI.

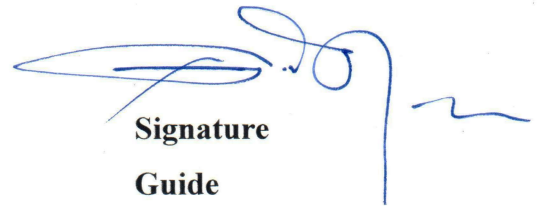
I/We hereby certify that I/we have read this thesis prepared under my/our direction and recommend that it may be accepted as fulfilling the thesis requirement.

Date: 12.12.2020

Place: MUMBAI.

Signature

Co-guide (if any)

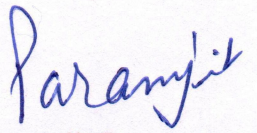


Signature

Guide

## DECLARATION

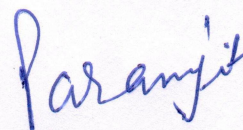
I, hereby declare that the investigation presented in the thesis has been carried out by me. The work is original and has not been submitted earlier as a whole or in part for a degree / diploma at this or any other Institution / University.

  
Paramjit Rana

## STATEMENT BY AUTHOR

This dissertation has been submitted in partial fulfillment of requirements for an advanced degree at Homi Bhabha National Institute (HBNI) and is deposited in the Library to be made available to borrowers under rules of the HBNI.

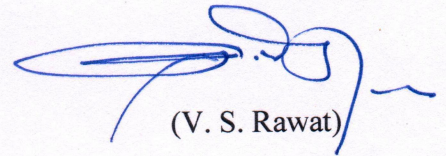
Brief quotations from this dissertation are allowable without special permission, provided that accurate acknowledgement of source is made. Requests for permission for extended quotation from or reproduction of this manuscript in whole or in part may be granted by the Competent Authority of HBNI when in his or her judgment the proposed use of the material is in the interests of scholarship. In all other instances, however, permission must be obtained from the author.



Paramjit Rana

## Certificate

I hereby certify that i have read the thesis titled" Study of Spectral Beam Combination Techniques for High Power, Pulsed, Dye Laser Applications " by Paramjit Rana. This thesis has been prepared, compiled and completed under my supervision.



(V. S. Rawat)

Guide

## LIST OF PUBLICATIONS ARISING FROM THE THESIS

### JOURNALS:

1. “Characteristics of a cascaded grating multi wavelength dye laser”, **Paramjit Rana**, G.Sridhar, K.G. Manohar, *Optics and Laser Technology*, **2016**, Vol. 86, 39-45.
2. “Measurement of Thermo Optical Coefficient for Commonly used Dye solvents ”, S.K. Mishra, **Paramjit Rana**, S.P. Sahoo, S.K. Agarwalla, G.Sridhar, D. Bhale, N.O. Kawade, V.S. Rawat, *International Journal of Photonics and Optical Technology*, **2018**, Vol. 4, Iss. 2, 12-16.
3. “Co-amplification: An Efficient Spectral Beam Combination Approach for High Power, Closely Separated Dual Wavelength Dye Laser Systems”, **Paramjit Rana**, S.K. Mishra, D. Bhale, S.P. Sahoo, G. Sridhar, V.S. Rawat, *Optics Communications*, **2019**, Vol. 451, 367-373.
4. “Characterization of dye cells for a high repetition rate pulsed dye laser by particle image velocimetry (PIV)”, S.K. Mishra, **Paramjit Rana**, Siba P. Sahoo, Nitin O Kawade, V.S. Rawat, *Laser Physics*, **2019**, Vol.29, 065001; 1-8.
5. “Thin Film Design of IR Reflector Window for Reduced Thermal Lensing in Copper Vapor Laser”, **Paramjit Rana**, V. S. Rawat, *AIP Conference Proceedings*, **2019**, 2115, issue 1, 030281, pp 1-4.
6. "Multilayer Dielectric Coated Fabry Perot Spectral Beam Combiner for High Power, Tunable Laser Applications", **Paramjit Rana**, C. Mukherjee, S.K. Mishra, Rajiv Kamparath, S.P. Sahoo, Jaya Mukherjee, V.S. Rawat; *Optics & Laser Technology*, **2020**, Volume 128, 106210, pp 1-9.

7. "Multilayer Dielectric Thin Film Optical Coating Design for Single Wavelength Operation of Inherently Dual Wavelength Copper Vapor Laser", **Paramjit Rana**, S.K. Mishra, Jaya Mukherjee, V.S. Rawat, *Springer Proceedings in Physics* 258, **2021**, chapter 196, pp 1-5.
8. "Thermal Lensing in Copper Vapor Laser Oscillator-Amplifier Configuration: It's Measurement, Role and Compensation", **Paramjit Rana**, S.K. Mishra, V.S. Rawat, *Under review (Optik)*.

### **CONFERENCES:**

#### **International:**

1. Multilayer Dielectric Thin Film Optical Coating Design for Single Wavelength Operation of Inherently Dual Wavelength Copper Vapor Laser, **Paramjit Rana**, S.K. Mishra, Jaya Mukherjee, V.S. Rawat, Proceedings of International Conference on Optics and Electro-Optics (ICOL) 2019, I.R.D.E. Dehradun.

#### **National:**

1. Spectral characteristics of three wavelength laser in dye mixture, **Paramjit Rana**, G. Sridhar; Proceedings of National Laser Symposium – 2015.
2. pH modulated photophysical characteristics of Rh101 dye for CVL pumped dye lasers, **Paramjit**, S.K. Mishra, V.S. Rawat, S.P. Sahoo, S.K. Agarwalla, G.Sridhar, A.K. Ray, K.G. Manohar, Proceedings of National Laser Symposium 2015.
3. An efficient spectral beam combination technique for closely separated wavelengths for high power CVL pumped dye laser oscillator amplifier chains; **Paramjit**, S.K. Mishra, V.S. Rawat, S.P. Sahoo, S.K. Agarwalla, G. Sridhar, K.G. Manohar, Proceedings of National Laser Symposium – 2015.
4. Comparison of Hydraulic Resistance in Different Dye Cells Used in the High Repetition Rate Pulsed Dye Lasers, S K Mishra, **Paramjit**, V S Rawat, S P Sahoo, S

- K Agrawalla, G Sridhar, K G Manohar, Proceedings of National Laser Symposium – 2015.
5. Jitter tolerance studies on dye laser oscillator amplifier configuration, **Paramjit Rana**, S.K. Agarwalla, S.P. Sahoo, S.K. Mishra, D. Bhale, G. Sridhar, V.S. Rawat; Proceedings of National Laser Symposium – 2016.
  6. Design of multifunctional window for polarized green copper vapor laser oscillator amplifier chain, **Paramjit Rana**, R.B. Tokas, V.S. Rawat, S. Thakur, N.K. Sahoo Proceedings of National Laser Symposium – 2016.
  7. Multi wavelength narrowband dye laser, G.Sridhar, **Paramjit Rana** Proceedings of National Laser Symposium – 2016.
  8. Measurement of Thermo Optical Coefficient for Commonly Used Dye Solvents, S K Mishra, **Paramjit**, S P Sahoo, S K Agrawalla, G Sridhar, N Kawade, V S Rawat, Proceedings of National Laser Symposium – 2016.
  9. Design optimization and deposition of laser beam combiner, C. Mukherjee, Rajiv Kamparath, A.S. Joshi, **Paramjit Rana**, V.S. Rawat, R.K. Rajawat, N.K. Sahoo and P.A. Naik, Proceedings of National Laser Symposium – 2017.
  10. Computationally Generated Dye Cell for High Repetition Rate Pulsed Dye Lasers, S K Mishra, **Paramjit**, S P Sahoo, S K Agrawalla, G Sridhar, V S Rawat, Proceedings of National Laser Symposium – 2017.
  11. Characteristics of SulfoRhodamine 101 dye laser in ethanol-water binary solvent mixture, S.K. Mishra, **Paramjit Rana**, S.P. Sahoo, S.K. Agarwalla, G. Sridhar, V.S. Rawat, Proceedings of National Laser Symposium 2018.
  12. Comparative study of Copper Vapour Laser Master Oscillator Power Amplifier configurations, **Paramjit Rana**, S.K. Mishra, S.P. Sahoo, S.K. Agarwalla, G. Sridhar, V.S. Rawat, Proceedings of National Laser Symposium 2018.

**Book/Book Chapter/Bulletin:**

1. “Multi-wavelength Narrowband Dye Laser System”, G. Sridhar, **Paramjit Rana**, *KIRAN-A Bulletin of the Indian Laser Association*, Vol.29, No.3, pp 8-14, December 2018.
2. "Experimental and theoretical studies of multi wavelength dye laser system", G. Sridhar, **Paramjit Rana**, Sandeep Kumar Agarwalla, Jaya Mukherjee; *BARC newsletter*, pp 11-14, July-August 2020.

**Other Publications not included in the thesis:**

1. “Computationally Optimized Dye Cell Flow Geometry for High Repetition Rate Pulsed Dye Lasers”, S.K. Mishra, **Paramjit Rana**, S.P. Sahoo, V.S. Rawat, *International Journal of Photonics and Optical Technology*, **2018**, Vol. 4, Iss. 3, 12-16.
2. “Evaluation of Hydraulic Resistance of Flow Cells with Commonly Used Solvents for Dye Lasers”, S.K. Mishra, **Paramjit Rana**, S.P. Sahoo, V.S. Rawat, *International Journal of Photonics and Optical Technology*, **2018**, Vol. 4, Iss. 4, 17-23.

*Dedicated to.....*

*My family*



## ACKNOWLEDGEMENTS

*Though only my name appears on the cover of this thesis, many people have contributed to its completion. These pages reflect the support of many generous and inspiring people who contributed in many ways to the success of this study and made this journey an unforgettable experience for me. The list is long, but I would like to express my gratitude to all of them who have encouraged and contributed both academically and emotionally during the tenure of my research.*

*At this moment of accomplishment, first of all I pay my sincere gratitude to my guide, **Dr. V. S. Rawat**, for being a constant source of motivation, guidance and continuous encouragement throughout the course of this work and giving me a chance to accelerate my research skills in the field of lasers. His expertise, understanding and patience have added greatly to my research experience. I am also thankful to him for his assistance and guidance in improving my writing skill and for constant help by means of productive discussions, showing me how to improve the presentation of my work, which will surely be helpful in the future also.*

*Sincere thank are due to the former and present doctoral committee members **Dr. K. Dasgupta, Dr. N.K. Sahoo, Dr. Vasdev, Dr. S.G. Nakhate, Dr. S.K. Dixit, Dr. Padma Nilaya, Dr. Jaya Mukherjee and Dr. S. Pradhan** in helping me for years to work in the correct direction. It gives me an immense pleasure to place on record my sincere thanks to **Dr. K.G. Manohar** for giving me a proper direction and opportunity to work and develop the skills required for my thesis. He was truly instrumental in selection of the core field during the most crucial stage of my PhD. I am grateful to **Dr. B.K. Nayak and Dr. Dinesh Udupa**, Dean, Physical & Mathematical Sciences, HBNI for providing me the correct guidance for timely fulfilling the documentary requirements of the HBNI.*

*I gratefully acknowledge **Dr. C. Mukherjee, Dr. R.B. Tokas, Sh. Rajeev Kamparath** for their support in the thin film beam combiner development. I thank **Dr. K.S. Bindra, Dr. P.K. Mukhopadhyay and Sh. Amarjeet Singh** for providing diode pumped solid state lasers for the dye laser testing. The support received from **Dr. G. Sridhar** during initial experiments is greatly acknowledged. The inspiration, help and suggestions received from all the colleagues (**Sh. S.K. Mishra, Sh. Bhagyesh Gangawane, Sh. S. Mandal, Sh. Dheeraj Singh, Sh. Anil Nayak, Smt. Rajasree Vijayan and Sh. S.P. Sahoo,**) are beyond words.*

*There can be no adequate acknowledgement for the loving encouragement I have received from my all family members. Blessings from my father **Sh. Ramkanwar Rana** cannot be acknowledged in words. Last but not least, I would like to express my heartfelt gratitude and high regards to my cute and loving daughter, **Zinnia** and son, **Ivaan**. I have no words to thank my wife, **Dr. Suman Rana** whose love, selfless support, generous care, encouragement and inspiration always cheered me up during the trying moments. Moral support provided by **Sh. Ravinder Kumar, Mrs. Urvashi** and lovely **Arnav** enhanced positivity and self belief. My family members were always beside me during the happy and hard moments to push me and motivate me to overcome the difficulties. Without their constant support and inspirations all this would never have been possible.*

**Paramjit Rana**

# CONTENTS

ABSTRACT.....	XXI
SYNOPSIS.....	XXIII
LIST OF FIGURES.....	XXXIII
LIST OF TABLES.....	XLI
CHAPTER-1: INTRODUCTION TO SPECTRAL BEAM COMBINATION TECHNIQUES FOR PULSED DYE LASERS.....	1
1.1. Introduction.....	1
1.2. Classification of Laser Beam Combination Techniques .....	3
1.2.1. Side by Side Beam Combination.....	4
1.2.2. Coherent Beam Combination.....	4
1.2.3. Spectral Beam Combination.....	5
1.2.4. Other Laser Beam Combination Schemes.....	7
1.3. Copper Vapor Laser Pumped Dye Laser System.....	10
1.4. Spectral Beam Combination Techniques for Pulsed Dye Lasers.....	13
1.4.1. Intra-cavity Beam Combined Multi-wavelength Dye Lasers.....	13
1.4.2. External Cavity Beam Combination.....	32
1.5. Motivation.....	33
1.6. The Organisation of The Thesis.....	35
CHAPTER-2: HIGH POWER COPPER VAPOUR LASER SYSTEM.....	37
2.1 Introduction.....	37
2.2 Indigenously Developed Copper Vapour Laser System.....	39
2.3 Characteristics of CVL Oscillator Configurations.....	44
2.3.1 Resonator Configuration.....	44
2.3.2 Laser Beam Divergence Measurement.....	46
2.3.3 Results and Discussions.....	48
2.4 Emission Wavelength of Copper Vapour Laser Oscillator.....	50
2.4.1 Measurement of Green to Yellow Power Ratio.....	51
2.4.2 Optical Designs for Single Wavelength Emission.....	53
2.4.2.1 Multilayer Thin Film Design of Single Wavelength.....	53
2.4.2.2 Window Design for Polarised Single Wavelength Emission.....	57

2.5	Master Oscillator Power Amplifier (MOPA) configurations.....	61
2.5.1	Designs for CVL MOPA Configurations.....	63
2.5.1.1	Single Long Chain.....	63
2.5.1.2	Splitted Chain After Oscillator.....	64
2.5.1.3	Splitted Chain After First Amplifier.....	65
2.5.1.4	Periodic Power Withdrawal Configuration.....	65
2.5.2	Results and Discussions.....	66
2.5.2.1	Determination of Amplifier Gain.....	66
2.5.2.2	Comparison of CVL MOPA Chain Designs.....	68
2.6	Thermal Lensing in CVL.....	70
2.6.1	Experimental Setup for Measurement of Thermal Lensing.....	71
2.6.2	Estimation of Thermal Focal Length for Amplifier Module.....	73
2.6.3	Effect of Operating Power on Thermal Lens.....	75
2.6.4	Effect of Operating Pressure on Thermal Lens.....	76
2.6.5	Evaluation of Thermal Lensing.....	77
2.6.5.1	Oscillator Configuration.....	78
2.6.5.2	Thermal Lens Effect in The Oscillator-Amplifier Configuration.....	79
2.6.6	Thermal Lensing Compensation Techniques.....	83
2.6.6.1	Individual Laser System.....	83
2.6.6.2	Thermal lens compensation in MOPA Configuration.....	93
2.7	Conclusions.....	104
CHAPTER-3: THE DYE GAIN MEDIUM.....		107
3.1	Introduction.....	107
3.2	Effect of pH on Photophysical Properties of Rh 101 Dye.....	109
3.2.1	Variation in The pH of The Dye Solution by Acetic Acid.....	110
3.2.2	Effect of pH on Absorption Spectra of Rh 101 Dye Solution.....	111
3.2.3	Effect of pH on The Emission Spectra of Rh 101 Dye.....	112
3.2.4	CVL Pumped Dye Laser with Acidic Solution of Rh 101 Dye.....	113
3.3	Measurement of Thermo-optic Coefficient of Dye Solvents.....	115
3.3.1	Experimental Set-up And Results.....	117
3.4	Sulfo-Rhodamine Dye Laser Performance in a Binary Solvent.....	120
3.4.1	Experimental Set-up.....	121
3.4.2	Tuning Characteristics of SRh 101 Dye Laser in a Binary Solvent.....	122

3.5	Widening of Tuning Range by Dye Mixture.....	125
3.5.1	Experimental Set-up for Tuning Range Widening by Dye Mixture .....	126
3.5.2	Effect of Concentration of PM 567 in PM 567-DCM Dye Mixture.....	128
3.5.3	Effect of Concentration of DCM in PM 567-DCM Dye Mixture.....	130
3.6	Conclusions.....	132
CHAPTER-4: INTRA-CAVITY BEAM COMBINATION TECHNIQUE FOR MULTI-WAVELENGTH DYE LASER .....		135
4.1	Introduction.....	135
4.2	Selection of Cavities for Narrowband, Multiple Wavelength Generation... ..	137
4.2.1	Linear Cavity With Intra-cavity Beam Expander.....	138
4.2.2	Folded Cavity With Intra-cavity Beam Expander.....	141
4.2.3	Linear Cascaded Cavity Without Intra-cavity Beam Expander.....	144
4.3	Cascaded Grating Cavity Set-up for Four-wavelength Generation.....	147
4.4	Characteristics of Cascaded Grating Cavity Configurations.....	149
4.4.1	Cascaded Grazing Incidence Grating (CGIG) Cavity.....	150
4.4.2	Hybrid Cascaded Grazing Incidence Grating (HCGIG) Cavity.....	155
4.4.3	Zone of Operations in CGIG and HCGIG Cavities.....	159
4.5	Five wavelength Generation in Hybrid Cascaded Grazing Incidence Grating Cavity.....	162
4.6	Conclusions.....	163
CHAPTER-5: EXTERNAL CAVITY BEAM COMBINATION TECHNIQUES FOR HIGH POWER, PULSED DYE LASER SYSTEM.....		165
5.1	Introduction.....	165
5.2	External Cavity Beam Combined Dye Laser Systems.....	166
5.2.1	Narrowband Dye Laser Oscillators.....	167
5.2.1.1	Copper Vapor Laser Pumped Dye Laser Oscillator.....	167
5.2.1.2	Diode Pumped Solid State Laser Pumped Dye Laser Oscillator.....	172
5.2.2	Spectral Beam Combination Post Power Amplification (Method-I).....	184
5.2.2.1	Amplification of Dye Laser Signal Beam.....	184
5.2.2.2	Spectral Beam Combination of Individually Amplified Laser Beams....	187
5.2.3	Co-amplification Based Spectral Beam Combination (Method-II).....	188

5.2.3.1 Theoretical Evaluation for Co-amplification of Composite Dye Laser Beam.....	188
5.2.3.2 Experimental Study on DCM Dye Common Amplifier.....	191
5.2.3.3 Characterization of Dual Wavelength Common Amplifier.....	192
5.2.3.4 Gain Competition in Common Amplifier.....	196
5.2.3.5 Performance of Spectral Beam Combination Scheme.....	201
5.3 Conclusions.....	203
CHAPTER-6: MULTILAYER DIELECTRIC COATED FABRY PEROT BEAM COMBINER FOR HIGH POWER, PULSED DYE LASERS.....	205
6.1 Introduction.....	205
6.2 Design of Multilayer Thin Film Interference Filters for Closely Separated Wavelength.....	207
6.2.1 Edge Filter Design of a Beam Combiner.....	208
6.2.2 Single Cavity Fabry Perot Beam Combiner Design.....	209
6.2.3 Dual cavity Fabry Perot Beam Combiner Design.....	210
6.3 Fabrication of Fabry Perot Laser Beam Combiner.....	212
6.4 Characterisation of the FP Laser Beam Combiner Using Spectrophotometer.....	213
6.5 Surface Morphology of The Laser Beam Combiner by Atomic Force Microscopy.....	214
6.6 Laser Induced Damage Threshold of FP Beam Combiner.....	217
6.7 Spectral Beam Combination by FP Beam Combiner.....	217
6.7.1 SBC by FP Combiner for Closely Separated Wavelengths.....	218
6.7.2 SBC by FP Combiner for Widely Separated Wavelengths.....	219
6.7.3 Amplified Spontaneous Emission (ASE) Filtering By FP Beam Combiner.....	220
6.7.4 FP Beam Combiner Implementation for Widely Tunable Lasers.....	223
6.8 Conclusion.....	226
CHAPTER-7: SUMMARY AND FUTURE SCOPE.....	229
REFERENCES.....	237

## **ABSTRACT**

Multi-wavelength, tunable dye lasers are required for DIAL based environmental applications. Spectral beam combination techniques are utilized for generating multi-wavelength tunable dye lasers. Three laser beam combination techniques namely intra-cavity beam combination, co-amplification based external cavity beam combination and multilayer dielectric coated Fabry Perot (FP) beam combiner were studied in detail for combining tunable dye laser beams with closely separated wavelengths of  $<10\text{nm}$ . Spectral beam combination using the FP beam combiner proved to be efficient among all three techniques studied. Co-amplification based external cavity spectral beam combination technique found to be compact and efficient as compared to other configurations for the closer wavelengths. Linear, folded cavity with prism beam expander (PBE) and cascaded cavity without PBE were used to obtain more than three narrowband wavelengths in a single dye laser cavity. Cascaded grazing incidence grating (CGIG) and hybrid cascaded grazing incidence grating (HCGIG) based intra-cavity beam combination configurations for dye lasers were characterized in detail and simultaneous multi-wavelength operation of 4 to 5 wavelengths has been established. The multilayer thin-film based FP beam combiner was developed. This FP combiner was tested for high power, pulsed dye laser beams of wavelength separated by less than 10 nm. It proved to be an efficient beam combiner for closer wavelengths and acts as an amplified spontaneous emission (ASE) filter for a dye laser. Indigenously developed a high repetition rate, high power copper vapor laser (CVL) MOPA system was characterized and utilized to pump the dye lasers. The evaluation of thermal lensing and its compensation for individual CVL and MOPA configuration was done. Multilayer dielectric thin film designs for the IR reflector

window, single color emission mirror and multi-functional window for the CVL were presented. The effect of pH and solvents on the photo-physical properties of the dye laser was investigated. Water based solvents and their mixture was found to be suitable for high power dye lasers due to lower thermo-optic coefficient. Thermo-optic coefficient of ethanol, water and ethanol-water binary solvent was experimentally measured using Michelson interferometer. As thermo-optic coefficient for ethanol-water binary solvent was measured to be lower than the pure ethanol, a SRh 101 dye laser was characterised using ethanol-water binary solvent at various volumetric ratios. Tuning range widening from 42 nm to 80 nm was achieved by using binary dye mixture of PM567 and DCM and simultaneous operation of a three-wavelength from a dye laser system was achieved.

## SYNOPSIS

Differential Absorption Lidar (DIAL) [1-4] Remote sensing [5], Laser Spectroscopy [6], non-linear frequency mixing [7] and trace measurement [8], etc. requires a composite laser beam of tunable multiple wavelengths. Several beam combination techniques such as side by side, spectral and coherent combinations are used to generate a composite laser beam as per the desired beam parameters and the type of lasers employed [9]. Narrowband, widely tunable dye lasers in visible to near-infrared spectrum are suitable for such applications. High repetition rate and power scalability extend its application regime to large scale industrial as well as commercial use such as laser isotope separation of medical isotopes [10]. DIAL based environmental and remote sensing applications require closely separated (<10nm) multi-wavelength tunable dye lasers with suitable power levels [3, 7]. Therefore, studies on spectral beam combination techniques for closer wavelengths, high power, pulsed dye lasers were taken up for the present research work.

Many researchers have studied various aspects of spectral beam combination to generate multi-wavelength dye lasers for different applications [11-14]. In this thesis, some of the unexplored areas in the spectral beam combination techniques and multi-wavelength dye laser generation were studied. The important aspects of intra-cavity and external cavity beam combination techniques for multi-wavelength (separated by less than 10 nm) dye lasers were explored during the current course of study. In the intra-cavity spectral beam combination technique, cascaded grating sub-cavities in a resonator for generating four to five wavelengths in a single dye laser has been studied, which was not explored yet. Tuning characteristics of all the cascaded grating sub-cavities were established to simultaneously operate four wavelengths in a single dye laser cavity [15]. Co-amplification based spectral beam combination technique for high power, closely separated wavelength was found to be less explored in the literature for oscillator-amplifier configuration. This was studied in detail to

generate high power (~8W), high repetition rate (~10 kHz), dual-wavelength (<10 nm separated) dye laser. The co-amplification of closely separated wavelengths proved to be an efficient approach over individually amplified dye laser beams for high power generation using oscillator-amplifier configuration [16]. Gain competition among the closely separated wavelengths was studied in the dye common amplifier. In both of these spectral beam combination techniques, gain competition among closer wavelengths limit the individual optimization of the participating laser wavelengths with the added complexity of intensity control. Therefore, gain competition free spectral beam combination technique was required to be studied. Hence, the development of spectral beam combining element suitable for closer wavelength combination was taken up as the third spectral beam combination technique.

Efficient spectral beam combination of multiple dye laser beams could not be realized without a beam combining optical device. Multilayer dielectric coated beam combiner was selected for studies among other beam combining elements such as grating, prism, etc., due to its ease of handling wide wavelength tunability and high power. The thin film Fabry Perot (FP) filter was chosen as a spectral beam combiner due to its capability of combining closely separated wavelengths (<10nm). Single cavity FP filter (19 layers, TiO<sub>2</sub>, SiO<sub>2</sub>) based beam combiner was designed, fabricated and tested with the dye laser beam. FP beam combiner was characterized in terms of transmission spectrum (spectrophotometer), surface roughness (atomic force microscopy) and damage threshold (laser-induced damage threshold). This FP beam combiner was successfully tested for spectral beam combination of two dye laser beams with closely separated wavelengths of less than 10 nm as well as widely separated wavelengths of 30 nm. FP beam combiner was found to be an efficient device for closer wavelength beam combination as compared to conventional broadband beam splitter based combination. This FP beam combiner served the dual purpose of spectral beam combiner as well as amplified spontaneous emission (ASE) filter. ASE filtering was advantageous for

combining the dye laser beams operated at the end of the tuning range as ASE in the laser beam is relatively higher while tuned to the end of the tuning range. A novel mechanism for varying the FP transmission peak along with dye laser wavelength tuning was established using a combination of precision rotation and translation stage.

Pump laser plays a key role in the high power dye laser generation. An indigenously developed copper vapor laser (CVL) was thoroughly characterized to pump the dye lasers. One of the objectives of this current study was to generate a high power pump laser for generating a high power multi-wavelength dye laser beam for spectral beam combination. The high pump power was generated by six CVLs configured in one oscillator followed by five amplifiers in a Master Oscillator Power Amplifier (MOPA) configuration. Various MOPA configurations were theoretically analyzed using an individual CVL as an amplifier, whereas amplifying capabilities have been experimentally established. Thermal lensing was found to be a key factor to maximize the power extraction from a CVL in the longer MOPA chain. A novel technique was established to measure the effective thermal focal length of an amplifier using the oscillator beam as the probe beam. The compensation techniques were theoretically analyzed to minimize their impact on a longer MOPA chain of eight modules.

The dye laser was chosen for spectral beam combination experiments due to its versatile capabilities. Fluorescent laser dye, dye cell, dye solvent are crucial components for any narrowband dye laser system. The study of beam combination techniques for multi-wavelength dye laser needs these elements to be utilized to their best possible capabilities. The use of different solvents, their mixture, for shifting the absorption and emission characteristics of a laser dye is used for obtaining the desired wavelength. Mixing two or more laser dyes notably widens the wavelength tunability range and also shifts the emission peak wavelength. These areas were not explored much, especially for multi-wavelength dye laser systems. We have studied these aspects of the dye gain medium during this thesis work:

effect of pH on photophysical characteristics of Rh 101 dye, measurement of thermo-optic coefficient of dye solvents and their mixtures, characterization of SRh 101 dye in water-ethanol binary solvent and extension of tuning range for three-wavelength dye laser using binary dye mixture.

The motivation behind this elaborated study was to advance the knowledge of spectral beam combination techniques for high power dye lasers and its associated technologies. We could achieve narrowband, multi-wavelength, high power, high repetition rate, pulsed dye laser using three spectral beam combination techniques. Intra-cavity and external cavity beam combination techniques along with its associated important elements (high power pump laser and dye laser gain medium) were studied in this thesis work. The complete study is organized into seven chapters as follows.

### **Chapter-1: Introduction to Spectral Beam Combination Techniques for Pulsed Dye Lasers**

Several spectral beam combination techniques for multi-wavelength dye laser generation are discussed in chapter-1. Laser beam combination techniques used for various applications and experiments are summarized in this chapter. The classes of laser beam combination schemes i.e. side by side beam combination; coherent beam combination and spectral beam combination are presented in detail. An elaborate literature survey on multiple wavelength dye laser generation using various beam combination techniques is presented and the review of existing knowledge in the field of spectral beam combination is presented.

### **Chapter-2: High Power Copper Vapor Laser System**

Copper vapor laser (CVL) is the most suitable pump laser source for pumping the dye lasers to generate high power and high repetition rate. We have studied and characterized the indigenously developed CVL system operating at 9 kHz pulse repetition rate in MOPA configuration. Analysis of several MOPA configuration designs is discussed in chapter-2 of

this thesis. Thermal lensing in the CVL plays a significant role in the output beam size management, divergence and power extraction capability in longer MOPA chains. The thermal lensing of the CVL amplifier system was experimentally measured using a collimated CVL oscillator probe beam in an oscillator-amplifier configuration. The effect of neon buffer gas pressure and input electrical power on the resultant thermal focal length of the CVL system was studied. Various compensation techniques were theoretically analyzed for the CVL MOPA chain, which is elaborated here in this chapter.

### **Chapter-3: The Dye Gain Medium**

The dye gain medium is responsible for a versatile, tunable, multi-wavelength dye laser system, which is described in this chapter- 3. The possibility of spectral tailoring of photophysical properties of the gain medium by simple techniques adds the versatility and application potential of the dye laser. The effects of various solvent environments such as pH variation, binary solvent, polar and non-polar solvents on the photo-physical properties of few of the laser dyes of interest for spectral beam combination experiments were studied. The photophysical properties of Rh 101 and SRh 101 dyes were studied in detail. Thermo-optic coefficient of solvents plays a significant role in the high power operation of the dye lasers, which was measured using the Michelson interferometer based technique for commonly used dye solvents and their mixture. Broadening of the wavelength tuning range of three wavelength dye laser was achieved using DCM and PM 567 binary dye mixture with optimized concentration. Studies on the dye gain medium properties are presented in this chapter in detail.

### **Chapter-4: Intra-cavity Beam Combination Techniques for Multi-wavelength Dye Laser**

Intra-cavity beam combined multi-wavelength dye laser configurations are described in this chapter. Linear cascaded resonator without intra-cavity beam expansion was chosen to

configure the cavity to generate two to five wavelengths in a single composite output laser beam. A single laser beam consisting of four wavelengths were generated from the linear cascaded grazing incidence grating configuration (CGIG). This configuration was studied to achieve the tuning range for simultaneous four wavelength operation. A hybrid cavity configuration (HCGIG) consisting of three GIG cavities and one Littrow cavity was studied to understand the effect of sub-cavity on the overall emission characteristics. Characteristics of these intra-cavity beam combined CGIG and HCGIG cavities are discussed in this fourth chapter of the thesis.

### **Chapter-5: External Cavity Beam Combination Techniques for High Power, Pulsed Dye Laser System**

High power, dual-wavelength laser beam generation is elaborated in the chapter-5 of this thesis. MOPA configurations were employed for enhancing the power of the dye laser beams. High power generation using external cavity beam combination was investigated using two techniques i.e. spectral beam combination post-amplification of the individual laser beams and co-amplification of the composite (spectral beam combined) dye laser beam. Both these methods of high power, multi-wavelength dye laser generation are presented in this chapter. Studies on amplification include narrowband grazing incidence grating (GIG) oscillator (CVL and Diode Pumped Solid State Laser pumped oscillators) for individual dye laser beam generation and its amplification using transverse pumped amplifiers. The effect of pump power and dye concentration on amplifier extraction efficiency is presented here. The common amplifier of DCM pumped by CVL for closely spaced wavelength (<10nm) was studied. Gain competition in a common amplifier was characterized by varying individual input intensities as well as pump power. This efficient spectral beam combination technique is described in detail.

## **Chapter-6: Multilayer Dielectric Coated, Fabry Perot Beam Combiner for High Power, Pulsed Dye Laser**

Efficient, gain competition free and effective combination of two or more laser beams requires a beam combining element. A single cavity FP filter was designed using 19 layers of  $\text{TiO}_2$  and  $\text{SiO}_2$ . It was fabricated using an ion-assisted e-beam evaporation technique. The filter was characterized using spectrophotometer, atomic force microscopy (AFM) and laser-induced damage threshold (LIDT). This filter was used for laser beam combination of high power (~8W) dye laser beams of closely separated wavelength. This combiner was also utilized for filtering the amplified spontaneous emission (ASE) present in the dye laser beam. The tuning mechanism to match the dye laser wavelength tunability was established. The development, characterization, and implementation of this FP beam combiner are elaborated in this chapter.

## **Chapter-7: Summary and Future Scope**

An elaborated study on spectral beam combination techniques for high power, pulsed, dye laser is presented in the thesis. The important conclusions drawn from the current thesis work are described in this chapter, which is as follows:

- ✓ Three laser beam combination techniques namely intra-cavity beam combination, co-amplification based external cavity combination and multilayer dielectric coated Fabry Perot beam combiner were studied in detail for combining laser beams with closely separated wavelengths (<10nm). Spectral beam combination using the FP beam combiner proved to be efficient and gain competition free technique as compared to the other two techniques.
- ✓ CGIG and HCGIG based intra-cavity beam combined configurations were characterized in detail to determine simultaneous multi-wavelength operation. These techniques were

found to be suitable for the generation of four to five, narrowband wavelengths in a compact resonator cavity.

- ✓ Laser beam combination after amplification was suitable for widely separated wavelengths whereas co-amplification of the combined beam was proved to be more efficient for closely spaced wavelengths.
- ✓ Tailoring of the dye emission spectrum could be achieved by changing the solvent pH environment and ethanol-water binary solvent. Widening of the tuning range from 40 nm to 82 nm in a three-wavelength dye laser using a concentration optimized binary dye mixture of PM567 and DCM demonstrated.
- ✓ Multilayer thin-film FP based filter was designed, fabricated and used as a beam combiner. It was characterized for transmission spectrum, surface morphology and damage threshold using a spectrophotometer, AFM and LIDT techniques respectively.
- ✓ This beam combiner was successfully tested for a combination of laser beams wavelength separated by less than 10 nm, which was proved to be more efficient as compared to beam splitter based combiner with the added advantage of ASE filter for the transmitted laser beam operating at the end of its tuning range. A tuning mechanism for the FP beam combiner for widely tunable laser systems was successfully established for combining closely as well as widely separated wavelengths.
- ✓ An indigenously developed copper vapor laser MOPA configurations were characterized and optimized to generate maximum possible pump power. Theoretically studied thermal lensing compensation techniques seem to be effective for maximum power extraction using longer CVL MOPA chains.

In the future, remotely operable, optical fiber pumped, intra-cavity beam combined dual-wavelength system will be developed. Application of multi-wavelength dye laser in trace

analysis and environmental application will be explored. Remote gas sensing based exploration will be an important work towards environmental monitoring and control.

### **Bibliography:**

- [1].A.L. Jones Jr., et. al., Compact solid-state dye polymer laser for ozone lidar applications, *Opt. Eng.* 41(11), pp 2951–2958, (2002).
- [2].Takuya Nayuki, et.al. , Development of a differential-absorption lidar system for measurement of atmospheric atomic mercury by use of the third harmonic of an LDS-dye laser *Applied Optics*, Vol. 43(35), pp. 6487-6491, (2004).
- [3].Takashi Fujii, et.al., Dual differential absorption lidar for the measurement of atmospheric SO<sub>2</sub> of the order of parts in 10<sup>9</sup>, *Applied Optics*, Vol. 40( 6) pp. 949-956 (2001).
- [4].S. Chudzy! nski A. Czy'zewski et. al., Multi wavelength lidar for measurements of atmospheric aerosol, *Optics and Lasers in Engineering*, 37, pp 91-99 (2002).
- [5].D.J. Gray, et.al. Using a multi-wavelength LiDAR for improved remote sensing of natural waters, *Applied Optics*, Vol. 54(31), pp F232-F242 (2015).
- [6].Y. Oki et.al., Multiwavelength distributed-feedback dye laser array and its application to spectroscopy, *Optics Letters*, Vol. 27(14), pp. 1220-1222 (2002).
- [7]. Takuya Nayuki, et.al., Sum-frequency-generation system for differential absorption lidar measurement of atmospheric nitrogen dioxide, *Applied Optics*, Vol. 41(18), pp. 3659-3664, (2002).
- [8].Takashi Fujii, et.al., Trace atmospheric SO<sub>2</sub> measurement by multi-wavelength curve-fitting and wavelength-optimized dual differential absorption lidar, *Applied Optics*, Vol. 41(3), pp. 524-531 (2002).
- [9].T.Y. Fan, Laser beam combining for high power high radiance sources, *IEEE Journal of selected topics in quantum electronics*, Vo. 11(3), pp 567-577 (2005).
- [10].H. Park et.al, Laser Isotope Separation of 176-Yb for Medical Applications, *Journal of the Korean Physical Society*, Vol. 49(1), pp. 382-386 (2006).
- [11].Yu. G. Basov, Optical designs of two frequency dye lasers (Review), *Zhurnal Prikladnoi Spektroskopii*, Vol. 49(6), pp. 887-899 (1987).
- [12].Y. Oki et.al. Multi-wavelength distributed-feedback dye laser array and its application to spectroscopy. *Optics Letters*. 27(14):1220-1222, (2002).
- [13].S. Jevlani, B. Khodadoost, Gain competition effect in dual-wavelength dye lasers, *Optics & Laser Technology*; Vol. 39(1), pp 182-188 (2007).

- [14]. R.Khare. et.al., A tunable three-wavelength copper-vapor laser pumped dye laser with collinear output, *Optics Communications*, Vol. 114 (3–4), 1 February 1995, Pages 275-279
- [15]. Paramjit Rana et.al., Characteristics of a cascaded grating multi-wavelength dye laser, *Optics and Laser Technology*, Vol. 86, pp 39-45 (2016).
- [16]. Paramjit Rana et.al., Co-amplification: An Efficient Spectral Beam Combination Approach for High Power, Closely Separated Dual Wavelength Dye Laser Systems, *Optics Communications*, vol. 451, pp 367-373 (2019).

## LIST OF FIGURES

Figure 1.1: Side by side beam combination.....	4
Figure 1.2: Coherent beam combination.....	5
Figure 1.3: Spectral beam combination (SBC).....	6
Figure 1.4: Equal frequency beam combination using interference.....	7
Figure 1.5: Energy level diagram of the fluorescent laser dye.....	12
Figure 1.6: Tunable multi-wavelength dye laser.....	15
Figure: 1.7: Schematic of simultaneous two-wavelength dye laser.....	16
Figure 1.8: Schematic of the cavity used by C.Y. Wu.....	17
Figure 1.9: Multi-wavelength tunable dye laser.....	17
Figure 1.10: Three cavities for dual-wavelength dye laser.....	20
Figure 1.11: Simultaneous two-wavelength operation of dual-wavelength dye laser.....	21
Figure 1.12: Schematic of the orthogonal polarized dual-wavelength generation.....	23
Figure 1.13: Grazing incidence cavity based dual wavelength dye laser.....	24
Figure 1.14: Prism beam expander based dual wavelength cavity.....	25
Figure 1.15: Prism and grating beam expander based variable output power cavities.....	26
Figure 1.16: Grazing incidence grating based dual wavelength configuration.....	27
Figure 1.17: Cavity configuration used by S. Jelvani.....	30
Figure 2.1: Energy level diagram of the CVL system.....	40
Figure 2.2: Picture of the indigenous CVL: 40 system used for the studies.....	41
Figure 2.3: Schematic of the plane-plane configuration.....	44
Figure 2.4: Schematic of the unstable resonator configuration.....	46
Figure 2.5: Schematic of the divergence measurement technique.....	47
Figure 2.6: Focal spot estimation for divergence measurement.....	48

Figure 2.7: Variation of divergence with magnification.....	48
Figure 2.8: Effect of Neon gas pressure on optical output power.....	50
Figure 2.9: Schematic of the experimental setup used for the green to yellow ratio measurement.....	51
Figure 2.10: Green to Yellow ratio of a CVL oscillator.....	52
Figure 2.11: Variation of output power with electrical input power.....	52
Figure 2.12: Schematic of a plane parallel resonator for single wavelength emission.....	54
Figure 2.13: Reflectance curve of green emission mirror achieved by the design.....	56
Figure 2.14: Reflectance curve of yellow emission mirror design.....	56
Figure 2.15: Fresnel loss variations with the angle of incidence (Single layer MgF <sub>2</sub> ).....	58
Figure 2.16: Spectrum for Green and yellow filtering design.....	59
Figure 2.17: s and p polarization selection in the specialised window design.....	59
Figure 2.18: Schematic of the MOPA configuration for the experiment.....	62
Figure 2.19: Single long chain configuration.....	64
Figure 2.20: Splitted chain after oscillator configuration.....	64
Figure 2.21: Splitted chain after amplifier configuration.....	65
Figure 2.22: Periodic power withdrawal configuration.....	66
Figure 2.23: Dependence of input signal power on power addition from the second amplifier.....	67
Figure 2.24: Dependence of input signal power on power addition from the fifth amplifier..	68
Figure 2.25: Schematic of CVL oscillator test beam for amplifier thermal lens measurement.....	72
Figure 2.26: Effective thermal lensing assessment setup.....	73
Figure 2.27: Determination of the effective thermal lens of the amplifier.....	74
Figure 2.28: Effect of input electrical power on the effective focal length.....	76

Figure 2.29: Effect of buffer gas pressure on the effective focal length.....	76
Figure 2.30: Oscillator (PBUR) and its equivalent thermal lens model.....	78
Figure 2.31: MOPA chain with equivalent thermal lens.....	80
Figure 2.32: Schematic of the amplifier ray-tracing model (beam parameter definition).....	81
Figure 2.33: Diameter of the beam and power gain after each amplifier in the MOPA.....	83
Figure 2.34: Schematic of the heat radiation model for the window heating.....	84
Figure 2.35: Transmittance curve of the designed IR reflector window.....	89
Figure 2.36: Effect of bore diameter on absorbed power and effective focal length.....	90
Figure 2.37: Effect of window distance on effective thermal lensing.....	92
Figure 2.38: Optimization of the solid angle for minimum thermal lens.....	92
Figure 2.39: Extractable MOPA output power with a slightly divergent beam to the amplifier.....	96
Figure 2.40: Extractable power due to stage-wise re-collimation in MOPA chain.....	97
Figure 2.41: Schematic of thermal lensing compensated (proposed) MOPA.....	103
Figure 3.1: Molecular structure of Rh101 dye in neutral/acidic form (AH) and its equilibrium process with anionic ( $A^{-1}$ ) form at the ground ( $S_0$ ) and excited ( $S_1$ ) states, respectively.....	110
Figure 3.2: Variation of pH by addition of acetic acid in Rh 101 dye in ethanol.....	111
Figure 3.3: Effect of pH on peak absorption wavelength and peak optical density (OD).....	112
Figure 3.4: Effect of pH on peak emission wavelength and peak intensity.....	113
Figure 3.5: Dye laser cavity set up for performance testing of acidic dye laser.....	114
Figure 3.6: Experimental setup (Michelson Interferometer) for measurement of thermal coefficient of refractive index for commonly used dye solvents.....	118
Figure 3.7: Schematic layouts of the experimental set-up.....	122
Figure 3.8: Tuning range of SR 101 in ethanol solvent.....	123

Figure 3.9: Comparative tuning range of SR 101 in Ethanol in a binary solvent mixture.....	123
Figure 3.10: Effect of water to ethanol ratio on spectral sifting in the tuning range.....	124
Figure 3.11: Performance enhancement with increasing water to ethanol ratio.....	125
Figure 3.12: Schematic of the resonator configuration for three-wavelength.....	127
Figure 3.13: Spectrograph of three wavelength dye laser.....	127
Figure 3.14: Starting wavelengths of the tuning range with increasing PM 567 Concentration.....	129
Figure 3.15: Ending wavelengths of the tuning range with increasing PM 567 concentration.....	129
Figure 3.16: Starting wavelengths of the tuning range with the dilution of PM 567 concentration.....	130
Figure 3.17: Ending wavelengths point variation of the tuning range with dilution of PM 567 concentration.....	131
Figure 3.18: Starting wavelengths of the tuning range with DCM concentration dilution.....	131
Figure 3.19: Ending wavelengths of the tuning range with DCM concentration dilution.....	132
Figure 4.1: Linear cavity with a prism beam expander.....	139
Figure 4.2: Gain competition effect in the wavelength tuning curve in a linear cavity with a prism beam expander.....	140
Figure 4.3: Spectrograph showing a two-wavelength operation.....	141
Figure 4.4: Folded cavity with a prism beam expander.....	142
Figure 4.5: Linear cascaded grating cavity without PBE.....	145
Figure 4.6: Wavelength tuning characteristics of three sub-cavities in the cascaded grating cavity without PBE.....	145
Figure 4.7: Three wavelength operation in the linear cascaded grating cavity.....	146
Figure 4.8: Schematic of Cascaded Grazing Incidence Grating (CGIG) resonator	

configuration.....	148
Figure 4.9: Schematic of hybrid CGIG (HCGIG) with Littrow resonator configuration.....	148
Figure 4.10: Tuning curves of four CGIG sub-cavities.....	151
Figure 4.11: Variation of output intensities due to wavelength tuning of sub-cavity C-1, keeping wavelength of C-2, C-3, and C-4 at fixed values (CGIG).....	151
Figure 4.12 Variation of output intensities due to wavelength tuning of sub-cavity C-2, keeping wavelength of C-1, C-3, and C-4 at fixed values (CGIG).....	153
Figure 4.13: Variation of output intensities due to wavelength tuning of sub-cavity C-3, keeping wavelength of C-1, C-2, and C-4 at fixed values (CGIG).....	154
Figure 4.14: Variation of output intensities due to wavelength tuning of sub-cavity C-3, keeping wavelength of C-4, C-1, and C-2 at fixed values (CGIG) but wavelength values of C-1 and C-2 interchanged.....	155
Figure 4.15: Tuning curves of four HCGIG sub-cavities.....	156
Figure 4.16: Variation of output intensities due to wavelength tuning of sub-cavity C-1, keeping wavelength of C-2, C-3, and C-4 at fixed values (HCGIG).....	156
Figure 4.17: Variation of output intensities due to wavelength tuning of sub-cavity C-2, keeping wavelength of C-1, C-3, and C-4 at fixed values (HCGIG).....	157
Figure 4.18: Variation of output intensities due to wavelength tuning of sub-cavity C-3, keeping wavelength of C-1, C-2, and C-4 at fixed values (HCGIG).....	158
Figure 4.19: Variation of output intensities due to wavelength tuning of sub-cavity C-4, keeping wavelength of C-1, C-2, and C-3 at a fixed value (HCGIG).....	158
Figure 4.20: Representative Fabry Perot (15GHz FSR) etalon fringes of sub-cavity C-1(CGIG).....	160
Figure 4.21: Picture of the intra-cavity beam combiner four wavelength laser system.....	161
Figure 4.22: Simultaneous four wavelength generation in CGIG resonator.....	162

Figure 4.23: Simultaneous five wavelength generation in HCGIG resonator.....	162
Figure 5.1: Yellow beam pumped oscillator characterization set up.....	168
Figure 5.2: Tuning characteristics of Rh 101 dissolved in ethanol.....	169
Figure 5.3: Tuning curve with PM 650 dye in ethanol.....	170
Figure 5.4: Comparison of the tuning curve of Rh 101 dye in ethanol and water, ethanol binary mixture.....	171
Figure 5.5: Tuning range of the yellow pumped Rh 101 dye in ethanol and methanol.....	172
Figure 5.6: Characterization of output power (W) with input diode current.....	174
Figure 5.7: Variation of temporal pulse width (ns) with input diode current (A).....	174
Figure 5.8: Variation of pulse rise time (ns) with diode input current (A).....	175
Figure 5.9: DPSSL pumped dye laser in Littrow configuration.....	176
Figure 5.10: Effect of pump pulse width on dye laser output pulse width.....	177
Figure 5.11: Effect of pump pulse width on dye laser output power.....	177
Figure 5.12: Effect of pump pulse rise-time on dye laser output power.....	178
Figure 5.13: Effect of pump pulse rise-time on dye laser output pulse rise-time.....	179
Figure 5.14: Effect of pump pulse rise-time on dye laser pulse width.....	179
Figure 5.15: DPSSL pumped dye laser in GIG configuration.....	180
Figure 5.16: Tuning range of DPSSL pumped GIG cavity at various OC reflectivity.....	181
Figure 5.17: Narrowband operation of DPSS pumped GIG dye laser with FP etalon of FSR 7.5GHz.....	182
Figure 5.18: Temporal pulse of DPSS pumped GIG dye laser along with pump pulse.....	183
Figure 5.19: Experimental setup for yellow pumped Rh 101 dye oscillator amplifier study (One laser beam).....	185
Figure 5.20: Optimization of the concentration in yellow pumped Rh 101 dye amplifier.....	185
Figure 5.21: Pump power effect in yellow pumped Rh 101 dye amplifier.....	186

Figure 5.22: Schematic of the spectral beam combination setup.....	187
Figure 5.23: Schematic of high power, dual-wavelength dye laser generation using external cavity beam combination (Individual Amplification scheme).....	190
Figure 5.24: Schematic of high power, dual-wavelength dye laser generation using external cavity beam combination (Common Amplifier scheme).....	191
Figure 5.25: Optical layout of the experiment.....	192
Figure 5.26: Pump power effect on amplifier extraction efficiency of individually amplified $\lambda_1$ beam.....	193
Figure 5.27: Input power effect amplifier extraction efficiency of individually amplified $\lambda_1$ beam.....	193
Figure 5.28: Amplifier extraction efficiency of individually amplified $\lambda_2$ beam (Pump power effect).....	194
Figure 5.29: Amplifier extraction efficiency of individually amplified $\lambda_2$ beam (Input power effect).....	194
Figure 5.30: Pump power effect on extraction efficiency of the common amplifier with the composite input beam.....	195
Figure 5.31: Input power effect on extraction efficiency of the common amplifier with the composite input beam.....	196
Figure 5.32: Input-output correlation of dual-wavelength common amplifier.....	197
Figure 5.33: Output relation for the individual and co-amplified scheme in the common Amplifier.....	197
Figure 6.1: Transmission spectrum of edge filter designed for closer wavelength.....	208
Figure 6.2: Transmission spectrum (p-polarised) of the designed FP beam combiner (at AOI of 0 and 45 degree).....	210

Figure 6.3: Designed transmission spectrum of the dual cavity FP combiner.....	211
Figure 6.4: The measured transmission spectrum of the fabricated FP combiner.....	214
Figure 6.5: Height-height correlation function.....	216
Figure 6.6: 2-D &3-D AFM surface image of the beam combiner.....	216
Figure 6.7: Schematic of spectral beam combination setup.....	218
Figure 6.8: Experimental set up for ASE measurement.....	221
Figure 6.9: ASE filtering feature in the transmission spectrum of the FP filter (both cases).	222
Figure 6.10: Shift in the transmission spectrum (calculated) due to change of AOI.....	223
Figure 6.11: Spectral variation with the change of AOI (calculated).....	224
Figure 6.12: Schematic of spectral beam combination of widely tunable lasers.....	225

## LIST OF TABLES

Table 2.1: Characteristics of 9 kHz CVL in Plane-Plane resonator.....	45
Table 2.2: Divergence measurements with various resonator magnification.....	49
Table 2.3: Layer thickness pattern of green emission mirror.....	55
Table 2.4: Layer thickness pattern of yellow emission mirror.....	55
Table 2.5: Design of multifunctional window for CVL.....	60
Table 2.6: Comparison of power extracted from various configurations.....	69
Table 2.7: Design description of IR reflector CVL window.....	88
Table 2.8: Layer thickness of IR reflector thin film coated window.....	88
Table 2.9: Effect of the diverging beam on stage-wise power gain in the CVL MOPA chain.....	95
Table 2.10: Effect of re-collimation on stage-wise power gain in CVL MOPA chain .....	97
Table 2.11: Effect of re-collimation after two stages on power gain in CVL MOPA chain....	99
Table 2.12: Relative output power after dual re-collimation (DR).....	100
Table 2.13: Effect of RBDR on stage-wise power gain in CVL MOPA chain.....	101
Table 2.14: Relative output power after re-collimation and beam diameter recovery (RBDR).....	101
Table 2.15: Relative comparison of the compensation schemes in amplifiers.....	102
Table 3.1: Measured values of thermo optic constant for ethanol, demineralised water and their mixture by Michelson interferometer.....	119
Table 4.1: Zone of individual sub-cavities in both the configurations for sustained four wavelength operation in DCM dye laser.....	159
Table 5.1: Characteristic of the DPSS pump laser system.....	173

Table 5.2: Calculations for individual and common amplifier scheme selection.....	189
Table 5.3: Input-output power ratio correlation and Gain Competition Coefficient (GCC)..	198
Table 5.4: Effect of pump power polarisation on extraction efficiency.....	200
Table 5.5: Expected performance of the individually amplified scheme.....	202
Table 5.6: Measured performance of the co-amplified scheme.....	202

# Chapter: 1

## Introduction to Spectral Beam Combination Techniques for Pulsed Dye Lasers

---

### **1.1. Introduction:**

The laser is a versatile light source having enormous applications in the field of engineering, chemistry, physics, and biology due to its unique properties such as coherence, monochromaticity, and directionality [1.1-1.4]. These properties can be further tailored by utilizing various techniques, devices and methods to widen the scope of its application potential. Beam combination techniques are one of such techniques, which can help in generating high power, high repetition rate and multiple wavelength laser sources for special applications ranging from military, defence, communication, pulse repetition rate scaling, power scaling, brightness scaling, frequency mixing, laser spectroscopy and laser fusion etc.[1.5-1.7]. Pulsed laser beams with a smaller pulse repetition frequency are combined to increase the repetition frequency, which is termed as multiplexing of the laser beams [1.8]. Power obtained from a single laser system is usually limited by thermal effects and damage mechanisms [1.9]. Combining several high power laser beams coherently can enhance the total achievable power as well as brightness at the target location for desired applications. Similarly, several lasers operating at different wavelengths can be combined to generate a multi-wavelength composite laser beam for a suitable application. Side by side, coherent and spectral beam combination are the major mechanisms of the laser beam combination techniques used by several authors [1.9]. In the spectral beam combination technique, several laser beams operating at different

## CHAPTER - 1

---

wavelengths are combined to generate a composite laser beam. Spectral beam combined multi-wavelength dye lasers have applications in atmospheric probing, non-linear frequency mixing, differential absorption lidar (DIAL), resonance ionization spectroscopy (RIS), remote gas sensing, and trace analysis [1.10-1.17]. For all these applications, multi-frequency, collinear and wavelength-tunable lasers are required [1.10-1.17]. Simultaneous operation of twin wavelengths in a single dye laser has been reported by many researchers [1.18] and widely used for DIAL applications. In the DIAL applications, two closely separated (difference <10nm) laser wavelengths are utilized. One of the wavelengths is on-resonance with the target molecules, while the second is at the off-resonance. Variation in the scattering of these two wavelengths from the target molecules gives the concentration and range of the molecules. The dye laser is a versatile tool having high power, narrow bandwidth, high repetition rate, and wide tunability finds direct application in these areas. The generation of wavelengths from 400 nm to 1100 nm is achieved using several dye chromophores optically pumped by a suitable pump source [1.19-1.23]. The wavelength spectrum of dye laser can be widened by either using a mixture of dye chromophores or by generating the harmonics [1.23]. A further spectral shifting in the photophysical properties (absorption-emission) is achieved by using several solvents (polar and non-polar) and their binary mixtures [1.23]. Fluorescent laser dyes can be used in liquid as well as in solid phase. The liquid phase of dye lasers was selected for the present studies. The gain medium in the liquid phase facilitates heat removal, which can be operated at a high pulse repetition rate and higher power levels. Dye lasers in the liquid phase can be configured in oscillator-amplifier chains to enhance the average output powers [1.24]. A master oscillator generates the desired quality of the signal beam, which can be further amplified using several amplifier modules in a master oscillator power

amplifier (MOPA) configuration [1.24, 1.25]. The enormous potential applications of dye lasers along with versatile spectral coverage, high repetition rate capability, and operability at high average power motivated to study the spectral beam combination techniques for high power, pulsed dye laser systems. The copper vapour laser (CVL) pumped dye laser systems were utilized for the spectral beam combination experiments. Multiple wavelengths were generated using dye lasers following the intra-cavity and external cavity beam combination techniques. Because of the potential candidate for vast application ranging from environment monitoring to basic sciences, the study of spectral beam combined multi-wavelength dye laser was taken up as the scope of this thesis work. The spectral beam combination techniques (intra-cavity and external-cavity) have been studied to generate high power, pulsed, narrow bandwidth, multi-wavelength dye laser beams having closer wavelengths ( $<10\text{nm}$ ) [1.26,1.27], which is described in the subsequent chapters of this thesis. An elaborate study on the high pump power generation using CVLs and dye gain medium was carried out to meet the requirement of high power, pulsed laser systems for spectral beam combination experiments.

### **1.2. Classification of Laser Beam Combination Techniques:**

Spatial overlapping of several laser beams to generate a single composite laser beam is termed as the beam combination. The selection of beam combination technique is governed by the requirement for the application and the properties of the constituent laser beams. The number of laser beams to be combined, spectral region, wavelength separation, polarization, power levels, and their repetition rates are some of the important parameters for selecting a suitable combination technique. Three classes of the beam combination techniques are defined based on these parameters [1.9]. Most of the schemes fall in one of the following categories:

## 1.2.1. Side by Side Beam Combination:

In this technique, laser beams are placed side by side to each other emitting towards one targeted direction. These individual laser beams are kept close enough with each other to spatially overlap the output beams in near and far-field. Figure 1.1 shows the typical schematic of the side by side beam combination technique.

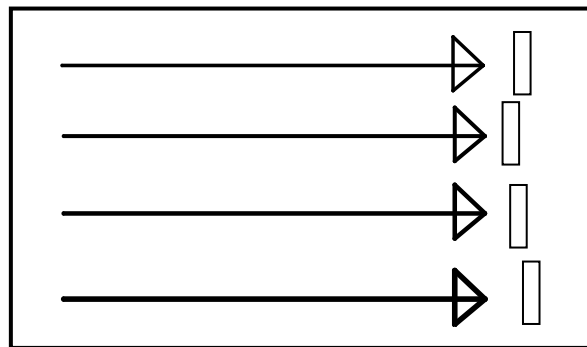


*Figure 1.1: Side by side beam combination [1.9]*

Wavelengths may or may not be the same. Phases are not controlled in this technique. Radiance of combined laser beams by this technique cannot be greater than the radiance of a single array element; therefore diffraction-limited beam cannot be achieved using this technique. Linear bars and two-dimensional arrays of diode lasers fall in this category.

## 1.2.2. Coherent Beam Combination (CBC):

Coherent beam combination (CBC) is a technique in which all of the constituent sources operate with the same spectrum. The relative phases of the constituent elements are controlled, such that they interfere constructively. In CBC, the electric fields of the elements must add constructively (vectorially). This requires controlling the polarizations and the amplitudes of the elements at every instant in time. Figure 1.2 shows the basic scheme of the CBC scheme. Implementation strategies under this class are elaborated as follows:

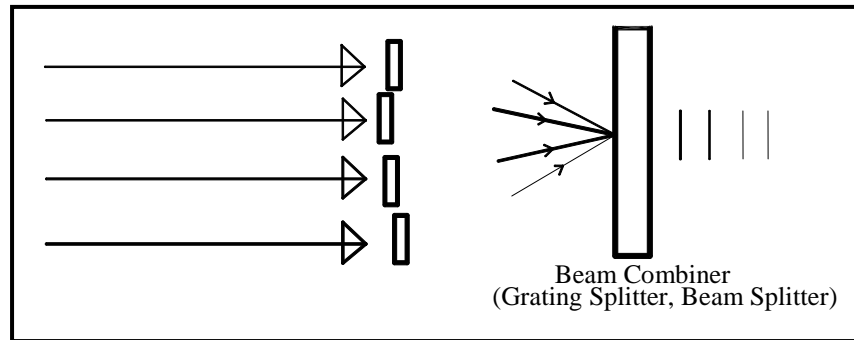


*Figure 1.2: Coherent beam combination [1.9]*

**1.2.2.1. Tiled Aperture Implementation:**

In this, individual elements have outputs that are adjacent to each other, which interfere only in the far-field. This type of implementation can be thought of as a synthesized plane wave. To minimize the side lobes and to obtain the maximum far-field intensity, the fill factor must approach unity i.e. the spaces between tiles (laser modules) must be minimized.

**1.2.2.2. Filled Aperture Implementation:**

In the filled-aperture implementation, the interference occurs in the near field. The beam combiner in the filled aperture system can be thought of as the inverse of a beam splitter with proper phase, amplitude and polarization relations among the multiple beams must be maintained for efficient combination. The highest possible brightness and modular power scaling are the advantages of this approach. Controlling the relative phases is comparatively difficult in this scheme. Fill factor approaching to unity is very difficult, which results in the side lobes for this implementation.

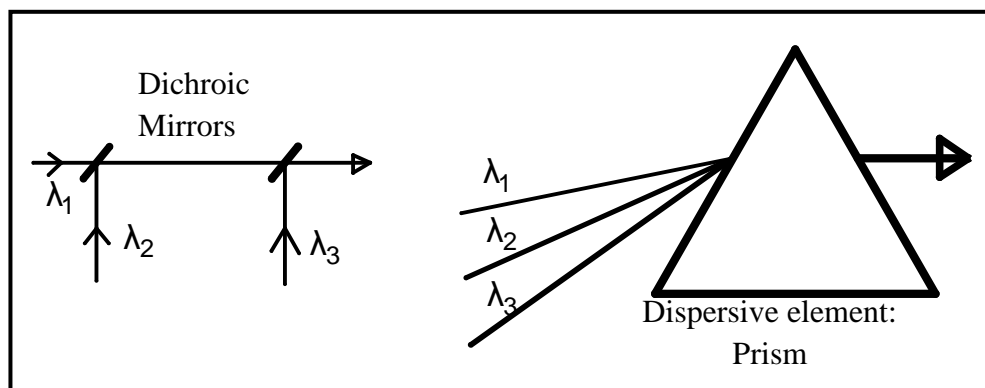
**1.2.3. Spectral Beam Combination (SBC):**

In Spectral, wavelength or incoherent beam combinations, individual beams of different wavelengths are overlapped using dispersive or non-dispersive elements in the near and far-field. Power in this scheme is added but not vectorially as in

CBC. Optical elements used in this technique are broadband beam splitters, dichroic filters, polarizers, and dispersive elements.

### 1.2.3.1. Serial Implementation:

In the serial implementation as shown in fig. 1.3, all the beams are added or combined one by one serially. The broadband beam splitter and dichroic filters based combination fall under this scheme. These elements have advantages of handling high power as well as the polarization but shows lower efficiencies for combining closely separated wavelengths.



1. Serial Implementation

2. Parallel implementation

*Figure 1.3: Spectral beam combination (SBC) [1.9]*

### 1.2.3.2. Parallel Implementation:

In the parallel implementation, all the constituent beams are incident simultaneously (fig. 1.3) on the combining element. Grating and prism are used to implement this type of beam combination. This implementation is dependent on the polarization of the incident beams. Polarization of the constituent beams should be the same for grating and prism-based beam combination, whereas polarizer beam combiners can combine only two mutually orthogonal polarizations of the laser beams.

## 1.2.4. Other Laser Beam Combination Schemes:

Apart from these well-classified laser beam combination schemes, many other techniques are used by researchers to combine several laser beams. A few of the recent combination techniques are described below.

### 1.2.4.1. Beam Combination Using Interferometer Technique:

D. Haubrich et.al. have demonstrated interferometer based beam combination techniques to combine two laser beams with the same linear polarizations and very closely spaced frequencies as shown in fig. 1.4 [1.28].

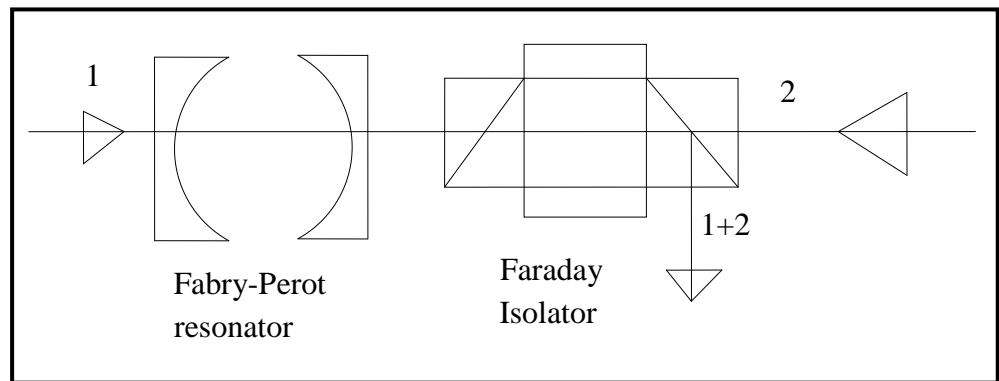


Figure 1.4: Equal frequency beam combination using interference [1.28]

They have investigated three configurations using Faraday isolator, polarizing beam splitter, and Mach-Zehnder interferometer. Linearly polarised laser beams separated by few GHz were combined with good combination efficiencies greater than 90%. A Fabry Perot (FP) resonator and Faraday isolators were arranged together in the first configuration. The FP resonator was tuned on resonance for first laser frequency while being far off-resonant for second laser frequency so that the first beam (1 in fig. 1.4) is transmitted completely, while the second beam (2 in fig. 1.4) is reflected. After interaction with the resonator, both beams were travelled

## CHAPTER - 1

---

towards the Faraday isolator where both of these beams were combined in the reverse exit of the Faraday isolator.

The second method was based on a polarizer beam splitter (combiner) instead of the isolator. A similar setup using a combination of a quarter-wave plate and a polarizing beam splitter instead of isolator was investigated [1.28]. A third arrangement using modified Mach Zehnder interferometers was tested [1.28]. Each laser beams enter through one of the two input ports of the two-beam interferometer. The length of the second path was chosen such that the first path and second path lead to completely constructive interference at the first output port for both the beams. In effect, both laser beams emerge at the same output port with ideally all their input power while no light comes out of the other output port. One of them is named as bright and another is the dark output port depending on the overall phase difference accumulated along the first and second paths. By changing it over the range of half a wavelength the splitting ratio of 100:0 can continuously be tuned all the way to 0:100. These techniques are efficient for equal wavelength beam combination but less suitable for high power, tunable laser beams.

### **1.2.4.2. Fiber Optic Beam Combiner:**

For attaining multi-kW power levels, beam combining has become the method of choice to reach higher powers using diode and fiber lasers. C. Lei et.al. have demonstrated a tapered fiber bundle based incoherent beam combiner to combine 2kW fiber lasers and generated a combined output beam of 14.1 kW power [1.29]. In this technique, there are four steps to fabricate a combiner [1.29] namely; (1) Make a fiber bundle and place them

centro-symmetrically within a low-index fluorine-doped glass capillary, (2) The fiber bundle is tapered until all the fiber cores can be covered by the core of the output fiber, (3) The tapered fiber bundle is then cleaved by ultrasonic cutter at the taper waist, (4) The input fiber bundle is spliced with the delivery output fiber. It is a promising technology, which has shown the potential to enhance the level of power achieved using all-fiber combiners.

### **1.2.4.3. Beam Combination Based on Material Optical Non-linearity:**

Phase conjugation, Raman and Stimulated Brillouin scattering based non-linear effects are used to combine the coherent beams of laser in a CBC approach [1.9]. Stimulated Brillouin scattering (SBS) is a non-linear optical process that generates backward scattered phase conjugate waves [1.30-1.33]. SBS phase conjugate mirror (PCM) is the device, which generates the phase conjugate wave by the SBS process. High power laser beams are generated by the SBS-PCM beam combination technique. The realization of the CBC technique using phase conjugation relied on SBS in bulk media, which has a relatively high threshold requirement, which needs high-peak-power lasers [1.9]. Recently, lower thresholds have been obtained by using guided wave configurations [1.9]. This is a technique used for laser fusion driver applications [1.34,]. Issues with non-linear optical beam combining include scaling to large numbers of elements, having a low threshold, handling the bandwidth and dynamic range of the required phase corrections [1.9].

Recently in 2018, a plasma-based beam combiner was used for the combination of very high fluence lasers [1.7]. R.K. Kirkwood et.al. have demonstrated plasma itself as the beam combiner [1.7]. They have used

nonlinear interactions of multiple beams in plasma, which has the potential to produce optics that can operate at a much higher intensity and fluence than possible in solids. It was used for laser-driven inertial confinement fusion experiments. In this experiment, many laser beams overlapped in the plasma inside a hohlraum. Cross-beam energy transfer by Brillouin scattering has been employed to redistribute energy between laser beams within the target. In hot, under-dense plasma the energy of many input beams can be combined into a single well-collimated beam which generates a fluence that was more than double. The diffractive type optical element produced here was plasma and is inherently capable of generating higher fluencies in a single beam than the solid-state refractive or reflective optics. Polariser based beam combination for increased repetition rate was used by I. Balboa for the LIDAR experiment [1.8]. Their beam combination method was suitable for current ITER and Jet applications as well.

After studying all these classes of beam combination, diffraction grating was selected for the intra-cavity beam combiner element and the thin film based multilayer-coated Fabry Perot interference filter as a beam combiner for the external cavity beam combination studies carried out during this thesis work.

### **1.3. Copper Vapour Laser Pumped Dye Laser System:**

Tunable pulsed dye laser with narrow bandwidth is an extremely versatile instrument [1.19-1.23] for studying the beam combination technique. Dye lasers are optically pumped by a suitable pump source. Flash lamp and lasers are generally used as a pump source for pumping the dye lasers. Lasers are more suited to pump the dye laser due to better overlap with the absorption band of the dye chromophores. Therefore,

## CHAPTER - 1

---

nowadays pumping with a laser source is preferred for the dye lasers [1.19-1.23]. These pump sources primarily include nitrogen laser, Ar-ion laser, copper vapor laser (CVL), second harmonic of Nd: YAG laser and diode lasers, etc. Nitrogen laser emits the blue wavelengths (337.1 nm) whereas CVL is in the green and yellow wavelength range (510.6 nm & 578.2 nm). Second harmonic of Nd: YAG (532 nm) lies in the green wavelength range. Argon-ion lasers emit at 13 different wavelengths in the visible and ultraviolet spectra, including 351.1 nm, 363.8 nm, 454.6 nm, 457.9 nm, 465.8 nm, 476.5 nm, 488.0 nm, 496.5 nm, 501.7 nm, 514.5 nm, 528.7 nm, and 1092.3 nm. However, the most commonly used wavelengths of Ar ion laser are in the blue-green region (488 nm, 501.7nm, 514.5nm) of the visible spectrum. The CVL pump laser was selected for pumping the dye laser for studying the beam combination techniques, due to its high repetition rate and power scaling capability. Individual CVL of 40W operating at 9 kHz repetition rate was utilized, whose details are described in the next chapter. It can be cascaded in the master oscillator power amplifier (MOPA) chains to generate higher power levels. The indigenously developed CVL system arranged in a MOPA chain were utilized for pumping the present dye laser system intended to study various spectral beam combination techniques for closer wavelengths.

Several classes of dye laser chromophores and their variants have been developed covering the wider spectral range efficiently [1.23]. The laser dyes used majorly for generating tunable laser sources are coumarin, rhodamines, pyromethenes, pyridine, etc. The selection of laser dye depends on the required emission wavelength range and the available pumping source. Dye chromophores have a shorter upper laser lifetime in the range of 4-10 ns, which imposes the requirement of the sharp rise time of the pumping pulse for the efficient optical conversion. The CVL and diode-

## CHAPTER - 1

pumped solid-state laser pumped dye lasers meet this stringent demand of dye chromophores. Hence these two pump sources were utilized for this study.

The dye laser is a four-level system, which is a tunable source and can be operated in the pulsed as well as in continuous wave mode of operation. The energy level diagram of a dye is shown in fig. 1.5.

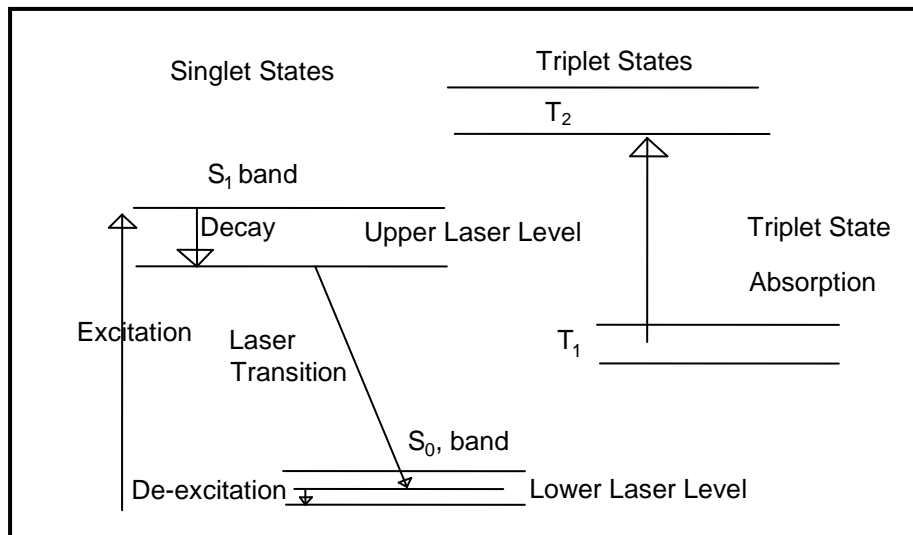


Figure 1.5: Energy level diagram of the fluorescent laser dye

It can be seen from the energy level diagram that, ground state, upper laser level, and lower laser level are singlet states. There are triplet states adjacent to these singlet states having slightly lower energy levels. Dye chromophores are excited to upper levels of the  $S_1$  band and relax to the lowest level of the  $S_1$  band by internal conversion. Lasing action takes place between the lowest  $S_1$  levels to any of the levels in the  $S_0$  band. The transitions to these bands result in the continuous tuning of the dye laser wavelengths. The dye gain medium when used in the resonator cavity with dispersive optical elements emits the narrowband tunable radiation at the desired wavelength. The liquid dye gain medium is studied in detail during the present thesis work. Tailoring the photo-physical properties and CVL pumped dye laser performance by using polar, non-polar solvents, their mixtures, and binary dye mixtures make the

dye laser an ideal candidate for the spectral beam combined multi-wavelength laser system for applications like DIAL based environmental and remote sensing. Studies on the dye gain medium are presented in the subsequent chapters of this thesis.

### **1.4. Spectral Beam Combination Techniques for Pulsed Dye Lasers:**

Composite laser beam consisting of multiple wavelengths is generated by spectral beam combination techniques. In this scheme, spatial overlap among constituting laser beams is achieved by an optical component or a geometrical arrangement inside a resonator cavity. This optical component can be a grating, a prism, an interference filter (broadband beam splitter or dichroic beam splitter), a polarizer, a Fabry-Perot interferometer (etalon), thin-film lasers, or a distributed feedback (DFB) laser system; depending on the power, wavelength separation, compactness and polarization of the constituent beams [1.35]. In dye lasers, a combination of the laser beams can be done intra-cavity at the oscillator or outside (external) the oscillator cavity.

#### **1.4.1. Intra-cavity Beam Combined Multi-wavelength Dye Lasers:**

A multi-wavelength composite laser beam is generated from a resonator cavity using intra-cavity beam combination techniques. Sub-cavities generating separate laser wavelengths are coupled inside the main cavity using a suitable optical element or a special geometry. Several intra-cavity beam combined cavity configurations are studied by many researchers for multi-wavelength dye laser generation [1.29-1.65].

Multi-cuvette and single cuvette systems are being used for intra-cavity beam combined multi-wavelength dye laser generation [1.35]. In multi-cuvette systems, separate cuvette containing dye solutions are used for each wavelength, whereas in a single cuvette system, the same cuvette is used for all the wavelengths. The advantages of the multi-cuvette system include the absence of

## CHAPTER - 1

---

chemical compatibility requirements, dye mixture requirement, and reduced gain competition. However, in a single cuvette (dye cell) system, the common gain volume is utilized for all the constituent wavelengths. This results in gain competition among constituent laser wavelengths. Maintaining the co-linearity and temporal synchronization is easier in the single cuvette configuration. Sharing the common gain volume acts as the inherent aperture for ensuring the co-linearity. This scheme is suitable for developing compact multi-wavelength tunable laser sources. Therefore, a single cuvette system based spectral beam combination techniques were reviewed in detail and are presented in this section.

Yu.G. Basov has reviewed the optical designs of two frequency dye lasers in 1988 [1.35]. Multi-cuvette, single cuvette systems including optical devices and their geometries were summarised [1.35]. Researchers have continued interest in multi-wavelength dye lasers due to its wide applicability. Literature about intra-cavity beam combiner multi-wavelength dye laser system is reviewed in detail.

Zalewski et.al. have reported dual-wavelength operation by flash lamp pumped 0.1 mM Rh 6G dye in ethyl alcohol in a dual grating resonator cavity [1.36]. Two mutually coupled sub-cavities using grating and partially transmitting mirror pairs were used to generate the intra-cavity beam combined, dual-wavelength dye laser beam as shown in the fig. 1.6.

Two gratings at the Littrow angle were used at both the end of the cavity, which formed two linear sub-cavities. Partially transmitting mirrors at normal incidence were inserted in between dye gain medium and the grating. The wavelength tuning range of both the sub-cavities was determined by blocking the grating of another sub-cavity. The tuning range of 50Å and 130Å was measured for first (G-1/M-1) and second (G-2/M-2) sub-cavities respectively. Wider tuning range

## CHAPTER - 1

in the second cavity was due to the higher transmission of mirror M-2 (40% as compared to 10% of the M-1) in the second cavity.

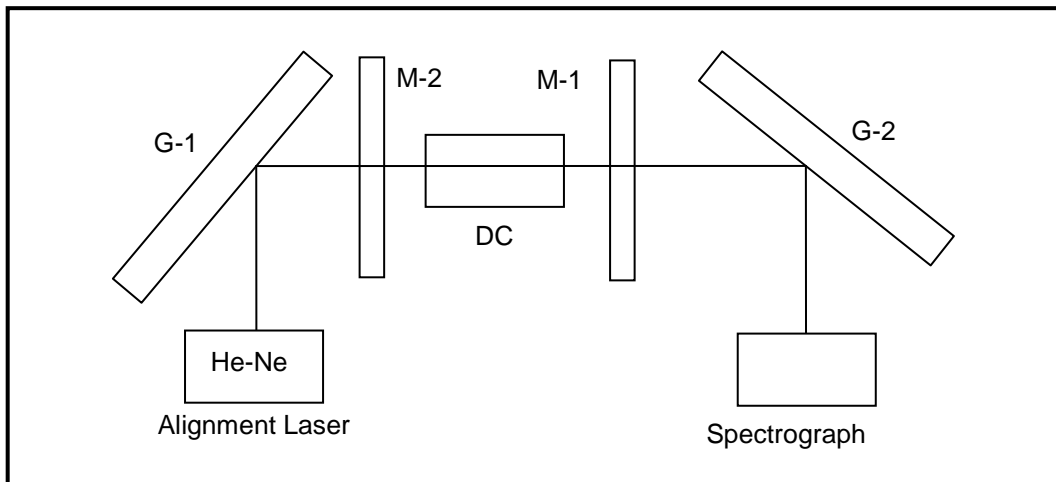


Figure 1.6: Tunable multi-wavelength dye laser [1.36] (G-1, G-2: Gratings, M-1, M-2: Mirrors, DC: Dye cell)

Taylor et.al. have demonstrated the dual-wavelength oscillation in a dye laser using an acousto-optic switch and electronic tuning [1.37]. A simultaneously operable, continuously tunable two-wavelength operation in a Nitrogen ( $N_2$ ) laser pumped dye laser was demonstrated by H.S. Pilloff [1.38]. Intra-cavity beam combined dye laser resonator using a polarizer and Littrow angled gratings was used to generate two wavelengths. As both the wavelengths were mutually orthogonal, they could be simultaneously tunable across the full range of tuning without severe gain competition. A  $N_2$  laser of 100 kW peak power, 10ns pulse duration, with the operating frequency of 100 PPS, was used to pump the 4-methylumbelliferone (4-MU) dye solution in ethanol to generate a dye laser wavelength around  $5000\text{\AA}$ . The time-averaged spectral bandwidth of this dye laser was less than  $2\text{\AA}$  at  $5000\text{\AA}$  and peak output power of the order of 10kW was obtained. Temporal delay between both the dye laser wavelength pulses was studied and temporally synchronized by varying the cavity lengths of the sub-cavities.

## CHAPTER - 1

Schematic of their cavity configuration is shown in fig. 1.7.

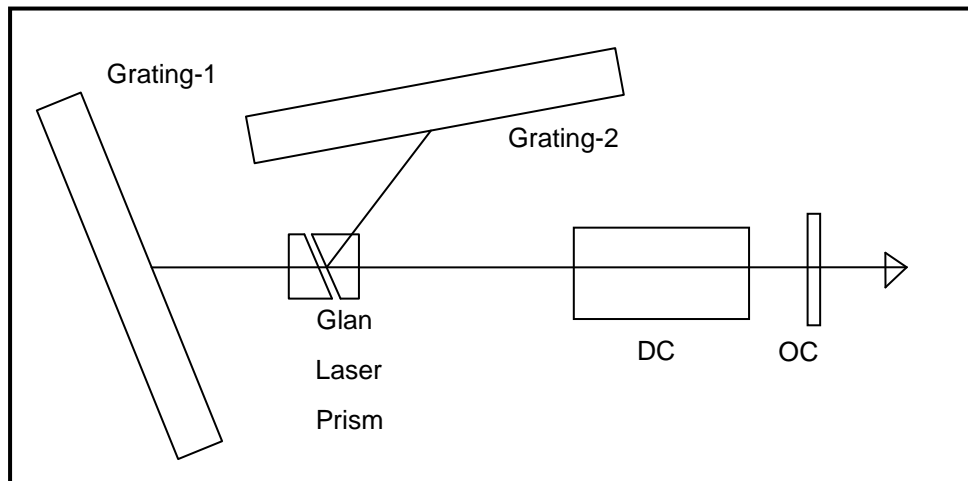


Figure 1.7: Schematic of simultaneous two-wavelength dye laser [1.38] (DC: Dye Cell, OC: Output coupler)

C.Y. Wu had used beam splitter of an aluminum-coated glass slide with 30% reflectivity as an intra-cavity beam combination device instead of the polarizer as used by H. S. Pilloff to generate two wavelengths in an  $N_2$  laser pumped Rhodamine 6G solution of concentration  $10^{-2} \sim 10^{-3}M$  in methanol [1.39]. Suitable neutral density filters and polarizers were used to alter the losses in the sub-cavities to maintain the equal proportion of output power from each wavelength. Two wavelength beams could be simultaneously tuned from  $5,790 \text{ \AA}$  to  $6,070 \text{ \AA}$ . Spectral narrowing of  $0.1 \text{ \AA}$  (FWHM) was achieved by inserting intra-cavity beam expanders.

The salient feature of this cavity configuration was that each wavelength could be configured to either the same or mutually orthogonal polarization orientation by simply adding the required polarizer in the sub-cavity arm. One of the wavelengths could be un-polarized, if the polarizer is not inserted in that arm. Figure 1.8 shows the schematic of the cavity used by CY Wu [1.39].

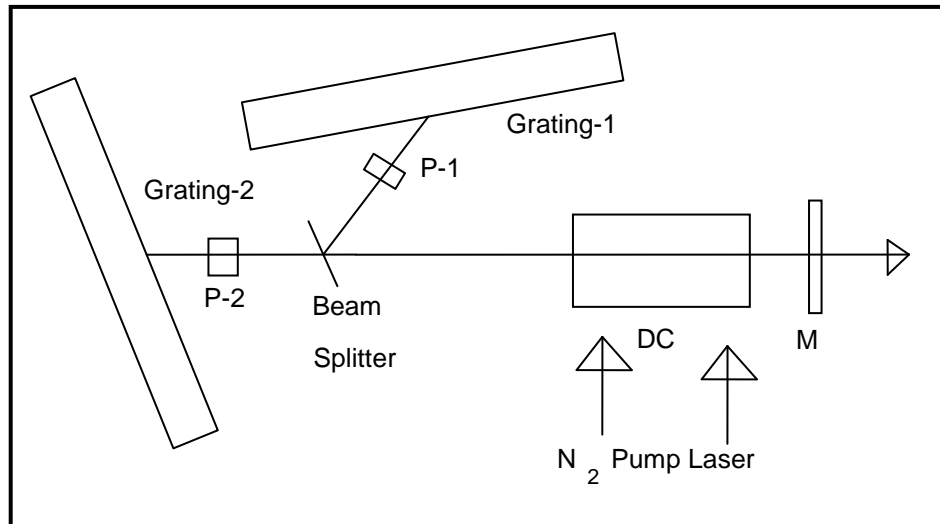


Figure 1.8: Schematic of the cavity used by C.Y. Wu,[1.38] (P-1 & P-2: Polarisers, DC: Dye Cell, M: Partially transmitting mirror)

Another technique for simultaneous and collinear emission of two wavelengths was demonstrated by Friesem et.al. using a pair of holographic wavelength selectors (Reflectivity in visible ~90%) [1.40]. One of the holographic reflectors has acted as a combiner as well as the wavelength selector. This reduced the intra-cavity losses due to the absence of additional intra-cavity combining optics. The schematic of their experimental is shown in fig. 1.9.

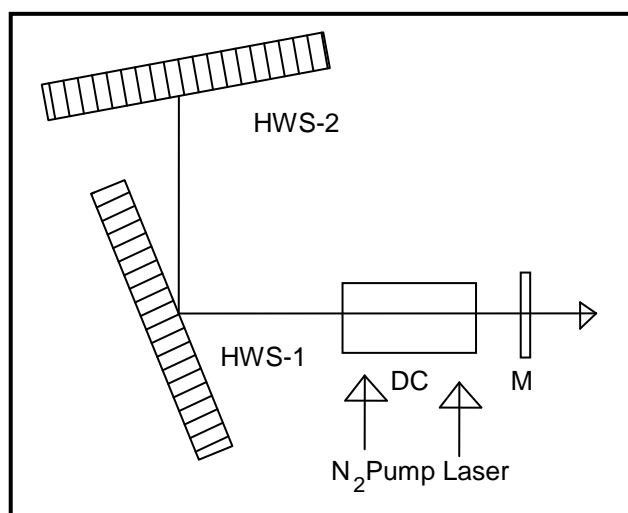


Figure 1.9: Multi-wavelength tunable dye laser [1.40], (HWS: Holographic wavelength selector, M: Output mirror, DC: Dye cell))

## CHAPTER - 1

---

Gain competition behavior in the tuning range was studied by measuring the relative peak power of one wavelength while keeping another wavelength as a constant. Short length cavity including two holographic wavelength selectors and one output coupling mirror makes this cavity suitable for shorter pulse operation. The performance of the laser was tested using several dye solutions (Rh6G, 7D4MC, 4MU, etc.) pumped by nitrogen laser (75kW peak power, 8 ns pulse width). The output of single wavelength (500nm) operation (another holographic reflector blocked) was measured to be 10kW peak power with 5 ns pulse duration and a tuning range of 85 nm was observed with a linewidth of 0.2 Å.

The simultaneous two-wavelength output from an N<sub>2</sub> pumped dye mixture of Rh 6G-Cresyl violet (CV) and a mixture of coumarin - Rh 6G was observed by R.C. Hilborn et.al. [1.41]. They have partially pumped the dye cell and two different wavelengths were emitted from each end. No additional beam combination element was used in their cavity; as, a combination of dyes inherently emitted the composite dual-wavelength laser. Excitation and emission mechanisms for the case of dye mixtures were determined for various concentrations of the individual dyes in the dye mixtures. The superradiant emission from dye mixtures was detected using fast photodiodes from both the ends of the partially pumped dye cell. Characterization of Rh6G and CV dye mixture was done by gradually adding CV in pure Rh6G (5mM in Methanol). Two distinct wavelength output with equal power in the 10 nm bandwidths were observed at 570 nm and 630 nm with CV concentrations of 0.55 mM. Similarly, in 7D4M coumarin and Rh6G mixture, simultaneous emission at 470 nm and 580 nm was achieved. Both the mixtures were studied in detail at various dye concentrations. The time delay of the order of rise time of the donor's emission concluded the dominant mechanism as the radiative excitation transfer process. They have suggested

## CHAPTER - 1

---

using separate dye cells for each dye pumped by a common pump is the simpler way to generate multiple wavelengths.

The operation of two coupled dye laser cavities using an absorbing cell was demonstrated by G. Marowsky et.al. [1.42]. Flash lamp pumped ring dye laser pumped a secondary intra-cavity dye laser using Rh6G and CV dye combination to generate independently tunable dual wavelengths covering the spectral range from 580 nm to 652 nm. The tuning range was found to be changed by changing the concentration of the constituent dye solutions. The influence of intra-cavity absorbing dye cell in a flash lamp pumped ring dye laser was studied experimentally. The conversion efficiency of 30% was obtained for  $2 \times 10^{-4}$  molar solution of Rhodamine 6G and a  $2 \times 10^{-5}$  molar solution of cresyl violet (CV) in methanol. The conversion efficiency was found to be independent of the bandwidth of the exciting laser emission due to homogenous broadening. The output power of the secondary laser was slightly dependent on the first wavelength. The typical output powers were 20kW for the Rh6G laser and 6 kW for the CV dye laser at input energy of 60J. In their experiments, both wavelengths had the same pulse shape. They were synchronized within 10ns at a pulse duration of 200 ns to 600 ns depending on input energy.

C. Kittrell et.al. had studied three cavity arrangements for independently tunable, simultaneous operation of two or more wavelengths in a single dye laser with a bandwidth of  $1\text{cm}^{-1}$  in the visible spectrum [1.43]. In the first cavity configuration, the wavelength was generated by reflection from the grating at the Littrow angle whereas the second wavelength was obtained from the cavity formed by end mirror, grating, and retro-reflection of the grating diffracted beam using the additional mirror.

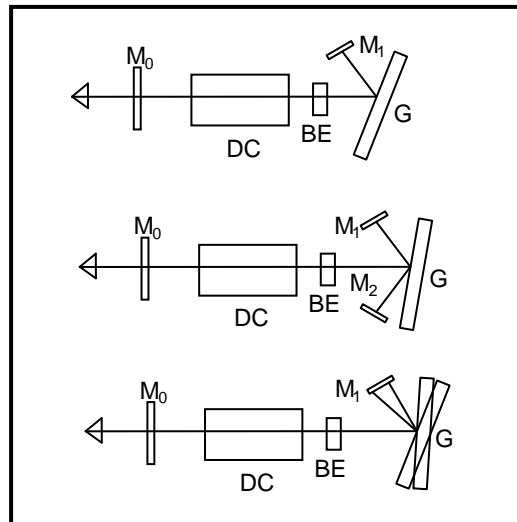
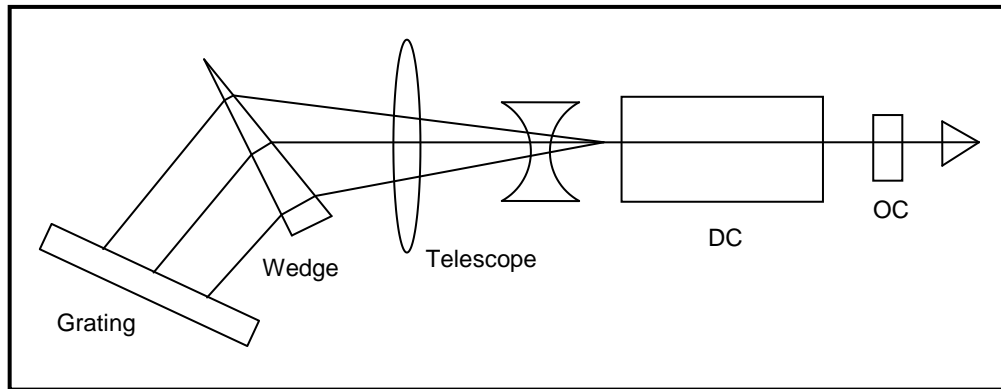


Figure 1.10: Three cavities for dual-wavelength dye laser, [1.43], ( $M_0$ : Output mirror,  $M_1, M_2$ : Mirrors, DC: Dye cell. BE: Beam expander, G: Grating)

Figure 1.10 shows the schematic of three configurations demonstrated by C. Kittrell et.al. [1.43]. The second configuration consisted of two retro-reflection mirrors to form the cavity with a slightly tilted grating. Wavelength tunability was obtained by tilting the retro-reflecting mirrors. Two wavelength laser beams were obtained with reduced gain competition by employing two separate paths through the gain medium achieved by careful alignment and focusing. In the third configuration, fractional power output at each wavelength was adjusted by translated the first and second mirrors perpendicular to the beam path so that the beam is intersected more by one than the other. The narrowest linewidth achieved was between  $0.5\text{cm}^{-1}$  and  $1\text{cm}^{-1}$ .

A.J. Schmidt et.al. have obtained two wavelengths by intersecting part of the beam using a wedge placed in front of the tuning grating [1.44]. Inserting the wedge in the cavity forms two separate beams having different feedback for different wavelengths. Partially transmitting an output mirror, a dye cell, a telescopic beam expander, a wedge for partially reflecting the part of the beam and a diffraction grating formed the resonator cavity. The schematic is shown in fig. 1.11.



*Figure 1.11: Simultaneous two-wavelength operation of dual-wavelength dye laser (DC: Dye Cell, OC: Output Coupler)*

The relative intensities of the two outputs could be changed by adjusting the position of the wedge in the z-direction. The polarization of the two beams was the same. They obtained tuning range for the wavelength difference of the two beams from  $50\text{\AA}$  to  $246\text{\AA}$  with a wedge of  $3^\circ$  (52 mrad). They proposed the tuning range of  $8\text{\AA}$  to  $50\text{\AA}$  by using a wedge angle of  $0.46^\circ$  (8mrad).

H. Lotem et.al. used a partially inserted wedge into the beam to obtain two different cavity paths for two different wavelengths similar to the configuration used by A.J. Schmidt [1.45]. The difference in the two approaches is the usage of Glan prism polarizer and tuning by rotation of the wedge. Cavity demonstrated by H. Lotem had two vertically separated sub-cavities, one with the wedge and another without the wedge. This ensured that different wavelengths pass through the different regions of the active medium. This minimized the gain competition as well as allows the usage of two separate dyes for different sub-cavities. Glan prism was inserted to get the polarized output beam and wedge axis was aligned parallel to the grooves of the grating. Rhodamine 6G dye laser was pumped with a 50kW nitrogen laser of the repetition rate of nearly 5-10 pulses per sec. They could generate the second wavelength by inserting a circular wedge with 11nm shifted towards the red side. The

## CHAPTER - 1

---

wedge was rotated about its axis to tune the second wavelength by around 2 nm. Second harmonic and sum-frequency generation using this dual-wavelength laser was demonstrated by them.

Marx et. al. have modified their Hansch type cavity to generate dual-wavelength, narrow-band dye laser [1.46]. A partially transmitting mirror was inserted horizontally into the beam after the beam expander and the diverted beam again routed to fall on the same Echelle grating. This resulted in the formation of two independent sub-cavities as both the beams falling on the grating at different angles hence generated separate wavelengths. Insertion of the solid etalon in both the arms resulted in the reduction of the line width to 400 MHz. The relative intensities of both the wavelengths could be varied by changing the extent of the insertion of the mirror. Tuning was achieved by rotating the grating and tuning of individual wavelength was achieved by changing the angle of the mirrors. Two wavelengths over 20 nm separation could be generated by using mixtures of Rh6G and Rh 110 dye solution. They had carried out experiments of the two-photon absorption process by using laser generated by this method.

Simultaneously tunable dual-wavelength dye laser in ultraviolet has been developed by Inomata et.al.[1.47]. Pulses from a pump laser (both nitrogen and a frequency-doubled ruby laser) were focused by a lens into a dye cell in a transverse pumping configuration. Rhodamine B dye solution of concentration  $5 \times 10^{-3} \text{M}$  in ethanol was used. A beam splitter was utilized to split and direct two cavity beams on to a grating. One beam travelled directly to the grating through the beam splitter and another indirectly via a fully reflecting mirror. An intra-cavity telescope (10X), a fully reflecting mirror and an output coupler with 70% reflectivity were aligned to obtain the narrowband laser beam. Intra-cavity frequency doubling has been obtained by

## CHAPTER - 1

using angle tuned KDP crystal in the wavelength range of 305 nm. Pair of wavelengths with a difference from 0 to 10 nm was generated for their DIAL based measurements of SO<sub>2</sub>

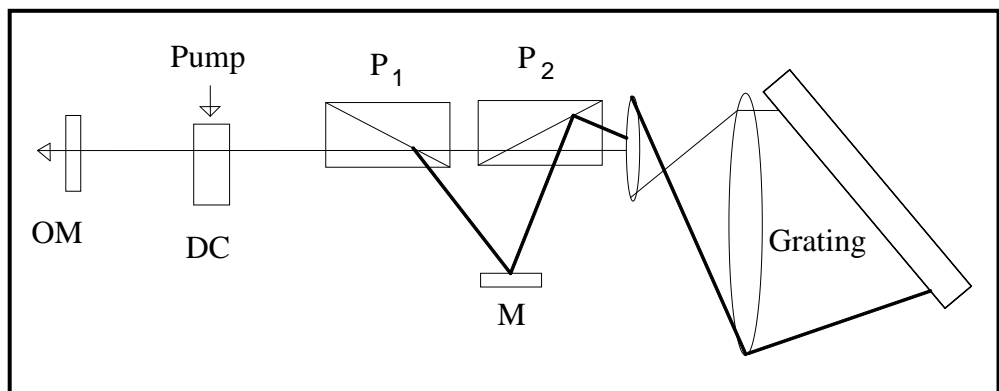


Figure 1.12: Schematic of the orthogonal polarized dual-wavelength generation (OM: Output Mirror, DC: Dye Cell, M: Mirror, P<sub>1</sub>& P<sub>2</sub>: Glan-Thomson prisms, Thin line: E ray path; Thick line: Ordinary ray path to Grating) [1.48]

Depending on its polarization a light beam travelled different paths and incident on the grating at different angles. Hence, two separate feedback pathways were established for two separate wavelengths. A maximum wavelength difference of the two beams of about 1.5 nm was obtained by using a coumarin 102 laser dye with grating aligned at the 6<sup>th</sup> order.

Longitudinal pumped, simultaneously operable, dual-wavelength dye laser was demonstrated by Dorsinville [1.49]. This was done by inserting a prism in the cavity, positioned at a very high angle of incidence, to separate the two wavelengths. An

## CHAPTER - 1

intra-cavity Glan prism with an open escape window was used to separate the pump beam from the stimulated emission.

A two-frequency dye laser using grating at the grazing incidence angle was demonstrated by M. A. Priya [1.50]. Total mirrors were used to reflect different order of diffraction of two different frequencies. The higher order from the laser cavity at the exit side of the grating is Glan prism. The first order of the diffracted beam additional from grating and second order using (1.48) Figure 1.13 Schematic of system used by Peromys setup used by Winter.

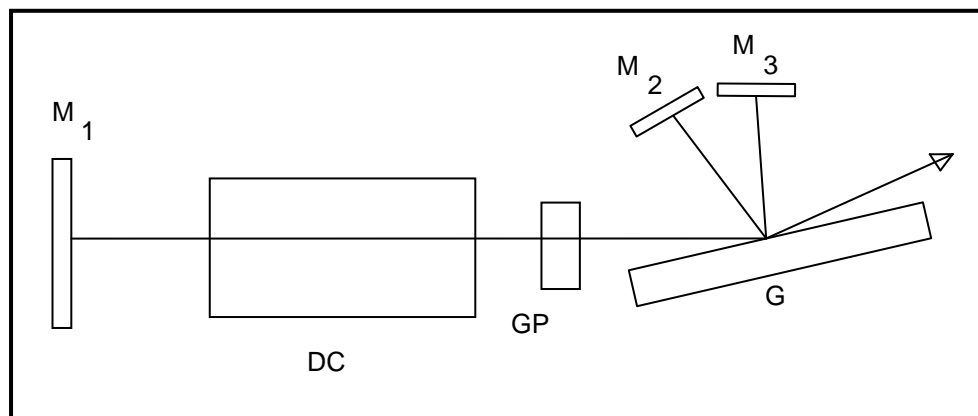


Figure 1.13: Grazing incidence cavity based dual wavelength dye laser [1.50], ( $M_1$ ,  $M_2$ ,  $M_3$ : High reflectivity mirror,  $G$ : Grating,  $GP$ : Glass plate,  $DC$ : Dye cell)

The cavity was closed with the high reflectivity mirror, whereas the zeroth-order diffracted beam was taken as the output beam. Nitrogen pumped Rh6G dye of concentration 5mM was used. They could achieve linewidth of the order of 0.01 to 0.02 nm from their dye laser system.

L.G. Nair has demonstrated orthogonal polarized, narrowband, dual-wavelength laser beam using nitrogen pumped Rh6G, RhB laser dyes [1.51]. She had used dual prism combination as the intra-cavity beam combiner as well as the beam expander. The experimental schematic used by Nair is shown in fig. 1.14. Intra-cavity beam incident on the prism was partially transmitted while the remaining portion was reflected. The

reflected beam was again expanded using another prism. The transmitted and the reflected beam from the first prism were incident at near grazing angle on the separate diffraction gratings.

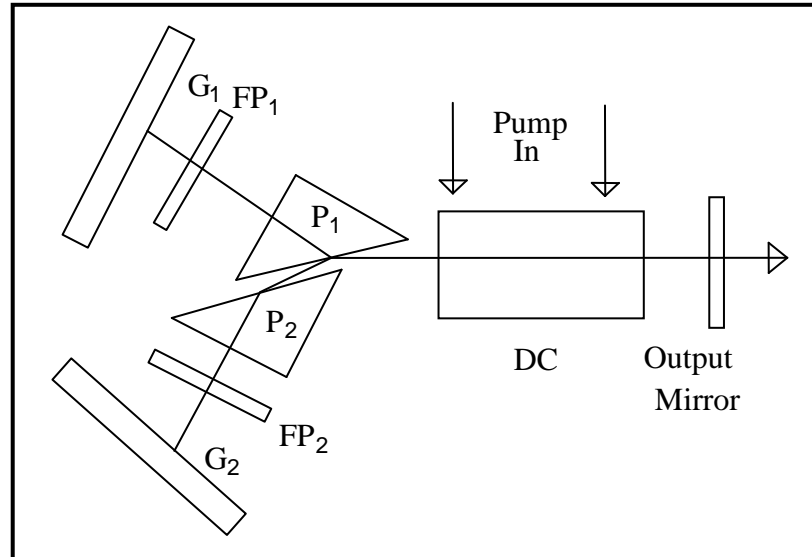


Figure 1.14: Prism beam expander based dual wavelength cavity [1.51], ( $G_1$ ,  $G_2$ : Gratings,  $P_1$ ,  $P_2$ : Prisms,  $FP_1$ ,  $FP_2$ : FP etalons, DC: Dye cell)

These two arms made sub-cavities for separate wavelengths, combined at the prism. Without intra-cavity etalons in the resonator and with the prisms oriented for  $88^\circ$  angles of incidence, a bandwidth of  $0.6 \text{ cm}^{-1}$  was achieved for each dye laser wavelength.

S. Chandra et.al. have studied two designs for independently tunable double frequency dye lasers with continuously variable power as shown in fig. 1.15 [1.52]. Each sub-cavity incorporates a movable dye cell and two tuning elements (gratings or mirrors) intercepting an expanded beam inside the laser cavity. The power ratio can be set at any desired value, regardless of relative positions of the two frequencies within the dye tuning curve. They have studied two designs for a double-frequency grazing angle dye laser with easily controlled and continuously variable power ratios. One design

## CHAPTER - 1

was based on a prism beam expander and another was using the grating beam expander in the cavity.

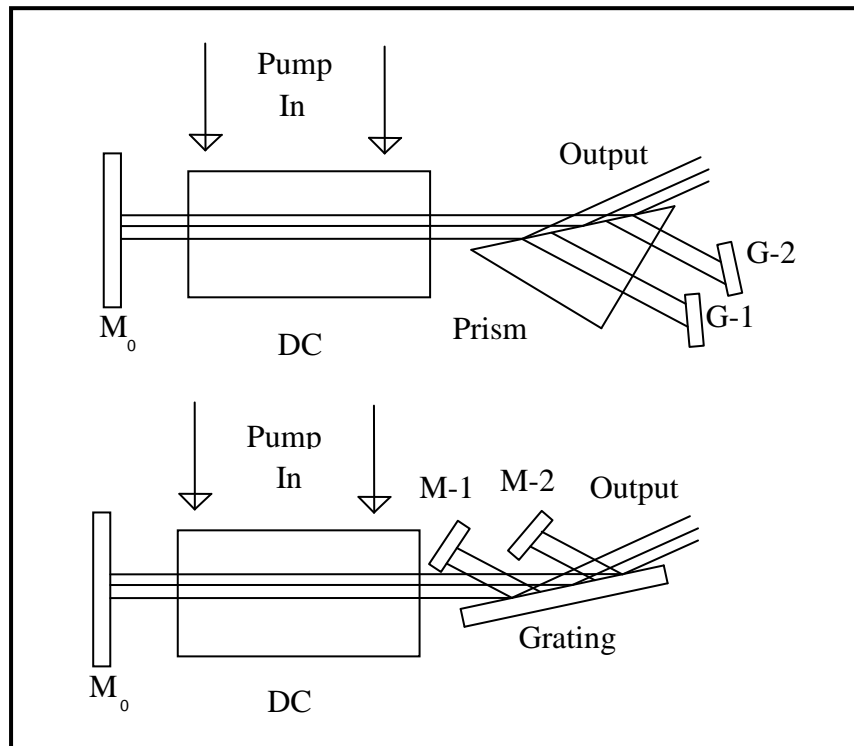
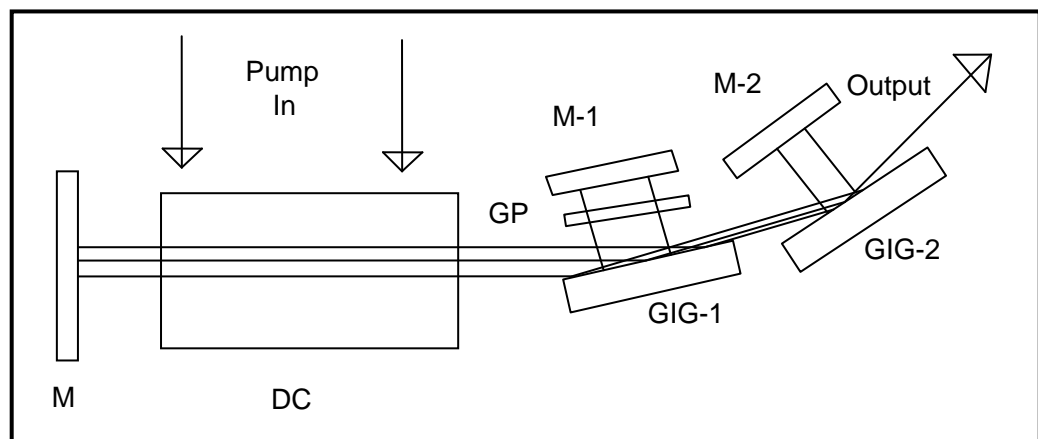


Figure 1.15: Prism and grating beam expander based variable output power cavities ( $M_0$ ,  $M-1$ ,  $M-2$ : Mirrors, DC: Dye cell, G-1, G-2: Gratings) [1.52]

Both designs use a fully reflecting mirror and a dye cuvette with a stirrer mounted on a translation stage. For the prism beam expander design, expanded, transmitted part of the beam was retro-reflected using two diffraction gratings aligned at the Littrow angle. These formed two sub-cavities for two separate frequencies, whereas the output was taken by reflecting part of the prism beam expander. In this geometry, prism (isosceles right angle set at  $89.3^\circ$ ) was utilized as a beam expander as well as beam combiner. In the second design, diffraction grating was utilized as the beam expander and combiner for both the frequencies. The first-order diffracted beam was intercepted by two mirrors, whereas the zeroth order beam was taken as the output laser beam. Both the configurations were pumped by a 250kW, 10ns pulse-duration nitrogen laser

operating at 15 Hz PRF with Rhodamine 6G and coumarin laser dyes were used for generating required wavelengths. Spectral widths were found to be around  $0.4 - 0.6 \text{ cm}^{-1}$  for the prism beam expander design while  $0.2-0.4 \text{ cm}^{-1}$  for the grating-based beam expander design.

L.G. Nair et.al. have used a compact dual grating cavity configuration for independently generating tunable, collinear dual-wavelength with variable linewidth dye laser as shown in fig. 1.16 [1.53]. Both gratings were aligned at a grazing incidence angle ( $\sim 87^\circ$ ) with their respective high reflectivity mirrors. The zeroth order beam was taken as the output dye laser beam.



*Figure 1.16: Grazing incidence grating based dual wavelength configuration, (M, M-1, M-2: Mirror, DC: Dye cell, GP: Glass plate, GIG-1&2: Grazing incidence gratings)*

A  $\text{N}_2$  laser with peak power of  $\sim 200\text{kW}$  and pulse width of  $4\text{ns}$  (FWHM) was used to pump the Rh 6G dye with a concentration of  $2.5\text{mM}$  for their experiment. Variable power was achieved using a tiltable glass plate (GP) in one of the sub-cavity.

S.G. Dinev et.al. have achieved independently tunable, dual-wavelength single-mode laser [1.54] by a short (cavity length  $\sim 4-5 \text{ cm}$ ) grazing incidence grating cavity with a pair of retro-reflectors. This Rh6G dye laser was pumped by a  $\text{N}_2$  laser. A single-mode spectrum of  $310 \pm 50 \text{ MHz}$  was achieved along with a tuning range of  $40 \text{ nm}$ .

## CHAPTER - 1

---

Kong et.al. have demonstrated a special dual-wavelength laser configuration which generated a dye laser beam having continuously variable polarization [1.55]. The grazing incidence prism beam expander with multilayer antireflection coating for the p-component while suppressing the s-component. They have coupled a Littrow mounted grating and the rotative wavelength selector. It was rotative with respect to the resonator optical axis as a single unit. By rotating the p-plane of the rotative wavelength selector, the polarization of the resonance beam was made continuously rotative. Knife-edge and a half mirror were used as a beam divider. The knife-edge beam divider method was proved to be better with no gain competition effect. They have used 5mM Rh 6G dye solution in ethanol, pumped by N<sub>2</sub> laser for their experiment. A tuning range of 570 – 615nm was achieved with a spectral linewidth of ~0.1nm.

Nenchev et.al. have used a reflecting Fizeau interferometer in their dual-wavelength Rh6G dye laser pumped by N<sub>2</sub> laser [1.56]. They have used the fact that the reflecting Fizeau wedge can ensure selective feedback once for a given wavelength and quasi-total reflection in another direction for all other wavelengths [1.56]. Fully independent tuning of two wavelengths with a linewidth of 0.02 nm was obtained using a single Fizeau wedge.

A simple dye laser system with a multilayer dielectric filter as a tuning element was demonstrated by Nomura [1.57]. J.P. Sage et.al. have characterized a dual-frequency oscillator-amplifier system, pumped by the second harmonic of a Nd: YAG laser [1.58]. They have used Glan polariser in the cavity as the polarization selector for the two frequency sub-cavities. The output of the oscillator was subsequently amplified using the amplifiers. Output energies up to 115 mJ with Rh 6G dye was achieved with

## CHAPTER - 1

---

pump energy of 250 mJ and linewidth was measured as 1.2pm at 589 nm with a 25 ns pump pulse duration.

Simultaneously operating and independently tunable, distributed feedback and grating tuned pulsed dye lasers following a Hansch type design was demonstrated by I. Golub [1.59]. Gain competition effects were shown to play an important role in a spatially modulated gain medium. The distributed feedback dye laser output exhibited sub-nanosecond pulses while the second laser had a few nano-second pulses. A CVL pumped Rh6G dye laser was used for this experiment.

A mode competition-free two-wavelength dye laser with power variability was demonstrated by Williams et.al. [1.60]. They have used a plane polarised pump laser which was splitted into two pump beams using birefringent beam splitter. A half-wave plate was used to vary the power in these splitted pump beams. This resulted in the two vertically displaced pumped dye gain regions; as a result, two separate gain channels were formed. One grating was used at the grazing angle for diffracting both the displaced intra-cavity beams at two different angles, which was retro-reflected using two mirrors. The linewidth of the output laser beams was 0.001 nm. This Rh6G dye of 5mM concentration in ethanol was pumped by N<sub>2</sub> laser for this system.

N.D. Hung et.al. have used a tunable alternate double wavelength single grating dye laser for DIAL experiments [1.18]. A rotatable parallel thick glass plate was used symmetrically to generate two separate beams at two orientations. A grating at grazing incidence was used to diffract both of these beams on to two separate mirrors. An alternate double wavelength laser beam was generated by rotating the glass plate in the desired direction. They have generated two wavelengths near 600 nm using a N<sub>2</sub> laser pumped Rh6G dye laser for SO<sub>2</sub> measurements.

## CHAPTER - 1

M. Schutz et.al. have developed a dual-wavelength dye laser in the UV range for simultaneous multi-element detection of lead (283.3 nm), manganese (279.5nm), nickel (232.0nm) and cadmium (228.8 nm) [1.61]. A grazing incidence grating with four prism beam expander was used, while two separate tuning mirrors intercepted the diffracted beam. The oscillator-amplifier system was utilized for power enhancement, whereas BBO crystal was used for the second harmonic generation in the UV range. Second harmonic of Nd: YAG laser was used to pump the Rh6G dye for this experiment.

Simultaneous dual-wavelength operation of a self-seeded dye laser was demonstrated by D.K. Ko [1.62]. Two grazing-incidence cavities and a standing wave cavity were used to generate an independently tunable, collinear, self-seeded dual-wavelength laser beam by a second harmonic Nd: YAG pumped Rh6G dye laser.

S. Jelvani et.al. have demonstrated a CVL pumped dual-wavelength dye laser using a Thomson prism as an intra-cavity beam combiner as shown in fig. 1.17 [1.63]. Two orthogonally polarised sub-cavities using a grazing incidence grating-tuning mirror pair, operating at different wavelengths was established with minimum gain competition effects.

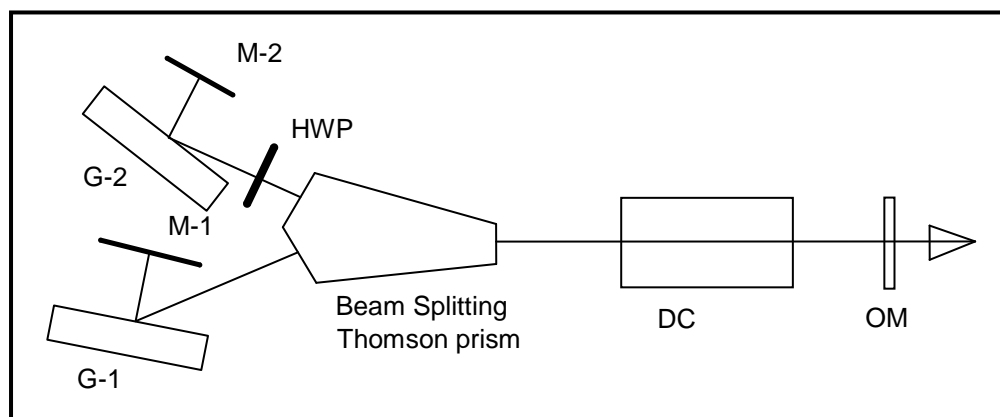


Figure 1.17: Cavity configuration used by S. Jelvani [1.63], (G-1, G-2: Gratings, M-1, M-2: Mirrors, OM: Output mirror, DC: Dye cell), HWP: Half wave plate

## CHAPTER - 1

---

They have shown that gain competition can be minimized for both the wavelengths if possessing mutually orthogonal polarizations. Jelvani had further theoretically analyzed, that gain competition is dependent on pump power, dye laser polarization, dye concentration, solvent viscosity, re-orientation rate of the dye molecules, etc. [1.64].

R. Khare et.al. [1.65] have obtained two coupled dye laser resonators to obtain independently tunable and collinear two-wavelengths having an adjustable delay between them. A single grating was used to provide dispersion and coupling [1.65]. The CVL beam of 510.6 nm and 578.2 nm was used to pump Rhodamine 6G and Sulforhodamine B dyes respectively. The collinear outputs could be tuned over 566 nm to 606 nm and 600 nm to 640 nm with individual bandwidths of  $0.24 \text{ cm}^{-1}$ . By changing the path-difference between the pump beam components, the delay between the two wavelengths could be varied from 21ns to 30 ns.

Recently, O.J. Zapata-Nava et.al. have demonstrated a simultaneous dual-wavelength dye laser using Littman-Metcalf and Littrow cavity configurations [1.66]. In their minimum cavity element design, the dual-wavelength operation was obtained by laser operation in two optical paths inside the cavity, one of which uses reflection in the circulating dye cell. Q-switched frequency-doubled Nd: YAG laser pumped Styryl14 laser operating in the 910 nm to 960 nm were used for the above demonstration.

M. Liu et.al. have generated tri-wavelengths in an organic solid-state laser from a holographic polymer-dispersed liquid crystal and a distributed feedback laser with a doped laser dye and a semiconducting polymer [1.67].

Tripple wavelength generation was demonstrated by R. Khare et.al. by utilizing a mutually coupled-cavity with different orders of the grating [1.68]. They could achieve the narrow line-width and co-linearity with the same linewidths. A Rh6G dye

laser, pumped by a CVL was operated at three wavelengths. Two of the three wavelengths can be independently tuned. Alternatively, two wavelengths with a fixed interval can be simultaneously tuned, keeping the third wavelength as constant.

Many researchers have studied diverse types of intra-cavity beam combined configurations. The cascaded grazing incidence grating cavities was selected for the intra-cavity multi-wavelength dye laser generation, due to its co-linearity, compactness, and operability at more than three wavelengths.

### **1.4.2. External Cavity Beam Combination:**

In this technique, beams are spatially overlapped external to the oscillator cavity using a suitable optical element. Resonator cavities of individual lasers may or may not have identical features. All the participating cavities may be different, generating different wavelengths, line width, power, beam aspect ratio, etc. In this scheme, every laser beam is generated using separate gain volumes; therefore it does not face any gain competition effects. Maintaining co-linearity and spatial overlap over a longer distance propagation may be tricky for this scheme. However, optimization of parameters for individual laser beams along with independent wide tunability is the salient feature of this technique. Further, amplification of individual laser beams can be done before combination to meet the desired power levels as per the applications.

Dispersive elements such as prism and grating and non-dispersive elements such as interference filters, splitters are used to combine the laser beam outside the oscillator cavity. Dispersive elements can combine closer wavelengths with relatively poor efficiency, whereas interference-filter based devices can combine widely separated wavelengths with improved efficiency. The interference filter based beam combiner i.e. thin-film multi-layer dielectric coated Fabry-Perot

beam combiner as the external cavity beam combiner for closely separated wavelengths.

### **1.5. Motivation:**

DIAL based environmental applications require collinear, tunable, multi-wavelength laser beam operating at wavelengths which are generally closer by less than 10 nm. Other applications namely frequency mixing, harmonic generation and commercial production of medical isotopes using atomic vapour laser isotope separation requires multi-wavelength collinear high power, narrowband tunable lasers. Dye laser meets these requirements; therefore many researchers have studied various aspects of multi-wavelength dye lasers for such applications [1.35-1.65]. However, spectral beam combination techniques for closely separated wavelengths are seldom reported in the literature. Hence, an elaborated study on spectral beam combination techniques for closely separated high power, pulsed dye laser became the motivation for this thesis work. Intra-cavity, as well as external cavity configurations along with the master oscillator power amplifier chain to boost the power levels, were planned to be studied during this research work.

Dual and triple wavelength generation using a dye laser is reported by many authors, however, no researcher had reported four and five wavelength generation using intra-cavity beam combined dye lasers. The selection of combining element and beam combination approach became necessary to select a technique that has the capability of closely separated, narrowband tunable, composite laser beam generation.

Multi-layer thin-film dielectric coated interference filter based beam combiner such as edge filter; bandpass filter is generally used for the combination of high power dye laser beams in an external cavity beam combination approach. However, these devices are not efficient for spectral beam combination of high power wavelengths

## CHAPTER - 1

---

separated by less than 10 nm. Therefore, the development of a multi-layer thin film coated Fabry-Perot filter was taken up for studying the spectral beam combination of high power laser beams of closely separated wavelengths.

A MOPA chain is used to enhance the power levels of the good quality signal beam generated by the dye laser oscillator. Spectral beam combination of closer wavelengths separated by less than 10 nm can be done using broadband beam splitters as no other suitable and efficient device is available for this purpose. This approach suffers huge losses in the beam combination process. The combination of closely separated wavelength with minimal combination losses motivated us to work towards the utilization of thin-film technology for combining the closely separated wavelengths. Therefore, the study of an alternate approach for efficient high power composite laser beam generation in an oscillator-amplifier system became one of the important objectives during this work.

CVL pumped liquid phase dye lasers were chosen for these studies. High power CVL system includes setting up an optimized MOPA configuration with minimum thermal lens was required to be studied for generating high pump power levels for these experiments. Dye chromophores in the liquid phase is a versatile gain medium suited for the intended applications. Therefore, the exploration of tailoring the dye gain medium by various methods was necessary to widen the application potential of these studies on spectral beam combined dye lasers. Because of the enormous applications, studies on spectral beam combination techniques for less than 10 nm wavelength separated, high power pulsed narrowband dye lasers were taken up, which is described in the subsequent six chapters of this thesis.

### **1.6. The Organization of The thesis:**

The objective of this thesis work was to study intra-cavity and external cavity beam combined multi-wavelength dye laser and its associated technologies. The entire study is described in seven chapters. The first chapter deals with the introduction and literature survey of the techniques for multi-wavelength laser generation specific to the dye lasers. Studies related to the high power pump laser system are summarised in the second chapter. Thermal lens measurement, compensation techniques, and MOPA configuration are the main components of the study in this chapter. Studies related to dye cell, dye solvent, dye mixtures, the effect of pH on photo-physical properties of laser dyes, measurement of thermo-optic coefficient of solvents are summarized in the third chapter. The fourth chapter encompasses the intra-cavity beam combined multi-wavelength dye laser cavities. Tuning characteristics of cascaded grazing incidence grating (CGIG) and hybrid cascaded grazing incidence grating (HCGIG) cavities for sustained four wavelength operation zones are the main features covered in chapter-4. Next chapter-5 contains studies about high power generation using an external cavity beam combination approach. Studies on the beam combination after amplification and co-amplification after combination are the key features discussed in this chapter. Designs, fabrication, characterization of multilayer dielectric coated laser beam combiner, along with high power dye laser implementation are listed in the sixth chapter. The seventh chapter concludes the entire research work by summarising the key findings and proposing the future directions of the research work.

## CHAPTER - 1

---

# Chapter: 2

## High Power Copper Vapour Laser System

---

### 2.1. Introduction:

Copper Vapour Laser (CVL) is well known for its high power, high repetition rate, and pulsed laser source in the visible range (510 & 578 nm) of the electromagnetic spectrum [2.1, 2.2]. It has a wide range of commercial applications in micromachining, high-speed photography; research applications in pumping dye lasers for spectroscopy; bio-medical applications like dermatology oncology, angioplasty surgery, and photodynamic therapy. Other applications namely seas and oceans, marine and air force navigation, atmospheric probing, and synthesis of multi-wall nanotubes [2.1-2.7] have driven the research for continuous improvement in the CVL systems. UV light (generated by the second harmonic of CVL laser beam) is used in writing fiber Bragg grating and dicing of sapphire, gallium nitride and micro LED devices, etc. [2.8, 2.9]. A combination of attributes namely high average output power, high pulse repetition rate, beam quality available from CVL and its improved variants are unmatched to even solid-state lasers [2.10]. These laser properties are unique in the visible spectrum around 500 to 600 nm, which can be extended further by tunable lasers using dye and dye mixture pumped by CVLs. These features keep the demand high and growing for this laser even after decades of its discovery [2.11]. This special laser has been studied for pumping dye laser systems intended for spectral beam combination applications. One of the objectives of this thesis work was to study spectral beam combination techniques for high power, pulsed dye laser beams and CVL was chosen due to its power scaling capabilities [2.12]. CVL and its master oscillator power amplifier (MOPA) configuration studies were taken up for generating

## CHAPTER - 2

---

a high average power pump laser source. An indigenously developed CVL operating at 9 kHz pulse repetition rate, excited by an all-solid-state based pulse power supply was used for the present study and is briefly described in this chapter. The resonator configuration for this system was optimized to obtain a reasonably good quality beam. Multilayer thin-film interference filter-based optical designs were analyzed for single wavelength emission from the CVL system.

MOPA chains are used to boost the average power of a laser beam [2.1, 2.2, 2.13]. A laser beam of desired beam quality is generated from the oscillator and subsequently, the power is enhanced using amplifier modules in the MOPA chain. Amplification characteristics of an amplifier at various input powers were experimentally determined. Percentage Fresnel and reflection losses were higher at higher incident power. This prevented the maximum power addition from the subsequent amplifiers in the longer CVL MOPA chain. Several possible MOPA chain configurations were analyzed theoretically to reduce such losses to extract maximum output power from the MOPA chain.

CVLs are operated at higher discharge tube temperatures of  $\sim 1600$  °C [2.1, 2.2, and 2.11] and result in the lensing effect due to gas and window heating [2.11, 2.14]. The thermal lensing effect present in each amplifier reduces the beam diameter due to the resultant converging effect [2.14]. The thermal lens changes the beam diameter in the CVL MOPA chain, which reduces the power extraction capability from the amplifier modules in the MOPA chain. It is due to reduced overlap between extracting beam diameter and the available gain diameter in the amplifier. The thermal lens focal length of an amplifier unit in the MOPA chain was experimentally determined by using the oscillator beam as the probe beam. Effective focal length was calculated using ray optics based novel technique. An equivalent lensing model based on ray

tracing matrix manipulations was established to estimate the beam diameter reduction at every amplifier stage in an eight module MOPA chain. Compensation techniques are proposed to minimize the thermal lensing effect in the individual laser system as well as for the eight modules MOPA chain. An experimental set up of a six-module MOPA chain with optimized parameters for pumping the dye laser system has been utilized to study the spectral beam combination at higher power levels. All these aspects pertaining to high power CVL systems are described in the subsequent sections of this chapter.

### **2.2. Indigenously Developed Copper Vapour Laser System:**

The CVL system is a self-discharge heated, pulsed laser system [2.1, 2.2 and 2.11]. Electrical discharge across a ceramic tube is applied to raise the temperature of the discharge tube. Neon as a buffer gas is used to assist in striking the discharge during cold conditions. Pure copper pellets are placed at 8 to 10 locations in the discharge tube (alumina). The temperature of the tube is raised to approximately 1600 degrees Celsius using the electrical pulse energy [2.1, 2.2]. Copper evaporated in the vapor form due to this heating. Atoms excite to higher energy level using electrical energy in the discharge. It is a three-level laser system with an upper energy level having a lifetime of around 500 ns, whereas a lower energy level is a meta-stable with a lifetime of milliseconds. Therefore, it is an inherently pulsed system due to a higher lifetime of the lower laser level than that of the upper laser level [2.1, 2.2]. The  $[\text{Ar}]3d^{10}4p^1$  ( $^2P_{3/2}$  and  $^2P_{1/2}$ ) is the upper laser level of the atoms in Cu vapor, whereas  $[\text{Ar}]3d^94p^2$  ( $^2D_{3/2}$  and  $^2D_{5/2}$ ) is the lower laser level. These levels have the degeneracy, defined by their total angular momentum values. The upper laser level is the resonance level of the copper atom. Radiation trapping helps to maintain the ground state population to achieve excitation and population inversion.

## CHAPTER - 2

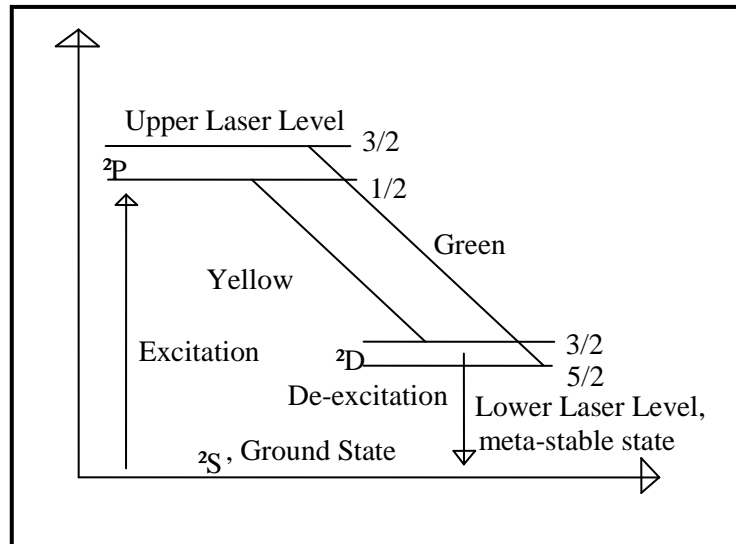


Figure 2.1: Energy level diagram of the CVL system

The energy level diagram of the copper atom is shown in fig. 2.1. A certain ground state copper density is required to be maintained to achieve the radiation trapping. This is achieved by maintaining a partial pressure of around 0.1 torr. The partial pressure of copper atoms is maintained by regulating the required temperature of 1550 to 1650 degrees Celsius. Laser action takes place following the allowed transitions. The lower laser level is the metastable state, which is not radiatively connected with the ground state, due to the parity selection rule violation. Therefore, population inversion is maintained for a very short time using an electrical excitation pulse having a very sharp rise time in the range of 80 to 100 ns. The migration of the copper atoms and collisions with the discharge tube wall helps to de-excite the meta-stable level. This collisional decay is the main mechanism for depopulating the lower level and super elastic collision of copper atoms with the electron is another important mechanism.

The time taken for the de-excitation mechanism limits the pulse repetition rate of the CVL system. Therefore, a higher repetition rate operation is supported in a small diameter discharge tube which results in the lower gain volume and hence the lower

## CHAPTER - 2

average output power. CVL is a volumetric system, where higher volume results in higher output power. Mixing special gases and their mixtures along with buffer gas in the discharge assists in tailoring the relaxing mechanism. The faster inter-pulse plasma relaxation facilitates the enhanced pulse repetition rate operation. These improvements lead to an efficient and higher repetition rate variant of the elemental CVL with large bore diameter system. HyBrID and kinetically enhanced CVL are the improved variants, which utilizes  $H_2$  and  $HCl$  gas mixture along with neon buffer gas [2.1, 2.2 2.15]. The elemental CVL system has been studied as per the available technology and due to simple and rugged operation capability at moderately high pulse repetition rate operation of 9 kHz.

An indigenously developed elemental CVL system operating at a 9 kHz repetition rate was used for the present study. The average output power of the individual CVL system was measured to be around 40 W in the plane-plane oscillator configuration.

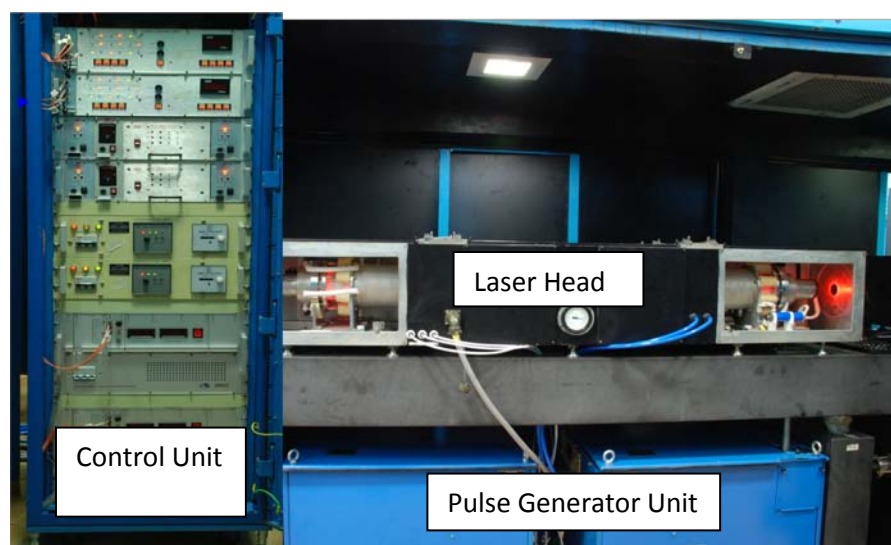


*Figure 2.2: Picture of the indigenous CVL: 40 system used for the studies*

A picture of an individual CVL including its sub-systems is shown in fig. 2.2. This system is referred to as the CVL-40 system in the rest of this chapter, wherever

required. This system comprised of three main sub-systems, namely the laser head (LH), pulse generation unit (PGU) and the control unit.

### **2.2.1. The Laser Head:**

The laser head is the main sub-system, which emits the laser radiation. It consists of an insulated alumina tube in-housed in a glass tube, pair of electrodes for applying the electrical discharge, a water-cooled SS outer jacket providing the desired cooling, the essential water and regulated buffer gas system fitted in an encasement. AR coated Quartz windows are used at the two ends of the electrodes for laser radiation emission, which provides the vacuum boundary. Buffer gas pressure was maintained at 40-50 mbar with neon gas purging at a flow rate of around 1 liter-atmosphere per hour. This helps in removing the impurities from the discharge, generated during the hot operation. A gas handling unit and vacuum handling unit having the solenoid and needle valve were used for regulating the neon gas flow rate through the laser head discharge tube. Alumina tube discharge length of 1800 mm with an inner diameter of 38 mm and the outer diameter of 45 mm was used and the copper pellets of nearly 50-60 grams were distributed at equidistant locations in this discharge tube. The pair of electrodes with a bore diameter of 55 mm and length 200 mm was attached to both ends of the discharge tube. A water-cooled, SS, double-walled jacket housed the discharge tube, in which electrodes are attached to strike the electrical discharge.

### **2.2.2. Pulse Generation Unit:**

A sharp rise time electrical pulse is generated using a solid-state switch based pulse forming network. Direct current power from SMPS of 450V, 20A was fed to the pulse formation circuit. The voltage across the storage capacitor was

doubled using the resonant charging circuit. Four insulated gate bipolar transistor (IGBT) switches were used to convert dc power to pulse electrical signal. This electrical pulse voltage further enhanced using a pulse transformer of the turn ratio 1:32. The rise time of the electrical pulse after the pulse transformer was round 1.5  $\mu$ s. Three magnetic pulse compression (MPC) stages were used to reduce the rise time from 1.5  $\mu$ s to less than 100 ns. This circuit is submerged in the transformer oil-cooled tank. Transfer oil, in turn, was cooled using water in the heat exchanger. This entire unit was termed as a pulse generator unit (PGU). The electrical pulse was transmitted to the laser head electrode using co-axial cables. The electrical discharge was applied to the laser head which transfer this electrical power to the laser head using a peaking capacitor connected across the laser head.

### **2.2.3. Control Unit:**

Control unit comprises of switch-mode power supply (SMPS), low voltage power supplies, controlling and interfacing unit. All these components were housed in a 19-inch rack. SMPS generates the dc voltage by using three-phase electrical input power. Low voltage power supplies were used for operating the solenoids of the gas/vacuum handling units and timer, trigger card in the pulse power supply. The laser control unit interfaces the interlock and status signals from the PGU. Status of the cooling water flow and the interlocks for tripping the power supply for the safe operation were implemented using this laser control unit. All these sub-systems were connected and the complete assembly was tested for its design values. Several such modules were cascaded together to configure in the MOPA chain to generate desired power levels. The

## CHAPTER - 2

characteristics of the resonator configurations are described in the subsequent sub-sections.

### 2.3. Characteristics of CVL Oscillator Configurations:

Divergence of the CVL beam plays a vital role when propagated to longer distances [2.1, 2.2]. Divergence is generally controlled by resonator configurations [2.16-2.19]. The radius of curvature of mirrors, distances between mirrors, resonator geometry and the number of round-trips govern the output laser parameters. The beam divergence of a laser beam provides the information about the increase in beam diameter with travel distance. It becomes costly, cumbersome and complex to handle the large size beams. Further, it becomes difficult to focus high divergence beam to smaller spot sizes. The focal spot requirement is very important to pump the dye laser efficiently. Therefore because of the advantages of the low divergence beam, a suitable resonator configuration was studied to generate the low divergence laser beam using a CVL system.

#### 2.3.1. Resonator Configuration:

Indigenously developed 9 kHz laser was used to perform the resonator studies. A resonator consisting of a high reflectivity plane mirror and a normal glass window as an output coupler was aligned parallel to each other across the CVL laser head [2.1]. The schematic of this configuration is shown in fig. 2.3.

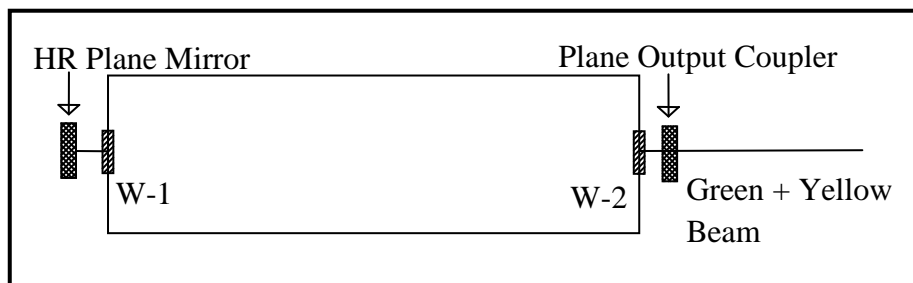


Figure 2.3: Schematic of the plane-plane configuration

## CHAPTER - 2

---

Parameters of the laser beam emitted from this resonator configuration were measured. The properties of the laser beam generated using a plane-parallel resonator is tabulated in table-2.1.

*Table 2.1: Characteristics of 9 kHz CVL in Plane-Plane resonator*

Sr. No.	Characteristic parameter	Measured values
1	Output Average power	40 W
2	Laser beam diameter	38 mm
2	Divergence	2 mrad
3	Green to Yellow ratio	3:2
4	Pulse width (FWHM)	45 ns
5	Rise time	7-10 ns
6	Wall plug efficiency	0.65 %
7	Type of Pulsed Power Supply	IGBT based Pulse Power Supply

It was observed that the divergence of the laser beam was around 2 mrad. This was not sufficient; therefore unstable resonator configuration was setup. An off-axis positive branch unstable resonator in confocal geometry was used to reduce the beam divergence. A concave mirror of focal length 2500 mm, diameter ~ 75mm and a convex mirror of various focal lengths with of diameter 8 mm were utilized to form the resonator cavity in confocal geometry. Convex mirror of small diameter assured minimum beam cutting in the off-axis configuration. The resonator confocal length was approximately 2400 mm. Magnification of the unstable resonator plays a significant role in reducing the divergence of the output laser beam [2.16-2.20]. The beam divergence studies have been carried out at various resonator magnifications. To vary the resonator magnification, the focal length of the concave mirror was kept fixed at  $f = 2500$  mm and the focal length of the convex mirror was varied from 25 mm to 44 mm. The schematic of the unstable resonator configuration is shown in fig. 2.4.

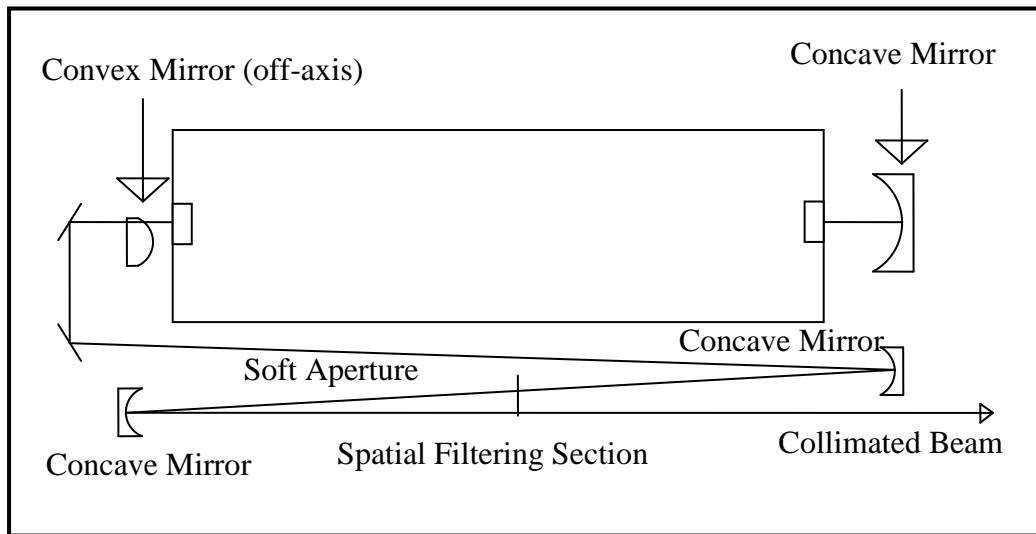


Figure 2.4: Schematic of the unstable resonator configuration

These experiments were performed at a neon gas pressure of 45 mbar and input electrical power of approximately 5.4 kW. A spatial filter (SF) was used after the optimization of the resonator magnification to further improve the beam quality. An external spatial filter was incorporated using two concave mirrors of focal length 1300 mm each to filter the higher divergence components. This mirror pair aligned in the confocal configuration and an aperture of 700 microns was used to filter out the higher divergence component of the laser beam.

### 2.3.2. Laser Beam Divergence Measurement:

The divergence was measured by aperture method and  $M^2$  meter (Spirikon make). It was measured using power in bucket method. The output laser beam was focused using a plano-convex lens of the focal length of 995 mm. The beam diameter of the focal spot was scanned by a 50-micron diameter aperture followed by photo-diode across vertical direction (Y-axis). It was done after centering the aperture with the focal spot in the horizontal direction (X-axis).

## CHAPTER - 2

Aperture was fixed on a X-Y translation stage. Laser pulse was monitored by using large area photodiode fixed behind the aperture. A digital storage oscilloscope (DSO) was used to record the photodiode signal. The area under the captured pulse was estimated using the integration function of the DSO. The experimental setup is as shown in fig. 2.5.

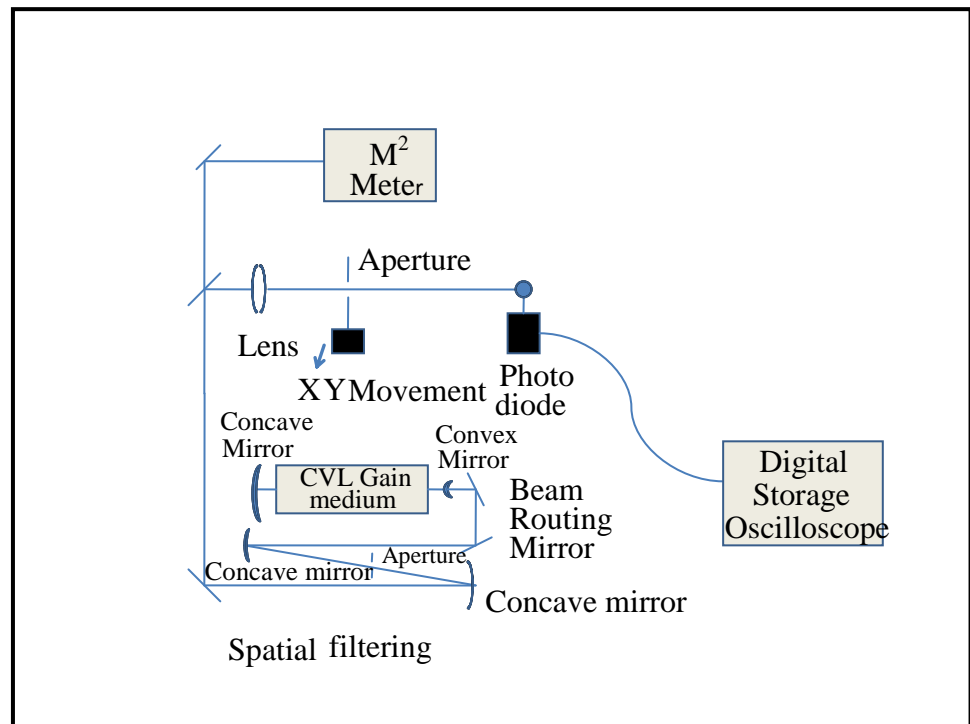


*Figure 2.5: Schematic of the divergence measurement technique*

The area under the curve resulted in pulse energy content in the pulse, which could pass through the aperture. This energy is proportional to the intensity transmitted through the aperture. The data is plotted for intensity variation versus aperture movement in microns as shown in fig. 2.6.

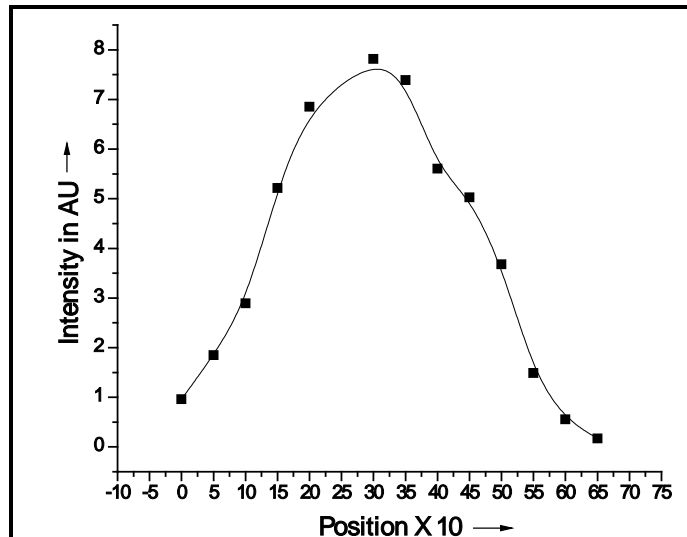


Figure 2.6: Focal spot estimation for divergence measurement

The focal spot size was calculated using a full-width half maximum (FWHM) of this fitted curve. The divergence of the beam was estimated by the relation  $f \times \theta = X$ , where  $f$ =focal length,  $\theta$  = divergence and  $X$  is the focal spot diameter. The beam divergence was also measured with an  $M^2$  meter, which was found to be matching with this aperture method.

**2.3.3. Results and Discussions:**

Parametric studies for different configurations were carried out. The effect of increasing magnification on the divergence is shown in fig. 2.7.

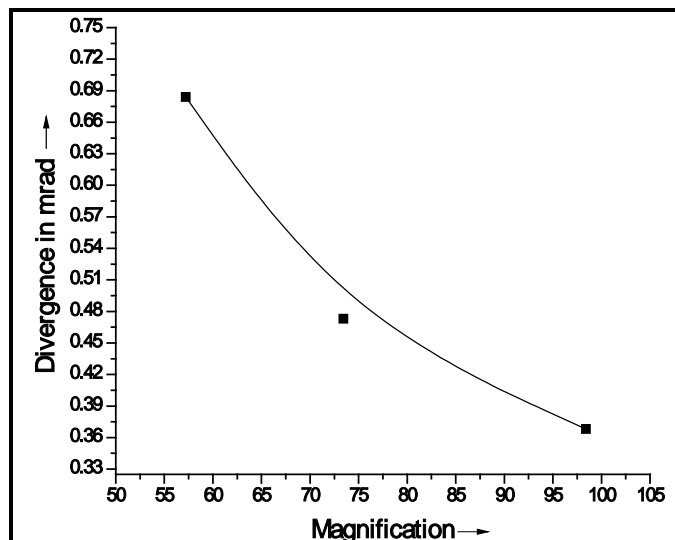


Figure 2.7: Variation of divergence with magnification

## CHAPTER - 2

---

It was observed that divergence decreased from 0.69 mrad to around 0.36 mrad for the increased magnification from 57.2 to 98.40. The effect of magnification on beam divergence was measured in different configuration and results are tabulated in table-2.2.

*Table 2.2: Divergence measurements with various resonator magnification*

Magnification	Divergence with aperture method	Divergence with aperture method after SF 700 $\mu\text{m}$	Divergence with $M^2$ Meter	Divergence with $M^2$ Meter after SF 700 $\mu\text{m}$
57.20	0.684 mrad		0.687 mrad	0.5884 mrad
73.43	0.473 mrad	0.368 mrad	0.4785 mrad	0.334 mrad
98.40	0.368 mrad	0.315 mrad	0.358 mrad	0.252 mrad

It was found that, as the magnification is increased, both average power and divergence decreased. It was because a good quality beam is obtained at the cost of power loss. The optimum performance was obtained to get a laser beam having a divergence of around 0.4 mrad. The magnification of 73 or higher was found suitable for the dye laser pumping as well as long-distance transportation.

Neon gas pressure was varied as a parameter and its effect on output power was measured. The variation of output power with Ne gas pressure is plotted in fig. 2.8. Optimum buffer gas pressure for maximum power was found to be around 45 mbar. The output power was measured at input electrical power of 5.3 kW for all buffer gas pressures. The optimized output power of around 30W was achieved in an off-axis unstable resonator with magnification 66.

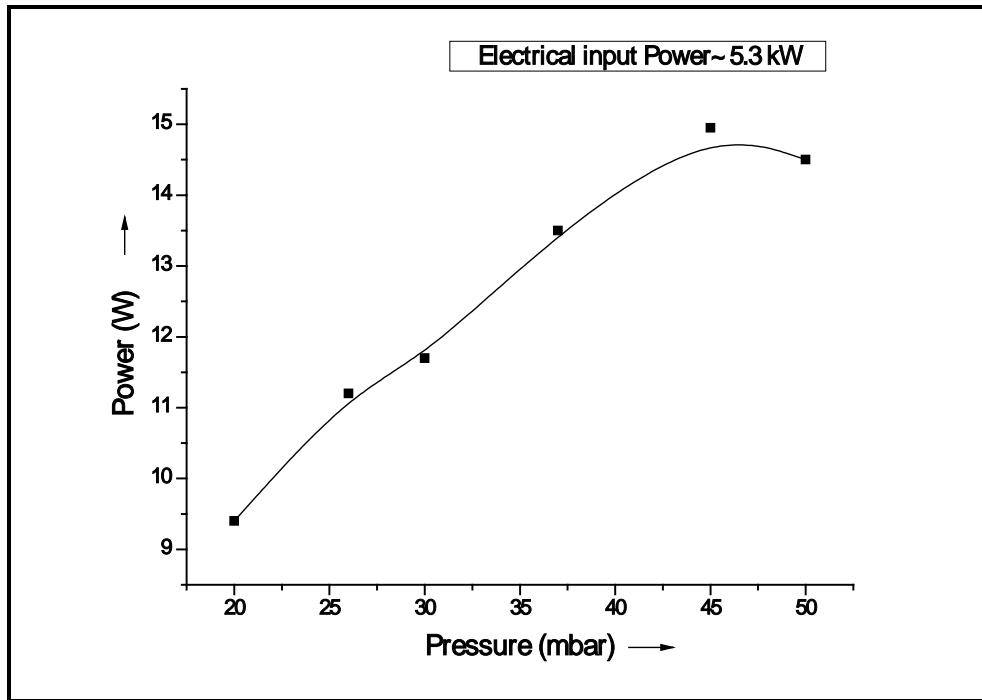


Figure 2.8: Effect of Neon gas pressure on optical output power

#### 2.4. Emission Wavelength of Copper Vapour Laser Oscillator:

CVL emits two wavelengths i.e. 510.6 nm (green) and 578.2 nm (yellow). The transition between  ${}^2P_{3/2}$  to  ${}^2D_{5/2}$  emits in the green region i.e. 510.6 nm, whereas yellow wavelength emission is obtained due to the transition between  ${}^2P_{1/2}$  to  ${}^2D_{3/2}$  levels. These wavelengths are emitted in a certain ratio, which is governed by discharge tube temperature [2.1, 2.2].

We have measured the green to yellow power ratio at the optimum operating conditions. The temperature of the discharge tube is directly proportional to the input electrical power. Therefore, the effect of input electrical power on the green to yellow ratio was established. Single wavelength is required for specific medical applications like treatment of port wine stains and photo-dynamic therapy etc. Therefore, few optical configurations are proposed and multilayer thin film coating designs to realize them, were studied. These emission wavelength characteristics and designs for single wavelength emission are described in the following section.

**2.4.1. Measurement of green to yellow power ratio:**

CVL:40 system was set up in a positive branch unstable resonator (PBUR) configuration with a magnification of 66. System was operated with minimum input power to obtain the laser beam. The output laser beam was splitted into green and yellow beams using a dichroic beam splitter. Ophir make (Model: FL 150) thermopile based power meter was used to measure the power of green and yellow beams. Subsequently, electrical power was varied from minimum lasing conditions to maximum operational limits. The schematic of the experimental setup for the measurement of green to yellow power ratio is shown in fig. 2.9.

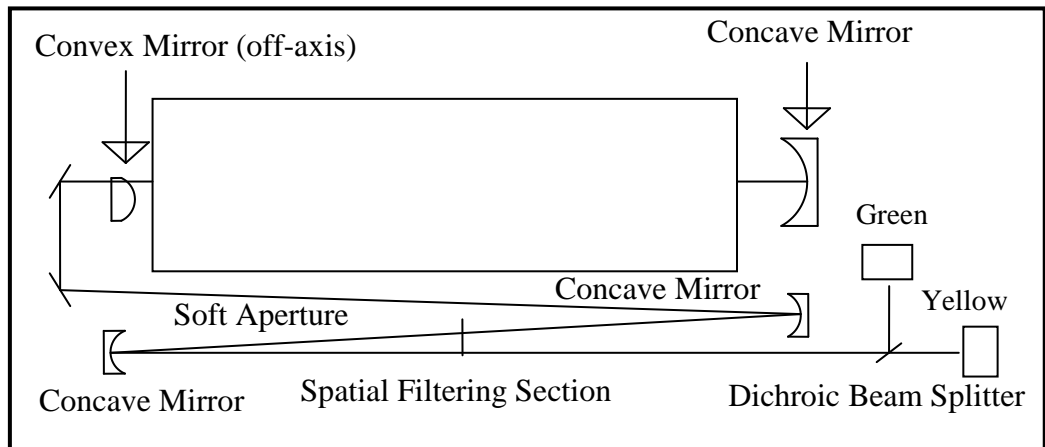


*Figure 2.9: Schematic of the experimental setup used for the green to yellow ratio measurement*

The green to yellow ratio was measured by taking the ratio of green and yellow average power measured at various electrical input power levels.

The measurement of green to yellow component of the laser beam was carried out using the experimental set up as shown in fig. 2.9. The green to yellow ratio with increasing electrical input is plotted in fig. 2.10. Green to yellow power ratio decreased from 3.1 to 1.1, as a result of increased input electrical power from 4.4 kW to 5.3kW.

## CHAPTER - 2

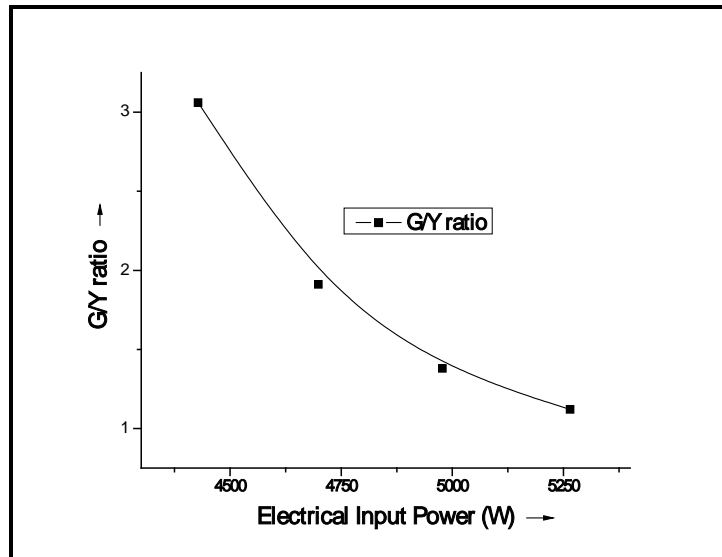


Figure 2.10: Green to Yellow ratio of a CVL oscillator

The variation of green power, yellow power and total power with the change of electrical input power is shown in fig 2.11.

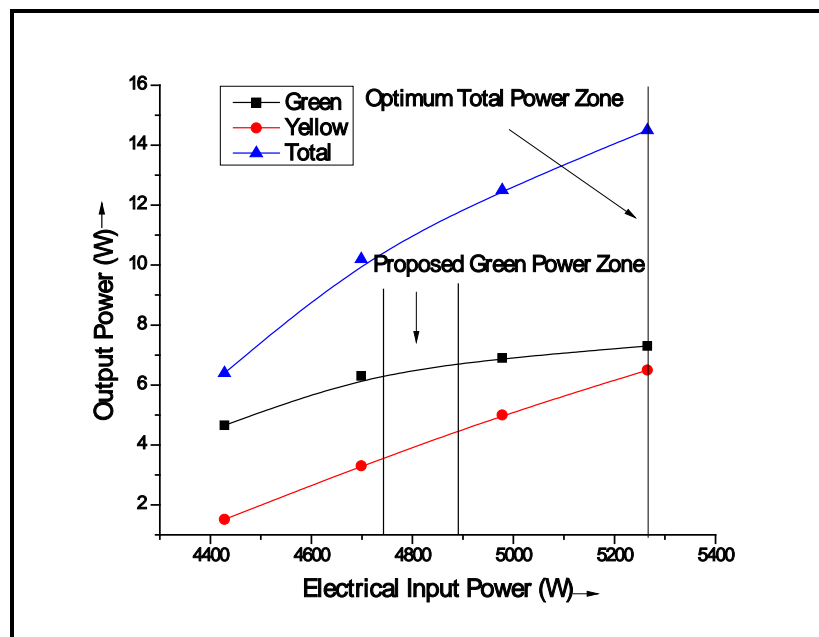


Figure 2.11: Variation of output power with electrical input power

The average power of the green beam increased from 4.65 W to 7.3 W and efficiency increased from 0.105 % to 0.138%, when electrical input power increased from 4.4 kW to 5.3 kW respectively. It was observed that efficiency of CVL increased only 2.98 % whereas input electrical power increased by

12%, which shows the saturation in the efficiency. An increase in yellow power from 1.52 W to 6.5 W and efficiency from 0.034% to 0.123% was observed when electrical input was changed from 4.7kW to 5.3 kW. Total optical power increased with increased electrical input, in which the dominance of green was observed at lower input electrical power whereas yellow dominates at the higher input electrical power. These observations lead to the conclusion that for efficient green beam emission, CVL should be operated at the lower input electrical power levels. Hence, the middle of the operating input electrical power range is optimum for the green beam. However, at higher input electrical power, net green power is higher without an increase in the efficiency. If we further increase the input electrical power then laser emission is quenched due to the thermal runaway. Lower energy levels get thermally populated at higher temperatures, therefore maintaining the population inversion becomes difficult and hence lasing quenches.

### **2.4.2. Optical Designs for Single Wavelength Emission:**

Two optical designs have been proposed to make this dual-wavelength CVL system to single wavelength system. These designs are proposed to be realized by following the thin-film design obtained by theoretical calculations. Both designs are described in this section.

#### **2.4.2.1. Multilayer Thin-Film Design of Single Wavelength:**

It is analyzed based on optical designs for plane-plane CVL resonator configuration. Generally, plane-plane resonator consists of one high reflectivity (HR) plane mirror ( $R \sim 99\%$  for both the wavelengths) and one partially transmitting plane mirror ( $R \sim 5\%$  for both the wavelengths) as an output coupler (OC), aligned parallel to each other across the gain medium

## CHAPTER - 2

[2.1]. An arrangement with modified roles of each mirror was investigated. In this arrangement, a pair of high reflectivity mirrors is designed in such a way that the first mirror act as HR mirror for yellow wavelength whereas OC for the green wavelength and vice-versa for the second mirror [2.21]. This modified plane-plane (P-P) resonator can generate a green laser beam from one side of the CVL laser and yellow beam from another side as shown in fig. 2.12. These designs convert a single side, dual-wavelength generating laser system into both side single wavelength operation. This arrangement will be useful for efficient generation of either green or yellow beam by operating the laser with suitable input electrical powers depending on the optimum green or yellow output power requirement.

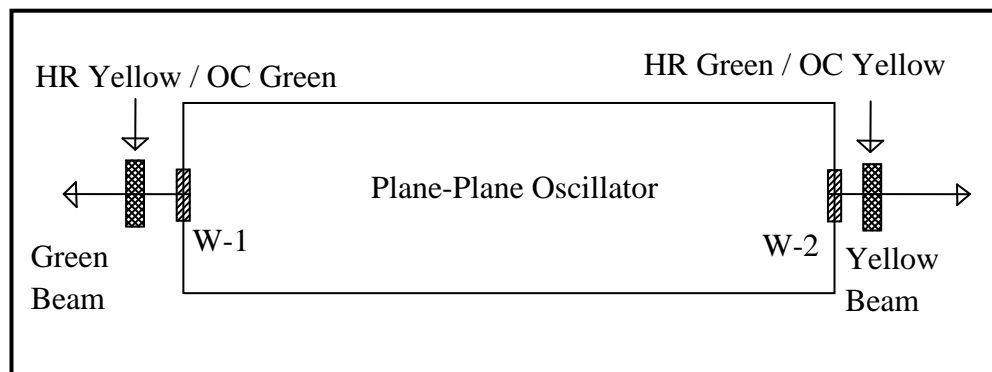


*Figure 2.12: Schematic of a plane plane resonator for single wavelength emission*

### **a. Multilayer Dielectric Thin Film Coating Designs for the Specialized Mirrors:**

Transmission and reflection properties of mirrors can be tailored to exhibit desired properties by suitably designing multilayer dielectric coatings. The design of special mirrors using the interference filter (low pass and high pass) based technique to function as per the application [2.37, 2.38].  $\text{TiO}_2$  and  $\text{SiO}_2$  were taken as high refractive index and low refractive index material respectively. Both the devices were designed for normal incidence angle. Green transmitting (emission) mirror functions as

## CHAPTER - 2

OC for green wavelength and green reflecting mirror as an OC for yellow wavelength. Design using a stack of  $((0.5L H 0.5L) ^ 7)$  with a reference wavelength of 608 nm optimized by tailoring first and last layer thickness of the stack as described in the table-2.3.

*Table 2.3: Layer thickness pattern of green emission mirror*

Layer No.	1	2	3	4	5	6	7	8	9
Material	SiO <sub>2</sub>	TiO <sub>2</sub>	SiO <sub>2</sub>						
Thickness	89.33	63.99	104.08	63.99	104.08	63.99	104.08	63.99	104.08
Layer No.	10	11	12	13	14	15			
Material	TiO <sub>2</sub>	SiO <sub>2</sub>	TiO <sub>2</sub>	SiO <sub>2</sub>	TiO <sub>2</sub>	SiO <sub>2</sub>			
Thickness	104.08	104.08	63.99	104.08	63.99	0.00			

Output coupler for yellow wavelength and high reflectivity for green wavelength was achieved using the design described in table-2.4. Yellow transmitting (emission) mirror was designed using a stack  $(0.5H L 0.5H) ^ 8)$  with a reference wavelength of 472 nm.

*Table 2.4: Layer thickness pattern of yellow emission mirror*

Layer No.	1	2	3	4	5	6	7	8	9
Material	TiO <sub>2</sub>	SiO <sub>2</sub>	TiO <sub>2</sub>						
Thickness	23.68	80.42	47.36	80.42	47.36	80.42	47.36	80.42	47.36
Layer No.	10	11	12	13	14	15	16	17	
Material	SiO <sub>2</sub>	TiO <sub>2</sub>	SiO <sub>2</sub>	TiO <sub>2</sub>	SiO <sub>2</sub>	TiO <sub>2</sub>	SiO <sub>2</sub>	SiO <sub>2</sub>	
Thickness	80.42	47.36	80.42	47.36	80.42	47.36	80.42	23.68	

### **b. Reflectance Spectrum of the Specialized Mirrors:**

Spectral characteristics of both the type of filtering mirror device designs are shown in fig. 2.13 and fig. 2.14. Reflectance for average polarization ( $R_{avg}$ ) of the green emission was achieved to be around 5.29% (fig. 2.13) by this design, which is required for output coupling. Reflectance for the yellow wavelength was observed to be 99.62% as a high reflective mirror. This coating design will function as OC for green wavelength and HR mirror for the yellow wavelength.

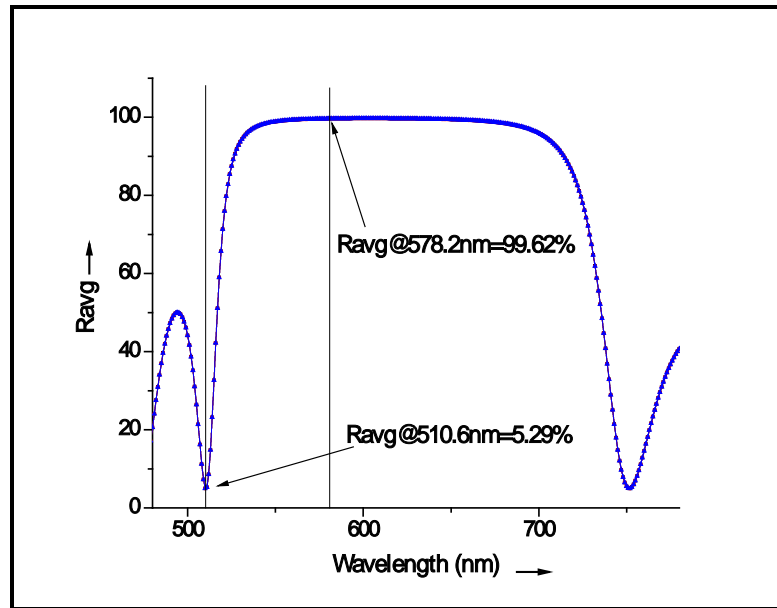


Figure 2.13: Reflectance curve of green emission mirror achieved by the design

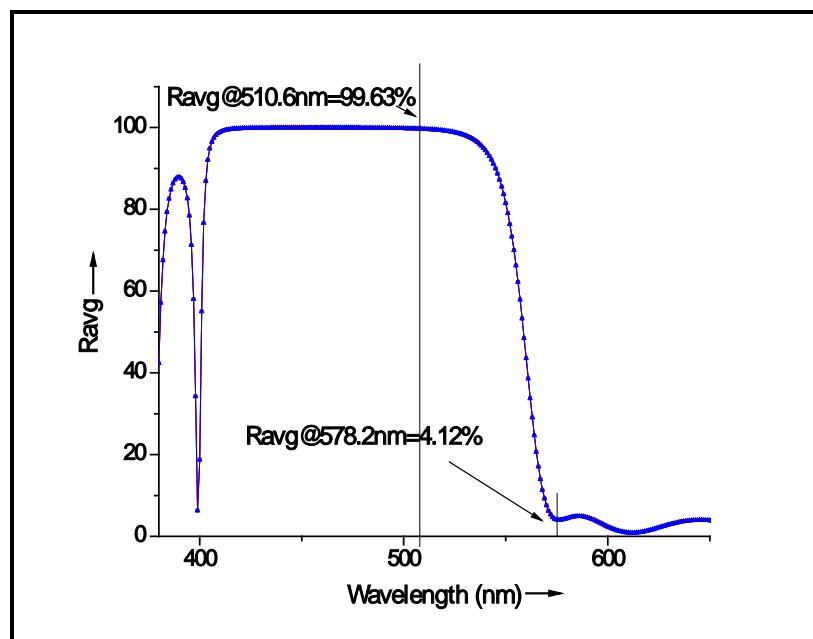


Figure 2.14: Reflectance curve of yellow emission mirror design

Figure 2.14 depicts the spectral performance of the yellow emission mirror coating design.  $R_{avg}$  for yellow wavelength was achieved to be 4.12% i.e. partially transmitting which acts as the output coupler. Green wavelength was found to be having a very high reflectivity of around 99.63% i.e. HR mirror for

green. A P-P resonator configured using this mirror is expected to behave as both side single wavelength emissions.

### **2.4.2.2. Window Design for Polarised Single Wavelength Emission:**

Conventionally, in the CVL MOPA configuration, both green and yellow wavelengths are generated and amplified simultaneously [2.17]. Polarization of the pump laser improves the conversion efficiency of the dye laser [2.1, 2.2]. The green and yellow parts are separated using suitable filters, subsequently, polarisers are used to polarize the green or yellow beam. Another approach for generating polarized laser output is by using a pile of Brewster windows [2.1, 2.2]. It is being proposed a new scheme for efficient generation of polarized green or yellow laser using interference filter based windows [2.22]. These windows can be used in all the laser heads of a CVL MOPA chain at optimized angles [2.37, 2.38]. This will filter out both the polarization of one wavelength either green or yellow, in which the propagation and amplification of desired wavelength of vertical polarization are supported. Multifunctional window design is expected to act as an antireflection window for reduced Fresnel losses, dichroic beam splitter for filtering one wavelength and polarizer for polarization selection throughout the MOPA chain [2.37, 2.38]. In the present design, the green polarized laser is targeted whereas a similar design may be adapted for yellow wavelength generation with suitable modifications in the design parameters.

Single-layer  $\text{MgF}_2$  design for inside AR coating was adapted over multilayer. Fresnel losses were reduced from 4% to 2.3% in a single layer coated window at  $0^\circ - 10^\circ$  angle of incidence. Variation of losses for vertical polarised green component (511 nm) versus angle of incidences from  $0^\circ - 56^\circ$

## CHAPTER - 2

degrees was studied (fig.2.15) to arrive at an optimized angle for minimum possible loss. It was achieved less than 0.5% loss for vertical polarisation of the green beam at 45 degree angle of incidence in a single layer AR coating design. The fig. 2.15 shows the variation of incidence angle with reflectivity of AR coated windows.

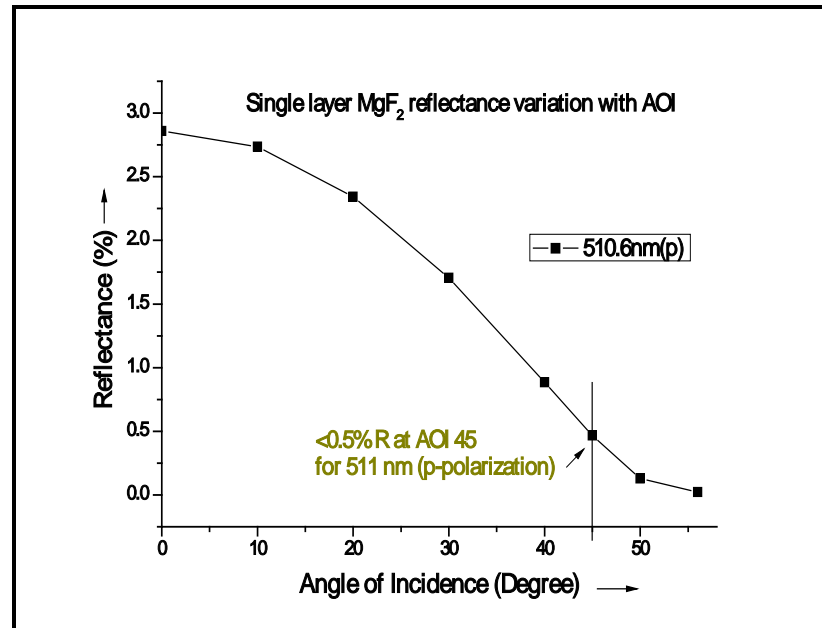


Figure 2.15: Fresnel loss variations with the angle of incidence (Single layer MgF<sub>2</sub>)

On the other side of the window, a multilayer interference filter based design was studied. A filter having a rejection band for a yellow beam and acceptance band for a green beam was designed. Reflection of the designed filter was assessed for various angles of incidences from 0 to 56° as shown in fig. 2.16.

Ripples in the passband are not optimized for angle variation studies, however, ripple minimized optimized design is shown in fig. 2.17. To achieve polarization selection, this design was further studied for reflection

## CHAPTER - 2

values corresponding to vertical and horizontal polarization of the green and yellow beam.

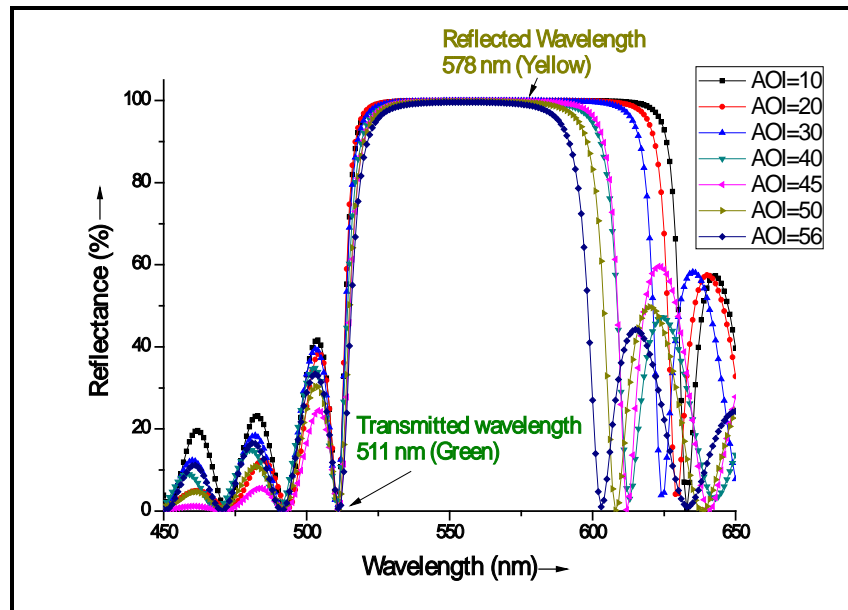


Figure 2.16: Spectrum for green and yellow filtering design

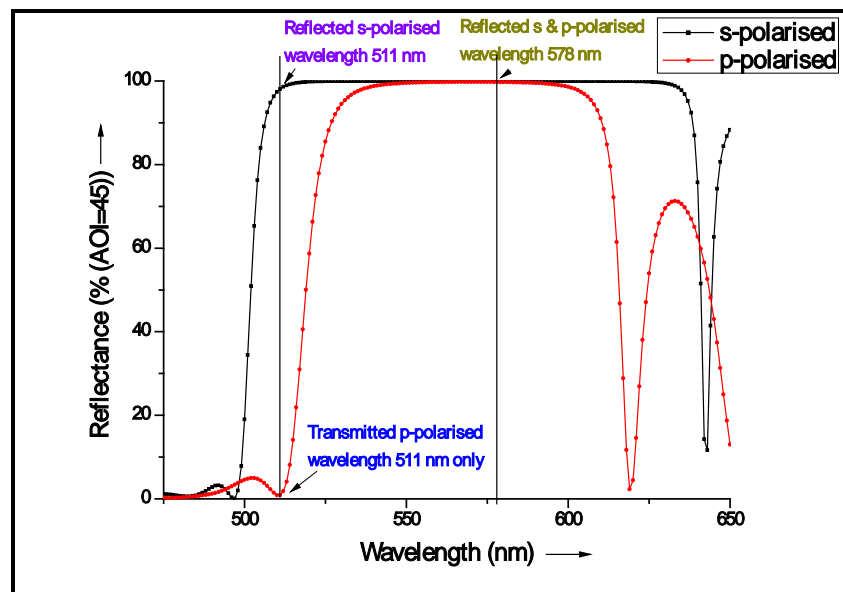


Figure 2.17: s and p polarization selection in the specialised window design

Figure: 2.17 shows the polarization selection of vertical (p) polarization of green beam ( $R < 1\%$ ) while as high reflectivity for another polarization of green ( $R > 99\%$ ) and both the polarization of yellow beam ( $R > 99\%$ ).

## CHAPTER - 2

*Table 2.5: Design of multifunctional window for CVL*

Layer No	Material	QWOT	Thick (nm)	Optimization	Layer No	Material	QWOT	Thick (nm)	Optimization
1	SiO <sub>2</sub>	1.5656 166.94	166.94	Yes	20	HfO <sub>2</sub>	1.0000	79.20	No
2	HfO <sub>2</sub>	1.2914	102.28	Yes	21	SiO <sub>2</sub>	1.0000	106.63	No
3	SiO <sub>2</sub>	1.1957	127.50	Yes	22	HfO <sub>2</sub>	1.0000	79.20	No
4	HfO <sub>2</sub>	1.1401	90.29	Yes	23	SiO <sub>2</sub>	1.0000	106.63	No
5	SiO <sub>2</sub>	0.5681	60.57	Yes	24	HfO <sub>2</sub>	1.0000	79.20	No
6	HfO <sub>2</sub>	1.3108	103.81	Yes	25	SiO <sub>2</sub>	1.0000	106.63	No
7	SiO <sub>2</sub>	1.0000	106.63	No	26	HfO <sub>2</sub>	1.0000	79.20	No
8	HfO <sub>2</sub>	1.0000	79.20	No	27	SiO <sub>2</sub>	1.0000	106.63	No
9	SiO <sub>2</sub>	1.0000	106.63	No	28	HfO <sub>2</sub>	1.0000	79.20	No
10	HfO <sub>2</sub>	1.0000	79.20	No	29	SiO <sub>2</sub>	1.0000	106.63	No
11	SiO <sub>2</sub>	1.0000	106.63	No	30	HfO <sub>2</sub>	1.0000	79.20	No
12	HfO <sub>2</sub>	1.0000	79.20	No	31	SiO <sub>2</sub>	1.0000	106.63	No
13	SiO <sub>2</sub>	1.0000	106.63	No	32	HfO <sub>2</sub>	1.2525	99.20	Yes
14	HfO <sub>2</sub>	1.0000	79.20	No	33	SiO <sub>2</sub>	0.8612	91.83	Yes
15	SiO <sub>2</sub>	1.0000	106.63	No	34	HfO <sub>2</sub>	1.0987	87.01	Yes
16	HfO <sub>2</sub>	1.0000	79.20	No	35	SiO <sub>2</sub>	1.6084	171.51	Yes
17	SiO <sub>2</sub>	1.0000	106.63	No	36	HfO <sub>2</sub>	0.8875	70.29	Yes
18	HfO <sub>2</sub>	1.0000	79.20	No	37	SiO <sub>2</sub>	0.9033	96.32	Yes
19	SiO <sub>2</sub>	1.0000	106.63	No					

A low pass edge filter design was taken as the basic design building block. A fused silica substrate of 10 mm thickness was chosen.  $\text{HfO}_2$  and  $\text{SiO}_2$  were taken as high refractive index and low refractive index material respectively for this design. Basic stack formula  $(0.5L H 0.5L)^{18}$  was considered for the design optimization and finalization of the coating. Reference wavelengths were suitably selected for optimization of the design for required wavelengths. Single-layer  $\text{MgF}_2$  was finalized as front layer AR coating. Layer thicknesses are tabulated in table-2.5. The first six and last six layers were optimized to achieve the desired target values. Ripples in the passband could not be eliminated as this is the unavoidable consequence of the polarizer functionality of the interference filter. However, these are less than 5 % at 510.6 nm.

This design has promising applications in the dye laser pumping where the single wavelength is used for overlapping with the absorption peak of the laser dye. The window design was found suitable for polarized single wavelength operation of an inherently dual-wavelength copper vapor laser. Single-layer AR coated design for the inside surface allows the possibility of using these windows in the CVL systems with an improved life. Filtering out the yellow component at every stage of MOPA enhances gain for the green component in the laser output.

### **2.5. Master Oscillator Power Amplifier (MOPA) Configuration:**

Power scalability is a key attribute of this laser which allows scaling up the average power by cascading multiple laser modules in a Master Oscillator Power Amplifier (MOPA) configuration [2.23-2.36]. In longer MOPA chains Fresnel losses arises due to windows and beam routing optics become significant to reduce the power gained

## CHAPTER - 2

from subsequent amplifier stages. It is proposed to analyze various MOPA configurations for maximizing the output power from a long MOPA chain [2.27]. A MOPA chain consisting of one master oscillator and five power amplifier stages was experimentally evaluated for the current study. An indigenous 40W CVL system was used for the experiments and analysis. The power gain was experimentally measured by varying input signal power to the amplifier. Higher power addition from amplifiers was experimentally observed at lower input signal power, which was the basis for pursuing this study. Total average power achievable from various configurations was evaluated. MOPA consisting of one oscillator and five amplifier stages was set up to study the effect of input signal power on the power addition of the amplifiers. An off-axis positive branch unstable resonator (PBUR) was set up across the oscillator to generate a good quality oscillator beam. A spatial filter consisting of concave mirrors and an aperture was used to filter out higher diverging components of the CVL beam. The oscillator beam was routed through five power amplifier stages to boost the average power. A pair of concave mirrors was aligned in confocal geometry for thermal lensing compensation after the third amplifier stage. Broadband beam splitters were used for varying the input signal power to the amplifying stages. A schematic of the MOPA configuration set up is shown in fig. 2.18.

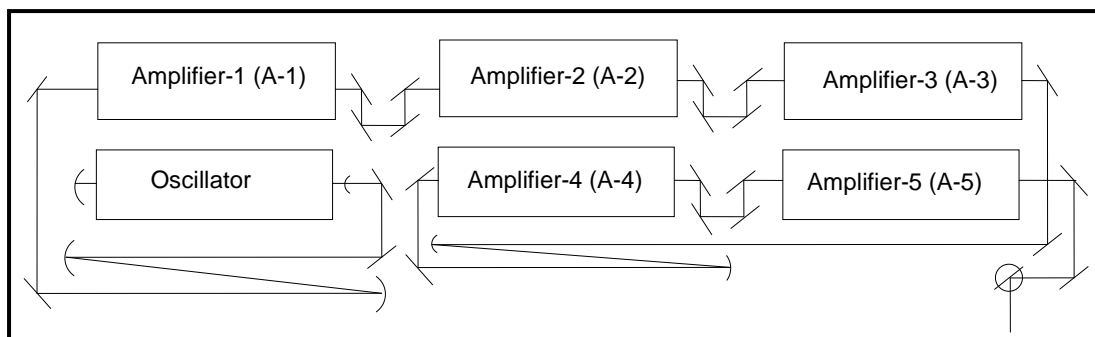


*Figure 2.18: Schematic of the MOPA configuration for the experiment*

Input electrical power was kept constant during these experiments. Ophir make (Model: FL 150) power meter was used to measure the average power of the laser beam.

### **2.5.1. Designs for CVL MOPA Configurations:**

A MOPA configuration design was based on splitting the signal beam to reduce the input to the next amplifier stage. Splitted part of the beam was either taken out or sends to the input of another amplifier module. The amplification using various arrangements of amplifier modules was analyzed using this splitted input signal. In all the configurations, one oscillator and five amplifier modules were considered to maintain the uniformity for a fair comparison. Thermal lens compensation was not considered in any of the configurations for this theoretical analysis. This was because no thermal lens correction is required in three of the four configurations owing to shorter constituent splitted MOPA chains of 2 to 3 amplifier stages. However, the thermal lens compensated six-module MOPA chain was used for experimental study. In all the design calculations, a PBUR was considered followed by spatial filter for filtering out the ASE having higher divergence components in the signal beam. We have studied four configurations, which are elaborated as below.

#### **2.5.1.1. Single Long Chain:**

In the first configuration, a single long chain of one oscillator and five subsequent cascaded amplifiers were considered. This design requires thermal lensing correction after the third or fourth stage. Four beam routing mirrors were considered in between the amplifier stages for the ease of alignment to attain maximum spatial gain volume utilization. Arrangement

## CHAPTER - 2

of the single long chain design without thermal lens compensation is shown in fig. 2.19.

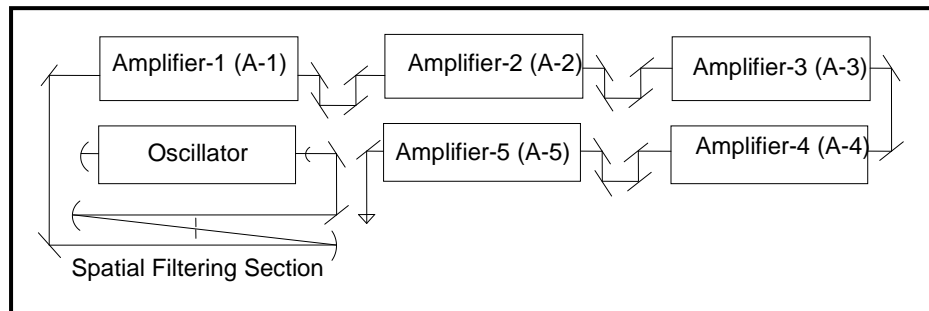


Figure 2.19: Single long chain configuration

### 2.5.1.2. Splitted Chain After Oscillator:

Splitted shorter chains instead of the single long chain were considered as the second MOPA configuration. This configuration is illustrated in fig. 2.20, which generates two CVL beams of different power levels.

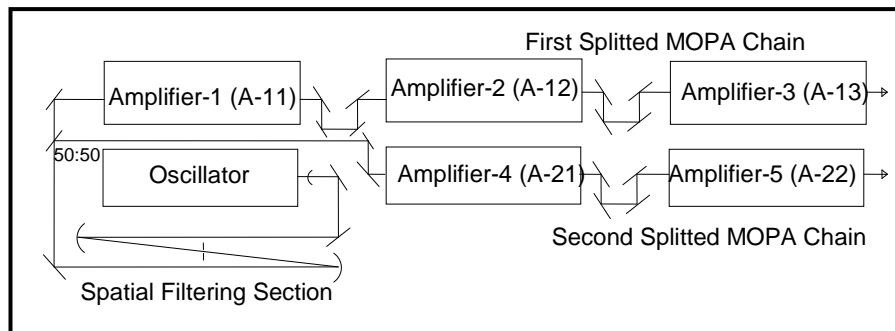


Figure 2.20: Splitted chain after oscillator configuration; (A-11, A-12, A-13: First, second and third amplifier in first splitted chain; A-21, A-22: First and second amplifier in second splitted chain)

In this scheme, the spatially filtered oscillator signal beam was equally splitted into two beams. These splitted beams were amplified using subsequent amplifier stages. The first beam was amplified using two amplifier stages, whereas the second splitted beam was amplified using three stages. This leads to a MOPA chain having one oscillator and three

amplifiers, whereas the second shorter chain consisted of two amplifiers.

Two amplified laser beams are generated at the end of this configuration.

**2.5.1.3. Splitted Chain After First Amplifier:**

In the third scheme, a spatially filtered oscillator beam was amplified using one amplifier module and this amplified beam then equally splitted into two beams. Each beam is routed through a pair of amplifier modules. This resulted in two high power output laser beams of equal power levels. This configuration of splitted chain after first amplifier is depicted in fig. 2.21.

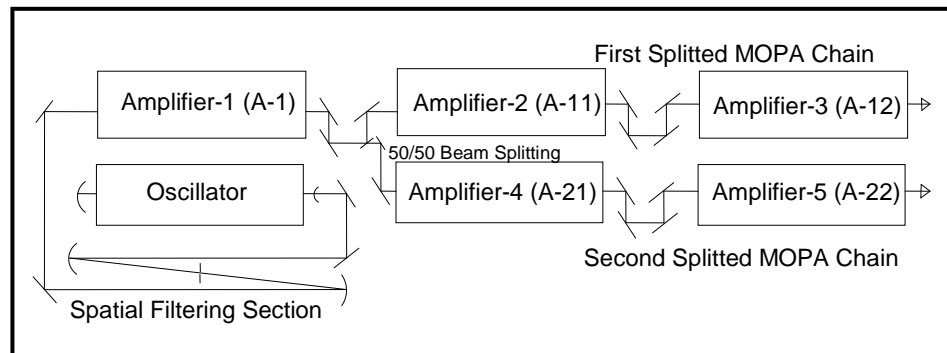


*Figure 2.21: Splitted chain after amplifier configuration, (A-11, A-12: First, and second amplifier in first splitted chain; A-21, A-22: First and second amplifier in second splitted chain)*

**2.5.1.4. Periodic Power Withdrawal Configuration:**

In another variation, which is suitable for fiber optic beam delivery is shown in fig. 2.22. In this configuration, the amplified beam is periodically withdrawn after every amplifier stage. The output power from laser beam after every stage was tapped so that only 10-12 W power of the beam is fed to the next amplifier, whereas the tapped part of the beam is taken out using a fiber optic beam delivery system. This delivery system is proposed to reduce transportation losses and better utilization of the laser power. This results in five output laser beams delivered using optical fibers. Reduced

## CHAPTER - 2

input signal power of  $\sim 12\text{W}$ , to each amplifier, ensures the maximum power gain utilization ( $\geq 33\text{ W}$ ) from every amplifier unit. Excess power is withdrawn periodically to enhance the overall extracted power from the MOPA chain which reduces Fresnel as well as routing mirror losses.

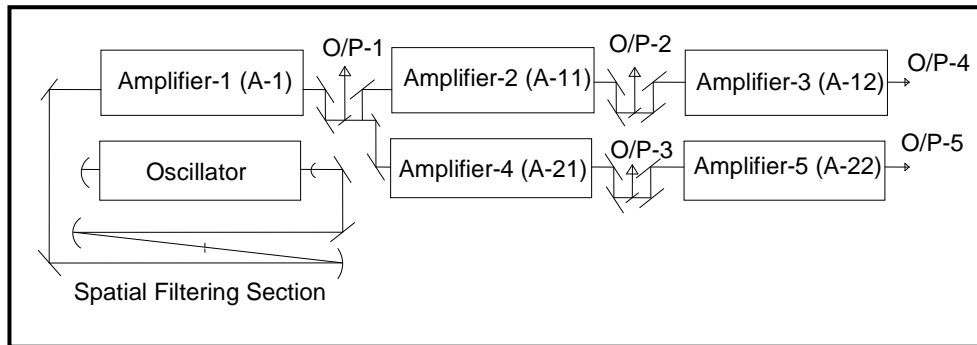


*Figure 2.22: Periodic power withdrawal MOPA configuration (A-11, A-12: First, and second amplifier in first splitted chain; A-21, A-22: First and second amplifier in second splitted chain)*

### 2.5.2. Results and Discussions:

The variation in the input signal power of the amplifiers and power gain behavior was recorded. Various MOPA configurations were theoretically analysed and compared for their maximum extractable power levels. The calculations are based on experimentally determined power gain from the individual amplifier module. Total extractable output power was estimated by the addition of average power in all the output laser beams.

#### 2.5.2.1. Determination of Amplifier Gain:

The power gain of amplifier modules was determined at various input signal powers from  $12\text{W}$  to  $80\text{W}$  in different amplifiers. Figure 2.23 and fig. 2.24 depicts the extractable power behavior of second and fifth amplifier in a six-module CVL MOPA chain. We have found that the power addition in every amplifier is maximum or greater than  $33\text{ W}$  when input signal power

## CHAPTER - 2

is between 10 and 15 W. The power addition found to be to minimum of nearly 22 W by the amplifier when the input signal beam was 80 W as shown in fig. 2.24. This result suggested that input to the amplifiers must be kept in between 10-15 W only to extract the maximum gain. The available gain in the higher input signal powers results in underutilization i.e. fourth, fifth amplifier stages where input signal power exceeds 80 to 100W. These observations were the basis for the CVL MOPA configuration design approach.

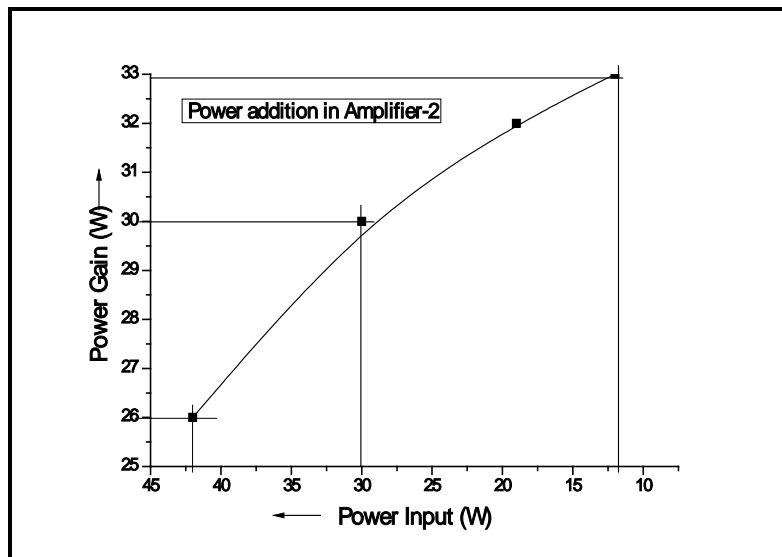


*Figure 2.23: Dependence of input signal power on power addition from the second amplifier*

The power gain of 33, 30 and 26 W was determined with an input signal of 12, 30 and 42W respectively in the second amplifier module. In amplifier-5, the power addition of 32.5, 28 and 22 W was measured at an input power of 32, 60 and 77 W respectively.

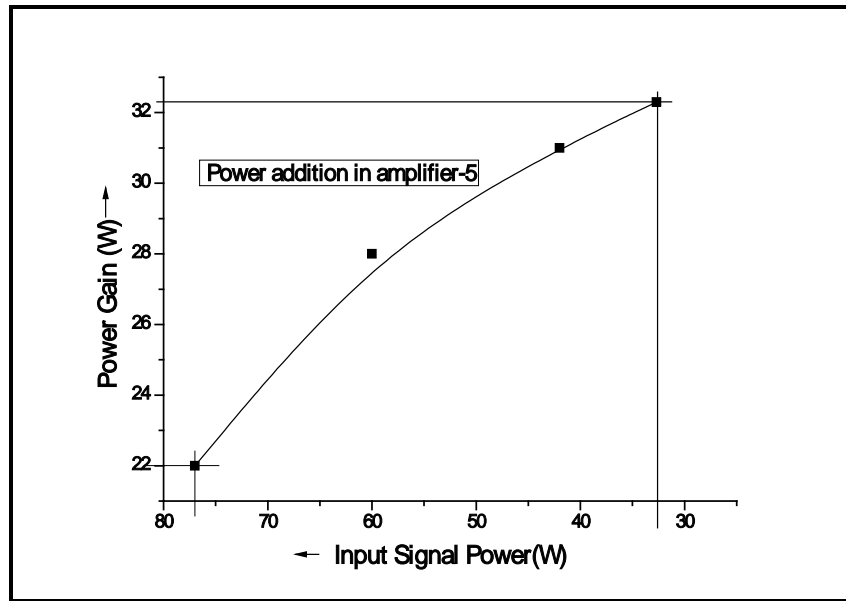


Figure 2.24: Dependence of input signal power on power addition from the fifth amplifier

#### 2.5.2.2. Comparison of CVL MOPA Chain Designs:

A comparison among four MOPA configurations suggested that MOPA chains with a smaller number of amplifiers are advantageous than the more number of amplifier modules in a single chain. The shorter chain not only extracts optimum output power but also minimizes the thermal lensing compensation and further prevents power losses occurred in additional correction optics. Table-2.6 depicts the calculated power levels at each stage with the expected gain factor and total extracted power for comparison in all these schemes. It was observed that net extractable power in a single long chain, splitted chain after an oscillator, splitted chain after the amplifier; periodic power withdrawal configuration has the capability of delivering the power levels in the range of 136W, 161W, 168W, and 179W respectively. The first configuration generates full power in a single output beam, second and third configuration emits two output beams whereas the fourth configuration emits in five different beams of similar power levels.

## CHAPTER - 2

*Table 2.6: Comparison of power extracted from various configurations*

Amplifier	Single long chain			Splitted chain after the oscillator			Splitted chain after the amplifier			Periodic power withdrawal configuration		
	In put	Gain	Out put	In put	Gain	Out put	In put	Gain	Out put	In put	Gain	output
Oscillator			15			15			15			15
A- 1,A11,A1. A1	15	33	48	7.5	33	40.5	15	33	48	15	33	48, OP1=24
A-2, A12, A11, A11	48	26	74	40.5	26	66.5	24	33	57	12	33	45, OP2=32. 5
A-3, A13 ,A12, A12	74	22	96	66.5	28	94.5	57	28	85	12.5	33	45, OP3=32. 5
A-4, A22, A22, A22	96	20	116	7.5	33	40.5	24	33	57	12	33	45, OP4=45
A-5, A21, A21, A21	116	20	136	40.5	26	66.5	57	28	85	12.5	33	45, OP5=45
Net output			136 W			161W, 18% extra			170W, 25% extra			179W, 31.6% extra

### 2.6. Thermal Lensing in CVL:

The temperature of the discharge tube needs to be raised to 1550 °C to 1650 °C to obtain the required partial pressure of the lasant copper atoms [2.1]. Double-walled SS housing of the discharge tube is cooled with flowing water through it. Temperature and water flow rates are controlled to maintain the required cooling rate to achieve sustained, stable temperature of 1600 °C of the discharge tube. This results in the high temperature at the axis while the lower temperature at the walls, and hence the axial temperature gradient is created. The steep radial thermal gradient causes a corresponding refractive index gradient in the buffer gas. The radial thermal gradient is known to have a parabolic profile [2.14, 2.28, 2.30, and 2.31]. The gradient of buffer gas density follows this parabolic temperature variation which causes a corresponding refractive index profile. This temperature-induced refractive index gradient generates an optical path difference between rays passing through the axis and at the periphery of the gain cylinder, which results in the lensing effect. The optical thickness due to buffer gas density variation is smaller at the center as compared to that at the periphery, which causes a negative lensing effect due to this buffer gas temperature gradient. Therefore, an equivalent concave lens is considered in the ray-tracing approach of the analysis. A pair of transparent glass windows is used in the laser head to provide the interface for the vacuum. The hot discharge tube emits heat radiations following Stephen's radiation law. This radiation reaching the windows and gets absorbed in it. The amount of heat radiation absorbed in the window depends on the fraction of emitted radiation based on a solid angle subtended by the window diameter or bore diameter [2.31]. The refractive index profile inside the glass window depends on the material of the window, its refractive index coefficient (sign and magnitude) and the geometry dependent solid angle. Generally fused silica windows

are used which has negative  $dn/dT$  [2.2]. A positive lensing effect is created due to this mechanism, which behaves like a convex lens. A system of an equivalent lens is a combination of a concave lens followed by the convex lens is formed, with a resultant positive lensing effect [2.14, 2.31]. This converging effect reduces the beam diameter passing through the laser head. An equivalent convex lens at the center of the CVL head has been taken for further simulations and analysis by the optical ray-tracing method.

### **2.6.1. Experimental Setup for Measurement of Thermal Lensing:**

A novel experimental technique for measurement of effective thermal lens in an amplifier module was demonstrated. A 40 W CVL (CVL-40), operating at 9 kHz repetition rate was used for this experiments and theoretical studies. The experimental setup and procedure for the estimation of effective thermal lens of this CVL system is described in the following sections.

The experimental setup for thermal lens determination comprises of three parts. The first part deals with ensuring the collimation of the CVL oscillator beam using a Shear interferometer wedge plate. The effect of amplifier thermal lens on the beam diameter of the collimated beam propagated through an amplifier module is discussed in the second section. The effect of electrical input power and buffer gas pressure on the effective focal length of the thermal lens is described.

A CVL oscillator was set up in the positive branch unstable resonator (PBUR) configuration. A concave mirror of the focal length of 2500 mm and a small diameter convex mirror of the focal length of 37.5 mm were set up in an off-axis confocal geometry. The oscillator output beam was collimated by optimizing the distance between convex and concave mirrors. The Shear interferometer plate

## CHAPTER - 2

was used to ensure the collimation of the oscillator probe beam before launching it in the amplifier module. Horizontal parallel fringes formed by the Shear plate confirmed the collimation of the oscillator output beam [2.14, 2.23, 2.30]. Collimated oscillator beam without any focusing effect is used as the probe beam for the measurement of focussing effect in the amplifier module. Oscillator operating parameters such as electrical power, buffer gas pressure were kept constant during the entire experiment to avoid any ambiguity in the probe beam. Two concave mirrors of an equal radius of curvature of 2600 mm were used for spatial filtering. An aperture 700- $\mu\text{m}$  diameter was used at the focal plane to achieve the filtering of the higher divergence components. Fig. 2.25 shows the schematic of the experimental setup for the measurement of collimation of the CVL oscillator beam, which was used as a probe beam for the thermal lens measurement of the CVL amplifier module.

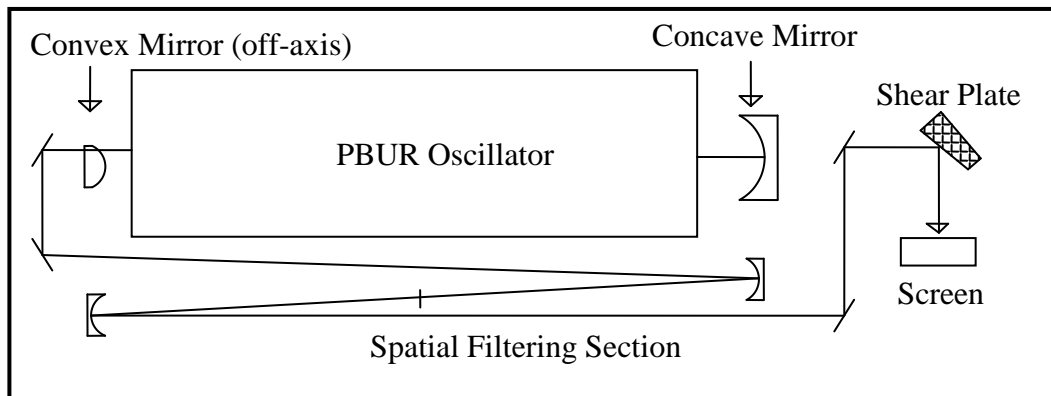


*Figure 2.25: Schematic of CVL oscillator beam used for thermal lens measurement*

The collimated beam manoeuvred through the amplifier using high reflectivity mirrors. The schematic of the experimental setup is shown in fig. 2.26 for the measurement of the thermal lens in the amplifier module.

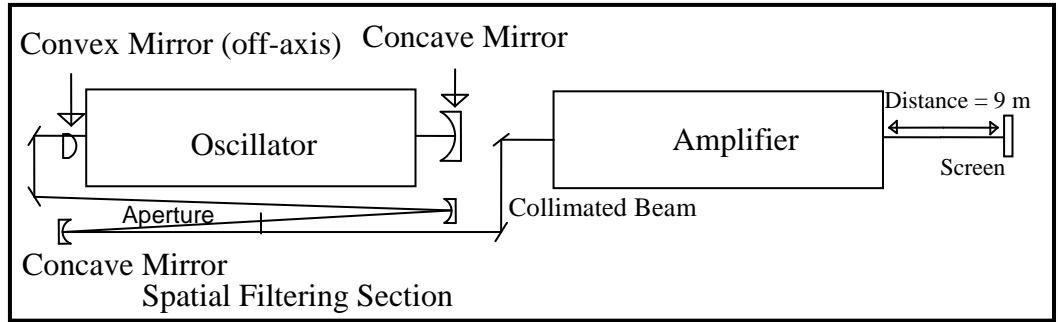


Figure 2.26: Effective thermal lensing assessment setup

The diameter of the probe beam entering the amplifier was measured. The diameter of the probe beam emerging out of the amplifier was measured at two locations, just after the amplifier exit plane as well as at 9 m away from the amplifier exit plane.

### 2.6.2. Estimation of Thermal Focal Length for Amplifier Module:

The diameter of the CVL beam at two locations separated by a distance of 9 m was measured. The converging nature of the resultant lensing effect was confirmed by reduced beam diameter at a distant location. These diameter values were used to estimate the effective focal length of the amplifier thermal lens using the ray diagram as shown in fig. 2.27. R1 and R2 were the radii of the beam just after the amplifier exit beam and at 9 m away from it respectively. A virtual focus point at 'C' was assumed at a distance 'F' from the amplifier due to the thermal generated lens in the amplifier. Ray diagram instead of Gaussian optical formulation was used to estimate the focal length because CVL is a superradiant laser system having a higher number of modes with large  $M^2$  ( $>20$ ) values.

In the ray diagram (fig.2.27) two similar triangles ABC and DEC, subtending a common angle 't' can be used to write the following equations:

## CHAPTER - 2

$$\frac{AB}{BC} = \tan(t) \quad (1)$$

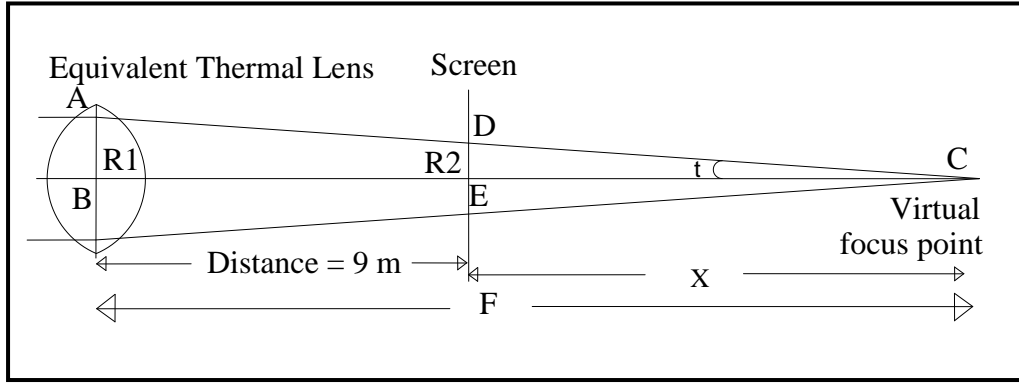


*Figure 2.27: Determination of the effective thermal lens of the amplifier*

$$\frac{DE}{EC} = \tan(t) \quad (2)$$

from Eqn. 1 and 2, we get

$$\frac{AB}{BC} = \frac{DE}{EC} \quad (3)$$

By definition,  $AB = R1$ ,  $DE = R2$ ,  $EC = X$ ,  $BE = 9$ ,  $BC = F$  eqn. 3 becomes

$$\frac{R1}{F} = \frac{R2}{F-9} \quad (4)$$

By simplifying eqn. 4, we get

$$F = \frac{9R1}{R1-R2} \quad (5)$$

The effective focal length of the amplifier thermal lens ‘F’ was calculated from Eqn. 5, using measured values of R1 and R2. This simple technique can be used for any amplifier stages in the CVL MOPA chain by simply re-routing the CVL beam in between the amplifier modules of the MOPA chain and measuring the diameter variation at two different locations of known distance to estimate the resultant thermal focal length (cumulative). The effective thermal focal length of the first amplifier in the chain at various operating parameters was measured. These focal length values were assumed to be the same for all the amplifier modules, at the optimized operating parameters. The

experimentally measured focal length value and CVL-40 dimensions were taken in further theoretical calculations and projections of compensation techniques.

### **2.6.3. Effect of Operating Power on Thermal Lens:**

Input electrical power causes the heating of the discharge tube in a self-heated CVL system. It is already established [2.14, 2.28, 2.30, 2.31] that, the negative lens effect is due to the buffer gas and the positive lens effect is due to the optical windows. At higher temperatures, the positive lens effect is more dominant in this combination of lenses, which results in the more converging power to the CVL amplifier system. Electrical input power is the controlling parameter for the operation of the CVL system to get the desired output beam parameters. Therefore, the characterization of the CVL amplifier thermal lens at various operating electrical power became mandatory. The effective focal length of the thermal lens at various operating input power was measured while keeping the buffer gas (Neon gas) pressure constant at  $\sim 40$  mbar. It was observed that the effective thermal focal length of the amplifier was 306 m at the input electrical power of 3.5 kW, it reduces to approximately 50 meters at a relatively higher input power of 6.2 kW. Reduction in focal length confirms that power (inverse of focal length, in dioptr) of the thermal lens increases at higher input electrical power. The focal length of the resultant thermal lens at operating electrical power was found to be approximately 50 m. The effect of input electrical power on the effective thermal focal length (thermal lens) is shown in fig. 2.28.

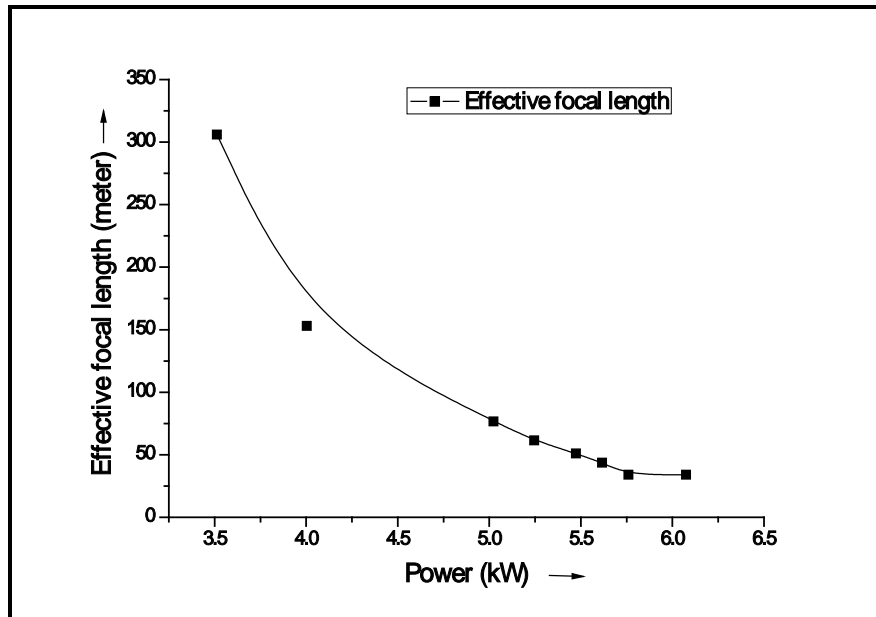


Figure 2.28: Effect of input electrical power on the effective focal length

#### 2.6.4. Effect of Operating Pressure on Thermal Lens:

Buffer gas contributes to the negative lens effect in the overall thermal lensing effect [2.14, 2.31]. It was necessary to characterize the amplifier for its effect on the resultant focal length of the equivalent thermal lens. Neon buffer gas pressure was varied from 18 mbar to 120 mbar at a constant input electrical power of approximately 6 kW. Effective focal length at various buffer gas pressure was measured and plotted as shown in fig. 2.29.

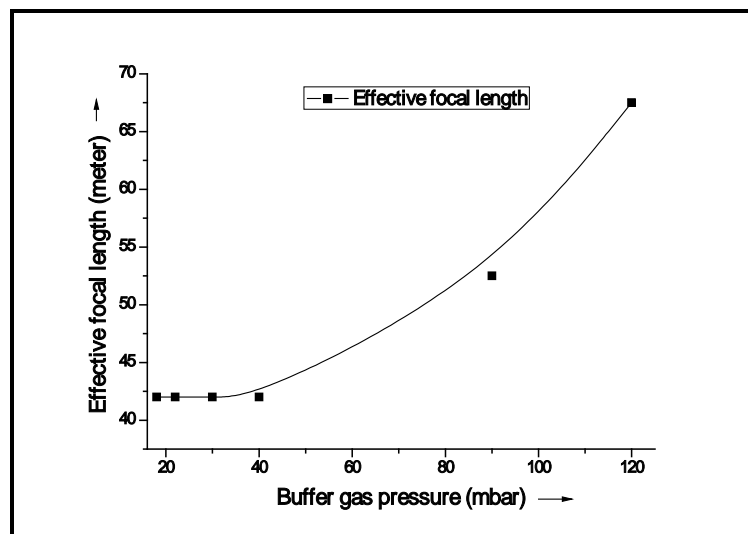


Figure 2.29: Effect of buffer gas pressure on the effective focal length

Effective thermal focal length changed from 42 m to 70 m when neon gas pressure varied from 18 mbar to 70 mbar. It can be seen that the power of an equivalent thermal lens reduces at higher gas pressure. It is postulated that, at higher gas pressure, the density variations caused due to thermal gradients are relatively lower than those at lower gas pressure. Therefore, higher buffer gas pressure is suitable for lowering the thermal lens effect, which is in agreement with the studies reported by other authors [2.14, 2.31]. This reduction in the power of thermal lens occurs with a cost of the increased impedance of the discharge tube at higher gas pressure. This impedance mismatch results in the lower dumped input electrical power and hence reduces the amplifier power gain. It is also observed in the CVL-40 system, the output power was reduced at higher operating pressure (>80 mbar). The optimized operating buffer gas pressure for this system is 40-50 mbar. It was observed (fig. 2.29) that, effective focal length was approximately 40 to 50 m at this optimum operating gas pressure. It can be seen from fig. 2.28 and 2.29 that, the effect of electrical input power was more prominent than that of buffer gas pressure. It is found that the effective resultant focal length of the thermal lens is 50 m at the optimum operating pressure of 40 mbar and electrical input power of 6 kW. Hence, for all theoretical extrapolations and compensation analysis, these parameters were kept the same.

### **2.6.5. Evaluation of Thermal Lensing:**

Thermal lens has a significant impact on the power extraction capabilities of the CVL module due to smaller gain volume utilization. It changes the effective separation distance between the mirrors in an unstable resonator and reduces the total extractable power in a MOPA configuration. These issues are discussed in the following section of this chapter.

2.6.5.1. Oscillator Configuration:

An oscillator comprises a set of concave and convex mirrors separated by confocal distance across the laser gain medium. The mirror separation distance is the sum of focal lengths of the mirrors in a confocal geometry. Cavity distance between the resonator mirrors gets modified if a lens or equivalent lens is present in between the mirrors. The equivalent cavity model for both the cases is shown in fig. 2.30.

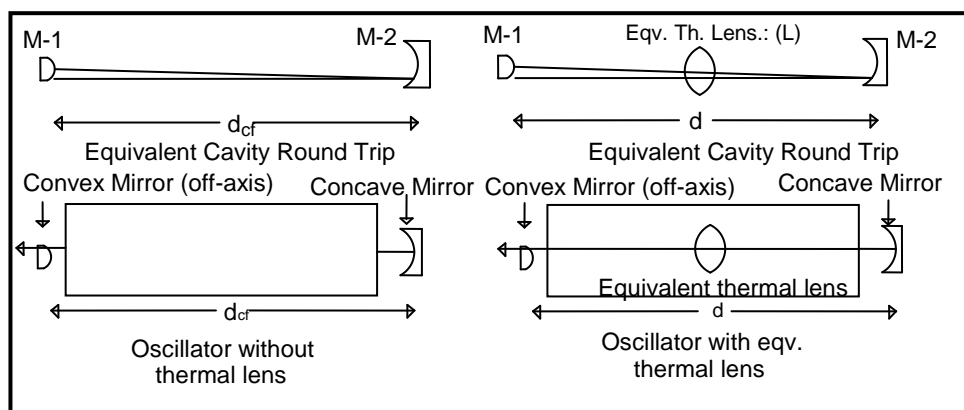


Figure: 2.30. Oscillator (PBUR) and its equivalent thermal lens model

(M-1: Convex mirror, M-2: Concave mirror,  $d^{cl}$ : Confocal distance, L: Equivalent thermal lens)

The modified optical system in the presence of an equivalent converging lens can be analyzed by using a ray-tracing matrix formulation. Let us consider  $M_1$ ,  $M_2$ ,  $M_d$ ,  $M_{d/2}$ , and  $M_L$  be the matrices for the first mirror (convex), the second mirror (concave mirror), free space propagation matrix between both the mirrors ( $d$ ), propagation matrix for the half cavity distance ( $d/2$ ) and thermal lens respectively. Cavity round trip matrix starting from the mirror (M-1, convex mirror) can be formulated as below for both the cases. System matrix for the first case (without thermal lens) and second

case (including thermal lens) are defined as  $M_{WTL}$  and  $M_{ITL}$  respectively.

Both of these matrices formulations can be described as:

$$M_{WTL} = [M_d \cdot M_2 \cdot M_d \cdot M_1] \quad (6)$$

$$M_{ITL} = [M_{d/2} \cdot M_L \cdot M_{d/2} \cdot M_2 \cdot M_{d/2} \cdot M_L \cdot M_{d/2} \cdot M_1] \quad (7)$$

The individual system matrices for optical components (sign convention included) can be written as:

$$M_d = \begin{bmatrix} 1 & d \\ 0 & 1 \end{bmatrix} ; M_{d/2} = \begin{bmatrix} 1 & d/2 \\ 0 & 1 \end{bmatrix} ;$$

$$M_1 = \begin{bmatrix} 1 & 0 \\ 1/f_1 & 1 \end{bmatrix} ; M_2 = \begin{bmatrix} 1 & 0 \\ -1/f_2 & 1 \end{bmatrix} ; M_L = \begin{bmatrix} 1 & 0 \\ -1/f_{th} & 1 \end{bmatrix}$$

By solving the above matrix manipulations, we can calculate the cavity distance for the collimated output of the oscillator for both the cases by employing the condition of collimation. It was experimentally observed that distance between convex and concave mirror in PBUR was 2410 mm instead of 2462.5 mm of confocal distance for the collimated output laser beam. Other researchers also observed a similar effect as well in their resonator system [2.35]. This was due to the presence of the thermal lens effect as can be seen in the modified system matrix formulation.

#### **2.6.5.2. Thermal Lens Effect in Oscillator-Amplifier Configuration:**

The thermal lens effect plays an important role in setting up CVL MOPA configurations. An equivalent converging lens is required to be considered inside the laser system for configuring the CVL MOPA chain. The role of the thermal lens in an oscillator-amplifier system is more prominent as compared with the oscillator alone. The thermal lens in oscillator configuration modifies the resonator distance, whereas it governs the total extractable power, the number of efficient amplifier modules and output beam parameters in a CVL

## CHAPTER - 2

MOPA chain. The schematic of a CVL MOPA chain showing the equivalent thermal lens is shown in fig. 2.31. A chain of one oscillator and seven amplifier stages were analyzed theoretically. It was assumed that one converging lens with a focal length ( $f_{thl}$ ) of 50 m at the centre of each amplifier unit.

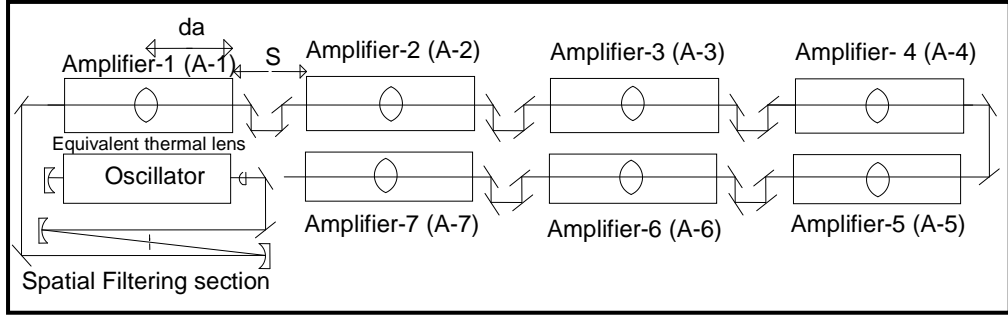


*Figure 2.31: MOPA chain with equivalent thermal lens*

One amplifier stage was divided into three optical parts for the ray tracing matrix formulation. In the first part, ray propagating a distance  $da$  (half of the CVL amplifier length i.e. 1125mm) before the equivalent thermal lens was considered. A similar matrix was assumed for the free space propagation ( $da$ ) after the thermal lens. The matrix for this beam propagation to a distance ' $da$ ' is defined as  $M_{da}$ . The equivalent thermal lens was modelled as a convex lens ( $f_{thl}=50m$ ) matrix,  $M_L$ . Free space propagation in between amplifier stages in a MOPA chain was considered in a translation matrix ( $M_s$ ) for separation distance  $S$ . These matrices are defined in the following manner:

$$M_{da} = \begin{bmatrix} 1 & da \\ 0 & 1 \end{bmatrix} ; M_s = \begin{bmatrix} 1 & S \\ 0 & 1 \end{bmatrix} ; M_L = \begin{bmatrix} 1 & 0 \\ -1/f_{thl} & 1 \end{bmatrix}$$

System matrix for the individual amplifier ( $M_A$ ) was defined such that:

$$M_A = M_{da} \cdot M_L \cdot M_{da}$$

System matrix for one amplifier stage including inter-amplifier distance ( $S=500$  mm) was defined as  $M_{AA}$ , which was calculated as:

## CHAPTER - 2

$$M_{AA} = M_s \cdot M_{da} \cdot M_L \cdot M_{da}$$

Seven such amplifier stages were considered for the calculations and simulated the beam radius and beam angle with respect to propagation axis in the MOPA chain using a paraxial approximation in matrix formulation.

The boundary line of the laser beam propagating through the amplifiers was defined as the ray. The height and angle of this ray with respect to propagation axis are governed by the optical elements encountered in the chain. The lens effect encountered during the propagation of this ray inside the CVL MOPA chain causes a reduction in the height and modulation of the angle as per the power of the thermal lens. The schematic of the model used for stage-wise diameter and angle calculations is shown in fig. 2.32.

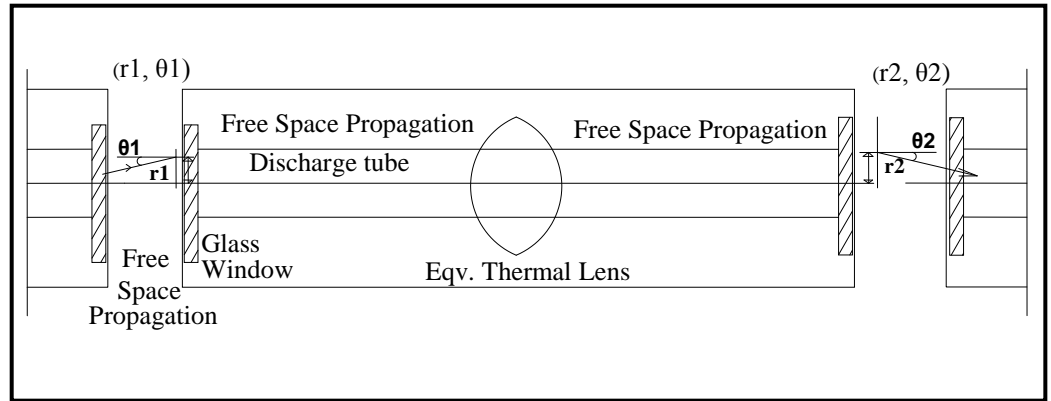


*Figure 2.32: Schematic of the amplifier ray-tracing model (beam parameter definition)*

The formulation used to determine the beam height (beam radius) and angle with the axis (central axis across the CVL MOPA chain amplifiers), can be written as,

$$\begin{bmatrix} r2 \\ \theta2 \end{bmatrix} = [M_{AA}] \cdot \begin{bmatrix} r1 \\ \theta1 \end{bmatrix}$$

Vertical distance of laser beam boundary line w. r. t. axis was considered as the height of the ray i.e.  $r$ . This ray defined at the laser beam boundary line

## CHAPTER - 2

---

subtends an angle with the propagation axis defined as the angle  $\theta$ . Radius and angle parameters  $r_1, r_2, \theta_1, \theta_2$  are the beam height and angle w.r.t. propagation axis at the entry and exit of the optical system. Initial values  $r_0$  and  $\theta_0$  are the starting point of the ray at the entry point of the first amplifier. It can be observed that  $r_0$  equal to 18.5 mm for the 37 mm laser beam from the oscillator launched to the first amplifier. Similarly, the beam diameter (twice the height ( $r$ ) of the ray) at every amplifier stage was calculated. Angle  $\theta_0$  was taken as 0 for collimated beam (for paraxial approximation), although beam will have some minimum divergence), positive for divergent beam and negative for convergent beam in the simulations.

CVL is a volumetric system having specific power per unit volume defined for a particular system. The specific power gain for the 40 W CVL system was calculated to be  $1.96 \times 10^4$  per  $\text{m}^3$ . Beam height values calculated using the ray-tracing model for all the amplifier stages were used to calculate the beam diameter and the effective beam volume in the amplifier. Effective amplifier gain was then calculated by multiplying specific power per unit volume (CVL-40 system) and thermal lens modulated beam volume at each amplifier stage. Beam diameter and corresponding amplifier gain was calculated for seven amplifier stages and plotted in fig. 2.33.

Beam diameter at every stage (black, square curve in fig. 2.33) reduces considerably and becomes too little to add any power after the fifth amplifier. Similarly, power gain (blue, triangle curve in fig. 2.33) in every amplifier stage reduces and vanishes after the fifth stage. It shows that a MOPA chain of five amplifiers is more efficient than seven amplifiers due to the thermal lens effect. Therefore, either reducing the power (inverse of focal length) of the individual

thermal lens or minimizing the effect by external means became essential to realize a longer MOPA chain to obtain higher extractable power.

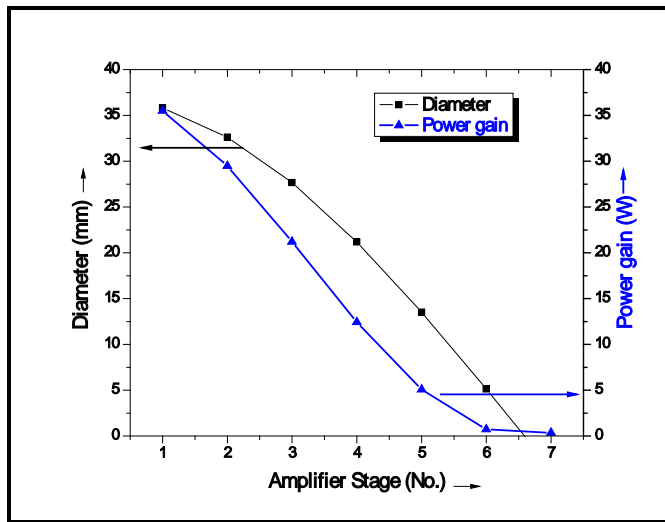


Figure 2.33: Diameter of the beam and power gain after each amplifier in the MOPA

The configurations and techniques, which mitigate the thermal lens were studied further and described in the subsequent sections.

**2.6.6. Thermal Lensing Compensation Techniques:**

Optical arrangements used to minimize the thermal lens effect are termed as compensation techniques. Compensation techniques for minimization of the thermal lens in the individual laser system and CVL MOPA chain were proposed and theoretically analyzed to compare the thermal lens compensated configurations. The design and analysis of the compensation techniques are described below.

**2.6.6.1. Individual Laser System:**

Heat absorbed by the windows is one of the main causes of the converging lens. This absorption depends mainly on two factors. The amount of heat radiation reaching and absorbed by the window is the main reason for the thermal lens effect. The solid angle subtended by the window dictates the

## CHAPTER - 2

amount of heat radiation reaching the window. The selection of low absorbing material or thin-film coating to minimize absorption of the heat will reduce the effect of lens [2.31]. Compensation techniques for individual laser systems by tailoring these effects were theoretically studied.

The schematic of the geometrical arrangement in the CVL electrodes is shown in fig. 2.34. It consists of a window fitted at the end of the electrode bore and the hot discharge tube separated by a distance (bore length,  $l$ ).

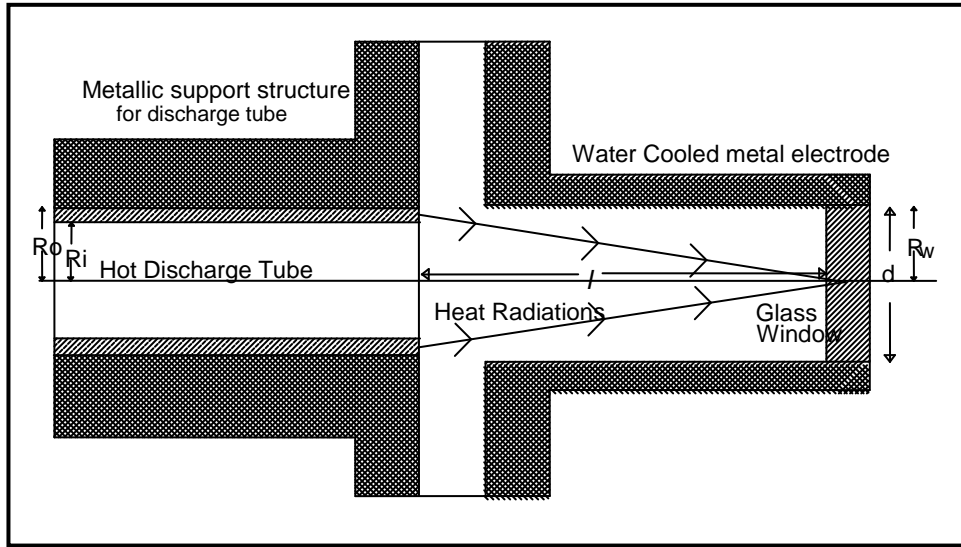


*Figure 2.34: Schematic of the heat radiation model for the window heating*

$R_i$  and  $R_o$  are the inner and outer radius of the discharge tube.  $R_w$  and  $l$  are the radii of the window (bore diameter) exposed to the radiation, the separation of the window from the discharge tube (bore length) respectively. The geometrical parameter dependent on the solid angle dictates the amount of heat radiation reaching the windows [2.14, 2.31].

Stephan's radiation law governs power radiated ( $P_{rad}$ ) by hot discharge tube, which is as follows:

$$P_{rad} = A. \epsilon. \sigma. T_0^4 \quad (8)$$

## CHAPTER - 2

---

Where end surface area,  $A = \pi \cdot (R_o^2 - R_i^2)$ ,

Alumina tube emissivity ( $\epsilon$ ) is 0.5 and Stephan-Boltzman's constant ( $\sigma$ ) is  $5.67 \times 10^{-8} \text{ Wm}^{-2}\text{K}^{-4}$ . Alumina tube temperature ( $T_0$ ), the inner radius of the alumina tube ( $R_i$ ) and outer radius of the alumina tube ( $R_o$ ) are 1650 degrees Celsius, 19 mm and 22.5 mm for this 40W CVL system respectively. The power of radiated heat was calculated to be around 176.8W.

The radiating alumina tube subtends a solid angle  $\Omega$  on the window.

Therefore, the amount of radiated power reaching the window is given by:

$$P_{rad} (W) = \left( \frac{P_{rad}}{4\pi} \right) \cdot d\omega; \text{ Where } d\Omega \approx \pi \cdot R_w^2 / l^2 \quad (9)$$

For our 40W CVL system, the radius of the window ( $R_w$ ) is 27.5 mm (55mm exposed diameter) and the distance between the discharge tube ends to the glass window ( $l$ ) is 200 mm. The estimated power reaching to the window is approximately 1.17 W.

The amount of radiation absorbed depends on the spectrum of the incident radiation. The fused silica windows have around 40% absorption for radiation of wavelength 1.51 to 1.68  $\mu\text{m}$  [2.31]. Therefore,  $P_{abs}(W)$  is the power absorbed by the window is given by Eq. 10.

$$P_{abs} = 0.4P_{rad} (W) \quad (10)$$

Power absorbed in the single window was 0.47W for the case of the bare fused silica window. The same amount of power was absorbed in the second window. Therefore, a total of 0.96 W of the heat radiation power absorbed by the pair of Quartz windows contributed to the converging thermal lens of 50 m focal length. Three configurations were theoretically studied to minimize the net absorption in the window so that the effect of the converging lens could be reduced. In the first configuration, the window reflects the heat radiation

reaching it to minimize the absorption and hence reduces the thermal lens effect. Optimization of the solid angle by varying bore diameter and bore length is described as the second and third methodology to reduce the net heat radiation reaching the window. A linear relation between the amount of heat absorbed and the effective focal length was assumed for all the compensation techniques. The same formulation for estimation of heat absorbed in the windows for CVL variants operating at two different temperature regimes was used by R. Biswal et.al [2.31] in their studies.

### **2.6.6.1.1. Infrared Reflector Windows:**

Among many compensation techniques reported, thin-film technology based solutions are not explored to best of the knowledge available. The compensation technique in which heat radiation incident on the multilayer-coated window is reflected on to the water-cooled metal electrode was analyzed. This may reduce the temperature rise of the window and hence decreased the thermal lens effect [2.36-2.38]. In this section, the design of a thin film multilayer dielectric coated window, which will be reflecting the incident heat radiation while transmitting the laser wavelengths.

Thin-film coating design was required to reduce heat radiation absorption in the glass window. This design was based on the wavelength band and power of emitted heat radiation, the amount of radiated heat reaching to the window and fraction of this power absorbed in the fused silica window.

The temperature of the discharge tube ranges from 1450 to 1650 degrees Celsius. Radiation emitted from hot discharge tube spreads

over wavelength range having a maximum wavelength ( $\lambda_{\max}$ ), which is governed by Wien's law as given below in Eqn. (9):

$$\lambda_{\max} = b/T_0 \quad (11)$$

Where  $b$  is Wien's displacement constant ( $2.898 \times 10^{-3}$  mK) and  $T_0$  is the temperature of the emitting material in Kelvin. The maximum wavelength of the emitted radiation was calculated to be  $1.51\mu\text{m}$  to  $1.68\mu\text{m}$  corresponding to a temperature of  $1650^\circ\text{C}$  and  $1450^\circ\text{C}$  respectively. The window design was planned to achieve maximum reflectance for the wavelength band.

### **A) Multilayer Dielectric Thin-Film Design:**

Multilayer dielectric coating manipulates the characteristics of the optical components as per the technological requirements. A multilayer (14 layers) dielectric coated fused silica window (10 mm thickness) was designed for reducing the absorption of incident heat radiation. The angle of incidence was taken as 5 degrees to avoid pseudo cavity effects. Multilayer design of sequential deposition of  $\text{TiO}_2$  and  $\text{SiO}_2$  layers was optimized by varying the thickness of the first two and last two layers. This optimization yielded the transmission of more than 99% at the lasing wavelengths of 511 & 578 nm. Reference wavelength for calculating the quarter-wave optical thickness was chosen as 1582 nm to get a reflection of greater than 98% for 1.51 to  $1.68\mu\text{m}$  wavelength band. Detailed design description is summarised in table-2.7, where design parameters and their description is tabulated. First, the second, thirteenth and fourteenth layers were varied to have

## CHAPTER - 2

non-quarter wave thickness, to optimize the transmission and reflection for the desired wavelength band.

*Table 2.7: Design description of IR reflector CVL window*

Design Parameter	Design description
Stack Formula	(LH) <sup>7</sup>
Material (High ref. Index (H) / Low ref. Index (L))	TiO <sub>2</sub> /SiO <sub>2</sub>
Angle of incidence	5 degree
Reference wavelength	1582 nm
No. of layers	14 Nos.
No. of optimized layers	Two starting layers and two ending layers
Transmittance	T <sub>avg</sub> at 510.6 nm =99.44 nm /T <sub>avg</sub> at 578.2 nm =99.59 nm  T <sub>avg</sub> at 1450 nm to 1780 nm <1%

The optical thickness of the optimized design is elaborated in table-2.8.

*Table 2.8: Layer thickness of IR reflector thin film coated window*

Layer No.	1	2	3	4	5	6	7	8
Material	SiO <sub>2</sub>	TiO <sub>2</sub>						
Layer thickness	280.80	172.93	272.38	171.57	272.38	171.57	272.38	171.57
Layer No.	9	10	11	12	13	14		
Material	SiO <sub>2</sub>	TiO <sub>2</sub>	SiO <sub>2</sub>	TiO <sub>2</sub>	SiO <sub>2</sub>	TiO <sub>2</sub>		
Layer thickness	272.38	171.57	272.38	171.57	299.52	149.76		

### **B) Characteristics of IR Reflector Window Design:**

The transmission characteristics of this design are shown in fig.2.35.

Transmittance at lasing wavelengths i.e. 510.6 nm and 578.2 nm are marked with arrows. It can be seen that these values are more than 99%, as desired. Transmittance for the undesired band of wavelengths i.e. 1.5 to 1.7 μm is less than 1-2%. Therefore, 98-99% of the incident

heat radiation power will be directed to the internal structure of the metallic electrode.

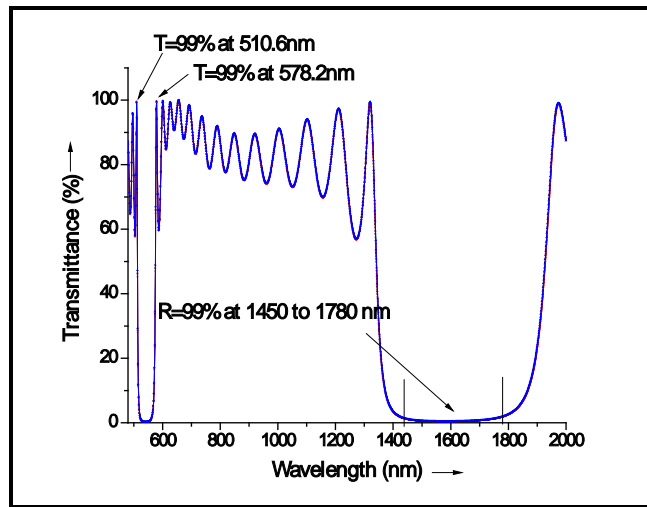


Figure 2.35: Transmittance curve of the designed IR reflector window

Therefore, the absorption of IR radiation in the window is prevented. This reflected heat on the electrode internal structure will be cooled by flowing cooling water through the electrode.

**C) Effect of IR Reflector Window on the Thermal Lens:**

The reflectance values achieved by this design (>98%) for IR wavelengths leads to the reduction of heat absorbed and the resultant benefit in the thermal lens has been evaluated. Heat absorbed by the window reduced from 0.47 W to 0.0094 W due to heat reflector thin-film coated windows. Since a resultant focal length of about 50 m was measured due to 1.17 W of absorbed heat, hence the increase in the resultant focal length from 50 m to 1250 meter was calculated at reduced absorbed heat of 0.0094 W due to IR reflector window. This results in the reduced thermal lens effect in the CVL amplifiers. A linear relation between absorbed heat and power of the resultant thermal lens was assumed for this estimation.

2.6.6.1.2 Reduction of Bore Diameter:

Heat radiated by a hot discharge tube reaching the electrode parts depending on its solid angle. The effect of varying the bore diameter on the solid angle was calculated. The amount of heat absorbed in the window manifested by this variation was analyzed and results are plotted in fig. 2.36.

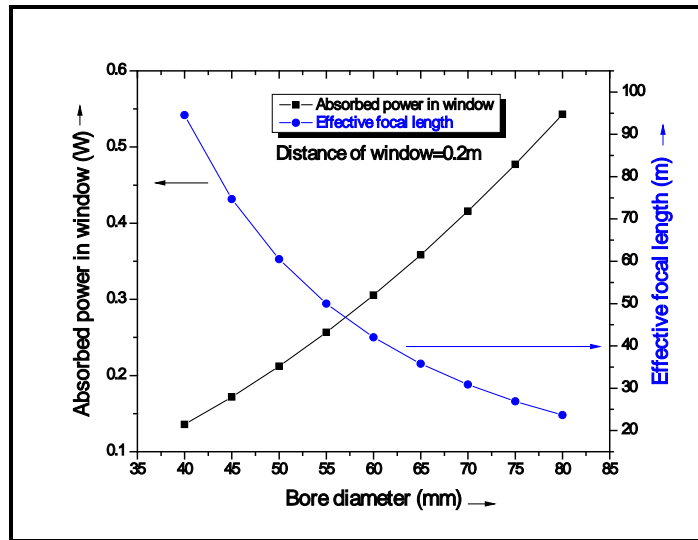


Figure 2.36: Effect of bore diameter on absorbed power and effective focal length

It was observed that on increasing the bore diameter (black, square in fig. 2.36) from 40 mm to 80 mm resulted in the increased absorbed power from 0.14 (single window) W to 0.54 W in the window. Consequently, a decrease in effective focal length (blue circle in fig. 2.36) from 94 m to 22 m was obtained. This result shows that thermal lensing is less effective for smaller bore diameter and shows severe effects for large bore diameter. This may be due to the direct proportionality of the bore area on the solid angle (eqn. 9). The smaller angle subtended at the window resulted in lesser heat reaching to the window and hence reduced thermal effect. The distance of the window from the hot discharge tube was taken as 200 mm (bore length of CVL-40 system)

for these calculations. The bore diameter of 45 mm calculated to be optimum for minimum thermal lens effect in this CVL-40 laser system. All these results were used for the design of a prototype system of the CVL.

### **2.6.6.1.3 Increasing the Bore Length:**

Increasing the separation between the window and the discharge tube proposed as the third method to reduce the effect of thermal lensing on the individual systems. In this case, a 55 mm bore (window, CVL-40 system) diameter for calculations was used. Variation of the separation from 100 mm to 600 mm (fig. 2.37) decreased the absorbed power in the window from 1.04 W to 0.1W. This has resulted in the increasing effective focal length from 12 m to 497 m. This concludes that the more the separation distance, the lesser will be the thermal lens effect. This is due to the inverse relation between solid angle and the separation distance. Higher separation distance resulted in a reduction of solid angle and hence reduced the heat radiation reaching to the window.

By comparing the results plotted in fig. 2.36 and fig. 2.37, it is found that the reduction of bore diameter and increasing separation distance minimize the thermal lens effect. Therefore, one has to consider both the effects together to arrive at the optimum geometry for minimum thermal lens effect, which is shown in fig. 2.38. Effective focal length was calculated for various bore diameter values from 40 to 80 mm. These were analyzed for different separation distances from 100 to 600 mm, which are plotted together.

## CHAPTER - 2

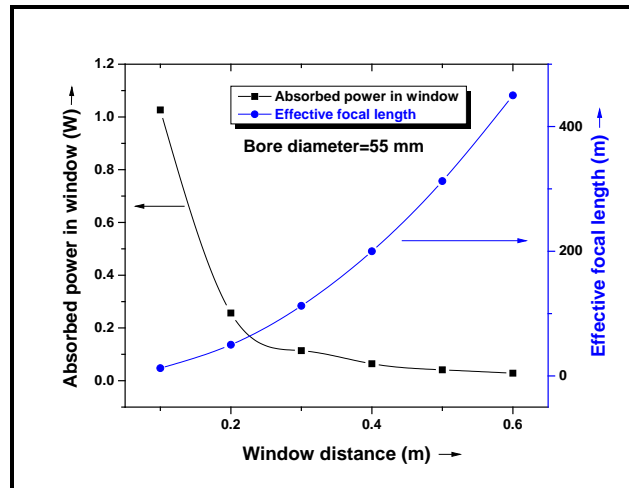


*Figure 2.37: Effect of window distance on effective thermal lensing*

Effective focal length was calculated for bore diameters varied from 45 mm to 70 mm at various separation distances ranging from 100 mm (0.1 m) to 600 mm are plotted together as shown in fig. 2.38.

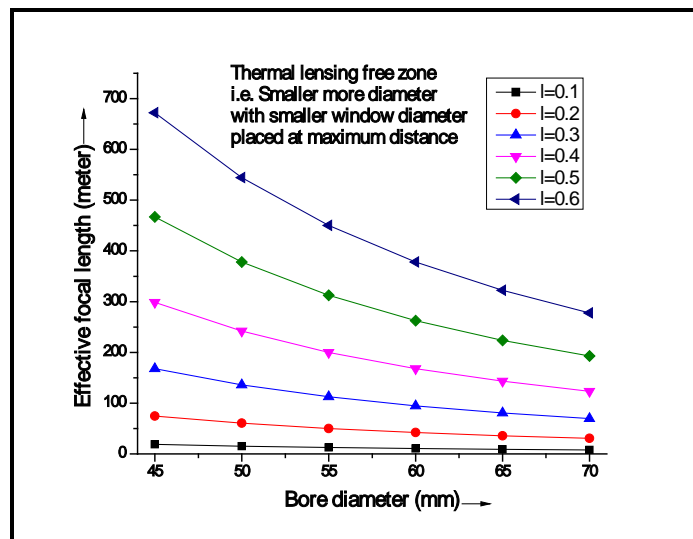


*Figure 2.38: Optimization of the solid angle for minimum thermal lens*

Calculated effective focal length at various separation distances at different bore diameters shows that, the thermal lens was least effective at minimum window (bore) diameter and maximum separation of the window from the discharge tube. This, in turn, is the manifestation of a solid angle to minimize the heat radiation reaching to the window. For 40 W, CVL system window

diameter of 45 mm and separation distance of 600 mm shows a minimum thermal lens effect (effective focal length  $\sim 650$  m) due to windows. Lens effect due to buffer gas pressure was neglected here because the focal length of the thermal gas lens at optimum gas pressure is constant. The higher separation distance between the hot discharge tube and the window will make the system lengthier. Therefore, this technique is not recommended. However, smaller bore diameters with IR reflector windows will minimize the thermal lens and make the system compact as well. The first and second options for compensation in an individual CVL system seem to be suitable based on these analyses.

### **2.6.6.2 Thermal lens compensation in MOPA Configuration:**

The role of the thermal lens becomes prominent for MOPA chains due to the presence of several equivalent lenses in series separated by some fixed distance. Efficient MOPA operation requires that the beam diameter should be the same as the every amplifier gain diameter. Therefore, compensation in between amplifier stages becomes essential to recover the beam diameter, reduced due to the presence of a positive lens effect in the amplifier unit. Four compensation approaches have been theoretically studied using the ray-tracing model. Analysis using a paraxial ray approximation based matrix method was carried out and discussed as follows.

#### **2.6.6.2.1 Slightly Divergent Beam to First Amplifier:**

A collimated beam of optimum beam diameter was launched in the first amplifier for subsequent amplification in the MOPA chain. It is assumed a perfectly collimated beam as a parallel ray (angle  $\sim 0^0$ ) having zero degrees angle with the propagation axis, although it should have resonator defined

## CHAPTER - 2

---

divergence. In the first scheme, it is considered a slightly divergent beam having an angle of 0.0001 degrees (1.75 micro-radian) with the propagation axis instead of 0 degrees (perfectly collimated beam) launched to the first amplifier. The effect of launching a slightly diverging beam on the beam diameter at the exit of every amplifier stage of a MOPA chain was calculated using the ray-tracing model. It was observed that beam diameter was increased at every amplifier stage of the MOPA chain. Beam diameter at first amplifier stage (38.5 mm) was larger than the gain dimension (38 mm) with a divergence angle of 0.0005 degrees. This results in the power loss at the gain boundaries. Therefore, the diverging angle limit is approximately 0.0005 degrees, beyond which this technique will have less advantage.

Power gain at every stage was calculated by estimated diameters at the exit of every amplifier stage and tabulated in table-2.9. The diameter will gradually reduce due to the presence of a thermal lens effect in an amplifier length of 2250 mm, which results in the higher beam diameter at the entry point than at the exit. Amplifier power gain values were calculated using diameter at the exit of the amplifier so that, actual extractable power values will always be higher than these estimated values. Enhancement in the amplifier power gain was observed at every stage when the angle of divergence was increased from 0 degrees (collimated beam) to 0.0005 degrees (slightly divergent). It can be seen that amplifier power gain at the seventh stage increased from 0 to 1.8 at a divergence angle of 0.0005 degrees. This implies that the compensation in the CVL MOPA chain is necessary to utilize the entire gain volume as well as length.

## CHAPTER - 2

*Table 2.9: Effect of the diverging beam on stage-wise power gain in the CVL MOPA chain*

Divergence angle	Power gain (W) at the amplifier stage of the CVL MOPA						
	1	2	3	4	5	6	7
Un-collimated	35.5	29.5	21.2	12.4	5.0	No gain	No gain
Collimated	35.5	29.5	21.2	12.4	5.0	No gain	No gain
0.0001	36.6	31.4	23.6	14.7	6.8	1.5	No gain
0.0002	37.6	33.4	26.0	17.2	8.8	2.6	No gain
0.0003	38.8	35.5	28.7	19.9	11.0	4.0	No gain
0.0004	39.9	37.6	31.4	22.8	13.5	5.7	0.9
0.0005	41.0	39.8	34.3	25.9	16.3	7.7	1.8

Sixth and seventh amplifier module was not contributing to the power gain in an un-compensated eight module MOPA configuration. These stages added the power of 7.7 W and 1.8 W respectively in the thermal lens compensated arrangement by launching a diverging oscillator beam.

These amplifier power gain values were added together to estimate the total extractable power in an eight module CVL MOPA chain. The oscillator output of 12.5 W after the spatial filtering was used for entire power gain estimations. Fresnel losses at the windows and reflections losses at mirrors were neglected for the output power calculations. Total calculated extractable power in eight modules MOPA was increased to 181W from 117 W with an increase in the diverging angle as shown in fig. 2.39.

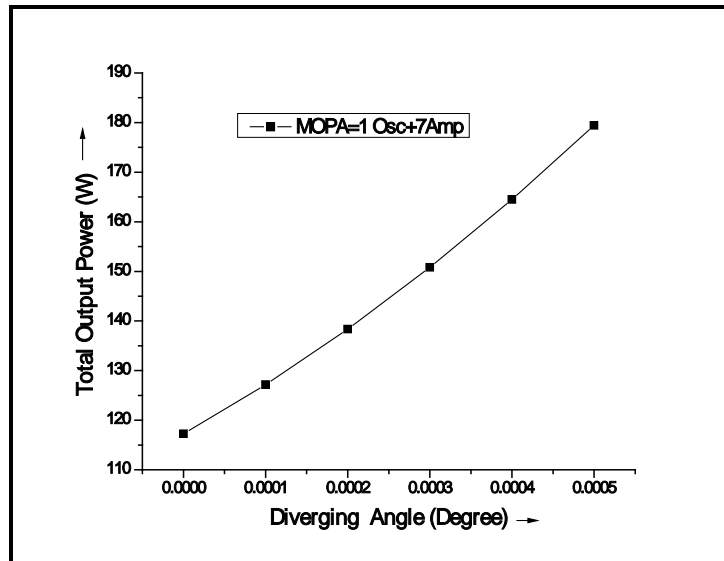


*Figure 2.39: Extractable MOPA output power with a slightly divergent beam to the amplifier*

This compensation scheme shows significant enhancement (55%) in the total extractable power. The proposed small divergence beam can be generated by changing the separation between the concave mirrors (unit magnification) in the spatial filtering unit of the oscillator. The diverging input beam compensated the converging effect that arises due to the thermal lens, which reduces the amount of decrement of the beam diameter at every stage of the MOPA chain. This resulted in more overlap between the gain diameter of the amplifier and the input beam diameter at every amplifier stage. This increases the extractable power from the longer MOPA chain.

#### **2.6.6.2.2 Single Stage Re-collimation:**

In the second compensation scheme, the thermal lens induced converging beam between amplifier stages of the CVL MOPA was collimated after one of the amplifier modules. The effect of re-collimation by adjusting the thermal lens induced convergence angle of the beam to zero for one of the amplifier stages. Beam diameter was calculated, by following the ray tracing matrices

## CHAPTER - 2

for remaining amplifier stages in the MOPA chain. Effect of re-collimation after 2<sup>nd</sup> to 5<sup>th</sup> amplifier stages on amplifier power gain one at a time for a seven-amplifier chain was evaluated and tabulated in table-2.10.

*Table 2.10: Effect of re-collimation on stage-wise power gain in CVL MOPA chain*

Re-collimation stage	Power gain (W) at the amplifier stage of the CVL						
	1	2	3	4	5	6	7
Un-compensated	35.5	29.5	21.2	12.4	5.0	No gain	No gain
After 2 <sup>nd</sup> amp	35.5	29.5	27.6	22.9	16.5	9.6	3.9
After 3 <sup>rd</sup> amp	35.5	29.5	21.2	19.8	16.5	11.8	6.9
After 4 <sup>th</sup> amp	35.5	29.5	21.2	12.4	11.6	9.7	6.9
After 5 <sup>th</sup> amp	35.5	29.5	21.2	12.4	5.0	4.8	3.9

It can be seen from the table-2.10 that, power gain at every stage increased as compared to the un-compensated case. Total MOPA output power with re-collimation after the 2<sup>nd</sup> to 5<sup>th</sup> stage is calculated and plotted in fig. 2.40.

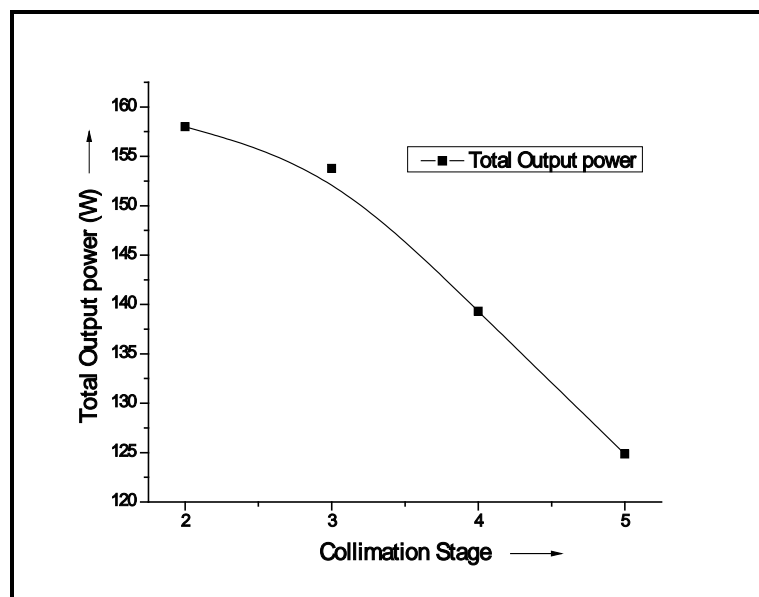


*Figure 2.40: Extractable power due to stage-wise re-collimation in MOPA chain*

Extractable power reduces when the re-collimation is done at the later stages (4<sup>th</sup> and 5<sup>th</sup>) as compared to earlier stages (2<sup>nd</sup> and 3<sup>rd</sup>). Power addition in the

sixth and seventh stages was less, while re-collimation was performed after the fifth stage. It is because, collimating the beam at later stages is less effective, due to diameter reduction to a smaller value to get the benefit of the re-collimation. The highest extractable power was achieved when the re-collimation was incorporated after the second stage as compared to the third stage. Re-collimation of the beam in between amplifier stages helps to reduce the converging history of earlier stages and the beam diameter reduces at a slower rate. This helps in an improved overlap of the extracting beam volume and available amplifier gain volume, which resulted in the increased extractable power from the entire MOPA chain.

As per the analysis, re-collimation after the second stage is recommended for the maximum power extraction in the MOPA chain. This compensation technique can be implemented by using a pair of concave mirrors with unit magnification placed at a suitable confocal distance after the second amplifier. Re-collimation of the converging beam can be achieved by adjusting the separation between concave mirrors.

### **2.6.6.2.3 Dual Stage Re-collimation:**

Re-collimation of the laser beam at two stages instead of a single-stage is proposed as the third compensation technique. Available power gain at the exit point of each amplifier of the MOPA chain was calculated using the compensated beam diameter values and tabulated in table-2.11. It was observed that amplifier power gain increased significantly as compared to the un-compensated case. Sixth and seventh amplifier starts contributing significantly in the power addition, whereas power gain in the fifth amplifier

## CHAPTER - 2

increased to a higher value. This shows an overall improvement in power extraction with more CVL units in a longer MOPA chain.

*Table 2.11: Effect of re-collimation after two stages on power gain in CVL*

### MOPA chain

Re-collimation stages	Power gain (W) at the amplifier stage of the CVL MOPA chain						
	1	2	3	4	5	6	7
Un-compensated	35.5	29.5	21.2	12.4	5.0	No gain	No gain
after 2&4 amp	35.5	29.5	27.6	22.9	21.5	17.8	12.8
after 3&5 amp	35.5	29.5	21.2	19.8	16.5	15.4	12.8
after 4&6 amp	35.5	29.5	21.2	12.4	11.6	9.7	9.0
after 2&5 amp	35.5	29.5	27.6	22.9	16.5	15.4	12.8
after 3&6 amp	35.5	29.5	21.2	19.8	16.5	11.8	11.1

Set of re-collimation stages were planned after 2<sup>nd</sup> and 4<sup>th</sup>, 3<sup>rd</sup> and 5<sup>th</sup>, 4<sup>th</sup> and 6<sup>th</sup>, 2<sup>nd</sup> and 5<sup>th</sup>, 3<sup>rd</sup> and 6<sup>th</sup> stage of the amplifier in the thermal lens model of the MOPA chain. The trend of stage-wise beam diameter variation and amplifier gain shows that the effectiveness of the dual-stage re-collimation is more for earlier stages (2<sup>nd</sup> and 4<sup>th</sup>) than at the later stages (4<sup>th</sup> and 6<sup>th</sup>). It was also noticed that the gap between the two stages (2<sup>nd</sup> and 4<sup>th</sup>) was more beneficial than that of three stages (2<sup>nd</sup> and 5<sup>th</sup>). There is no advantage of re-collimation at the later stages, as the beam size is reduced already too much to achieve the benefits gain from the re-collimation of the beam.

Extractable power in the MOPA chain of eight CVL modules was estimated by adding available amplifier gain at each amplifier stage with re-collimation at several different locations and is tabulated in table-2.12 for comparison. The advantage of re-collimation at earlier stages was evident from these output power values. Therefore, double re-collimation at earlier stages with a gap of

## CHAPTER - 2

two amplifier modules is the best possible technique among the dual-stage re-collimation configurations studied for the eight modules MOPA chain.

*Table 2.12: Relative output power after dual re-collimation (DR)*

Comparison parameter	No compensa tion	DR after A-2&4	DR after A- 3&5	DR after A- 4&6	DR after A- 2&5	DR after A- 3&6
Max. power	117	180	163	141	173	158
Rel. Benefit	Same	53.8%	39.3%	20.5%	47.9%	35%

### 2.6.6.2.4 Re-collimation and Beam Diameter Recovery (RBDR):

In the fourth method, the studies were concentrated on the effect of increased diameter and re-collimated beam. In earlier techniques, a unit magnification of the concave mirror was proposed, whereas in this technique magnification of more than 1 is proposed to increase the beam diameter to its initial value i.e. 37mm. Increasing the beam diameter to initial value is termed as beam diameter recovery. Stage wise re-collimation and beam diameter recovery after the 2<sup>nd</sup> to 6<sup>th</sup> amplifier stage was analyzed and illustrated in table-13. In this technique, beam diameter was adjusted to the initial values so that the lens effect history of previous stages becomes ineffective. Hence, the beam of restored diameter will see the thermal lens effect encountered in the following amplifier stages only. Re-collimation of the beam in addition to the diameter recovery is advantageous to eliminate the thermal lens effect of the previous amplifying stages. This becomes an equivalent arrangement of smaller MOPA chains (2-3 amplifiers) arranged together in tandem to set up a longer MOPA chain. Amplifier power gain calculated using the modified beam diameter is

## CHAPTER - 2

described in table-2.13. A significant advantage is observed in the calculated values of the power gain.

*Table 2.13: Effect of RBDR on stage-wise power gain in CVL MOPA chain*

CBDR stage	Power gain (W) at the amplifier stage of the CVL MOPA						
	1	2	3	4	5	6	7
Un-	35.5	29.5	21.2	12.4	5.0	~ 0	~ 0
After amp-2	35.5	29.5	35.5	29.5	21.2	12.4	5.1
After amp-3	35.5	29.5	21.2	35.5	29.5	21.2	12.4
After amp-4	35.5	29.5	21.2	12.4	35.5	29.5	21.2
After amp-5	35.5	29.5	21.2	12.4	5.1	35.5	29.5

The effect of implementing the technique in total extractable power is tabulated in table-2.14. It can be seen that the total extractable power was highest 197W after the 3<sup>rd</sup> stage. Total power was the same for compensation after 4<sup>th</sup> stage as well. Extractable power reduced to 181W when compensation was done after the 2<sup>nd</sup> and 5<sup>th</sup> stages. It may be because the extent of advantage of diameter recovery is higher at the 3<sup>rd</sup> stage as compared to the 2<sup>nd</sup> stage. However, losses have already occurred too much at the 3<sup>rd</sup> and 4<sup>th</sup> stage to get any advantage due to diameter recovery.

*Table 2.14: Relative output power after re-collimation and beam diameter recovery (RBDR)*

Compensation stage	No compensation	RBDR after A-2	RBDR after A-3	RBDR after A-4	RBDR after A-5
Max. power	117	181	197	197	181
Relative benefit	same	54.7%	68.4%	68.4%	54.7%

## CHAPTER - 2

---

Implementation of this scheme after 3<sup>rd</sup> stage was more advantageous because the diameter value at these stages significantly reduced due to the thermal lens effect and hence adjusting the beam diameter to initial value made a significant difference in the amount of the beam diameter recovery, which results in the highest MOPA output power.

This compensation technique can be implemented by incorporating a pair (non-unit magnification) of a concave mirror, setup in confocal geometry in-between stages. Magnification of the mirror pair is required to be chosen depending on the extent of the required beam diameter recovery. This will magnify the reduced beam diameter to initial value along with re-collimation.

### 2.6.6.2.5 Comparison of Compensation Techniques:

A comparison of maximum extractable power was carried out and values are tabulated in table-2.15. Among four compensation techniques analyzed, re-collimation and beam diameter recovery based techniques were found to be most suitable for thermal lens compensation.

*Table 2.15: Relative comparison of the compensation schemes in amplifiers*

Compensation scheme (MOPA: 1Osc.+7Amp.)	No compensation	Divergent Beam of the oscillator	Re-collimation after A-2	Dual re-collimation after A-2&4	RBDR after A-3 or A-4
Maximum power (W)	117	179	158	180	197
Comparison	same	53%	35%	54%	63%

Re-collimation at two stages increased the extractable power in the MOPA chain. Single-stage re-collimation is a simpler technique but it does not seem

## CHAPTER - 2

to be the most efficient scheme. Launching a slightly divergent beam to the first amplifier is capable of extracting higher powers but controlling the angle is very tricky. Higher than optimized angle may cause an increase in the beam diameter to more than the maximum gain volume and may suffer higher losses at the gain boundaries due to aperturing effect.

Eight module MOPA with thermal lensing minimization using hybrid compensation techniques is proposed in fig. 2.41. The layout is proposed by using minimum high reflectivity mirrors to reduce losses at later stages.

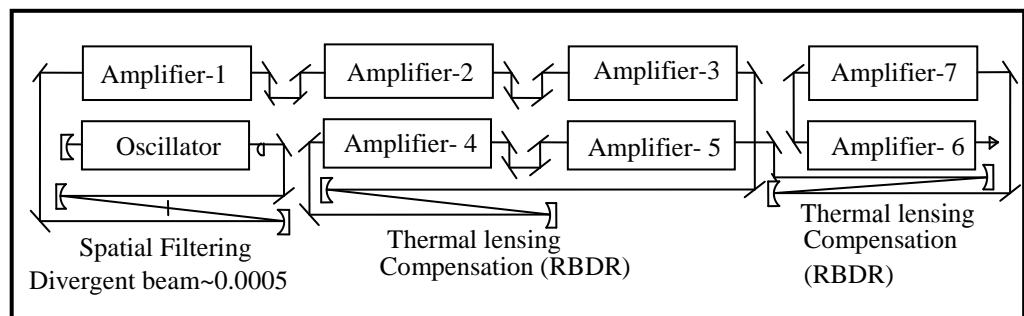


*Figure 2.41: Schematic of thermal lensing compensated (proposed) MOPA*

The hybrid technique includes the simultaneous implementation of two compensation techniques i.e. slightly divergent beam from oscillator to the first amplifier stage and re-collimation and beam diameter recovery (RBDR). These are implemented in the design shown in fig.2.41. The divergent beam was launched in the first amplifier, whereas re-collimation and beam diameter recovery is proposed after the third and fifth amplifier.

In this scheme, slightly divergent beam (0.0005 degree) is proposed to be generated by pair of mirror used in the spatial filtering section of the oscillator, whereas a separate pair of mirrors with suitable radius of curvature (magnification based on difference in beam diameter) are planned after third & fifth stage for re-collimation and beam diameter recovery in the MOPA chain.

## CHAPTER - 2

---

Maximum compensation can be achieved in this hybrid scheme, because a slightly divergent beam compensates up to 3<sup>rd</sup> amplifier stage, whereas re-collimation and beam diameter recovery compensate in the remaining stages. Total extractable power in the proposed eight modules CVL MOPA chain with hybrid thermal lensing compensation was calculated to be around 257 W, which is 2.2 times the total extractable power in the un-compensated case (117W). This shows the importance of the thermal lens compensation technique for CVL MOPA chains described in this chapter.

### **2.7 Conclusions:**

Indigenously developed CVL: 40 system with different resonator configuration was characterized for divergence and average power optimization. An unstable resonator with a magnification of 75 was optimized to generate a laser beam with a beam divergence of 0.4 mrad and an average power of around 30W. The green to yellow ratio was measured using this laser system. The effect of input electrical power on the G/Y ratio was studied which shows a decrease in green to yellow ratio for the higher input electrical input power. Multilayer thin-film designs for single wavelength emission were proposed. Multilayer dielectric thin film coating design to meet the optical design requirement was formulated. The optical design is capable of converting the dual-wavelength CVL to the single color laser system, which can be optimized for efficient green or yellow emission. This design will improve the efficiency and compactness of the CVL system which will have applications in laser-based medical treatments like photodynamic therapy. These have a promising application in a compact and efficient single wavelength CVL laser system.

## CHAPTER - 2

---

Power addition in an amplifier of the long MOPA chain was experimentally determined and it was found that lower power addition at higher input was due to higher percentage Fresnel losses occurring at the higher input power. Four CVL MOPA configurations for maximum power extraction from a six-module chain were theoretically analyzed using this input modulated power gain of the amplifiers. The single long chain has the advantage of a simpler configuration generating a single output beam but has a disadvantage of lower extractable power and the need for a thermal lens compensation technique to be implemented. Total power extracted is found to be maximum in periodic power withdrawal configuration owing to the maximum operable gain in all the constituent amplifiers. The third configuration is the best suited in terms of power but in this case, handling multiple beams using optical fibers is cumbersome. Splitted chain after amplifier came out to be the most efficient MOPA configuration with only two output beams at the similar end of the chain which is easier to utilize further. Splitted chain after the amplifier is the best configuration among all of them which generates maximum power in addition to the elimination of thermal lens compensation requirement.

The thermal lens is an inherent character of the metal vapor laser system such as CVL. Characterization of the thermal lens is important for choosing the appropriate configurations of the CVL MOPA system. A novel technique for effective focal length determination of the amplifier using a collimated oscillator beam was demonstrated. This technique proved to be simple and effective for oscillator-amplifier configuration without any additional laser beam. An effective focal length of the resultant convex lens at the optimum operating parameters was measured to be approximately 50 meters. Effect of input electrical power and

## CHAPTER - 2

---

buffer gas pressure on the resultant thermal focal length of the individual CVL was measured and the contribution of electrical power was found to be more prominent as compared to the buffer gas contribution. The thin-film coated IR reflector window shows its role in the reduced absorption of incident thermal radiation. The salient feature of this design was a lesser number of layers, high rejection ratio for undesired wavelength range and very high transmission in the desired laser wavelengths. This technique may contribute to the reduction of the thermal gradient along the length of the discharge tube as a rejected portion of the heat radiation is directed towards the electrode. The role of thermal lens in an 8-module MOPA chain was theoretically analyzed and suitable thermal lens compensation techniques for this MOPA configuration were suggested. The analysis was carried out by paraxial approximation using ray tracing system matrices. Reduction of the beam diameter and resultant amplifier gain due to beam volume and gain volume overlap was analyzed for several compensation techniques. Among four compensation techniques for MOPA configurations, re-collimation and beam diameter recovery technique using a non-unit magnification pair of concave mirrors was found to be yielding maximum output power in an eight-module MOPA chain. A hybrid compensation technique using a slightly divergent beam from oscillator and re-collimation with increased beam diameter after the third and fifth amplifier stage seems to be suitable for MOPA operation. The compensation techniques studied here will be useful for obtaining maximum output power in a longer MOPA chain. These compensation techniques can be employed for any MOPA system as per the required applications. Thermal lensing plays a crucial role in CVL MOPA configurations and its compensation is mandatory for efficient laser generation from a CVL MOPA chain.

# Chapter: 3

## The Dye Gain Medium

---

### 3.1 Introduction:

Dye gain medium is one of the important constituents for generating high power, high pulse repetition rate dye laser pumped by copper vapor laser (CVL). Tunable, high power dye lasers operating at different wavelengths were required for the spectral beam combination studies. Versatility in the dye lasers is a consequence of exceptional properties inherited by its gain medium i.e. fluorescent laser dyes. Fluorescent laser dye has higher gain suitable for high power applications [3.1-3.4]. Laser dyes can be used as a gain medium in liquid as well as the solid phase. The fluorescent laser dye dissolved in suitable solvents is used in the liquid phase. The heat removal becomes efficient in the liquid dye gain medium for generating high average power with a higher repetition rate of the dye laser. Multi-wavelength generation is well suited in the dye lasers due to its wide spectral range from 400 nm to 1100 nm, which is achieved by using various fluorescent laser dyes and their combinations. Fluorescent laser dye is dissolved in a solvent and circulated through a dye cell to form the gain medium for the dye laser. Hydrodynamically designed and characterized dye cell is the key to provide a superior quality gain medium. The quality of gain medium is an essential requirement to achieve narrow bandwidth laser from the dye oscillator which further generates high power using a master oscillator power amplifier (MOPA) configuration. Therefore, computational fluid dynamics (CFD) optimized and indigenously developed dye cell was characterized and used in the dye laser for this study.

Most of the laser dye molecules are polar, hence the polarity of the solvent is an important parameter that determines the shifting of the emission wavelength [3.6]. The heating due

## CHAPTER - 3

---

to non-radiative decay of the dye molecule in case of a large stoke shift can affect the laser characteristics more strongly than the lower stoke shift dyes. The quantum yields and fluorescence lifetimes are lower and strongly temperature-dependent in the non-polar solvents [3.6]. Several polar and non-polar solvents such as water, heavy water, ethanol, methanol, dioxane, n-heptane, ethylene glycol, dimethyl sulfoxide (DMSO), glycerol and mixtures of solvents were used to improve the thermo optical characteristics of a high repetition rate dye laser [3.7– 3.11].

Interestingly, absorption and emission characteristics of the laser dyes can be further tailored using different solvent environments. Therefore, studies were carried out to understand the behavior of the absorption and the emission characteristics of the dyes due to variation in the solvent environment by use of different solvents, their binary mixture and changing the pH of the solvent. The binary laser dye mixtures are used to extend the emission wavelength range [3.23]. Therefore, it becomes important to study the binary laser dye mixture to be pumped by second harmonic of Nd: YAG laser to extend the spectral emission from the dye laser for the spectral beam combination experiments. The effect of pH, various solvents, binary solvent mixtures, and binary dye mixtures was studied for shifting the dye emission wavelength during the present research work. SulfoRhodamine (SRh 101) and Rhodamine 101 (Rh 101) laser dyes were selected to be pumped by the yellow wavelength of the CVL and ethanol/methanol/water were used as the solvents for these laser dyes. The effect of pH variation as well as the effect of solvent polarity on the photo-physical properties of SRh 101 dye is described in the first section (3.2) of this chapter. Thermo-optic properties of the dye solvent play a significant role in the generation of high average power from dye lasers, hence the measurement of the thermo-optic coefficient for the commonly used dye solvents such as water, ethanol and their volumetric mixture (water + ethanol) were studied and presented in the second

section (3.3). The thermo-optic properties of the water-ethanol mixture motivated us to study the dye laser using this binary solvent. The emission characteristics of SRh 101 dye dissolved in the ethanol-water binary mixture was studied. The use of a binary solvent with SRh 101 laser dye not only red shifted the peak emission wavelength but also increased the conversion efficiency. A mixture of fluorescent laser dyes is well known for increasing the wavelength tuning range of the dye laser. Widening of the tuning range using PM567 and DCM dye mixture was demonstrated in an intra-cavity beam combined multi-wavelength dye laser. The utilization of the dye mixture for generating three wavelengths, which doubled the wavelength tuning range, is elaborated in the fourth section (3.5). The essential spectral aspects of the dye gain medium necessary for high power, pulsed dye laser generation required for spectral beam combination studies are presented here in this chapter, which are as follows:

### **3.2 Effect of pH on Photophysical Properties of Rh 101 Dye:**

The pH is a numeric scale used to specify the acidity or alkalinity of an aqueous solution. It is the negative of the logarithm to base 10 of the activity of the hydrogen ion. Solutions with a pH less than 7 are acidic and greater than 7 are alkaline. Acidified and basified solvent shifts the equilibrium for the dye molecule in the excited state [3.5]. This affects the photophysical properties of the laser dye in the solvent. Variation of concentration of H and OH ions in the solvents shifts the spectral characteristics of the dye. Generally, increasing pH shifts the emission towards higher wavelength (redshifting), whereas a decrease in pH results in a blue shift (shifting towards shorter wavelengths) [3.5]. The study was taken up to assess the spectral properties of the dye at various pH values. Rh 101 dye was found most suitable due to its peak absorption around 578 nm, which could be pumped by a yellow beam of the CVL. Its emission wavelength is from 606 nm to 640 nm [3.1].

## CHAPTER - 3

Interestingly, the Rh101 molecule in ethanol possesses equilibrium between its neutral (AH, A represents the chromophore molecule) and anionic forms ( $A^-$ ) in the ground ( $S_0$ ) state depending on pH value. In acidic pH (pH < 7) conditions, the majority of the molecule exists in the neutral form depending on its pH value. However, for excitation with a laser at the excited ( $S_1$ ) state, its  $pK_a$  (i.e; pH value in which both the forms have equal concentrations) value reduces, such that equilibrium shifts toward anionic form. The excitation and de-excitation processes of the Rh101 molecule along with its molecular structure are illustrated in fig. 3.1.

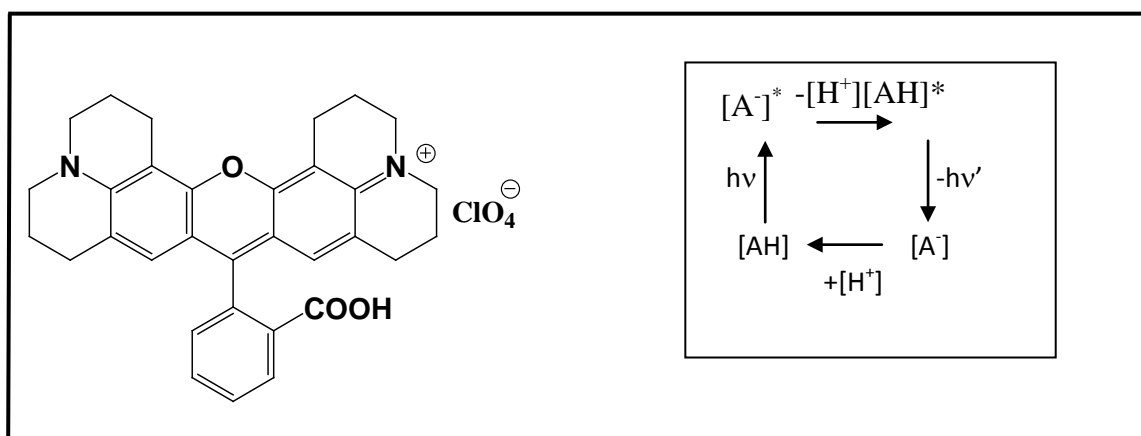


Figure 3.1: Molecular structure of Rh101 dye in neutral/acidic form (AH) and its equilibrium process with anionic ( $A^{-1}$ ) form at the ground ( $S_0$ ) and excited ( $S_1$ ) states, respectively.

With this background, it was intended to modulate the absorption and emission spectra of Rh101 dye in ethanol by suitably changing its pH to obtain efficient and photo-stable laser operation beyond 630 nm, which is scarcely reported. To investigate spectral shifting in the emission of Rh 101 dye, a study has been carried out on the absorption, emission and tuning characteristics of the Rh101 dye solution at various pH values.

### 3.2.1 Variation in The pH of The Dye Solution by Acetic Acid:

Acetic acid was used to vary the pH of the Rh 101 dye solution. High purity laser grade Rh101 dye, spectroscopy grade ethanol and acetic acid were used to study the effect of pH

on the photo-physical characteristics of the laser dye. The variation in pH of Rh101 dye in ethanol was achieved by the gradual addition of acetic acid in microliters. The variation of pH with the addition of acetic acid in the dye solvent is shown in fig. 3.2.

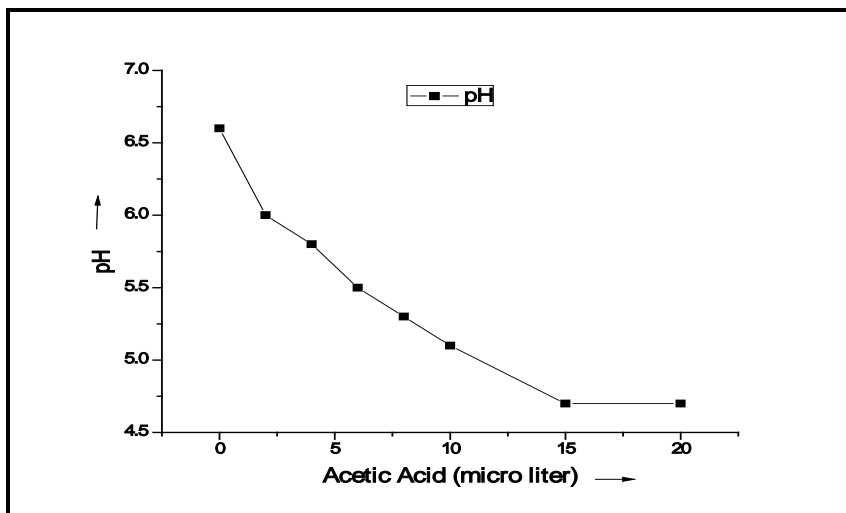


Figure 3.2: Variation of pH by addition of acetic acid in Rh 101 dye in ethanol

The pH of the ethanolic Rh101 dye solution (~40 ml) was found to decrease from 6.6 to 4.7 by the addition of 15  $\mu$ l (mcl) of acetic acid. An increase in the acidic nature of the dye solution was observed to be about 0.2 on the pH meter, while acetic acid in the step of 2  $\mu$ l per step was added. Absorption and emission spectra of a low concentration of Rh101 dye in ethanol (OD <1 for 1 cm cell), in the absence and presence of acetic acid, were obtained using absorption spectrophotometers (Thermofisher Scientific, UV 2700) and steady-state fluorimeter (Horiba, Fluoromax 4). Emission spectra and relative quantum yield of fluorescence of dye solutions were obtained by excitation at 578 nm around the absorption maxima of Rh 101 dye.

### 3.2.2 Effect of pH on Absorption Spectra of Rh 101 Dye Solution:

The absorption spectrum of the pH modulated Rh 101 dye solution was recorded at different pH values. Peak absorption wavelength ( $\lambda_a^{\max}$ ) and OD<sub>max</sub> values has been plotted with the pH of the dye solution and shown in fig. 3.3.

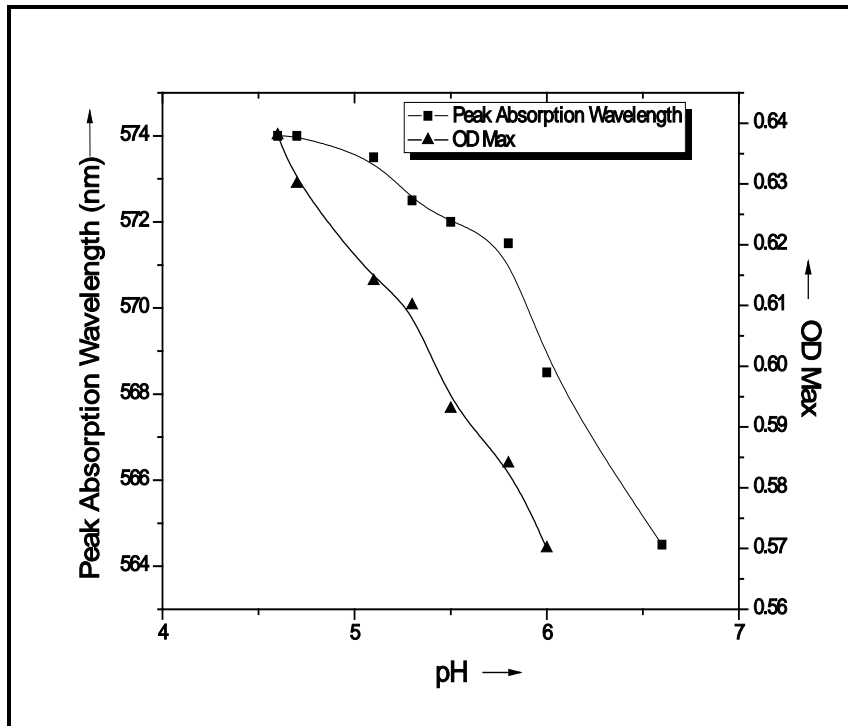


Figure 3.3: Effect of pH on peak absorption wavelength and peak optical density (OD)

The absorption peak of Rh101 dye in ethanol was found to be red-shifted by 9-10 nm with the addition of 10  $\mu$ l of acetic acid (pH  $\sim$  5.1). No further shift in the absorption peak was observed beyond the addition of 10  $\mu$ l of the acetic acid. Optical density (OD) was also found to be increased from 0.580 to 0.638. The higher OD results in the increased absorption of pump laser with increased acidic nature of the solution. A higher addition of acid for further increase in the OD was not tried to avoid corrosion-related complications in the dye circulation systems.

### 3.2.3 Effect of pH on The Emission Spectra of Rh 101 Dye:

Emission spectra of Rh101 (Rh 640) in ethanol at different pH values were measured using commercial fluorimeter (Horiba, Fluoromax 4). The emission characteristics of Rh 101 dye with variation in the pH of the solvent are shown in fig. 3.4.

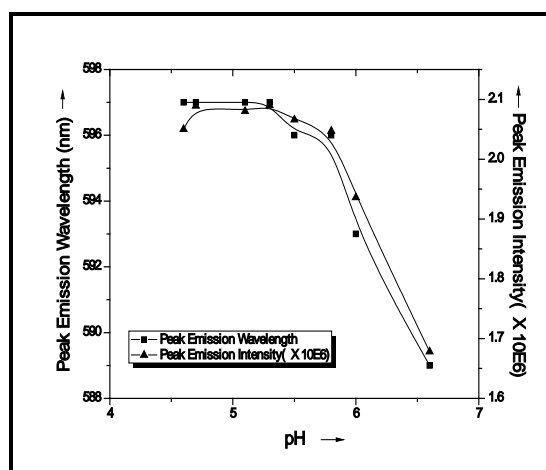


Figure 3.4: Effect of pH on peak emission wavelength and peak intensity

The emission peak was red-shifted by 8 nm by the addition of 8  $\mu$ l of acetic acid (pH~5.1). No significant shift of the fluorescence peak beyond the addition of 6-8  $\mu$ l of acetic acid was observed. The fluorescence characteristics were studied up to 20  $\mu$ l of acetic acid. The intensity of the emission peak was also found to be increased by 1.24 times. This increased fluorescence with increasing acidic nature of the solution indicated the improved quantum efficiency. The peak fluorescence intensity was found to saturate by a further increase of the acidity as shown in fig. 3.4. The inner filter effect is a common problem in fluorescence spectroscopy, affecting spectral measurements in particular. In highly concentrated solutions (O.D. >0.1) the excitation beam is attenuated by the sample so that only the surface facing the excitation beam fluoresces strongly. Due care has been taken during the above fluorescence measurements to minimize this effect. However, the measured tuning range was considered rather than fluorescence measurement for all of our relative studies."

#### 3.2.4 CVL Pumped Dye Laser with Acidic Solution of Rh 101 Dye:

About 200 $\mu$ l of high purity acetic acid was added in Rh101 dye (~pH 5.3) dissolved in ethanol, which measures the pH of the solvent to 5.3. A Grazing incidence Grating (GIG) configured dye laser oscillator with intracavity prism beam expander in non-

## CHAPTER - 3

compensation mode was set up. The acidic Rh101 dye solution was pumped using a yellow beam of CVL for studying the dye laser characteristics. The schematic of the indigenously constructed narrow-band dye laser is shown in fig. 3.5.

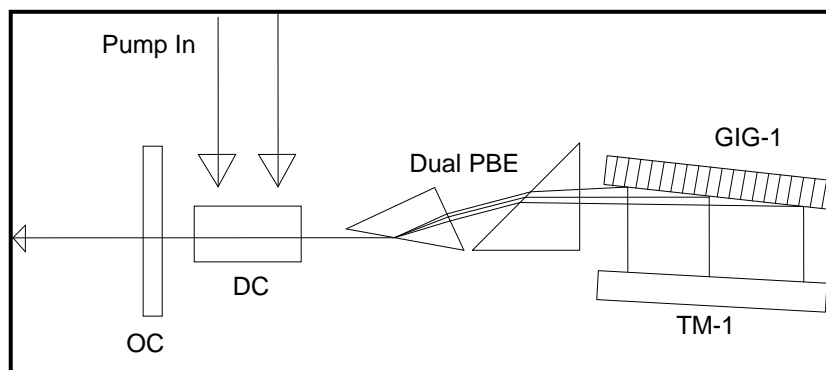


*Figure 3.5: Dye laser cavity set up for performance testing of acidic dye laser*

Laser emission was found to have maximum efficiency at 625nm in 0.5 mM Rh 101 dye solution in pure ethanol. Redshifting of the peak laser emission was achieved by increasing the concentration from 0.5 mM to 1 mM. Further, a redshift of about 2 nm was observed in the tuning range due to the addition of acetic acid. Transmission of the pump beam through the dye cell was found to be increased from 18% to 22 % after the addition of acetic acid. The reduced absorption is attributed to the redshifting in the absorption peak from 578 nm towards higher wavelengths, which resulted in reduced absorption of 578 nm. Dye laser efficiency was found to increase marginally in comparison to pure ethanolic dye solution, which is attributed to improved fluorescence efficiency even with reduced absorption of 578 nm. Photodegradation of the acidic Rh101 dye solution was also monitored during the cumulative operation of the dye laser while monitoring the transmission through the dye cell. No dye photo-degradation was observed for more than 50 hours of operation. Yellow pumped Rh 101 (acidic) dye laser demonstrated and the peak efficiency of approximately 10 % was achieved with a pump power of 20 W. The line width of the dye laser was measured using commercial wavelength meter (Angstrom, WS -7L) and found to be around 2-3 GHz.

### 3.3 Measurement of Thermo-optic Coefficient of Dye Solvents:

The laser dyes in appropriate concentration ( $\sim 0.01 - 10$  mM) dissolved in a suitable solvent play an important role in the overall performance of the dye laser system. As the dye concentration is too small, the physical properties of the solvent play a significant role in the generation of the high average power output from a dye laser. Thermo-optic property of the solvent is one of the important characteristics of the high power operation of the dye laser. It became essential to estimate the thermo-optic coefficient of the solvents and their mixtures during the high power generation intended for spectral beam combination experiments.

The absorption of the pump beam causes a corresponding change in the refractive index gradient due to optically heated dye volume that may cause optical in-homogeneities. The focusing and defocusing of the laser beam inside the gain medium depend on the sign of  $dn/dT$ . It can either lead to converging or diverging behavior. For most of the dye solvents, the temperature coefficient of the refractive index is negative, which results in a divergent thermal lens on the heating of the dye solvents. Adding a thermal lens to the dye laser intra-cavity degrades the wavelength selectivity, increases the beam divergence, frequency stability and random optical fluctuations in the dye laser output. The change in the refractive index with temperature is primarily due to a change in the density of molecules contributing to the polarization for both polar and non-polar solvents. The change in the refractive index with temperature  $dn/dT$  is of the order of  $-10^{-3}$  to  $-10^{-4}$ . The thermo-physical properties such as thermal diffusivity, thermal conductivity, absorption coefficient and fluorescence quantum yield of the dye solution are important parameters for the thermal lens.

It is reported in the literature that, about 25% of pump pulse energy converted into the heat in the dye gain medium, which expands the dye medium [3.12]. This expansion

## CHAPTER - 3

---

propagates outwards as an acoustic disturbance. The expansion time scales depends upon the relative time scales for the acoustic expansion and pump pulse duration. If the pump pulse is much larger than the acoustic transit time the thermal lens is essentially instantaneous. In this case, the change in the refractive index is linearly proportional to the pump pulse energy. In steady-state approximation the variation in the refractive index depends on the physical properties of the dye solvent, hence a figure of merit for the solvent is defined as

$$F_m = \left(\frac{dn}{dT}\right)/(\rho C_p) \quad (1)$$

Where,  $\rho$  is the density of the solvent ( $\text{g cm}^{-3}$ ),  $C_p$  is the specific heat at constant pressure ( $\text{J g}^{-1}\text{K}^{-1}$ ). The variation in the refractive index due to non-radiative relaxation follows the absorption of the pump beam in the dye solvent. The absorption of the pump beam in the dye solvent follows the exponential law (Beer-Lambert Law) in the linear region, which results in a non-uniform refractive index in the dye cell along the pump beam axis [3.12]. The magnitude of the refractive index non-uniformity increases with increasing the dye concentration and the pump power [3.11]. The temperature rise at the focal point in the dye solvent is proportional to  $\alpha P/(\rho C_p)$ , which is followed by the variation of the density in the medium. The refractive index variation is a function of temperature and change in density inside the dye medium [3.9].

$$\Delta n = \left(\frac{dn}{d\rho}\right) T \Delta\rho + \left(\frac{dn}{dT}\right) \rho \Delta T \quad (2)$$

Where  $(dn/d\rho)T$  is the change in the refractive index due to thermal expansion and  $(dn/dT)\rho$  is the temperature-dependent variation in the refractive index. The density change associated with heat source by the generation of the sound wave is relatively small in comparison to the density change that is associated with the thermal expansion of the medium due to heating.

If the  $(dp/dT)_p$  is very small or the constant for the solvent than the refractive index variation is determined by the thermal diffusion. The part of the pump energy absorbed by the dye molecule is converted into the kinetic energy of the molecules on a time scale shorter than the pulse duration. The liquid is heated by the laser beam and simultaneously cooled by the convection currents that arise in the medium due to the flow of the liquid. The heat generated in the gain region of the dye cell is removed by the motion of the liquid. The convection currents due to the motion of the liquid induce asymmetry in the temperature distribution of the gain medium in the dye cell. This asymmetry in the temperature leads to the deflection of the laser beam in its axis. It is known that the dye laser power decreases and the beam divergence increases with increasing dye temperature. An increase in the dye solvent temperature also causes the wavelength shift due to the temperature-dependent refractive index [3.13]. These investigations show that the formation of non-uniform refractive index gradients due to non-uniform heating in the dye gain medium has a major limitation in achieving high average power, narrow bandwidth (spectrally narrow) and spatially coherent (low divergence) dye laser. Therefore, the measurement of the thermo-optic coefficient of ethanol, water, and their mixture was carried out, which is described in the subsequent section.

### **3.3.1 Experimental Setup And Results:**

The temperature of dye solution changes due to heat coupled to the dye solution from the dye circulation pump of the dye flow system, by frictional energy near the dye cell walls and by the pump pulse energy as discussed above. The change in the dye solvent temperature could change the cavity length in the dye gain medium as well as in the glass windows of the dye cell in the resonator cavity. Since the optical path depends on the refractive index of the material in the cavity and the geometric length of the cavity, it can lead to a variation of the laser wavelength due to change in the cavity

## CHAPTER - 3

length. The ambient temperature change can change the cavity length in the air. These changes are relatively smaller than the thermo optical coefficient of the refractive index of the solvents hence can be neglected in the broad sense, but whenever the wavelength stabilities in the range of less than a ppm are required these effects cannot be ignored.

The variation of refractive index with temperature for some of the dye solvents and their mixtures have been studied using Michelson interferometer as a measuring instrument. A Michelson interferometer was illuminated with a 5 mW frequency stabilized He-Ne laser (SIOS make) of the wavelength of 632.8 nm. The dye cell ( $0.5 \times 10 \text{ mm}^2$ ) with a dye flow system having 200 Watt immersion heater for heating the dye solvent was inserted in the one of the arms of the Michelson interferometer as shown in fig. 3.6.

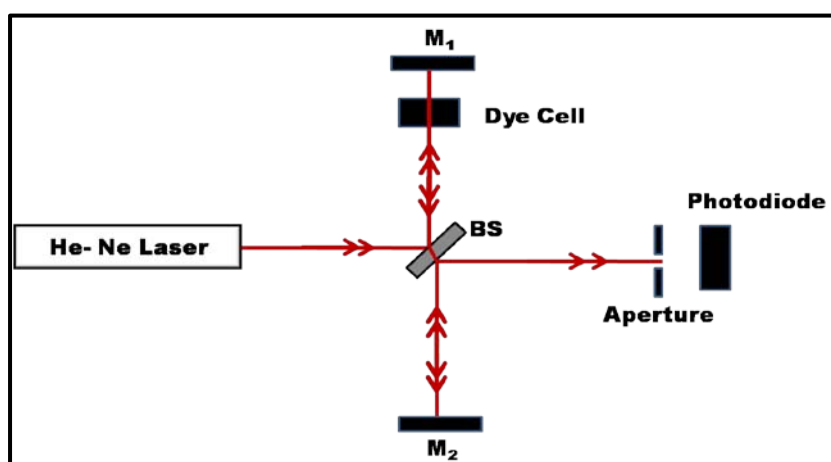


*Figure 3.6: Experimental setup (Michelson Interferometer) for measurement of thermal coefficient of refractive index for commonly used dye solvents*

The stabilized He-Ne laser beam of uniform magnitude is divided by the beam splitter into nearly two equal parts. By varying the dye solvent temperature, the optical path length of the solvent in the dye cell arm is changed resulting in the shift of the fringe

## CHAPTER - 3

pattern which was measured by a photodiode. By counting the number of fringes for the fixed temperature rise of the solvent the change in the path length was determined.

*Table 3.1: Measured values of thermo optic constant for ethanol, demineralized water and their mixture by Michelson interferometer.*

Sr. No.	Solvent	$-\frac{dn}{dT} \times 10^{-4}$
1.	Ethanol	3.955 <sup>[3.14]</sup>
2.	Ethanol (2 litter,66.66%) + Demineralized Water (1 Litter, 33.33%)	3.5595
3.	Ethanol (50 %) + Demineralized Water (50%)	3.2629
4.	Demineralized Water	0.9492 <sup>[3.15]</sup>

The dye solvent temperature was measured through a calibrated PT – 100 sensor and a temperature controller with a resolution better than 0.01<sup>o</sup>C. The temperature dependence of optical path length has two major attributes the thermal expansion coefficient( $\beta$ )and the temperature coefficient of the refractive index change ( $\frac{dn}{dT}$ ). The optical path length change with temperature( $\frac{dX}{dT}$ )is defined as the propagation characteristics of the laser beam within the material which can be defined as [3.16]:

$$\frac{dX}{dT} = \frac{dn}{dT} l + n\beta l = \frac{\lambda}{2l} \frac{dN}{dT} \quad (4)$$

In which,  $\beta$  is the linear thermal expansion coefficient,  $l$  is the length of the solvent in the dye cell,  $\lambda$  is the wavelength of the beam used for measurement and  $\frac{dN}{dT}$  is the rate of the fringe movement with temperature. The value of  $\beta$  is nearly one order smaller than the value of the  $\frac{dn}{dT}$  for the dye solvents, hence the contribution of the thermal

expansion was not considered in the calculation of optical path length measurements. The thermal coefficients of the refractive index for ethanol are closely matching to each other and reported value by Kita et al [3.14]. The measured value of the thermal coefficient of the refractive index by the interferometric technique for water is closely matching with reported value by Daimon and Masumura [3.15]. This interferometric technique can perfectly measure the coefficient of refractive index change for a mixture of the solvents at several volumetric ratios as per the requirement. We have demonstrated the measurement of the coefficient of the refractive index for the two volumetric mixtures of the ethanol and the demineralized water by this interferometric technique. These values were useful for studies of dye laser in the water-ethanol binary solvent mixture, which is described in the next section.

### **3.4 Sulfo Rhodamine 101 Dye Laser Performance in a Binary Solvent:**

Thermo-optic measurements of the water, ethanol and their mixture suggested that mixture of water and ethanol is superior to pure ethanol solvent in terms of the figure of merit for the solvents. Pure water seems to have a better figure of merit, but its implementation is restricted due to dimer formation [3.18, 3.19]. Therefore, a binary solvent of water and ethanol was tested in the dye laser system. SRh 101 dye was chosen due to solubility in the water as well as in ethanol and pumping band overlapping with a yellow beam of CVL.

Spectral shifting of the emission wavelength of laser dye by changing its solvent environment makes it more useful for generating an extended range of wavelengths. Different solvent environments namely ethanol, methanol, water, heavy water, propanol, DMSO, acetic/basic additives, etc are used to shift the emission peak of the dye laser [3.17 - 2.21]. The water is a very effective solvent used for high power and high repetition rate, pulsed dye lasers due to its favorable thermo-optic coefficient. S.Sinha [3.19] et. al.,

have studied the effect of heavy water and pure water on the dye laser characteristics. The operation of dye laser using a binary solvent mixture of DMSO and water was studied by Gayathri [3.20] et.al. Ray [3.21] et.al. has used water and propanol binary solvent mixture for their high power dye lasers. The Sulforhodamine 101 (SRh 101) dye laser in the ethanol-water binary mixture was studied for this thesis work. Characteristics of SRh101 dye dissolved in several volumetric ratios of water and ethanol as a binary solvent was studied. The advantages of the water-based solvents for generating high power dye lasers were the main motivation for this study. The tuning and performance characteristics of the Grazing Incidence Grating (GIG) laser system is studied using SRh101 dye dissolved in the water-ethanol binary solvent.

### **3.4.1 Experimental Setup:**

Indigenously developed, an all-glass dye cell was used for flowing the dye solution. A GIG laser cavity was made across the glass dye cell. A gain dimension of 0.5 mm X 16 mm was generated by focussing the yellow beam of the CVL using a cylindrical lens of 100 mm focal length. Two prism beam expander was utilized for unilateral expansion so that the large length of grating could be illuminated for obtaining anticipated grating resolution. An uncoated output coupler was utilized for generating the output laser beam from the dye laser. Green and yellow components of the CVL beam were separated using a dichroic beam splitter. A schematic of the GIG based cavity along with characterization setup is shown in fig. 3.7.

Ophir make power meter (Model: 10-A-PPS, accuracy 3%) was used for the measurement of average power from the dye laser. A small part of the dye laser beam was coupled to an optical fiber using a fiber coupler for measurement of the wavelength and bandwidth.

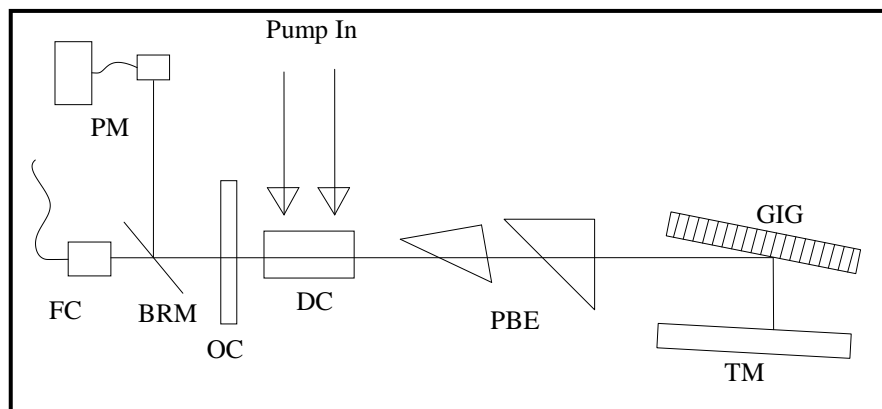


Figure 3.7: Schematic layouts of the experimental set-up;(PM: Power meter, FC: Fiber coupler, BRM: Beam routing mirror, OC: Output coupler, DC: Dye cell, GIG: Grazing incidence grating, TM: Tuning mirror, PBE: Prism beam expander)

The dye laser wavelength was measured using Angstrom make (Model: WS7) wavemeter. The SRh 101 laser dye was dissolved in a volumetric mixture of spectroscopy grade ethanol and de-mineralized (DM) water and dye (concentration of 0.5mM) was used for generating the dye laser. The bandwidth of the dye laser was measured to be 2-3 GHz.

### 3.4.2 Tuning Characteristics of SRh 101 Dye Laser in a Binary Solvent:

Tuning characteristics of SRh 101 dye at various volumetric ratios of water and ethanol in the binary mixture were measured. The tuning range of SRh 101 dye solution in pure ethanol was measured to be from 602 nm to 640 nm and maximum conversion efficiency of 2.35% was achieved at a peak wavelength of 613.6 nm. Redshifting in the tuning range from 607 nm - 640 nm to 611 nm - 642 nm was observed when the water to ethanol volumetric ratio was increased from 0.2 to 0.6. The pump power to the dye laser was kept fixed at 9-10 W for all the measurements. The redshift in the tuning range of around 6 – 7 nm was achieved with water to ethanol volumetric ratio variation from 0.2 to 1.0.

The tuning range in pure ethanol solvent is depicted in fig. 3.8.

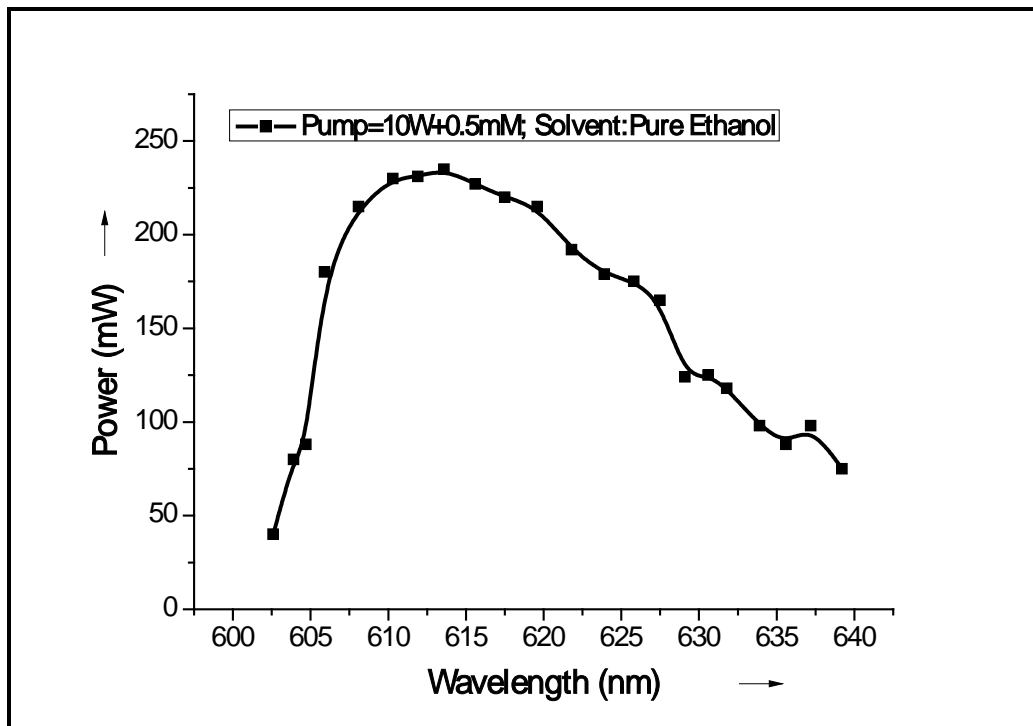


Figure 3.8: Tuning range of SR 101 in ethanol solvent

Tuning ranges of dye laser were recorded at various water to ethanol volumetric ratios (0 for pure ethanol to 1 for an equal portion of ethanol and water) is shown in fig. 3.9.

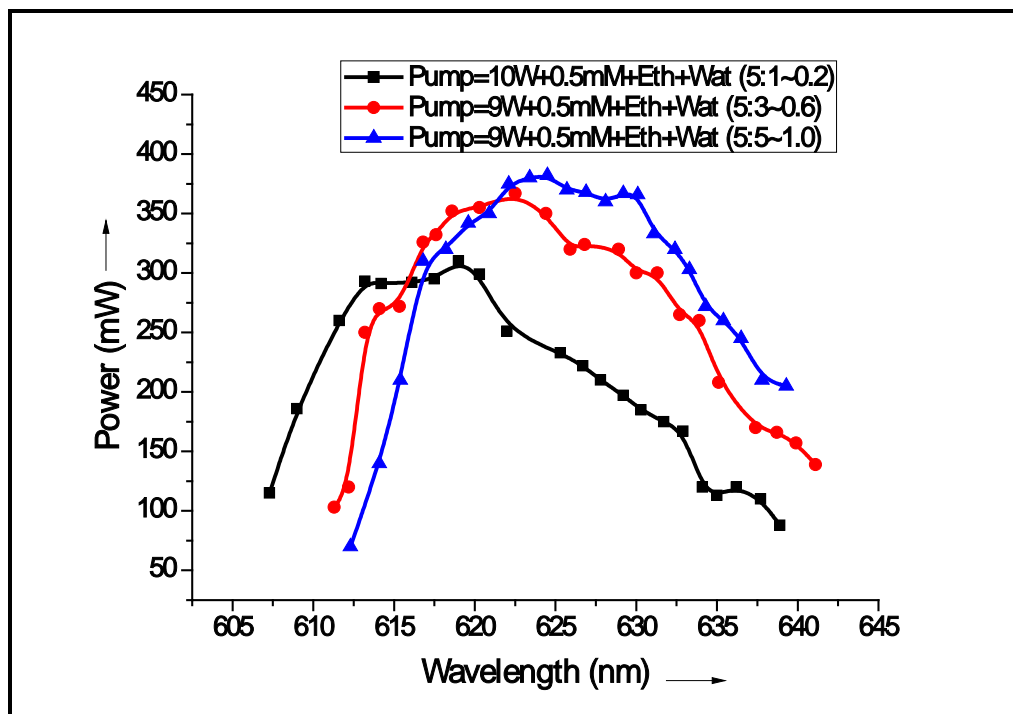
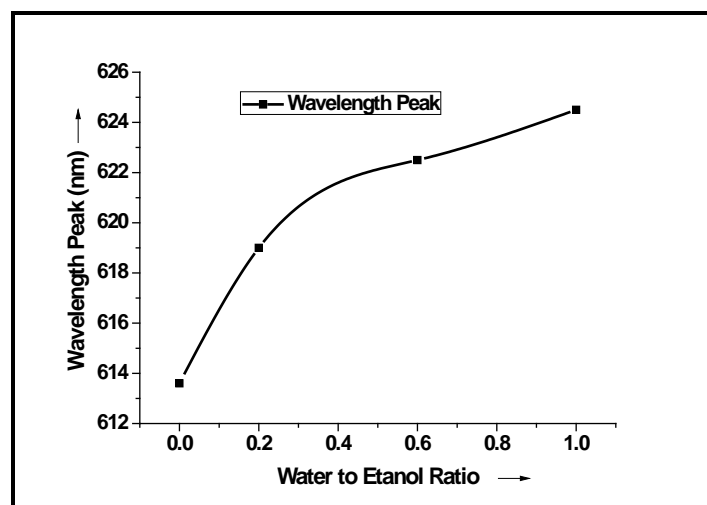


Figure 3.9: Comparative tuning range of SR 101 in ethanol in a binary solvent mixture

## CHAPTER - 3

A redshifting of 12nm in the peak wavelength from 613.6 nm to 624.5 nm was observed when pure ethanol solvent was changed to an equal proportion of water to ethanol in the binary solvent mixture. Figure 3.10 shows the shifting in the peak wavelengths towards the red side of the emission curves with an increasing volumetric concentration of DM water in the dye solvent. Water being more polar solvent than pure ethanol shows a higher red shifting of the peak wavelength with increasing concentration of DM water in the solvent.



*Figure 3.10: Effect of water to ethanol ratio on spectral shifting in the tuning range*

The addition of water in the solvent has not only red shifted the peak emission wavelength but also improved the conversion efficiency. Efficiency at the peak wavelength was increased from 2.35 % to 3.1% when water was added to the ethanol having a volumetric ratio of 0.2. A further improvement in the efficiency from 3.1% to 4.25% was achieved when the portion of water was gradually increased from 0.2 to 1.0 in the binary solvent mixture. Figure 3.11 shows the effect of the addition of the water to the ethanol on the conversion efficiency of the dye laser.

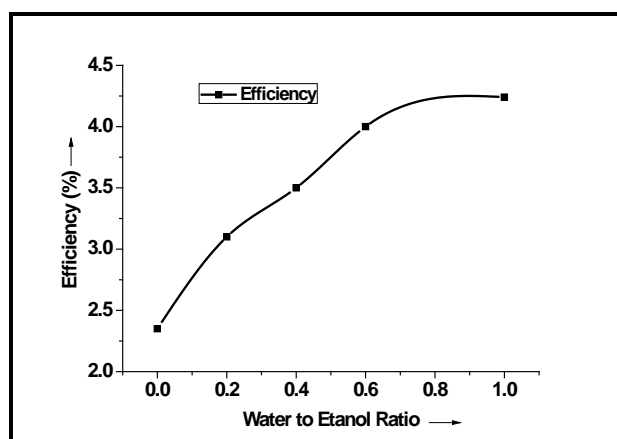


*Figure 3.11: Performance enhancement with increasing water to ethanol ratio*

The improvement in the performance of the dye laser was observed with water-ethanol binary solvent as compared to pure ethanol solvent.

Studies carried out in previous sections (3.3 & 3.4) have proved that the water-ethanol binary solvent has improved thermo-optic properties as compared to pure ethanol. Hence, a dye laser can be operated with improved performance using binary solvent at high average power as well as a higher pulse repetition rate.

Tailoring of spectral properties using pH, different solvents and their mixture was successfully demonstrated as described in this thesis. Mixing of laser dyes was studied to investigate the spectral advantage in spectral beam combination experiments using dye lasers. Widening of the tuning range using a dye mixture was demonstrated, which is described in the next section.

### **3.5 Widening of Tuning Range With Binary Dye Mixture:**

Dye mixture is widely used for tailoring the absorption and emission spectrum of the gain medium for the dye lasers. Several dye mixtures were studied by P. Burlamacchi et.al., for the generation of widely spread wavelengths for their dye laser system[3.22]. The dye mixture for studying the spectral shifting in a three-wavelength dye laser system was taken up for extending the tuning range. Generally, tuning range broadens for those dye mediums for which the emission spectrum is slightly overlapped. S. Sinha et.al. [3.23] had

studied the DCM and Rhodamine 6G dye mixture in the CVL pumped narrow-band dye laser system. Dye concentration and pump power play a crucial role in shifting of the absorption and the emission peaks of dye mixture either towards red or blue wavelengths. Hence, to study the effect of concentration on the tuning range of the multi-wavelength dye laser system using PM 567 and DCM as a dye mixture was taken up. In the first step, the concentration of PM 567 dye was increased in the dye mixture from 0.6 mM. Later on, the solution of DCM and PM 567 dye mixture was diluted to optimize the laser emission. The studies were carried out by keeping the dye concentration of one constituent fixed while changing the dye concentration of the other constituent in the dye mixture and results are presented in this section. However, the dye mixture poses serious concern of chemical reaction among them and accelerated photodegradation with reduced quantum and lasing efficiencies but this is a useful strategy for the spectral advantage. The extension of tuning range of the intra-cavity spectral beam combined three wavelength dye laser in a single cavity using the dye mixture has been demonstrated, which is described in the subsequent section.

### **3.5.1 Experimental Setup for Tuning Range Widening by Dye Mixture:**

A resonator with two grazing incidence grating arms splitted by inference filter was set up. Second harmonic of Nd: YAG laser operating at 20 Hz, pulse energy 2.5 mJ energy was used to pump the dye cell in the transverse geometry. A dye cell of 0.3 mm gain dimension was utilized to form the gain medium in the cavity. Dye mixture of DCM and PM 567 of the initial concentration of 2.66 mM and 0.6 mM respectively was prepared in spectroscopy grade ethanol. A dichroic beam splitter having passband (transmission) in the green wavelength and reflection band in red range was used for splitting the single-pass gain inside the cavity. In the reflected arm, two cascaded grating sub-cavities (C-1 and C-2) for lasing in red wavelength were set up, whereas

## CHAPTER - 3

grazing incidence grating sub-cavity (C-3) was set up on the transmitted beam for the third wavelength. The cylindrical lens of focal length 100 mm was used to line focus the pump beam on to the dye cell.

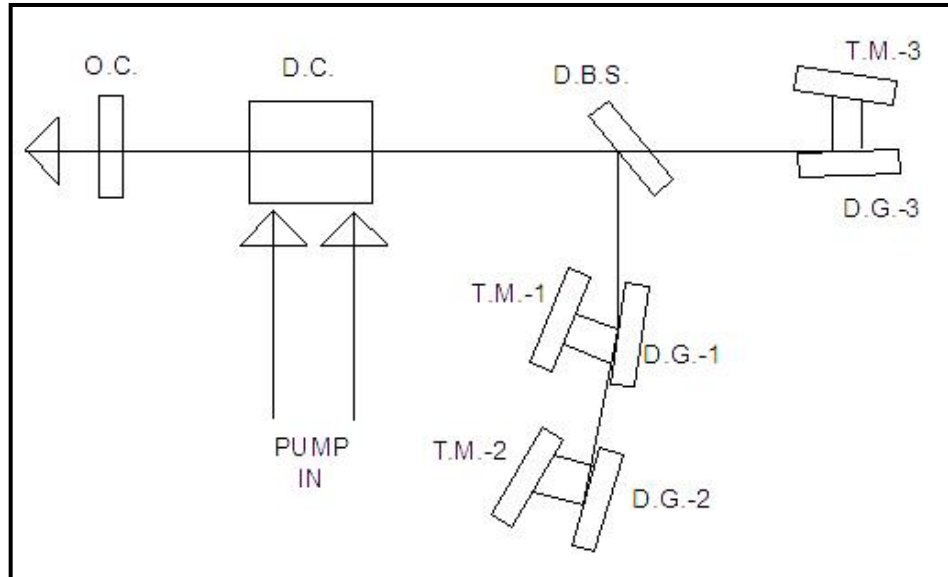


Figure 3.12: Schematic of the resonator configuration for three-wavelength, (OC: Output coupler, DC: Dye cell, DBS: Dichroic beam splitter, TM: Tuning mirror, DG: Diffraction grating)

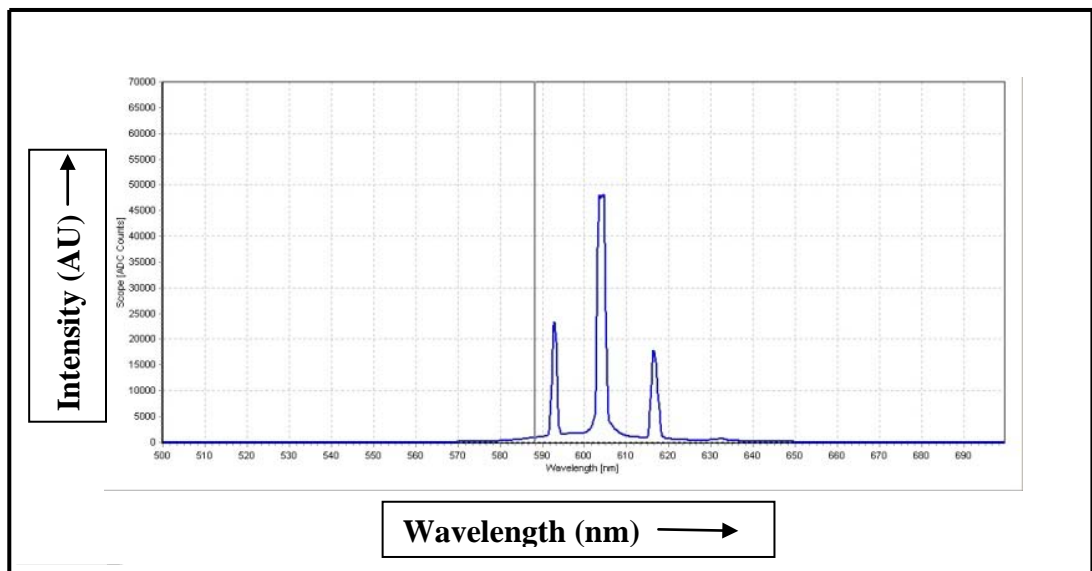


Figure 3.13: Spectrograph of three wavelength dye laser

Figure 3.12 and fig. 3.13 shows the schematic of the cavity implemented for simultaneous three-wavelength generation, and the spectrograph showing

simultaneous operation of three wavelengths, one at the peak and the other two at each end of the tuning range.

In the figure 3.12, sub-cavity, C-1 was formed by output coupler (O.C.), Dye cell (D.C.), Dichroic Beam Splitter (D.B.S.), Diffraction Grating-1 (D.G.-1), Tuning Mirror-1 (T.M.). The second sub cavity, C-2 was formed by O.C.- D.C.- D.B.S.-D.G.-1-D.G-2 and T.M.-2. The third sub-cavity, C-3 was set up using O.C.-D.C.-D.B.S.-D.G.-3 and T.M.-3 as the linear arm of the resonator. Spectroscopy grade ethanol was added in each step for the dilution of the dye mixture. Avantes make spectrophotometer (Model: AvaSpec 2048 XL) with a fiber probe was used to ensure the simultaneous operation of three wavelengths.

### **3.5.2 Effect of Concentration of PM 567 in PM567-DCM Dye Mixture:**

Tuning range of all the three sub-cavities i.e. C-1, C-2, and C-3 was observed for every change in concentration. Only the starting and ending values of the wavelength tuning range for each sub-cavity were considered for spectrum shifting experiments. This was a very effective method for the quick arrival of the final optimized tuning range ends of the configuration.

Figure 3.14 and fig. 3.15 shows the effect of an increase in PM 567 concentrations by keeping the concentration of DCM dye as constant. In sub-cavity, C-1, there was no change in the starting and ending point of the tuning range, while PM 567 concentration was increased. However, a slight blue shifting of the starting wavelength was observed in the tuning range of sub-cavity C-2. No change in the ending point of C-2 was observed.

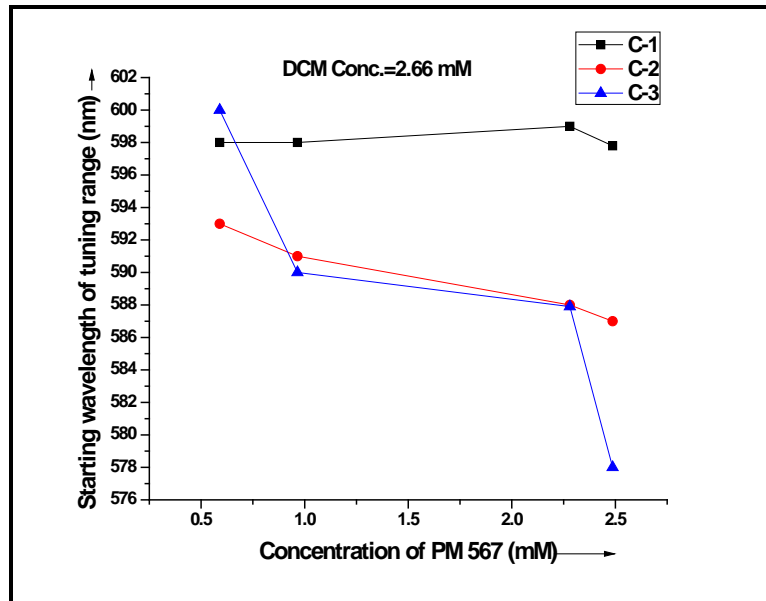


Figure 3.14: Starting wavelengths of the tuning range with increasing PM 567 concentration

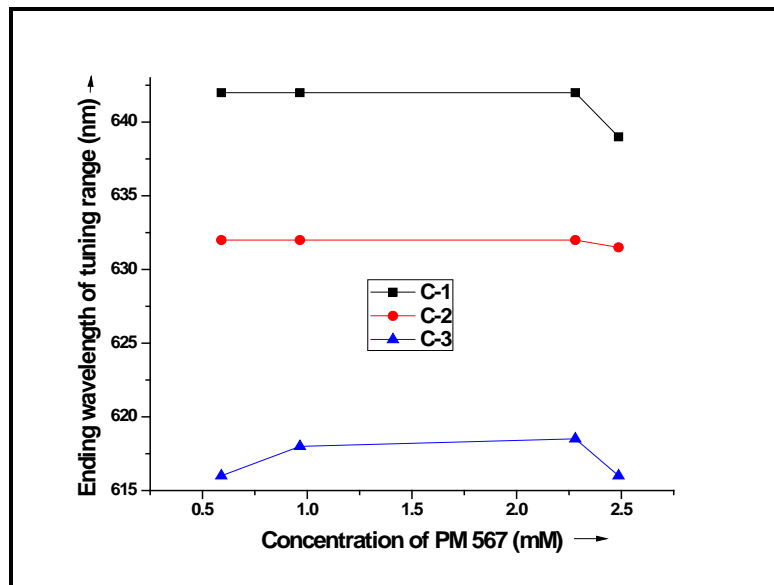
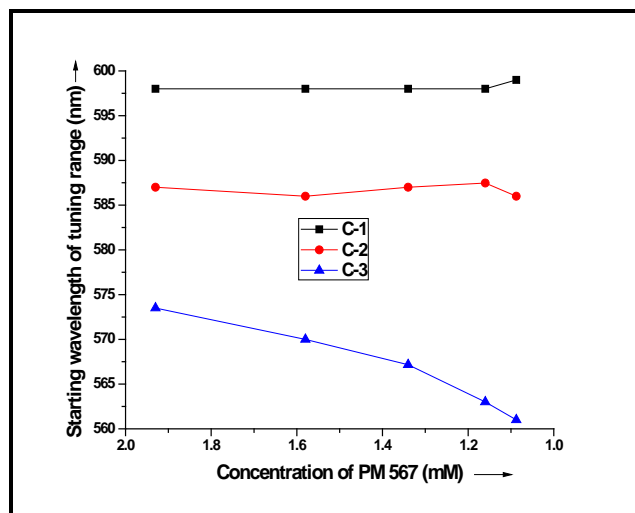


Figure 3.15: Ending wavelengths of the tuning range with increasing PM 567 concentration

A significant blue shifting from 600 to 578 nm due to increased PM 567 dye concentration was seen only in the tuning range of third sub-cavity (C-3). Figure 3.14 shows the starting wavelength whereas fig. 3.15 depicts the ending point of the tuning range due to an increase in concentration of PM 567.

**3.5.3 Effect of Concentration of DCM in PM567-DCM Dye Mixture:**

In the next step, dilution of the dye mixture was carried out and an effect on starting and endpoint of the tuning range was investigated. Concentration dilutions of PM 567 dye from 1.93 to 1 mM and DCM dye from 2 to 1.15mM was carried out. Simultaneous dilution was done by adding spectroscopy grade ethanol to the dye mixture. This has resulted in a further blue shift in the starting wavelength of the tuning range. However, the ending point of the tuning range was at 642 nm without any shift. This may be attributed to the ground state absorption effect in PM 567 dye. It was noted that DCM only plays an effective role in deciding the red region of the full tuning range, whereas PM 567 governs the spectrum in the green region.



*Figure 3.16: Starting wavelengths of the tuning range with the dilution of PM 567 concentration*

Figure 3.16 shows the starting wavelength whereas fig. 3.17 depicts the ending point of the tuning range due to dilution of PM 567 concentration

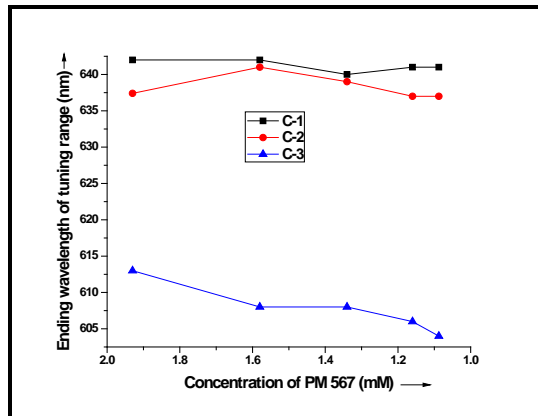


Figure 3.17: Ending wavelengths point variation of the tuning range with dilution of PM 567 concentration

The starting and ending point of the tuning range for C-1 and C-2 (fig. 3.16 & fig. 3.17) did not show significant shifting, whereas considerable blue shifting was observed in C-3 due to dilution of dye concentration.

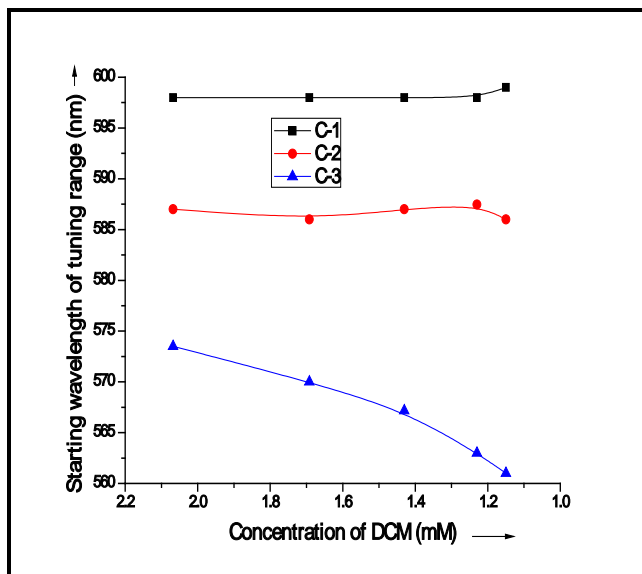


Figure 3.18: Starting wavelengths of the tuning range with DCM concentration dilution

Figure 3.18 shows the starting wavelength whereas fig. 3.19 depicts the ending point of the tuning range due to the dilution of DCM dye concentration

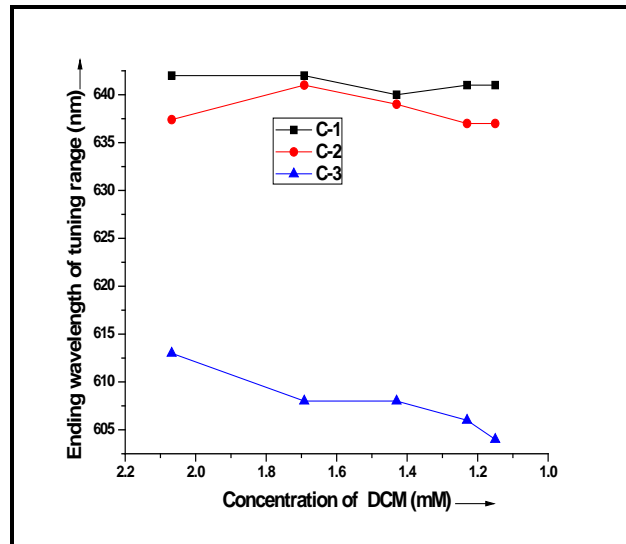


Figure 3.19: Ending wavelengths of the tuning range with DCM concentration dilution

Similar to the result obtained from PM 567 dilution, in case of DCM dilution (fig. 3.18 & fig. 3.19) blue shifting in the starting and ending point of C-3 output was seen, whereas no significant change was observed in tuning ranges of sub-cavities C-1 & C-2. The tuning range of the three-wavelength dye laser using PM 567 and DCM dye mixture was 42 nm, which was extended to 80 nm by optimizing the individual concentration of each dye in the dye mixture. This shows that only usage of dye mixture is not sufficient to achieve the extended spectral range, but optimization of the concentration is necessary to achieve desired spectral effects in the binary dye mixture.

### 3.6 Conclusions:

The environment of the dye solution plays a significant role in the spectral performance of the dye laser. Red shifted absorption and fluorescence spectra were observed with the addition of the optimized amount of acetic acid in the Rh 101 dye (~1 mM concentration) in ethanol. Improved laser efficiency with no dye photo-degradation (~ 50 hrs. operation) was observed for pumping with a high repetition rate (9 kHz) CVL at 578 nm. Reduced

absorption at 578 nm with red-shifted fluorescence spectra provides the red-shifted dye laser gain curve. Addition of acetic acid not only red shifted the absorption and fluorescence peaks but also enhanced the absorption and emission. In conclusion, the addition of a small quantity of acetic acid turns out to be a very useful methodology for red shifting of the Rh101 absorption and emission spectra.

Michelson interferometer proved to be a useful tool for the measurement of the thermo-optic coefficient of the dye solvents. Thermo-optic coefficient measured using this tool matched well with the values measured by other researchers. Measured thermo-optic coefficients suggested that ethanol and water-based solvents are well suited for high power operation. This binary solvent for SRh 101 dye laser was successfully demonstrated with high repetition rate. The addition of water in the ethanol solution not only redshifts the emission spectrum, but also enhances the peak efficiency of the dye laser output as well. A spectral shift of 11 nm was observed when pure ethanol solvent was replaced with a water-ethanol solvent of equal volumetric proportions. The volumetric composition of the water in the binary solvent can be varied to tweak the maximum efficiency at the desired wavelength from 613 nm to 625nm. Performance of SRh 101 dye laser in the water-ethanol solvent mixture was proved to be beneficial over pure ethanol solvent in terms of efficiency as well as the red-shifted emission wavelength. Three wavelength generation using DCM and PM 567 dye mixture was demonstrated. Blue shifting in the tuning range of the third sub cavity (C-3) was observed when the concentration of PM 567 was increased but the other two sub-cavities did not show any shift in their tuning range. Dilution of the mixture also resulted in the additional blue shifting of the tuning range of the third sub-cavity only. This study concludes that by adjusting the PM 567 and DCM dye concentration in the mixture, the tuning range can be increased. The blue shift of around 40 nm in the starting point of the tuning range from

## CHAPTER - 3

---

600 nm to 562 nm was obtained. This is achieved by keeping the red end of the range unchanged. In conclusion, the increase in the tuning range from 42 nm (600 - 642 nm) to 80 nm (562 – 642 nm) by concentration optimization was demonstrated. Therefore, it can be concluded that tailoring the solvent environment of the dye laser is a useful strategy for the generation of additional wavelengths. Laser dye mixtures with optimized concentration can further widen the tuning range of the CVL pumped dye laser system. It can be concluded that the dye gain medium is an important part of the dye laser system for studying the spectral beam combination techniques.

# Chapter: 4

## Intra-cavity Beam Combination Techniques for Multi-wavelength Dye Laser

---

### 4.1 Introduction:

In the intra-cavity beam combination technique, multi-wavelengths are generated by combining the different wavelength laser beams inside a common resonator cavity. Single or multiple dye cells (cuvette) are used inside the resonator cavity to generate different wavelengths. Generally, dye gain volume in the common dye cell is shared by several sub-cavities to generate the composite dye laser beam as compared to using separate dye volume in different dye cells for each wavelength. The common dye gain volume was utilized by all the sub-cavities for generating multi-wavelengths, which ensured the collinearity among multiple wavelength laser beams. Sharing the same gain volume by many wavelengths poses a challenge of gain competition in the homogeneously broadened gain profile of the fluorescent laser dye. Intra-cavity beam combined multi-wavelength dye laser generation has its own advantages and disadvantages. Shorter cavity lengths along with co-linearity of the output laser beams are the main attraction of this configuration. As a consequence of the gain competition in the dye gain medium, controlling the intensity of individual wavelength becomes tricky for this technique. Multi-cuvette systems are used to avoid gain sharing, which could minimize the gain competition effects for this configuration. However, this scheme becomes bulky and complex due to handling multiple dye mediums along with their respective flow systems and alignment becomes difficult to achieve the collinearity. Therefore, it was decided that the single dye cell configuration to be used to achieve collinear, multi-wavelength output beam from dye laser with several resonator

sub-cavities. This configuration promises a very compact dye laser system, which can provide multiple wavelengths simultaneously.

Intra-cavity beam combined scheme is capable of generating four to five wavelengths in a single compact dye laser system. The composite dye laser beam required to be propagated over long distance as per the applicability of this dye laser system. Maintaining the spatial overlap of the constituent dye laser beams over long propagation distance becomes difficult due to the extremely sensitive alignment of the combination and beam shaping optics. A further difficulty in achieving suitable spatial overlap is due to the unequal aspect ratios of different divergences for the major and minor axis of the dye laser beam. Common gain volume acts as an inherent spatial aperture in the intra-cavity scheme, which automatically results in a collinear output beam of the dye laser. These advantages of the intra-cavity beam combined systems were the main motivation for carrying out studies on this configuration despite of the gain competition behavior present in the dye laser medium.

Most of the well studied dual-wavelength designs pose extendibility to more than two wavelength operation. However, studies on a triple and four wavelength generation from single dye gain are very limited. Recently, R. Khare et. al. [4.1] had reported three-wavelength operation from copper vapor laser pumped Rh 6G dye laser. They have utilized two gratings coupled with different diffraction orders in a four prism beam expander cavity for their study. Two out of three wavelengths were independently tunable and laser line widths were of the order of  $0.3 \text{ cm}^{-1}$  (9 GHz). Y. Saito et.al. [4.2] had demonstrated the simultaneous three-wavelength operation in their laser system using a dielectric interference filter based cavity which provides broad linewidth and limited tuning range. Multi-color operation from dye mixtures

was achieved by Burlamacchi et.al. in a single grazing incidence grating with two separate tiltable mirror cavities[4.3].

Several techniques using multiple dispersive elements with telescopic beam expander, prismatic beam expander, and grating-based cavity designs are well studied by several groups. They had studied grazing incidence grating (GIG) cavities with and without intra-cavity expansion in greater details and reported in the published literature. Narrowband operation of dye laser using GIG cavity without beam expander had been achieved by I. Shoshan et.al [4.4] and Littman and Metcalf [4.5] with a line width of the order of 1GHz. In later versions, the single-mode operation had been obtained with a line width of 300 MHz [4.6, 4.7] using similar resonator configurations. Nair et. al. [4.8] had reported the double wavelength generation from a grazing incidence tunable dye laser without an intra-cavity beam expander. Prior [4.9] had used different orders of grazing incidence diffraction grating for narrowband double wavelength generation from a nitrogen laser pumped Rh 6G dye laser. Simultaneously operable, independently tunable, collinear, four wavelength dye laser was taken up for further studies as not reported in the literature. Hence, the generation of more than three wavelengths using intra-cavity spectral beam combination configurations was studied and described in subsequent sections of this chapter.

### **4.2 Selection of Cavities for Narrowband, Multiple Wavelength Generation:**

The multi-wavelength dye laser beam can be generated by coupling multiple sub-cavities inside a master resonator cavity. There are various possible configurations for coupling the sub-cavities operating at different wavelengths. A configuration having a common output coupler is termed as the intra-cavity beam combined configuration. This may or may not have the common dye gain medium as discussed in the previous section. The study for this thesis is limited to single dye cell (cuvette) configurations.

Few of the potential intra-cavity configurations, which are capable of generating narrowband, multiple wavelengths are described in the subsequent sections.

Configurations with inherent narrow linewidth generation capabilities were selected for experimental validation. Among various cavities, the GIG cavities with and without prism beam expander were studied. GIG cavities have been regularly used with intracavity prism beam expanders (PBE) and without PBE to generate very narrow line-width in the range of 1-3 GHz. Four wavelength operation in the GIG cavity with prism beam expanders was found to be difficult to achieve due to very high prism losses in comparison to the GIG cavity without prism beam expander. Various cavity configurations were tested to select the potential scheme, for a simultaneous generation of more than three wavelengths.

### **4.2.1 Linear Cavity With Intra-cavity Beam Expander:**

The first intra-cavity beam combined configuration tested, was a linear cascaded geometry, with grating as a beam combination element. In this configuration, gratings were cascaded linearly, so that zeroth-order beam of one grating is incident on another grating at either the Littrow or grazing incidence angle. Each grating had a corresponding tuning mirror to form sub-cavities for individual wavelengths. Output coupler, dye gain medium and prism beam expander were shared by all the sub-cavities. To generate a narrow-band laser beam, the grating is required to be employed at a higher resolution. Grating at a higher angle of incidence provides higher resolution, but at the cost of reduced diffraction efficiency. Higher resolution can also be obtained by illuminating the longer length of the grating. The intra-cavity expanded beam illuminates a higher number of lines on the grating and

achieves impaired resolution with improved efficiency. The schematic of this proposed geometry is shown below in fig. 4.1.

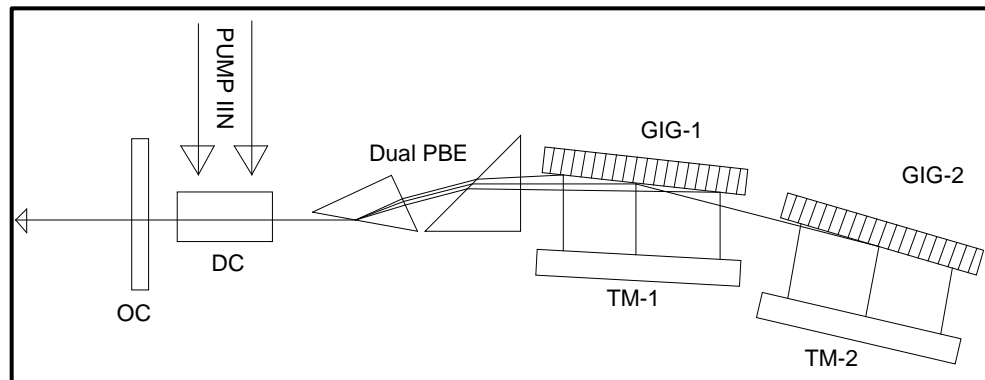
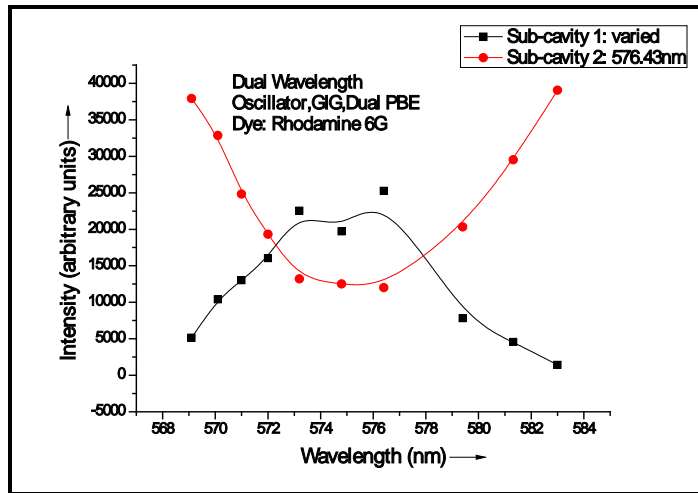


Figure 4.1: Linear cavity with a prism beam expander (OC: Output coupler, DC: Dye cell, PBE: Prism beam expander, GIG: Grazing incidence grating, TM: Tuning mirror)

An experiment was set up using two grazing incidence grating cavity in cascade to each other along with intra-cavity beam expander. Rhodamine 6G dissolved in pure ethanol was used as the gain medium. The concentration of dye was optimized for 70% of light absorption in 100 microns. A cylindrical lens of 100mm focal length was used to focus the pump laser onto the dye cell. The dimensions of the pump beam focus at the dye cell were approximately 20 mm X 0.5 mm. Diffraction gratings of 2400 lines per mm and length of 62.5 mm at a near grazing incidence angle was used for these experiments. High reflectivity ( $R \sim 99\%$ ) rectangular mirrors were used as tuning mirrors. A dual prism beam expander was incorporated in the cavity to achieve a linear magnification of 20. The salient feature of the configuration is its compactness, which is advantageous for utilizing a pump pulse of shorter pulse duration as well. This expanded beam was incident on the first grating (GIG-1) at the grazing incidence angle of nearly 81 degrees. A tuning mirror (TM-1) was aligned to reflect the first-order diffracted beam from the grating (GIG-1). This

formed the first sub-cavity (C-1), which generated one of the wavelengths. The second grating (GIG-2) was set up at grazing incidence to the zeroth-order beam from the first grating. A tuning mirror (TM-2) was aligned with the first-order diffracted beam from the second grating. This forms the second sub-cavity (C-2) and generated the second wavelength. The second sub-cavity was optimized by blocking the tuning mirror of the first sub-cavity. A dual-wavelength collinear output beam was obtained when both the tuning mirrors were optimized for individual sub-cavities. Pump laser used in this experiment was a 20 Hz repetition rate having pulse energies in the range of 1-2 mJ. Tuning characteristics of this cavity configuration were studied in detail. The wavelength of subcavity-2 was fixed at 576.4 nm and the wavelength of subcavity-1 was varied. Figure 4.2 shows the gain competition among the two wavelengths for Rhodamine 6G dye laser.



*Figure 4.2: Gain competition effect in the wavelength tuning curve in a linear cavity with a prism beam expander*

It was observed that the wavelength tuning range of C-1 shows a dip in the intensity when subcavity-2 (C-2) was tuned to its peak. It was a consequence of gain sharing among both the cavities. The effect of wavelength tuning of

subcavity-1 on the intensity of subcavity-2 with fixed wavelength clearly shows the gain competition effect, which is expected to occur as both the laser sub-cavities share a homogeneously broadened common dye gain medium.

The fig. 4.3 shows the simultaneous oscillations of twin wavelengths from this cascaded cavity with Rh6G dye, measured by Avantes spectrometer (Model no: AvaSpec-2048 XL).

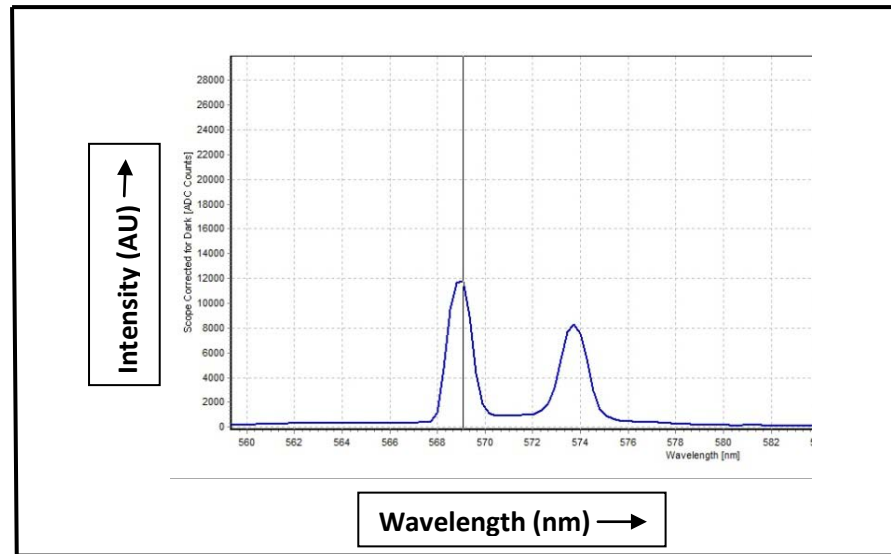


Figure 4.3: Spectrograph showing a two-wavelength operation

It was tried to add third grating to achieve lasing in the third sub-cavity, but it was very difficult to get the three-wavelength output using this configuration. Therefore, another cavity using an interference filter based beam combiner was planned to split the different wavelength zones for each sub-cavity to achieve three-wavelength operation.

#### 4.2.2 Folded Cavity With Intra-cavity Beam Expander:

In this configuration, the cavity is divided into two parts after the prismatic beam expander. Intra-cavity beam is splitted into one linear and another folded section using a broadband beam splitter or dichroic beam splitter. Both the sections have their grating and tuning mirror pair to form sub-cavity arms.

## CHAPTER - 4

This configuration can be used in separating two-wavelength zones in two orthogonal cavity arms using dichroic beam splitter (DBS) as the intra-cavity beam combiner. Each arm can be optimized separately by blocking another arm. Usage of beam splitter adds the advantage of achieving gain sharing variability among the orthogonal arms. It can be realized by changing the splitting ratio of the commonly available gain. This is useful for sharing gain to generate different power in each constituent wavelength.

Experimental set up using the DBS as beam combiner is shown in fig. 4.4. The linear and folded arm consists of primarily green and red wavelength range respectively. It was observed that this configuration is suitable for a dual-wavelength generation. Generation of three and four wavelengths using this configuration became difficult due to lower efficiency of the grating in GIG mode and higher intra-cavity losses occurring at the prism beam expander. Homogenous gain present inside the cavity fails to cross the net intra-cavity losses, resulted in limitation to generate more than two wavelengths.

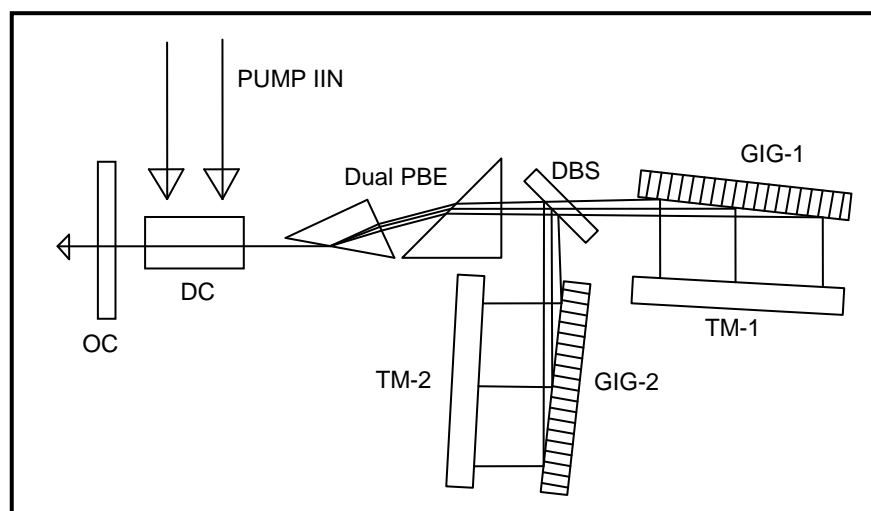


Figure 4.4: Folded cavity with a prism beam expander, (OC: Output coupler, DC: Dye cell, PBE: Prism beam expander, DBS: Dichroic beam splitter, GIG: Grazing incidence gratin, TM: Tuning mirror)

## CHAPTER - 4

---

To demonstrate the advantage of using DBS for wavelength zone separation, a binary dye mixture of Rhodamine 6G and DCM dye was studied. Intra-cavity dichroic beam splitter had a high transmission for wavelength less than 580 nm and high reflection for ( $R > 99\%$ ) wavelengths above 600 nm. Hence, the DCM dye laser was established in the folded arm with second grating (GIG-2) and corresponding tuning mirror pair. Lasing in green wavelength (Rh6G) was obtained in the linear arm using first grating (GIG-1) and its corresponding tuning mirror. A similar arrangement was established for the folded arm to form the second sub-cavity using GIG-2 and tuning mirror pair. Twin lasing with a wide wavelength difference was obtained. Sub-cavity: GIG-1 with grating-1 was observed to have wavelength tunability from 565 to 600 nm and sub-cavity: GIG-2 with a tuning range of 605 to 643 nm. This proved that intra-cavity beam combination using DBS is advantageous for reducing the gain competition in the case of well-separated wavelengths.

To generate three and more wavelengths, an additional grating tuning mirror pair was introduced at the zeroth order of grating on both sides of the cavities. Only feeble lasing was observed at the third wavelength. Intra cavity losses with dual PBE along with high grating losses were identified as the main culprit. This was replaced with four PBE at the Brewster angle with improved efficiency as compared to dual PBE. Though lasing at the third wavelength was improved inside the cavity, the output lasing was not appreciable. Even though single pass transmission efficiency was more, multiple round trips lasing at wavelength-3 suffered a huge loss due to low available gain for the third wavelength lasing. This was concluded after testing these two configurations with intra-cavity beam expander, that round trip losses at prism

surfaces are responsible for higher intra-cavity losses and hence poses the difficulty in more than two wavelength operation. Therefore, decided to test the cavity without a prism beam expander. Multi-wavelength operation using cavities without PBEs was demonstrated. This prism beam expander-less configuration is elaborated in the following section.

### **4.2.3 Linear Cascaded Cavity Without Intra-cavity Beam Expander:**

Resonator cavities without prismatic beam expander were analyzed to select the suitable cavity for narrowband, multi-wavelength beam generation. Losses occurring at the prism surfaces were eliminated in this configuration. This resulted in the lowering the threshold loss of the cavity. Consequently, available gain for the sub-cavities increased. This facilitated the gain required for the third and fourth sub-cavity. The absence of a prismatic beam expander made this cavity shorter in overall length. The compactness of this geometry has advantages of lower losses and the higher number of possible round trips to further narrowing of the linewidth. Two configurations under this class of geometries were studied in detail.

The cavity explored for a three-wavelength generation with minimal intracavity losses is shown in figure 4.5. This cavity is the extension of the dual-wavelength cavity reported by L.G.Nair et al [4.8] to three wavelength generation. The diffraction efficiency of the grating in the first order at an incidence of  $\sim 88^\circ$  was less than 5%. Therefore, only part of the gain was used for lasing and remaining gain was available for utilization in other sub-cavities. Zeroth order output carries more than 90% of the light incident on the grating. It was because the grating was functioning as a beam splitter of low reflectivity in this configuration.

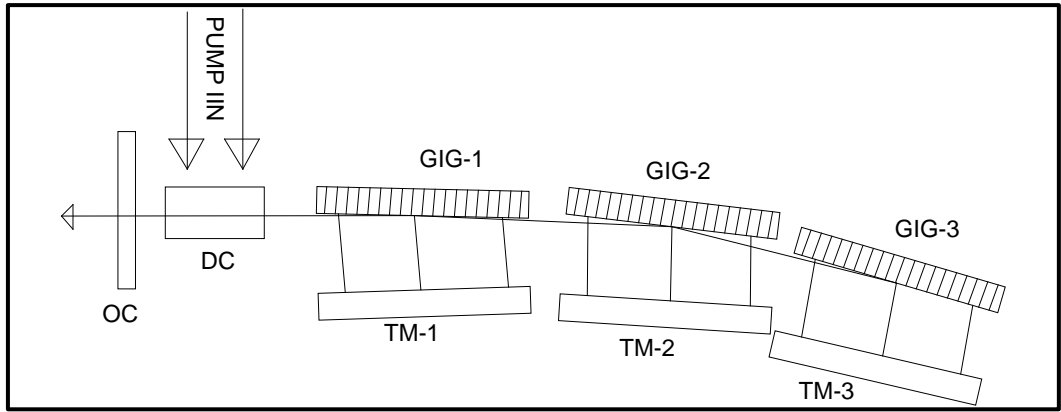


Figure 4.5: Linear cascaded grating cavity without PBE, (OC: Output coupler, DC: Dye cell, GIG: Grazing incidence gratin, TM: Tuning mirror)

Figure 4.5 shows the experimental setup used for the three-wavelength generation. Three gratings aligned in grazing incidence angle with their corresponding tuning mirror pair. All the three grating sub-cavities coupled via the zeroth-order output of adjacent previous gratings. DCM dye solution in ethanol pumped with second harmonic Nd: YAG laser was used as a gain medium for this investigation.

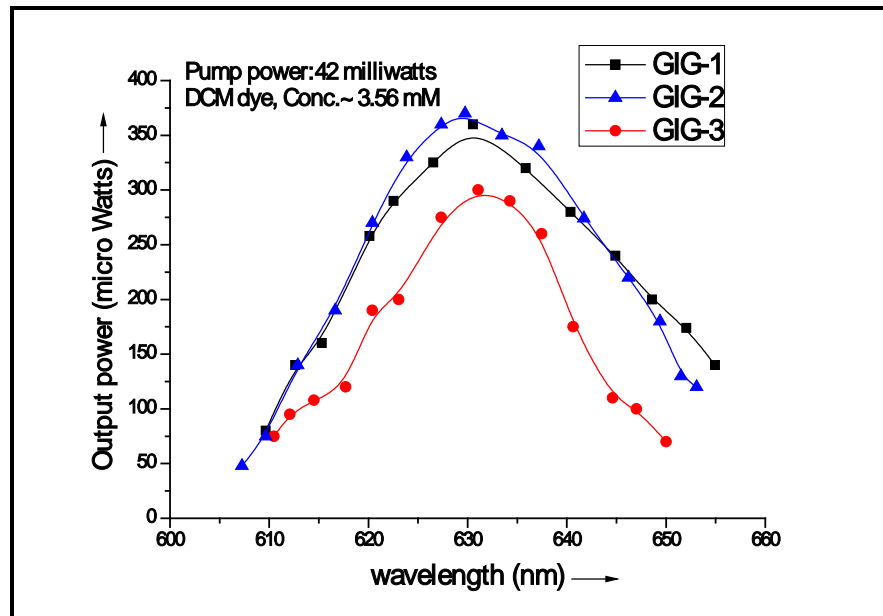
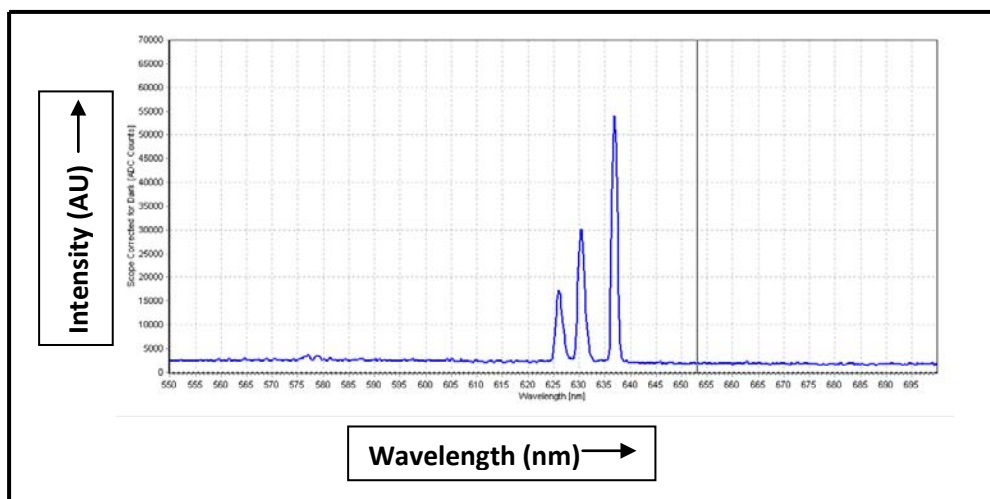


Figure 4.6: Wavelength tuning characteristics of three sub-cavities in the cascaded grating cavity without PBE

## CHAPTER - 4

Figure 4.6 shows tuning ranges of individual cascaded GIG cavities for DCM gain medium. These were measured for one sub-cavity at a time, while other cavities were physically blocked at the tuning mirror. Pump power of 42 mW and the grating is kept at  $\sim 89^\circ$  AOI having diffraction efficiency of  $\sim 1-2\%$ . At the first order. At full grating length of 62.5 mm was illuminated, most of the light falling on grating was available for successive cavities. From figure 4.6, GIG-1 and GIG-2 has nearly the same tuning range and GIG-3 has slightly reduced peak efficiency.

Figure 4.7 shows the simultaneous three-wavelength lasing for DCM dye laser. By reducing grating illumination length from 62 mm to 52 mm, peak efficiencies were increased to 2%.



*Figure 4.7: Three wavelength operation in the linear cascaded grating cavity*

The spectral linewidth at this illumination lengths was measured to be 2 GHz, 3 GHz and 4 GHz for GIG-1, GIG-2 and GIG-3 respectively. Cavity lengths of GIG-1, GIG-2 and GIG-3 were measured to be 210 mm, 350 mm and 490 mm respectively. An increase in line width from 2 to 4 GHz was attributed to increased round trip time from GIG-1 to GIG-3 and shorter pulse width of 8 ns of Nd: YAG pump laser.

We have extended this work on the three-wavelength laser to four and five lasers by adding additional grating and tuning mirror pairs. Two such cavities are described in detail in the next section.

### **4.3 Cascaded Grating Cavity Setup for Four Wavelength Generation:**

This cavity was finalized after initial experiments using various potential cavities to generate multiple wavelengths with narrow line-width. Two resonator configurations for simultaneous four wavelength generation using a common dye gain medium were studied. The first configuration i.e. cascaded grazing incidence grating (CGIG) resonator as shown in fig.4.8, utilized four diffraction gratings in cascade, aligned at near grazing incidence angle of  $\sim 87^{\circ}$  to  $89^{\circ}$  with their respective tuning mirrors. These sub-cavities were mutually coupled through the zeroth-order output from the preceding sub-cavities. The second configuration was hybrid CGIG (HCGIG) in which three diffraction gratings were set at a near grazing angle with their respective tuning mirrors, whereas fourth grating was aligned at Littrow angle configuration as shown in fig. 4.9. In HCGIG, individual sub-cavities were mutually coupled through the zeroth-order output from the preceding sub-cavity. Output coupler with 4% feedback was aligned for obtaining the collinear composite tunable dye laser output beam from the resonator. DCM dye (concentration 3.55 mM) dissolved in spectroscopy grade ethanol was circulated through a glass dye cell of 20 mm width and 0.5 mm depth. Typically, cavity lengths of first to fourth sub-cavities were 210 mm, 345 mm, 490 mm and 625 mm respectively for the CGIG resonator and fourth sub-cavity length reduces to less than 600 mm in case of HCGIG resonator configuration due to absence of tuning mirror arm.

## CHAPTER - 4

Figure 4.8 and figure 4.9 show the cavity configuration of CGIG and HCGIG. In CGIG configuration, basic resonator consists of output coupler (O.C.), dye cell (D.C.), tuning mirrors (T.M.) and a diffraction grating (D.G.) arranged in GIG configuration.

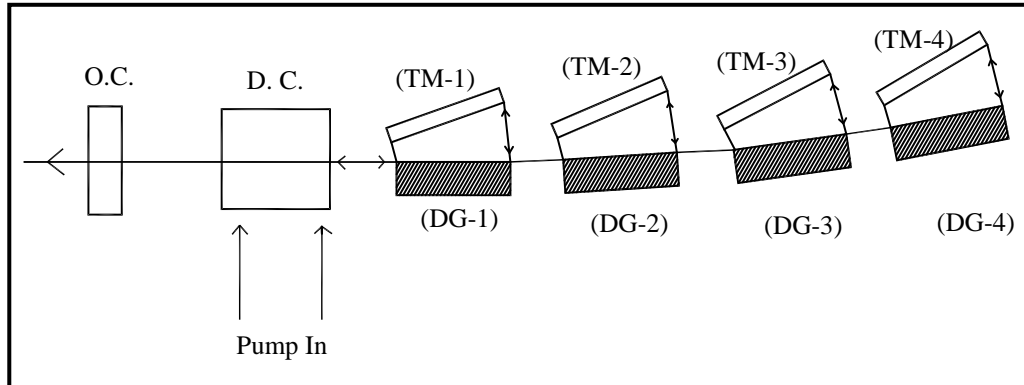


Figure 4.8: Schematic of cascaded grazing incidence grating (CGIG) resonator configuration (OC: Output coupler, DC: Dye cell, GIG: Grazing incidence grating, TM: Tuning mirror)

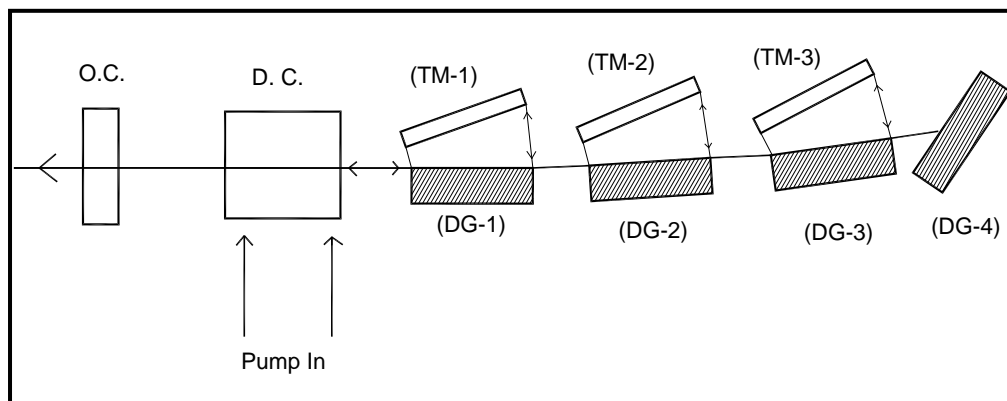


Figure 4.9: Schematic of hybrid CGIG (HCGIG) with Littrow resonator configuration (OC: Output coupler, DC: Dye cell, GIG: Grazing incidence grating, TM: Tuning mirror)

The dye laser was transversely pumped by the second harmonic of Nd: YAG. For this study, the grating illumination was maintained around 52 mm for all the gratings to ensure constant single pass spectral width. Cascaded GIG configurations have the advantage of variable line width and adjustable cavity losses by varying the angle of

incidence of the grating and hence the illumination length. In CGIG, as shown in fig.4.8, sub-cavities C-1 (O.C.→D.C.→D.G.-1→T.M.-1), C-2 (O.C.→D.C.→D.G.-1→D.G.-2→T.M.-2), C-3 (O.C.→D.C.→D.G.-1→D.G.-2→D.G.-3→T.M.-3) and C-4 (O.C.→D.C.→D.G.-1→D.G.-2→D.G.-3→D.G.-4→T.M.-4) correspond to the first, second, third and fourth sub-cavity respectively with nearest to longest distance from output coupler. In HCGIG configuration (fig.4.9), the sub-cavity C-4 (O.C.→D.C.→D.G.-1→D.G.-2→D.G.-3→D.G.-4) is aligned at Littrow angle instead of grazing incidence.

Avantes make spectrophotometer (Model no: AvaSpec-2048 XL) [4.10] was used with an optical fiber bundle to couple the dye laser beam for wavelength measurement and their relative intensity assessment. Ophir makes (FL250A & PD 300R; accuracy 3%) power meter was used for measurement of the input pump laser power and output dye laser power.

Line width was measured using Fabry Perot etalon (FP) of 15 GHz free spectral range and finesse of 30. An optical fiber was used to sample the dye laser beam and launch it into the FP etalon. A convex lens of 250 mm focal length was used for capturing the fringes formed by FP etalon, on the CCD camera which was interfaced using frame grabber card to the computer. The temporal parameter of the multi-wavelength dye laser output was measured using a fast photodiode and displayed on a Tektronix oscilloscope (4 channel, 1MHz bandwidth).

#### **4.4 Characteristics of Cascaded Grating Cavity Configurations:**

The performance characteristics of the four wavelength operation of dye laser in these two resonator configurations have been demonstrated. In the first configuration, tuning curves of four cascaded grazing incidence grating sub-cavities (CGIG) without intra-cavity beam expander similar to the dual-wavelength cavity by Nair et.al. [4.8] was

studied. In another resonator i.e. hybrid CGIG configuration (HCGIG), the fourth grating was aligned in a Littrow configuration instead of near grazing angle in CGIG configuration and tuning characteristics were recorded. Gain competition plays a significant role in dictating the intensity ratio, tuning range and sustained multiple wavelength operation for collinear output generation in a homogeneously broadened dye gain medium. Several authors [4.11, 4.12] have reported the gain competition behavior in various geometries and configurations but the detailed characterization is not reported to identify operable wavelength zones of individual sub-cavities for sustained multi-wavelength operation. Detailed characteristics of four wavelength oscillators and the role of gain competition effect in these two multi-wavelength dye laser resonator configurations (CGIG & HCGIG) are described in this thesis.

DCM dye was chosen due to its large tuning range spans from 590 to 680 nm. The wavelength tuning range of each dye laser was dictated mainly by the availability of gain and losses inside individual sub-cavities. The wavelength tuning range of each sub-cavity was measured one at a time, keeping the other three sub-cavities blocked at tuning mirrors to avoid gain competition effects.

### **4.4.1 Cascaded Grazing Incidence Grating (CGIG) Cavity:**

In CGIG configuration (Fig. 4.8), tuning range and efficiency of the first to fourth sub-cavity was observed to be reduced, which is attributed to the increased losses in subsequent sub-cavities as the cavity length is increased and the laser beam interacts with more number of gratings in the subsequent cavities.

All the four sub-cavities were aligned to lase simultaneously in four wavelengths for gain competition studies. Gain competition effects of one cavity on the output intensities of other cavities were studied in detail. In CGIG configuration, the wavelength of sub-cavities C-1, C-2, C-3, and C-4 were tuned one by one by

## CHAPTER - 4

setting the other three at a fixed wavelength. It was observed that the lasing in the fourth sub-cavity could be sustained only if sub-cavities C-1 & C-2 were tuned to either edge of the wavelength tuning range (fig. 4.10).

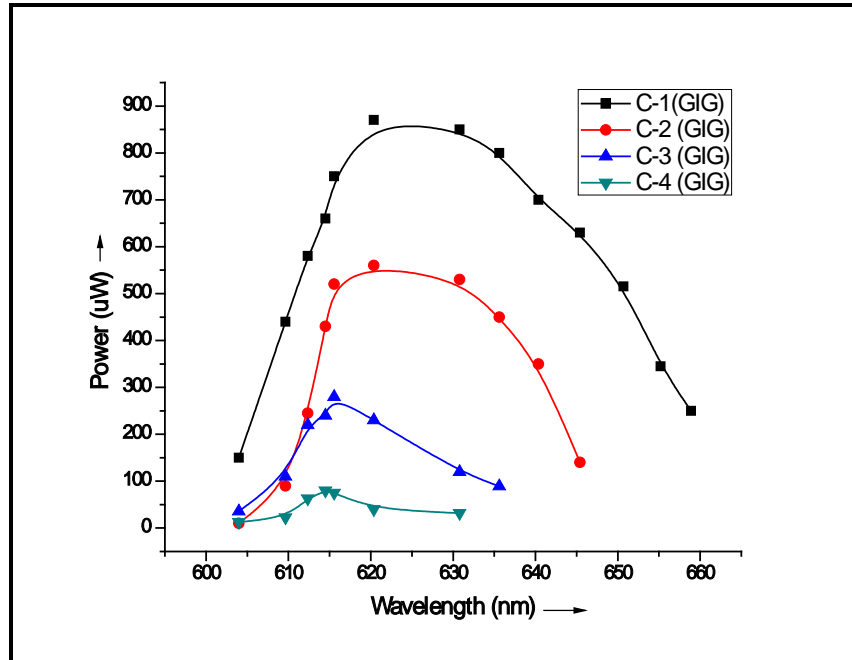


Figure 4.10: Tuning curves of four CGIG sub-cavities

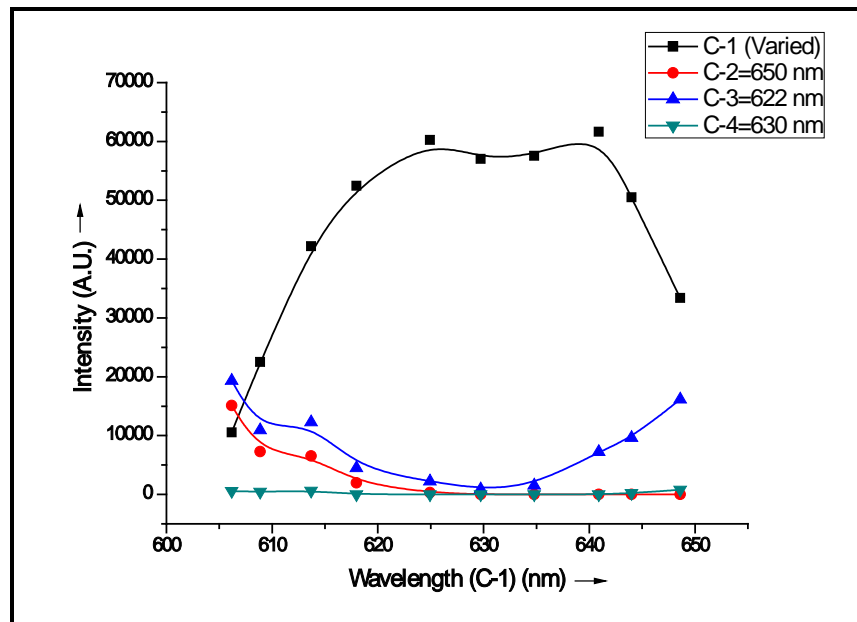


Figure 4.11: Variation of output intensities due to wavelength tuning of sub-cavity C-1, keeping wavelength of C-2, C-3, and C-4 at fixed values (CGIG)

## CHAPTER - 4

---

Figure 4.11 explains the effect of wavelength tuning in sub-cavity C-1 on the output intensity of the other three fixed wavelength sub-cavities. When the wavelength of sub-cavity C-1 was tuned from 606 nm to 616 nm and from 644 nm to 648 nm, all the four sub-cavities were lasing whereas four wavelength operation ceased when the wavelength of C-1 tuned through 616 nm to 644 nm. Sub-cavity C-2 was also ceased to lase when the wavelength of C-1 was tuned from 624 nm to 648 nm. It implies that sub-cavity C-1 is the most dominant cavity and can only be operated at the end of the tuning range i.e. 606 nm to 616 nm and beyond 650 nm for sustained four wavelength operation. During this experiment, wavelength of sub-cavity C-2 was set at either end of the wavelength tuning range, C-3 was set near the peak of the tuning range (622 nm) and C-4 (630 nm) was set at the peak of the tuning range for providing maximum gain in order to compensate for the associated cavity losses. The output intensity of fixed wavelength sub-cavities (C-2, C-3, and C-4) reduced when the wavelength of C-1 was tuned through its tuning range. A slight misalignment of tuning mirror of lower loss sub-cavity (C-1 and C-2) was found to play a significant role in sustained four wavelengths lasing. However, it deteriorates the collinearity of the beams at a longer distance of more than 15 meters.

Figure 4.12 shows the role of variation of wavelength in sub-cavity C-2 on output intensity variation of the other three fixed wavelength sub-cavities. It was observed that, when the wavelength of sub-cavity C-2 was tuned from 610 nm to 618 nm and from 642 nm to 649 nm, all four sub-cavities were lasing, whereas the fourth wavelength stopped lasing when the wavelength of C-2 was scanned from 618 nm to 642 nm. It implies that sub-cavity C-2 can only be operated at the end of the tuning range i.e. 610 nm to 618 nm and beyond 650 nm for sustained four

wavelength operation. The wavelength of sub-cavity C-1 was set at the start of the tuning range (607nm), C-3 was set near the peak of the tuning range (622 nm) and C-4 (630 nm) was set at the peak of the tuning range for this investigation. It shows sub-cavity C-2 is dominant but relatively less compared to sub-cavity C-1.

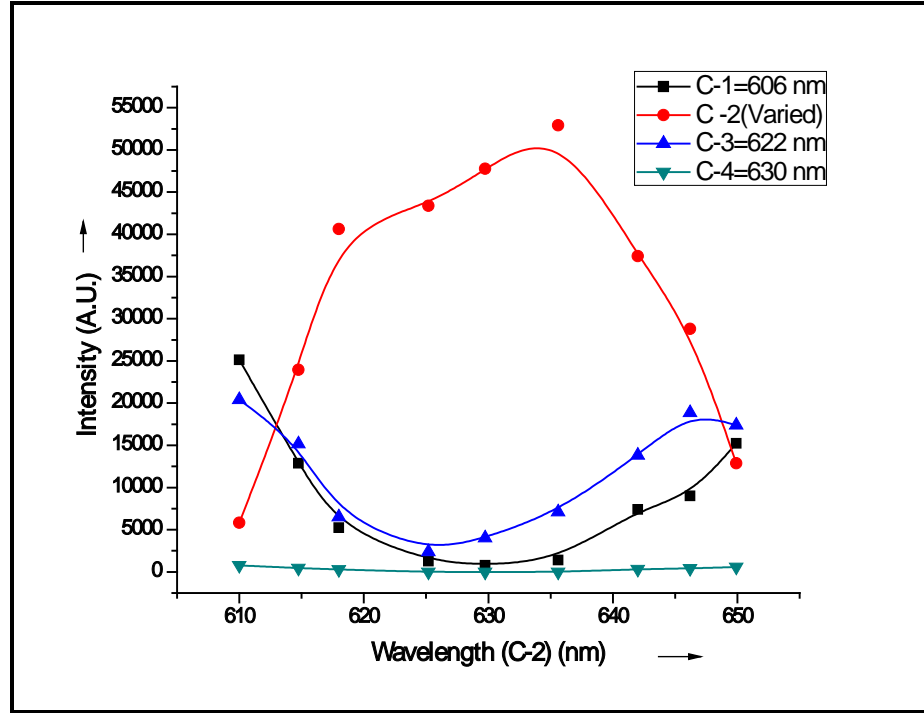


Figure 4.12: Variation of output intensities due to wavelength tuning of sub-cavity C-2, keeping wavelength of C-1, C-3, and C-4 at fixed values (CGIG)

Effect of wavelength tuning of sub-cavity C-3 on output intensities of sub-cavities C-1, C-2 and C-4 are depicted in fig. 4.13 and fig. 4.14. In this experiment, the wavelength of C-3 was tuned in two settings. In the first setting wavelength of sub-cavity C-1 was set (~610 nm) at beginning of the tuning curve (fig. 4.13) whereas C-2 was set (~650 nm) at the end of the tuning range. In the second setting (fig.4.14), the wavelength of sub-cavity C-1 was set (~654 nm) at end of the tuning range whereas C-2 was set at the beginning of the tuning range (610 nm).

The wavelength of sub-cavity C-4 (630 nm) was kept the same for both the settings. In both cases, sustained four wavelength operation was achieved

## CHAPTER - 4

throughout the tuning range of sub-cavity C-3 i.e. from 615 nm to 647 nm. This shows that C-3 was having the least effect on sustained four wavelength operation and can be tuned to any of the wavelengths inside its tuning range.

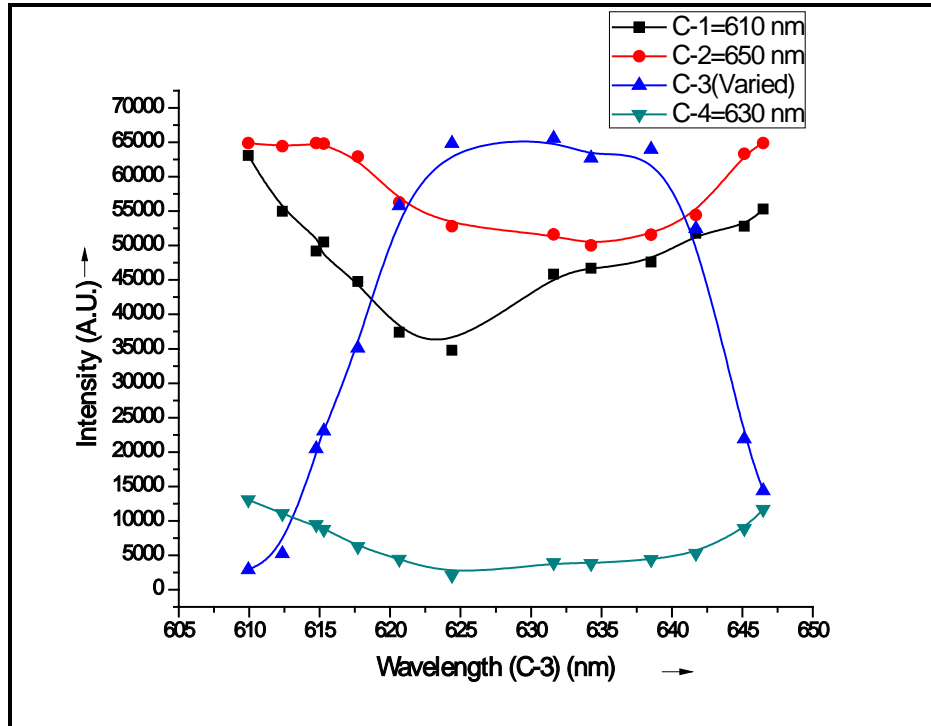


Figure 4.13: Variation of output intensities due to wavelength tuning of sub-cavity C-3, keeping wavelength of C-1, C-2, and C-4 at fixed values (CGIG)

However a reduction in the output intensity of sub-cavities C-1, C-2 and C-3 were observed when the wavelength of C-3 tuned through its tuning range.

The effect of wavelength tuning of sub-cavity C-4 was not studied as it was expected to be least influencing sub-cavity due to its highest loss. However, for sustained four wavelength operation, it was observed that the wavelength of the fourth sub-cavity has to be around the peak of the available gain (624 nm to 630 nm) medium.

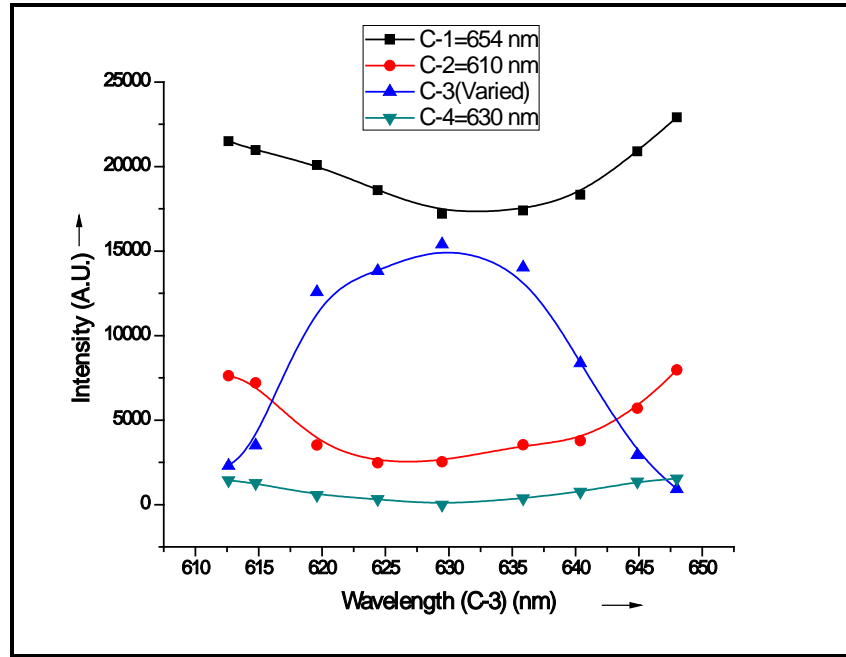


Figure 4.14: Variation of output intensities due to wavelength tuning of sub-cavity C-3, keeping wavelength of C-4, C-1, and C-2 at fixed values (CGIG) but wavelength values of C-1 and C-2 interchanged

#### 4.4.2 Hybrid Cascaded Grazing Incidence Grating Cavity (HCGIG):

In HCGIG, first to third GIG sub-cavities were also observed to behave similarly as for CGIG, whereas the fourth cavity (Littrow configuration) was observed to have the largest tuning range from 599 nm to 667 nm. The maximum efficiency of the sub-cavities in CGIG was observed to decrease from around 2% (first cavity) to 0.25 % (fourth cavity). In HCGIG, the fourth cavity was having the highest efficiency of nearly 7-8% whereas first, second and third cavities were having efficiencies of approximately 2%, 2%, and nearly 1% respectively, as shown in fig. 4.15. Pump beam pulse energy was 2 to 2.5 mJ. The efficiencies were measured when single sub-cavity was allowed to lase and the other three sub-cavities were blocked at tuning mirrors. In the second configuration i.e. HCGIG, gain competition behavior was different as cavity loss of the fourth sub-cavity reduced drastically as the grating was kept

## CHAPTER - 4

at the Littrow angle and take the most dominant role in deciding the gain competition effects.

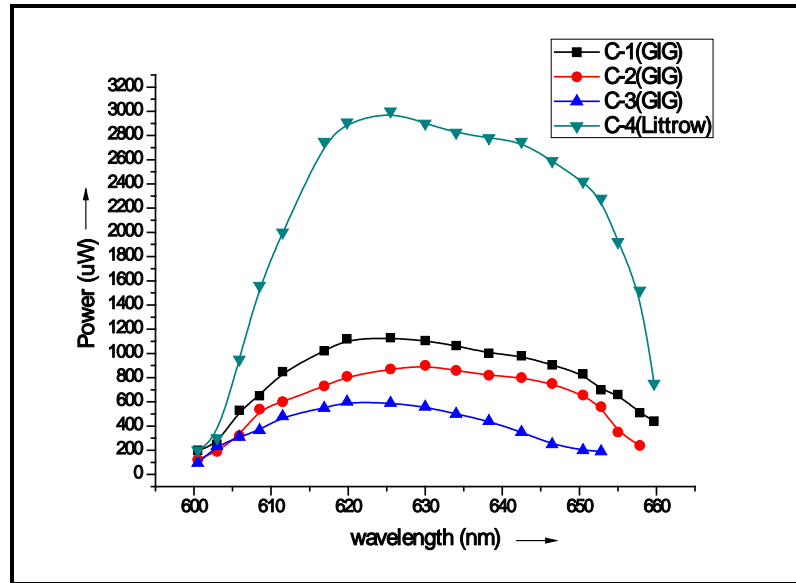


Figure 4.15: Tuning curves of four HCGIG sub-cavities

The wavelength of sub-cavity C-1 could be tuned (fig.4.16) only from 606 nm to 612 nm for the sustained four wavelength operation after that C-2 (~ 650 nm) ceased lasing but C-3 (~ 630 nm) & C-4 (660 nm) could still lase.

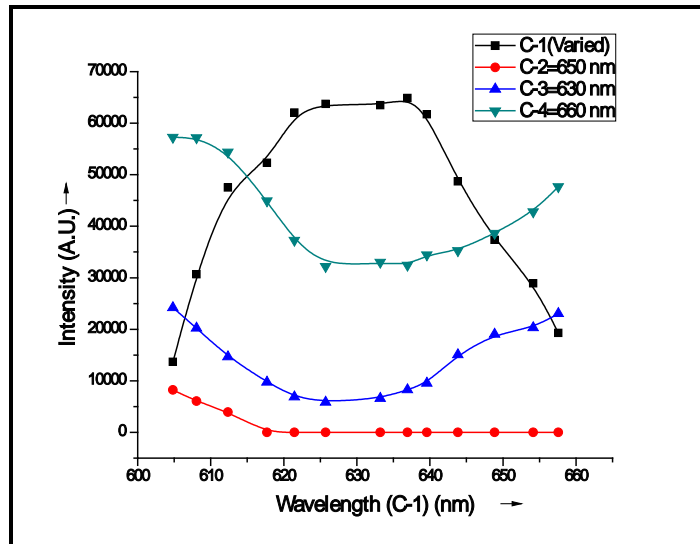


Figure 4.16: Variation of output intensities due to wavelength tuning of sub-cavity C-1, keeping wavelength of C-2, C-3, and C-4 at fixed values (HCGIG)

The wavelength of sub-cavity C-2 could be tuned from 611 nm to 624 nm and 636 nm to 650 nm for sustained multi-wavelength operation (fig.4.17).

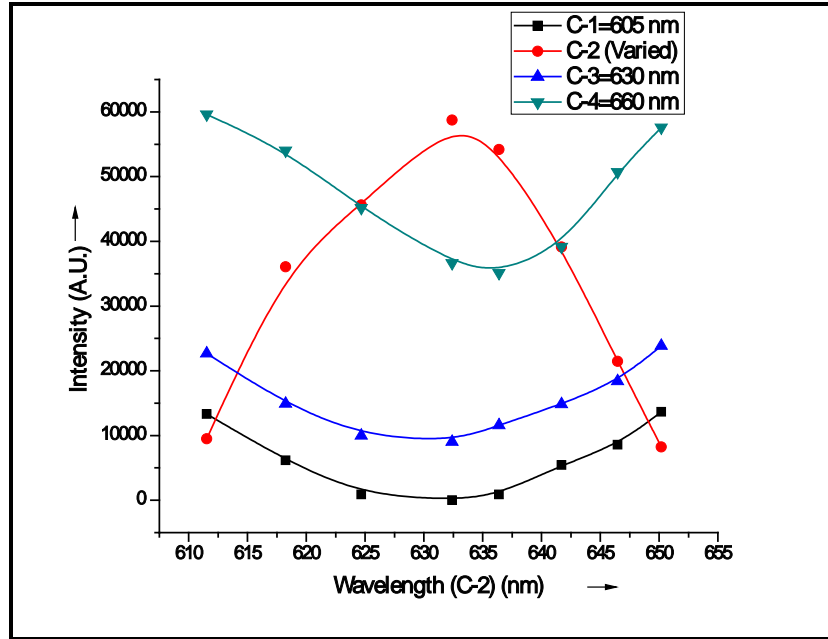


Figure 4.17: Variation of output intensities due to wavelength tuning of sub-cavity C-2, keeping wavelength of C-1, C-3, and C-4 at fixed values (HCGIG)

Sub-cavity C-1 ceased lasing when the wavelength of sub-cavity C-2 was tuned from 624 nm to 636 nm i.e. the peak of its tuning range. Similar to the CGIG resonator case, when the wavelength of sub-cavity C-3 was tuned through its entire tuning range from 612 nm to 645 nm, four wavelength operation was sustained. However, output intensities in sub-cavities C-1, C-2 and C-4 reduced due to gain sharing (fig.4.18). The major operational difference between CGIG and HCGIG configurations was the performance and efficiency of the fourth sub-cavity C-4.

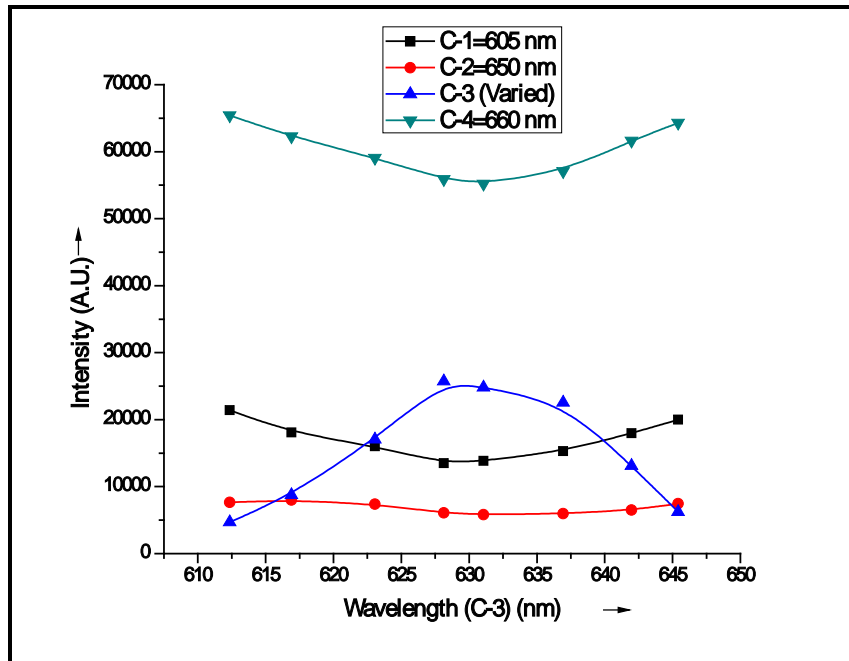


Figure 4.18: Variation of output intensities due to wavelength tuning of sub-cavity C-3, keeping wavelength of C-1, C-2, and C-4 at fixed values (HCGIG)

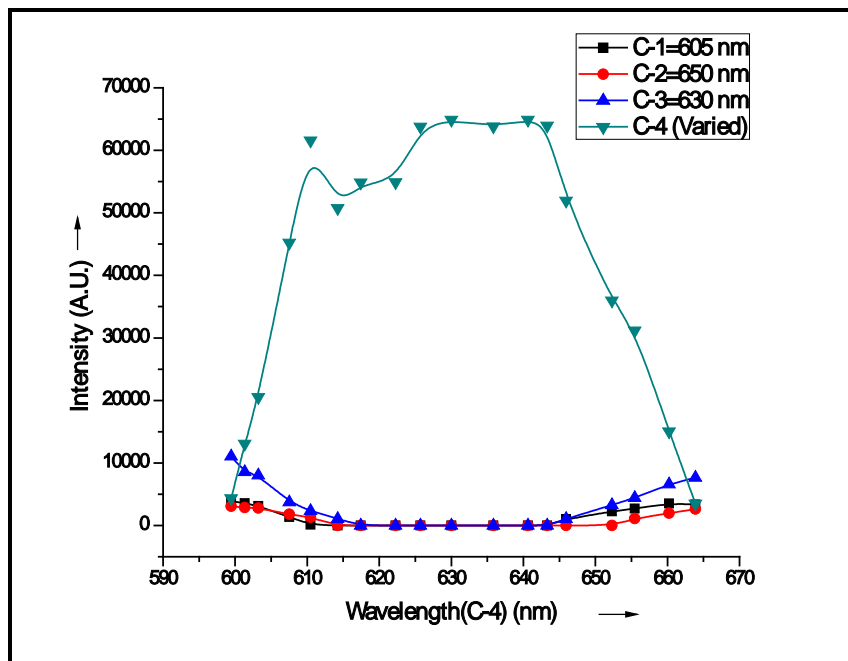


Figure 4.19: Variation of output intensities due to wavelength tuning of sub-cavity C-4, keeping wavelength of C-1, C-2, and C-3 at a fixed value (HCGIG)

Sub-cavity C-4 turned out to be the most dominant cavity in HCGIG whereas, in CGIG, C-4 was the weakest cavity with the lowest efficiency and smallest

tuning range. In HCGIG, wavelength tuning of C-4 from 610 nm to 650 nm stopped lasing in all the other three sub-cavities. Four wavelength generation could only happen when the wavelength of sub-cavity C-4 tuned (fig.4.19) from 599 nm to 610 nm and 650 nm to 667 nm. Contrary to this in the CGIG case, the fourth cavity had to be operated at the peak of the gain.

**4.4.3 Zone of Operations in CGIG and HCGIG Cavities:**

The gain competition behavior resulted in identifying the zone of operation for each sub-cavity for sustained four wavelength operation is summarized below in table-4.1.

*Table 4.1: Zone of individual sub-cavities in both the configurations for sustained four wavelength operation in DCM dye laser*

Resonator configuration	Tuning range of C-1	Tuning range of C-2	Tuning range of C-3	Tuning range of C-4
CGIG Resonator	606 – 616 nm 644 nm – 648 nm	610 – 618 nm 642 – 649 nm	615 – 647 nm	Independent due to high intracavity loss
HCGIG Resonator	606 nm to 612 nm	611 nm to 624 nm & 636 nm to 650 nm	612 nm to 645 nm	599 nm to 610 nm & 650 nm to 667 nm

The wavelength tuning zones for individual sub-cavities for sustainable four wavelength operation which is due to gain competition effect for generating a collinear, simultaneously operable, spatially and temporally overlapped output laser beam has been described in this chapter.

## CHAPTER - 4

---

In CGIG configuration, line width (FWHM) was measured to be around 2 GHz, 3 GHz, 4 GHz and  $> 5$  GHz for sub-cavities C-1, C-2, C-3, and C-4 respectively. Figure 4.20 represents the Fabry Perot etalon (FP) fringe of first sub-cavity in CGIG with a line width of the order of 2 GHz. Even though grating illumination of all the gratings was around 52 mm, deterioration of line width from shortest to longest sub-cavity is due to a reduced number of round trips as it goes from shortest to longest sub-cavity. For example, round trip time for sub-cavity C-4 in CGIG is 4.2 ns and it will hardly have two round trips during gain duration of  $\sim 7$  ns FWHM of the dye laser.

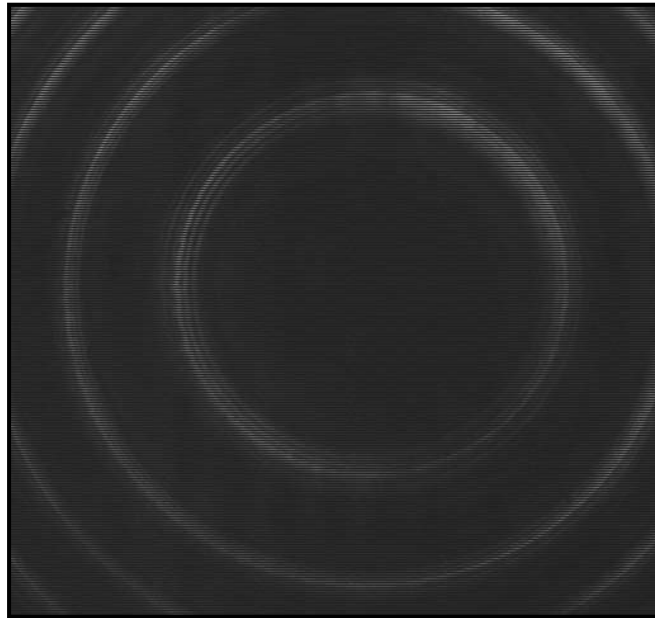


*Figure 4.20: Representative Fabry Perot (15GHz FSR) etalon fringes of sub cavity C-1(CGIG)*

Although four wavelengths had the same pulse shape, the four beams are not a priori automatically synchronized, because cavities having a lower loss and higher gain will reach threshold first with the result that delay times of 2-3 nsec or more have been observed between first and fourth wavelength. The

## CHAPTER - 4

---

pulse duration of 6, 5, 4 nsec was measured for output pulses from sub-cavities C-1, C-2, and C-3 respectively in CGIG configuration.

However, in HCGIG, the fourth cavity (Littrow configuration) has a pulse duration similar to the first cavity, which had the minimum losses. The temporal rise time of the output pulses from four wavelength dye laser was observed to be sharper in C-3 than in C-1. The identical linear polarization of all the four wavelength outputs was confirmed using a Glan laser polarizer. All the four laser beams were found to be collinear with the same aspect ratio up to a distance of 15 meters.



*Figure 4.21: Picture of the intra-cavity beam combined four wavelength laser system*

Picture of the intra-cavity beam combined four wavelength laser system is shown in fig. 4.21. Four cascaded gratings at near grazing angles are shown with all the intra-cavity elements.

Spectrograph recorded by Avantes make spectrophotometer (Model no: AvaSpec-2048 XL) is reproduced in fig.4.22 and fig.4.23 for the CGIG and HCGIG configurations respectively.

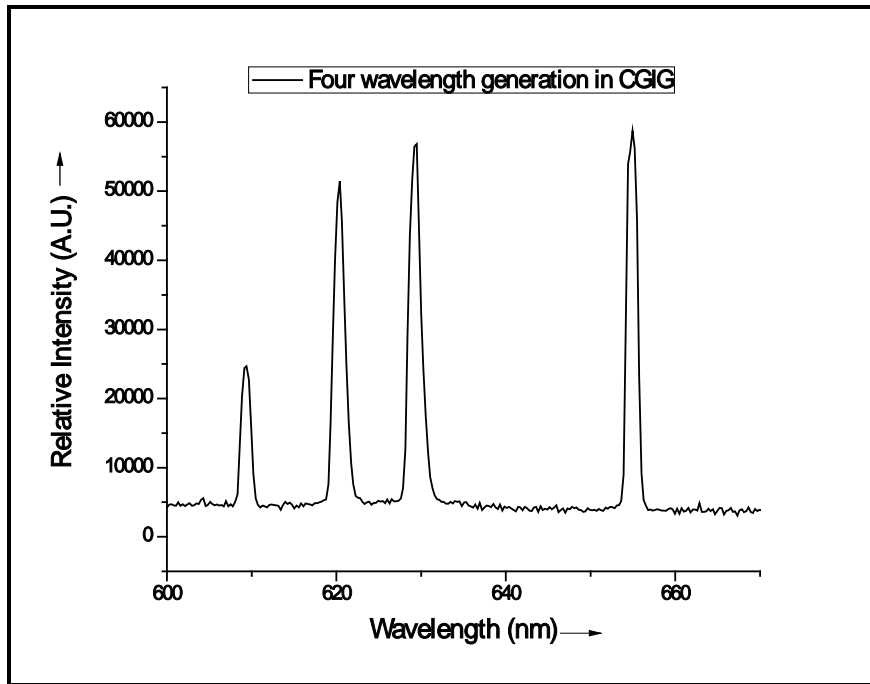


Figure 4.22: Simultaneous four wavelength generation in CGIG resonator

#### 4.5 Five Wavelength Generation in a Hybrid Cascaded Grazing Incidence Grating:

The study of HCGIG has been extended to five wavelength generation (Fig. 4.23), in which four wavelengths generated from four cascaded grazing incidence gratings and fifth wavelength in Littrow angle configuration.

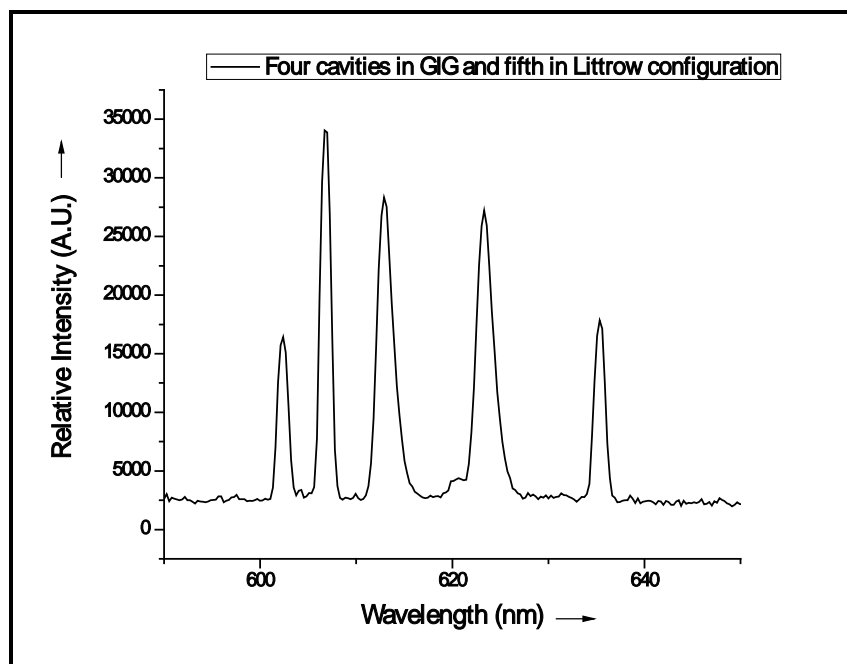


Figure 4.23: Simultaneous five wavelength generation in HCGIG resonator

This validates the studies for extended multiple wavelength generation from two to five. The generation of more wavelengths will depend on intracavity gain-loss dynamics of the cavity and pulse duration of the pump laser, which will have the limit on a maximum number of round trips.

As a comparison copper vapor laser has generally 4-5 times (30 nsec as compared to 7 nsec) longer pulses of pump beam which may facilitate longer zones of wavelength for each sub-cavity for sustained multi-wavelength operation and reduced linewidths.

### **4.6 Conclusion:**

A feasibility study of multi-wavelength generation from possible narrowband cavities were investigated and identified multi-wavelength generation (2 to 5) from cascaded GIG cavity without prism beam expanders. The advantages of this cavity are discussed in detail. This work will be useful for laser-based studies that require multi-wavelength with independent wavelength tunability and narrow bandwidth requirement. Various cavity configurations for multiple wavelength generation potentials were experimentally validated. Linear cascaded grating cavity configuration without prism beam expander was found most suitable for more than two-wavelength generation.

Four wavelength dye laser operation in cascaded grating-based two resonator configurations has been successfully demonstrated. Wavelength tuning ranges were observed to be reduced from first to third sub-cavity in both the configurations. The fourth sub-cavity (Littrow angle configuration) was having the widest wavelength tuning range in HCGIG configuration. Gain competition effects due to wavelength tuning of one sub-cavity on the performance of other sub-cavities are studied in detail. This resulted in identifying the operable wavelength zones for each individual sub-cavity in both the configurations for sustained four wavelength dye laser operation

which is interplay between available dye gain and intracavity losses. Intensity control and gain competition manoeuvring by tailoring the cavity loss by changing the angle of incidence of the diffraction grating but with variable line widths can be achieved. As an extension of these studies, equalized round trip time of all the sub-cavities by adjusting the grating - tuning mirror distance can be done and hence can achieve inherent temporal synchronization. Grating illumination length and round trip time of each sub-cavity will decide the resultant linewidth of the output laser beam. Further, it was observed that the first and second sub-cavity having lower losses needs to be operated at either end of the tuning range. The third sub-cavity observed to be less dominant in deciding the sustained four wavelength operation. Interestingly, the fourth cavity has to be operated at the peak of the gain curve in CGIG whereas at the end of the tuning range in HCGIG configuration. This concludes that sub-cavity with the lowest loss will be dominant in deciding the operable wavelength zones irrespective of their position in the cascade. Among both the configurations studied, HCGIG finds an advantage over CGIG, due to its wider tuning range with better efficiency and higher output power from the fourth sub-cavity. However, in all sub-cavities, output intensities of three fixed wavelength sub-cavities show a dip when the fourth sub-cavity is tuned to the peak of its tuning range which is a clear indication of the gain competition. Collinear, simultaneously operable, sustained four wavelengths dye laser operation with independent wavelength tenability has been demonstrated.

# Chapter: 5

## External Cavity Beam Combination Techniques for High Power, Pulsed Dye Laser Systems

---

### 5.1 Introduction:

Combining the laser beams external to the resonator cavity is utilized for spectral beam combination of the high power pulsed dye lasers. It provides the freedom for optimization of the individual laser cavities. The gain competition is known to be higher at higher pump powers [5.1, 5.2]. The stringent requirement of handling gain competition among the sub-cavities makes it difficult at higher pump power in the intra-cavity configuration. Therefore, the external cavity beam combination was studied in detail for spectral beam combination at higher power levels.

High power is generated by amplification of a few watts of oscillator output beam in a master oscillator power amplifier (MOPA) chain [5.4]. A high power dual-wavelength laser beam can be obtained by using two configurations namely amplification of individual laser beams before the spectral beam combination termed as individually amplified (IA) scheme and co-amplification (CA) of the composite laser beam combined before the amplification. IA and CA based external cavity beam combination techniques have been studied for this thesis work. Both the configurations were studied for the closely separated (<10nm) wavelengths generated by the dye laser MOPA chains pumped by a green and yellow beam of copper vapor laser (CVL) MOPA chains, which ensured complete utilization of the available pump power to obtain desired output power from the dye laser.

CVL and diode-pumped solid-state (DPSS) green lasers were used to pump the oscillators which were characterized to generate the low power, good quality dye laser beam. Detailed experimental setup of a narrowband oscillator, MOPA chains and characterization of the dye laser beam are described in this chapter. Two individual oscillator beams were tuned to wavelengths separated by less than 10 nm; IA and CA configurations were studied using these dye laser beams. The characterization of the co-amplification based spectral beam combination technique was studied. The gain competition effect in the co-amplification was due to the simultaneous amplification of two closely separated wavelengths uses common dye gain medium. It is less severe as compared to the intra-cavity beam combined system described in the previous chapter (chapter 3). It can be compensated by suitably adjusting the input intensities of the individual dye laser beams by using beam splitters before the co-amplification. The gain competition behaviour at various pump powers and input signal will be studied. These analyses will be very useful for fixing the input intensities, to obtain the desired output intensities from a CVL pumped DCM common amplifier. The entire work towards the efficient spectral combination technique studied for high power, pulsed dye laser is described in subsequent sections of this chapter.

### **5.2 External Cavity Beam Combined Dye Laser Systems:**

In MOPA configuration the dye laser oscillator was followed by amplifier systems to generate high power dye laser beams. The narrowband dye laser signal beam was generated in the grazing incidence grating (GIG) based oscillators. Two different dye laser oscillator beams were individually amplified to the higher power levels and then spatially overlapped using a suitable beam combiner. In the other set, laser beams of different wavelengths were spatially combined after the oscillators and this composite

dye laser beam was subsequently amplified to higher power levels using a common amplifier. Characteristics of both these methods were studied in detail, and presented in this chapter.

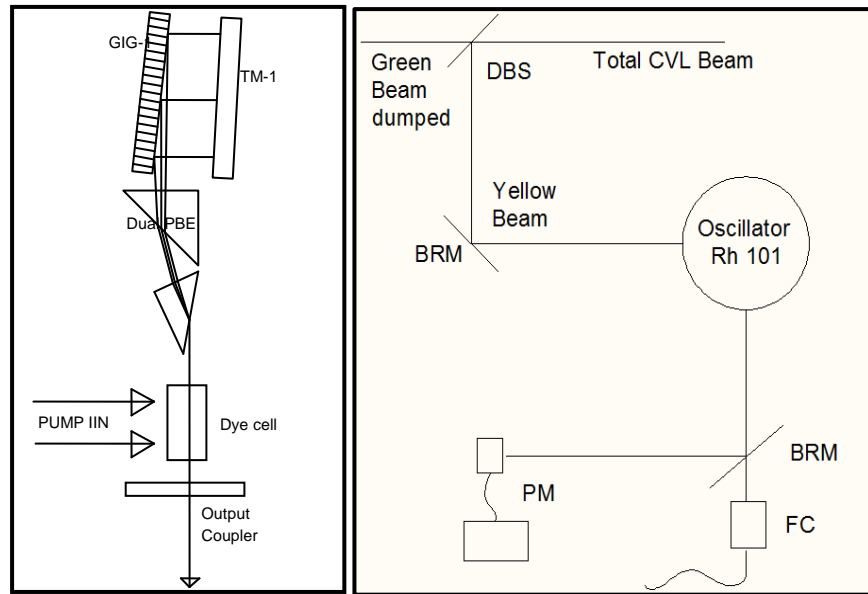
### **5.2.1 Narrowband Dye Laser Oscillators:**

A laser beam of required wavelength with desired attributes was generated using a resonator cavity consisting of dispersive and non-dispersive optical components. The CVL and DPSSL lasers were used as the pump source for pumping the dye laser oscillator.

#### **5.2.1.1 Copper Vapor Laser Pumped Dye Laser Oscillators:**

The CVL is well known as high power, high repetition rate pulsed laser source, which is widely used for pumping the dye lasers [5.5]. Power scaling of a CVL laser system is done by cascading several amplifier modules as per the power requirement described in chapter-2. The dual-wavelength (green & yellow) emission extends its use for pumping various laser dyes, which results in the wider emission range from 550 nm- 700 nm. These are some features, which were the key drivers for using CVL as the pump laser source for the current studies.

A Grazing incidence grating (GIG) cavity with an intra-cavity double prism beam expander (PBE) was set up as shown in fig. 5.1(a). The output coupler (OC), PBE, grating at a grazing incidence angle of  $81^{\circ}$  and tuning mirror (TM) were aligned across the dye cell (DC) to obtain the narrow-band dye laser beam of required wavelength. A combination of the spherical and cylindrical lens was utilized to obtain a line focal spot of pump beam around 400-500 micron diameter and 16 mm gain length.



(a) Grazing Incidence Grating Oscillator (b) Characterisation setup

Figure 5.1: Yellow beam pumped oscillator characterization set up

(GIG: Grazing Incidence Grating, TM: Tuning Mirror, DC: Dye Cell, OC: Output Coupler, PBE: Prism Beam Expander, DBS: Dichroic Beam Splitter, FC: Fiber Coupler, PM: Power Meter, BRM: Beam Routing Mirror)

The same configuration (GIG) was used to generate two wavelengths namely  $\lambda_1$  and  $\lambda_2$ . The narrowband dye laser beams for spectral beam combination experiment was generated and tuned to closer wavelengths. These beams were used in the common amplifier configuration. Two wavelengths around 632 nm were generated, among them,  $\lambda_2$  was 5-7 nm higher than  $\lambda_1$ . The Rh 101 dye dissolved in spectroscopy grade ethanol was used for both the oscillators with optimized dye concentrations of 0.8 mM and 0.9 mM for  $\lambda_1$  and  $\lambda_2$  oscillators respectively. The higher concentration for  $\lambda_2$  was used for higher efficiency and red shifting of peak wavelength in the tuning curve. The average output power of around 0.480 W and 1.25 watt was

obtained for  $\lambda_1$  and  $\lambda_2$  oscillators respectively. The pump power of 5.7 W and 25 W yellow beam of the CVL was used for  $\lambda_1$  and  $\lambda_2$  respectively. A small part of the oscillator beam was coupled to 125-micron core diameter optical fiber and fed to a wavemeter (Angstrom, WS-7L) for wavelength measurement as shown in fig. 5.1(b). Ophir make (FL150A, accuracy 3%) power meter was used for measurement of the average output power of dye laser as well as the pump laser. The linewidth of the dye laser was measured to be around 2-3 GHz using a wavelength meter.

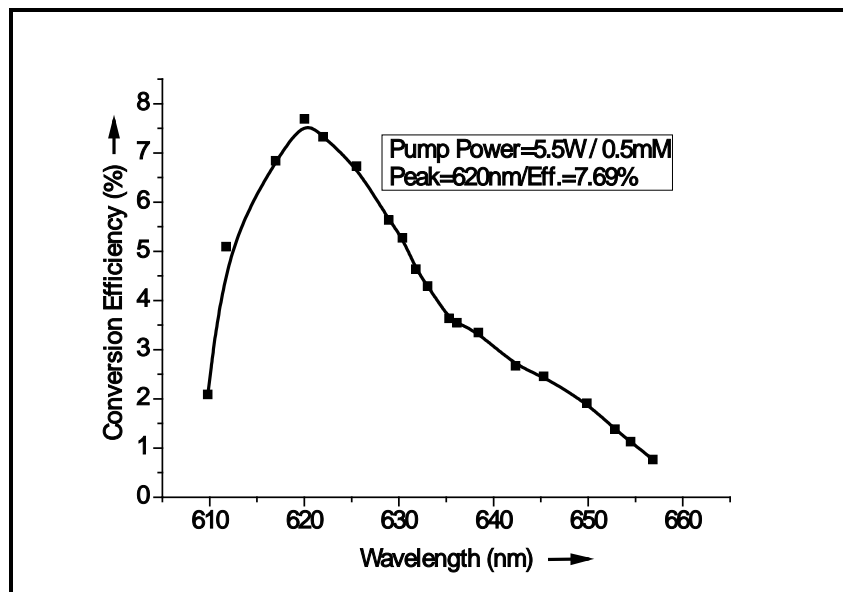
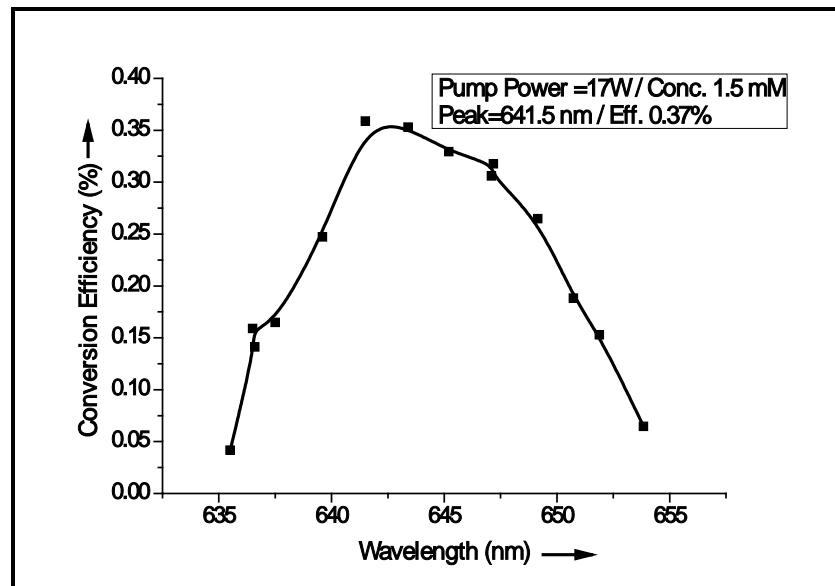


Figure 5.2: Tuning characteristics of Rh 101 dissolved in ethanol

The Rh 101 and PM 650 laser dyes were found to be suitable for pumping by yellow beam of CVL [5.3]. The tuning curve of the dye laser oscillator with Rh 101 and PM 650 dye was obtained as shown in fig. 5.2 and 5.3. In ethanol, Rh101 dye with 0.5 mM concentration shows maximum conversion efficiency at 620 nm. Redshifting in the peak wavelength was achieved by increasing the concentration from 0.5 mM to 1 mM. The tuning ranges of Rh 101 dye and PM 650 were

## CHAPTER - 5

compared. The tuning range for Rh101 in ethanol (fig. 5.2) was measured to be 610nm - 657 nm with a peak wavelength of 620 nm and a conversion efficiency of 7.69%. The wavelength tuning range of PM 650 with 1.5 mM concentration in ethanol dye was measured to be from 635 nm to 653 nm as shown in fig. 5.3 with maximum conversion efficiency of 0.36% at 641.5 nm. The PM 650 dye was pumped by 17 W of yellow beam of CVL. Hence, Rh 101 dye was selected for further studies. The Rh 101 dye in the binary solvent has been tested.



*Figure 5.3: Tuning curve with PM 650 dye in ethanol*

Figure 5.4 shows the spectral shifting of the tuning curve obtained with ethanol and ethanol-water binary solvents. The peak of emission wavelength has been shifted from 620 nm to 631.2 nm. This redshifting in the emission peak of Rh 101 laser dye was at the cost of reduced conversion efficiency to 2.54 % from 7.69%. Hence pure ethanol as the solvent was selected for establishing a yellow pumped dye laser with Rh 101 laser dye for the entire study.

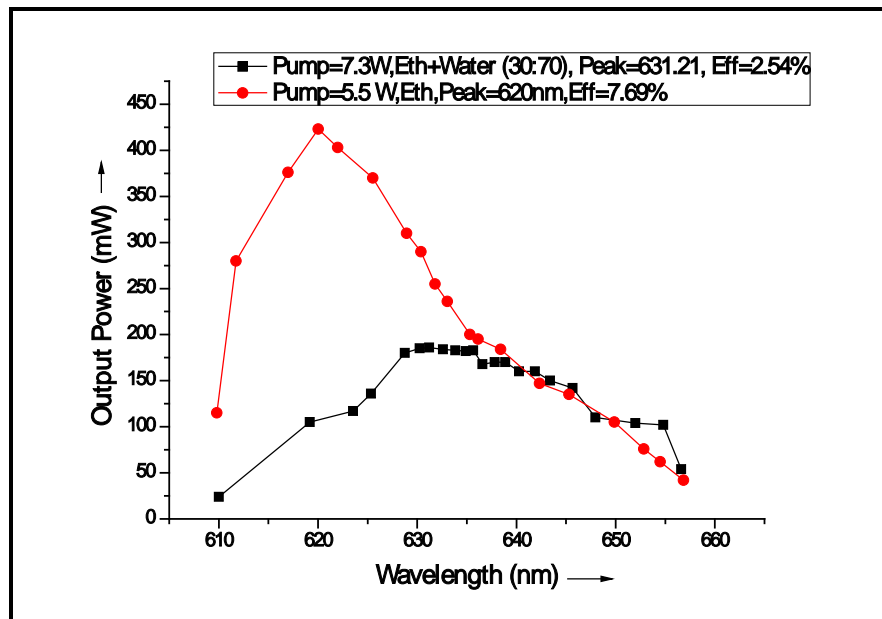


Figure 5.4: Comparison of the tuning curve of Rh 101 dye in ethanol and water, ethanol binary mixture

To extend the tuning range of yellow pumped Rh 101 dye, this dye was dissolved in methanol, as methanol is more polar solvent than ethanol, hence redshifting in the peak emission, as well as the extension of the tuning range, is observed. The tuning curve of the Rh 101 dye laser oscillator in ethanol and methanol is shown in fig. 5.5.

The wavelength tuning range of Rh 101 dye in ethanol and methanol was measured to be 607 nm to 637 nm with a peak wavelength at 618 nm and 611 nm to 650 nm with peak wavelength at 623 nm respectively. Redshifting of nearly 13 nm in the tuning range was achieved by changing the solvent from ethanol to methanol.

The two wavelengths have been generated, which are separated by 30 nm using the methanol as a solvent for Rh 101 dye. These red-shifted

wavelengths were utilized for testing of Fabry Perot (FP) beam combiner for widely separated wavelengths.

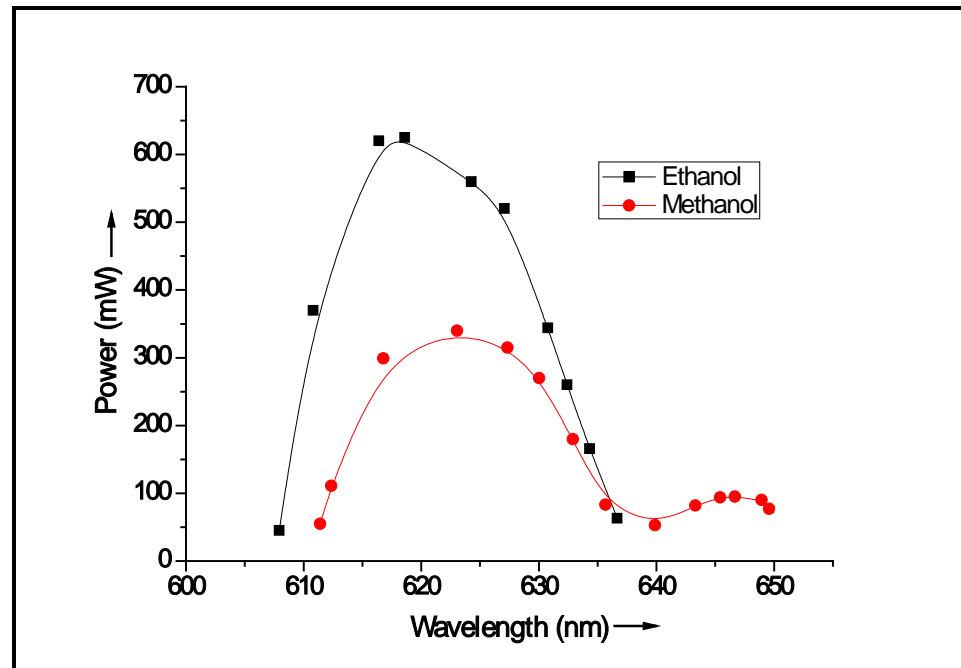


*Figure 5.5: Tuning range of the yellow pumped Rh 101 dye in ethanol and methanol*

Fabrication and characterization of FP spectral beam combiner using these dye laser beams will be discussed in the next chapter.

### 5.2.1.2 Diode Pumped Solid State Laser Pumped Dye Laser Oscillator:

Recent developments in solid-state lasers towards high power, high repetition rate, and efficient operation made them a suitable candidate for pumping the dye lasers. The second harmonic of an Nd: YAG laser operating at 532 nm wavelength is one of the best candidates for pumping dye lasers. Diode-pumped Nd: YAG lasers are an efficient pump source for the dye lasers. The diode-pumped Nd: YAG is a compact and efficient system in comparison to the CVL system. However, the pulse rise time is relatively slower for higher pulse repetition frequency (PRF) Nd: YAG

## CHAPTER - 5

lasers. The fluorescent laser dyes have shorter upper-level lifetimes of nearly a few ns, which demands a smaller rise time pump pulse. Therefore, the feasibility of the DPSS pumped dye laser oscillator was investigated.

DPSS laser system indigenously developed by Raja Ramanna Centre for Advanced Technology, Indore (MP) was used for pumping the dye laser system. The DPSSL system was characterized and relevant parameters are tabulated in table-5.1.

*Table 5.1: Characteristic of the DPSS pump laser system*

<b>Parameters</b>	<b>DPGL(9)#1</b>
Average output power	53W
Pulse Width (FWHM)	40 ns
Rise Time (ns)	23 ns
Fall Time (ns)	42 ns
Temporal propagation delay(ns)	1.80 $\mu$ s
Temporal Jitter (ns)	$\pm 2$ ns

The DPSS laser output power was measured using Ophir make power meter (model: FL 250A, accuracy 3%) and the variation of output power with increasing pump diode current is shown in fig. 5.6. It was observed that the DPSS laser power increased with increasing input current of the pumping diode. The diode input current was varied from 25 A to 40 A, which resulted in an increase of output power from 6.9 to 53.8 W. The effect of input diode current variation on the pulse width and risetime of the DPSSL output pulse was measured with a fast photodiode (FND 100) followed by oscilloscope (Make: Keysight (Agilent), Model: DSO X 3104).

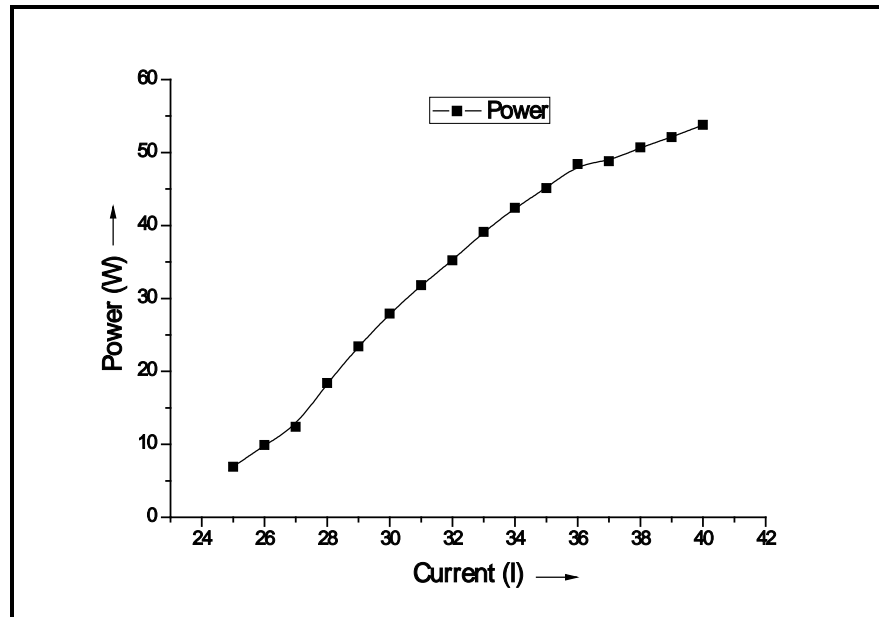


Figure 5.6: Characterization of output power (W) with input diode current

The variation of pulse width with input diode current is plotted as shown in fig. 5.7.

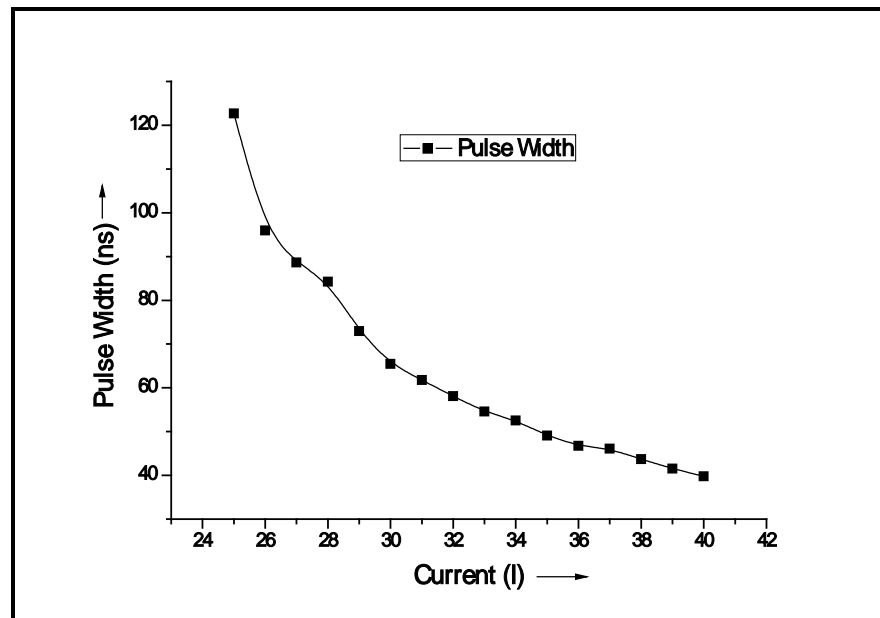
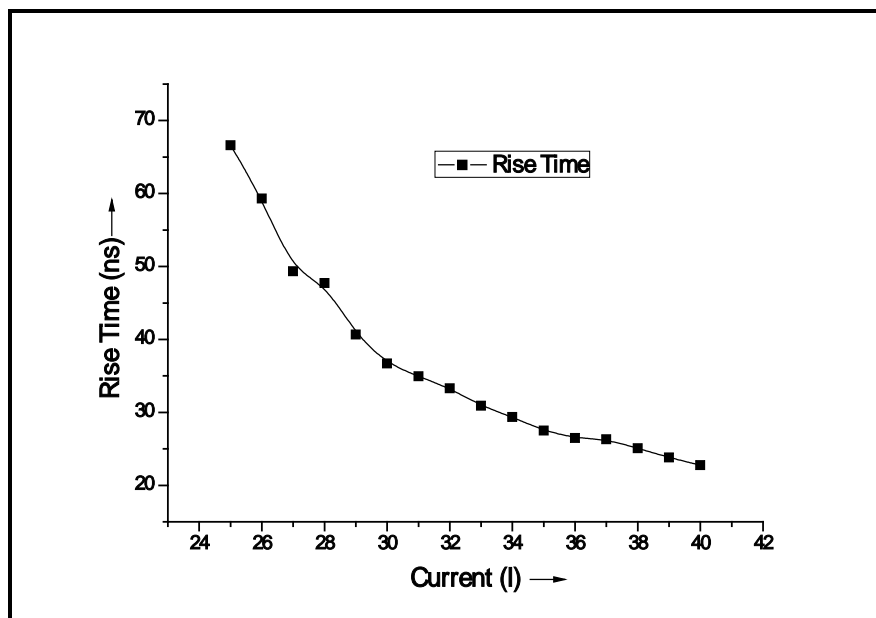


Figure 5.7: Variation of temporal pulse width (ns) with input diode current (A)

The fig. 5.8 shows the effect of input diode current on the pulse rise time of the DPSS laser. On increasing the diode input current from 25A

to 40 A resulted in the pulse width reduction from 122 ns to 40 ns while the rise time was reduced from 66 ns to 23 ns (fig. 5.8). After characterizing the pump laser, it was used for pumping the dye laser and results are presented in the subsequent section.



*Figure 5.8: Variation of pulse rise time with diode input current*

The experimental setup and results for this DPSS pumped dye laser oscillator is described as follows.

### 5.2.1.2.1 Characterization of DPSSL pumped Littrow Cavity Dye Laser:

The DPSS laser beam was routed to the dye laser oscillator using high reflectivity mirrors and suitable relaying optics. Beam expander of magnification 10X was used to match the pump beam size with the gain length in the dye cell. The Rh 19 dye was dissolved in the ethanol having dye concentration of 0.5 mM. As the absorption peak of Rh 19 dye matches with the emission wavelength of second harmonic of the DPSS laser beam.

A cavity with a grating at the Littrow angle was used to obtain the initial broadband laser emission. A Littrow cavity configuration without PBE is shown in fig. 5.9. This cavity was used for testing the temporal behavior of the DPSS pumped dye laser. The linewidth of this Littrow cavity was relatively higher which could not be measured by the FP etalon of 15GHz FSR and finesse of 30.

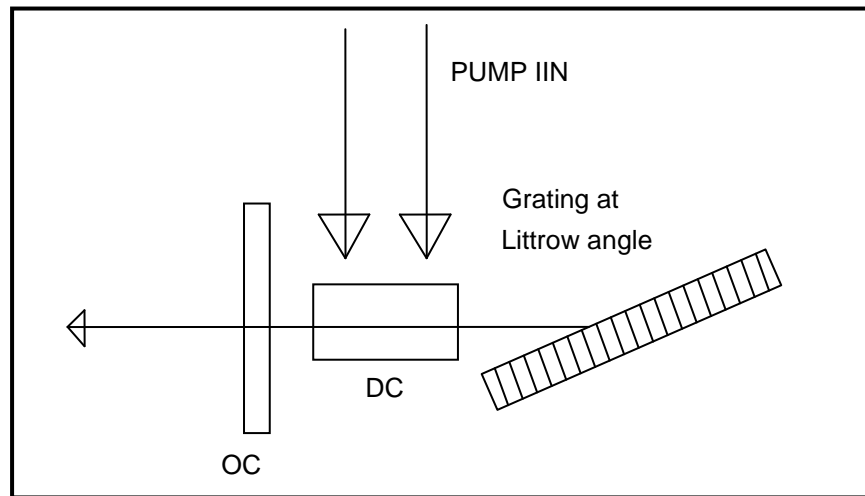


*Figure 5.9: DPSSL pumped dye laser in Littrow configuration (OC: Output coupler, DC: Dye cell)*

### 5.2.1.2.2 Temporal Behaviour:

Temporal parameters of the dye laser output beam were measured along with the DPSSL pump pulse. Effect of pump pulse rise-time and pulse width on the dye laser temporal parameters such as pulse width, rise-time and dye laser output power was studied. The temporal behaviour of the DPSSL pumped dye laser was studied. The effect of pump pulse on the temporal behaviour, power, pulse width and rise time of the dye laser was measured. The temporal characteristics of the dye laser pulse at various input pump pulse widths and rise times were

## CHAPTER - 5

studied. A constant input pump power of nearly 12 W was maintained by using an appropriate neutral density filter.

The effect of pump pulse width on the dye pulse width is shown in fig. 5.10. It was found that the dye laser pulse width follows the pump laser pulse width. Dye laser pulse width reduced from 44 ns to 30 ns with a variation of the pump pulse width from 65 ns to 42 ns respectively.

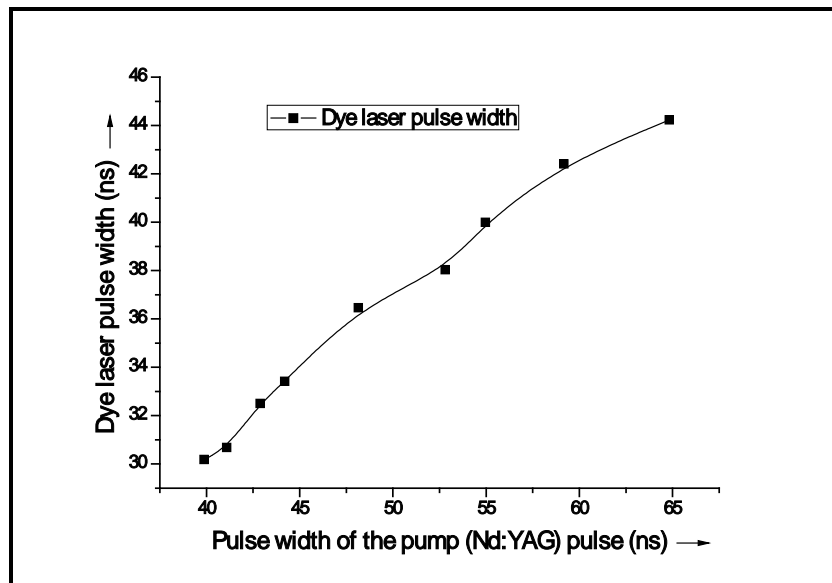


Figure 5.10: Effect of pump pulse width on dye laser output pulse width

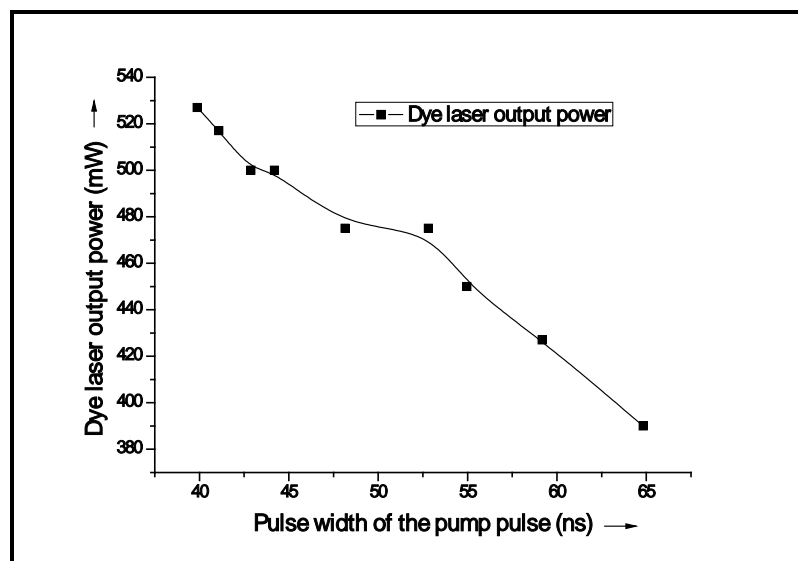


Figure 5.11: Effect of pump pulse width on dye laser output power

## CHAPTER - 5

The effect of the pump pulse width on the dye laser output power is shown in fig. 5.11. It can be seen that higher dye laser output power was obtained at the shorter pump pulse width. Dye laser output power increased from 390 mW to 530 mW on reducing the pump pulse width from 65 to 42 ns.

The effect of pump rise-time on the dye laser output is depicted in fig. 5.12. It can be seen that dye laser output power increased from 390 to 530 mW, due to reduction in rise-time from 38 ns to 22 ns respectively.

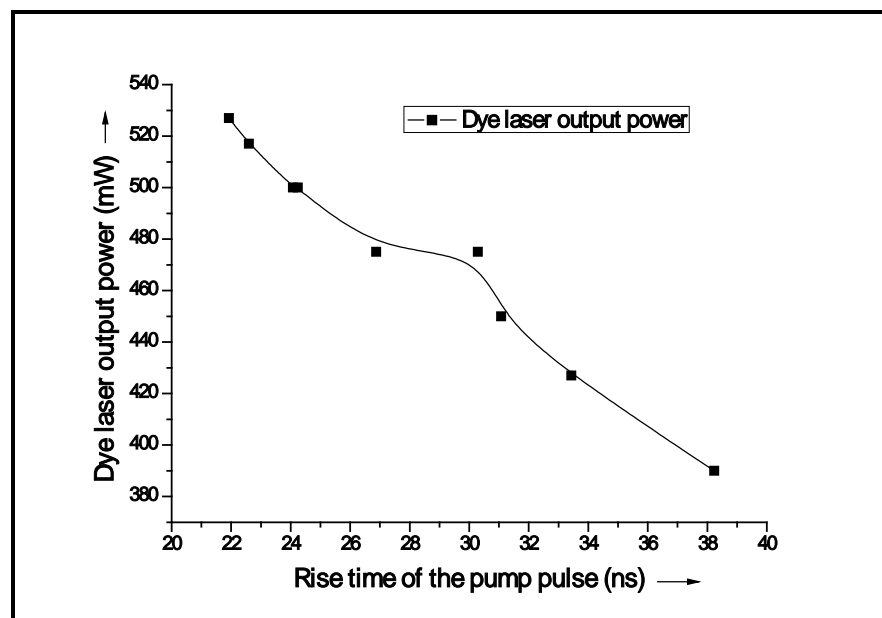


Figure 5.12: Effect of pump pulse rise-time on dye laser output power

The shorter pump pulse width provides an efficient dye laser operation. Similarly, it was also observed that dye laser pulse rise time is short for a shorter rise time pump pulse, which is shown in fig. 5.13. A reduction of pump pulse rise-time from 38 ns to 22 ns results in the shorter dye laser output pulse rise-time from 22 ns to 12.5 ns respectively.

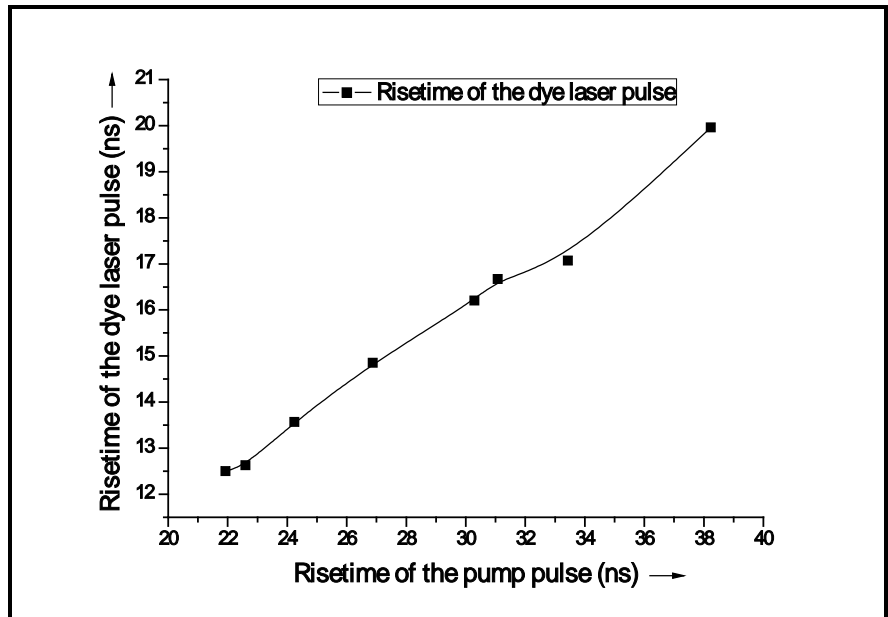


Figure 5.13: Effect of pump pulse rise-time on dye laser output pulse rise-time

Figure 5.14 shows the role of pump pulse rise time on dye laser pulse width

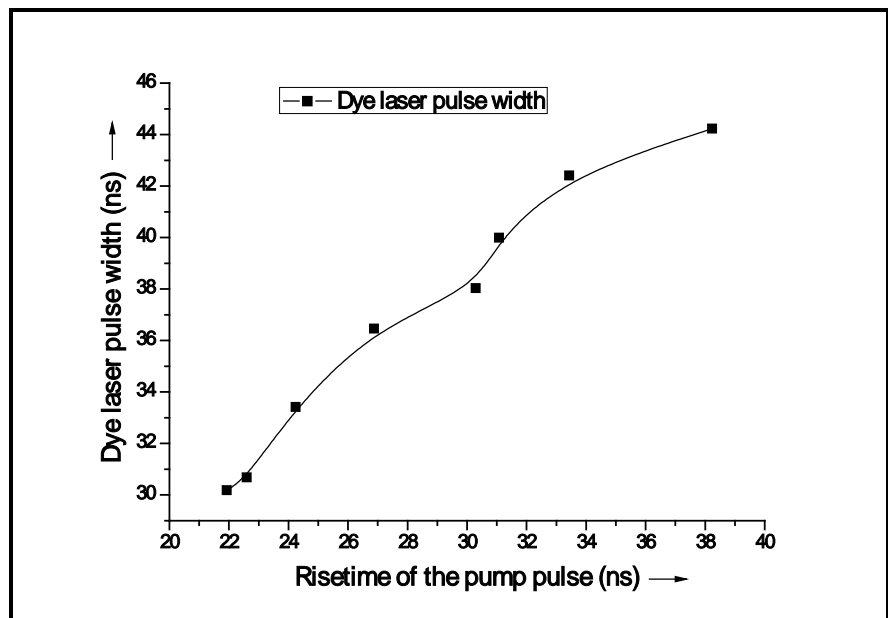
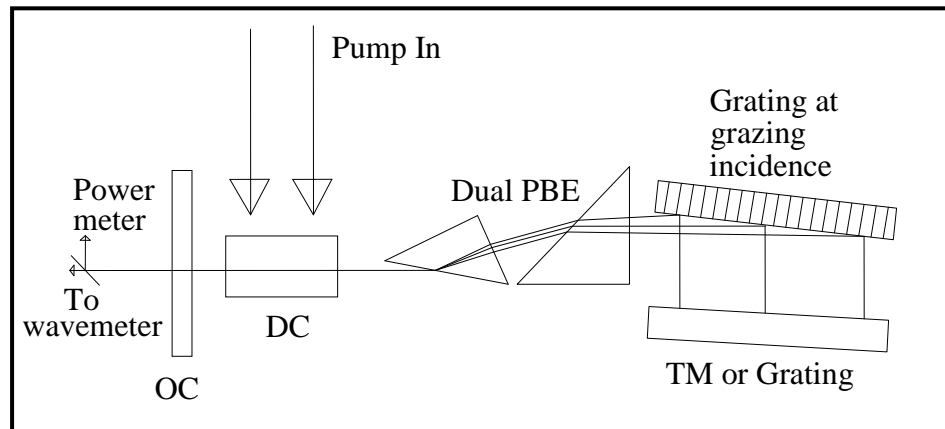


Figure 5.14: Effect of pump pulse rise-time on dye laser pulse width

A reduced pump pulse rise-time from 40 ns to 22 ns resulted in the reduced dye laser pulse width from 46 ns to 30ns. A shorter pump pulse seems to be good for an efficient dye laser with narrower pulse widths.

**5.2.1.2.3 Characterisation of DPSSL Pumped GIG Dye Laser:**

The grazing incidence grating (GIG) based cavity was set up to further narrow down the dye laser linewidth. The schematic of the DPSSL laser pumped narrowband dye laser system is shown in fig. 5.15. Dual prism beam expander of magnification 20X was used for utilizing the full grating length. A grating at a grazing incidence angle of  $\sim 81^\circ$  with a tuning mirror was aligned to obtain a narrowband tunable dye laser beam. The output coupler with 5% feedback was used to obtain the dye laser output.



*Figure 5.15: DPSSL pumped dye laser in GIG configuration*

A small part of the oscillator beam was coupled to 125-micron core diameter optical fiber and fed to the laser wavemeter of Angstrom make, model no.: WS-7L. Ophir make (FL150A, accuracy 3%) power meter (PM) was used to measure the average output power of the dye laser beam. The linewidth of the dye laser beam was measured using a Fabry Perot etalon of FSR: 7.5GHz and finesse of 30. A fast

photodiode (FND 100, rise time  $\sim 2$  ns) followed by an oscilloscope was used for the measurement of pulse width and the rise time.

A shortest possible pump pulse rise time  $\sim 22$  ns and pulse width of  $\sim 40$  ns (FWHM) was used for generating narrowband dye laser. A GIG cavity with PBE was used for these studies. The tuning range was measured to be less than 10 nm when output coupler reflectivity was 5%. The effect of increasing output coupler (OC) reflectivity on the tuning range of the dye laser was studied. It was found that on increasing reflectivity from 5 % to 70 %, the tuning range is extended to a larger range. The role of OC reflectivity on the tuning range is shown in fig. 5.16.

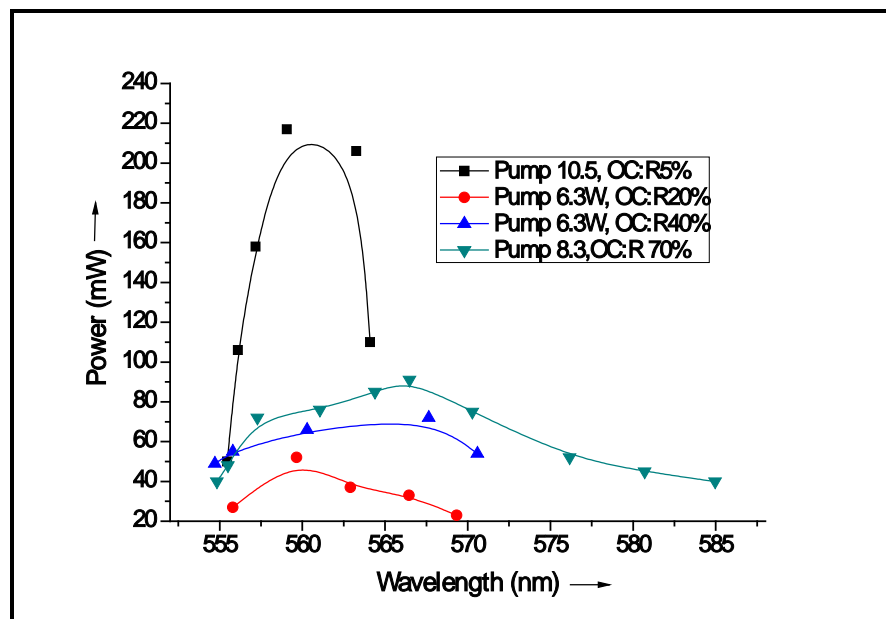


Figure 5.16: Tuning range of DPSSL pumped GIG cavity at various OC reflectivity

The tuning range was found to increase from 9 nm to 30 nm on increasing the reflectivity of the OC from 5 % to 70%. It was observed that on increasing the reflectivity of the OC increases the tuning range

## CHAPTER - 5

---

with reduced peak efficiency. Hence, the OC reflectivity of 20% was kept fixed for the narrowband operation of the dye laser.

The dye laser linewidth was measured more than 7.5 GHz using FP etalon of FSR 15 GHz. This GIG dye laser oscillator was operated with a high reflectivity tuning mirror (TM) and OC reflectivity kept at 5%. Further reduction in the linewidth of the dye laser of the order of 3-4 GHz was achieved, when the OC reflectivity was increased to 20% and the high reflectivity tuning mirror was replaced with a holographic grating at Littrow angle. FP etalon fringe of dye laser shows the narrowband operation of dye laser as shown in fig. 5.17.

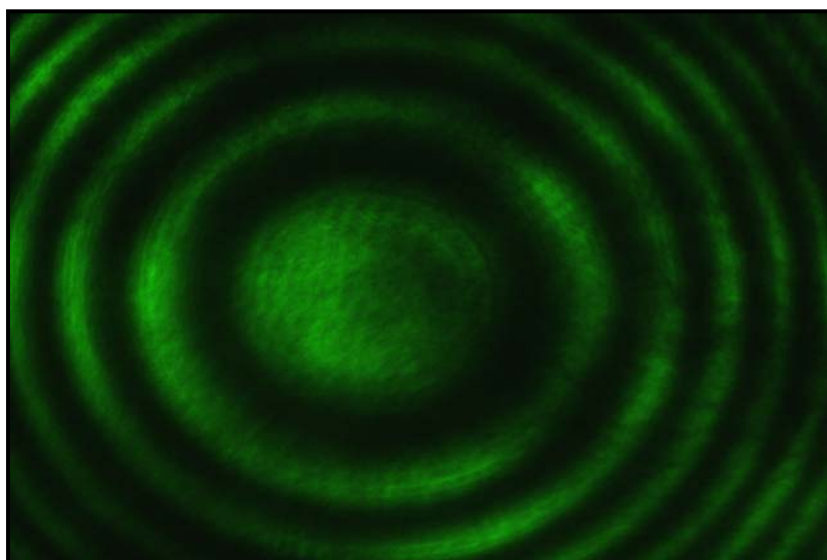


*Figure 5.17: Narrowband operation of DPSS pumped GIG dye laser with FP etalon of FSR 7.5GHz*

The tuning range of this narrow-band dye laser was measured to be from 555 nm to 564 nm with a pump power of 6.4 W. The temporal pulse of the DPSS pump laser along with dye laser output pulse is shown in fig. 5.18.

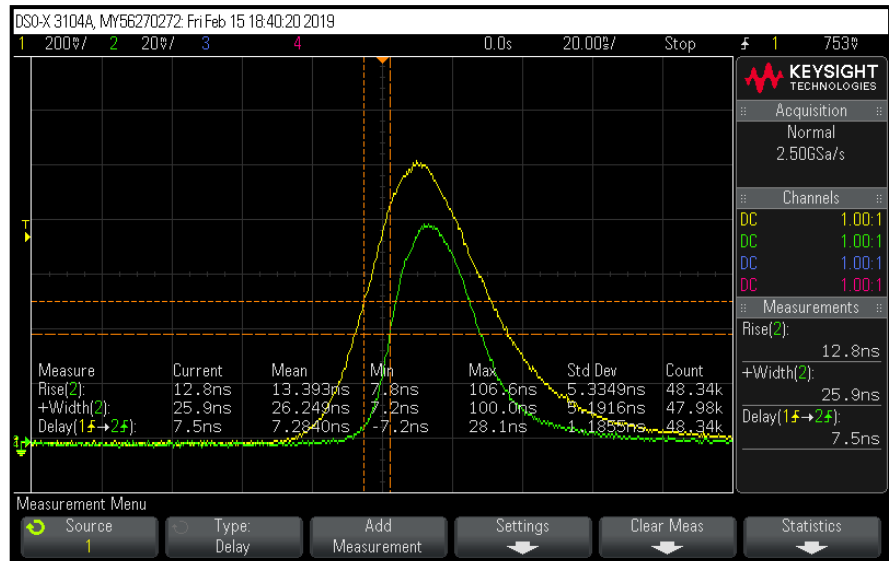


Figure 5.18: Temporal pulse of DPSS pumped GIG dye laser along with pump pulse (Yellow pulse: Dye laser, Green pulse: DPSSL pump pulse))

The DPSSL pump laser was used for pumping the dye laser amplifier module. The DPSSL beam was launched to the optical fiber of core diameter 600 micron and used for pumping the amplifier modules of the dye MOPA chain. The amplifier conversion efficiency of 15% was measured, which was comparable to CVL pumped amplifier system under similar pump and signal power levels. It was concluded that for DPSSL pumping, a special cavity configuration with additional grating in Littrow mode was required for the efficient narrowband operation in the oscillator mode while for amplifier it can be utilized without special care. Hence, CVL pumped dye laser oscillators and amplifier configuration was utilized for the external cavity spectral beam combination studies.

### 5.2.2 Spectral Beam Combination Post Amplification (Method-I):

In this method, CVL pumped Rh 101 dye oscillators were used to generate two laser beams, which are operating at closer wavelengths (<10 nm). These two laser beams were amplified to the desired power level using individual amplifier modules and these high power laser beams of closely separated wavelengths were then combined using beam combiner to generate a single composite beam of a higher power. This spectral beam combination scheme is discussed in subsequent sub-sections.

#### 5.2.2.1 Amplification of Dye Laser Signal Beam:

The enhancement of power levels of the dye laser beam was achieved by amplification of the oscillator signal beam using yellow pumped Rh 101 dye amplifiers. The CVL MOPA beam was distributed using broadband beam splitter (BBS) to the oscillator and amplifier modules. Rh 101 dye solution in ethanol was used in the amplifier module. An optical delay line was used to match the temporal delay of oscillator signal with the amplifier gain at the amplifier dye cell. A pair of the spherical lens (SL) and cylindrical lens (CL) was used to meet the required gain dimensions (16 mm length and 0.500 mm width) by the focussed pump beam at the dye cell. A plano-convex lens of focal length 400 mm was used to focus the oscillator signal beam into the amplifier dye cell. The schematic of the experiment setup is shown in fig. 5.19. Dye concentration and pump power optimization were done to achieve an efficient amplification of the oscillator output beam.



## CHAPTER - 5

0.825 mM respectively. However, there was no further increase in efficiency was obtained even for a higher concentration of 0.9 mM.

After dye concentration optimization, the effect of pump power was studied. Figure 5.21 shows an increasing pump power from 3W to 13W on the conversion efficiency of the dye amplifier increases from 1.4% to 3.47%. Saturation in the amplification efficiency was observed beyond pump power of 10 watts; however higher pump powers for the amplifier resulted in higher conversion efficiencies. Therefore, higher pump power (>10W) was used to amplify the dye laser signal beam to higher power levels, which was used to test the spectral beam combination schemes.

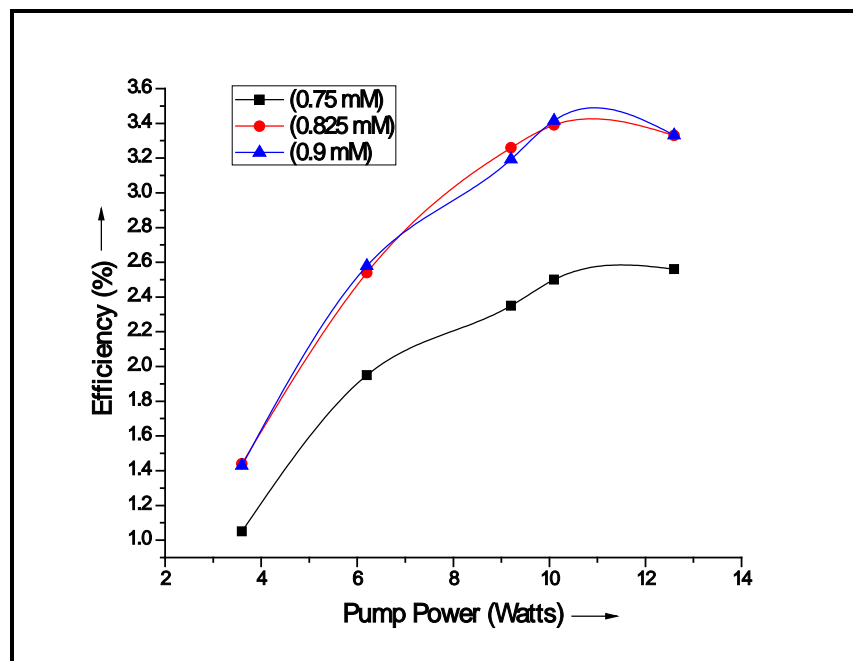


Figure 5.21: Pump power effect in yellow pumped Rh 101 dye amplifier

### 5.2.2.2 Spectral Beam Combination of Individually Amplified Laser Beams:

Spectral beam combination of two individually amplified CVL pumped dye laser beams (closer wavelengths less than 10 nm separated) was carried using

broadband beam splitter. A beam splitter (R: 70 / T: 30) was used to ensure lower combination losses for first (70% losses of the low power beam) and second wavelengths (30% losses of the higher power beam). Higher losses were allowed for the first wavelength as it's requirement seems to be lesser than the other wavelength for the specific spectroscopic experiments.

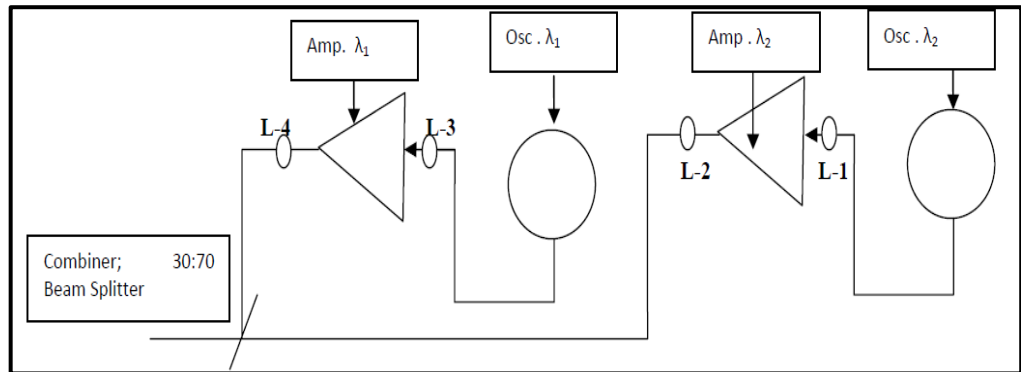


Figure 5.22 Schematic of the spectral beam combination setup

Two dye laser beams generated using MOPA chains are shown in the fig. 5.22. The power of the first and second wavelength beam was measured to be 2.65W and 5.5 W respectively. The average combined output power of 4.65 W (0.8 W of  $\lambda_1$  & 3.85 W of  $\lambda_2$ ) for the total incident power of 8.15 W was measured. The overall combination efficiency of 57% (Input power: 8.15W) was obtained from this combination technique. Another beam combination configuration with a co-amplification based scheme, where these losses expected to be lower needs to be study. This efficient co-amplification based spectral beam combination scheme is described in the next section.

### 5.2.3 Co-amplification Based Spectral Beam Combination (Method-II):

In the first method, high power lasers were generated in separate dye oscillators and successively amplified to the required power levels using individual amplifiers for each beam. A beam splitter (beam combiner) was utilized to combine these

laser beams. In the second scheme, the oscillator beams were combined before the co-amplification of the composite beam in a common amplifier

### **5.2.3.1 Theoretical Evaluation for Co-amplification of Composite Dye Laser**

#### **Beam:**

Two schemes for high power dual-wavelength generation were analyzed, which were closely separated. In the first scheme, laser beam combination is done after amplification of individual laser beams, whereas amplification (co-amplification i.e. CA) is done after beam combination in the second scheme. For these calculations, two scenarios were assumed, one with equal oscillator power combined by equal beam combiner ratio (50/50) and in another scenario unequal power of laser beams combined with unequal combiner ratio (30:70) were considered for comparison.

All the parameters were assumed to be the same to compare both the schemes under similar conditions. It was found that the total calculated combined output power was higher in the co-amplification scheme for both the assumed scenario in these sample calculations. These parameters were experimentally verified and presented in the later section, which is in the same lines as calculated. Amplifier efficiencies were taken the same (5.6%) for both cases. Pump power to the common amplifier (38 Watts) was assumed to be double the pump power to the individual amplifiers (19 W each).

## CHAPTER - 5

*Table 5.2: Calculations for individual and common amplifier scheme selection*

Scheme	Osc. $\lambda_1$ Output	Amplifier $\lambda_1$ Out put Pump:19W	Oscillator $\lambda_2$	Amplifier $\lambda_2$ Out put Pump:19W	Combiner ratio and Losses	Common Amp. Pump: 38 W	Total Output Power ( $\lambda_1 + \lambda_2$ )
I.A. scheme	300 mW	1.36 W (Efficiency = 5.6%)	600 mW	1.66 W (Efficiency = 5.6%)	30% $\lambda_1$ +70% $\lambda_2$ Losses = 70% $\lambda_1 + 30\%\lambda_2 =$ $0.952 + 0.498 =$ 1.45W		0.408 W ( $\lambda_1$ ) + 1.162 W ( $\lambda_2$ ) = 1.57 W
C.A. scheme	300 mW		600 mW		30% $\lambda_1$ +70% $\lambda_2$ Losses = 70% $\lambda_1 + 30\%\lambda_2 =$ $0.210 + 0.180 =$ 0.390W	2.7 W (Efficien cy = 5.6%)	Input to CA= 0.090 + 0.420 = 0.510 W Output = 2.7 W
I.A. scheme	300 mW	1.36 W (Efficiency = 5.6%)	300 mW	1.36W (Efficiency = 5.6%)	0.5 $\lambda_1$ +0.55 $\lambda_2$ Losses = 50% $\lambda_1 + 50\%\lambda_2 =$ $0.680 + 0.680 =$ 1.36W		1.36 W
C.A. scheme	300 mW		300 mW		0.50 $\lambda_1$ +0.55 $\lambda_2$ Losses = 50% $\lambda_1 + 50\%\lambda_2 =$ 0.150 + 0.150=0.300W	2.49 W (Efficien cy = 5.6%)	Input to CA= 0.150 + 0.150 = 0.300 W Output=2.49 W

## CHAPTER - 5

The calculated output power for two schemes is tabulated in table-5.2. Total power in the case of the individual amplifier was calculated after the amplification of both the laser beams. Combined output power after oscillators was taken as input to the common amplifier. A significant reduction in the combination losses in the co-amplification case has been observed as shown in table-5.2.

This advantage became the design basis for the study. This was attributed to a lower percentage of combination losses at lower power levels as compared to the combination of an amplified laser beam. The advantage of lower combination losses motivated to study the common amplifier configuration in detail. Schematic of individual amplification scheme (fig. 5.23) and common amplifier scheme (fig. 5.24) considered for the calculations is shown in fig.5.23 and 5.24.

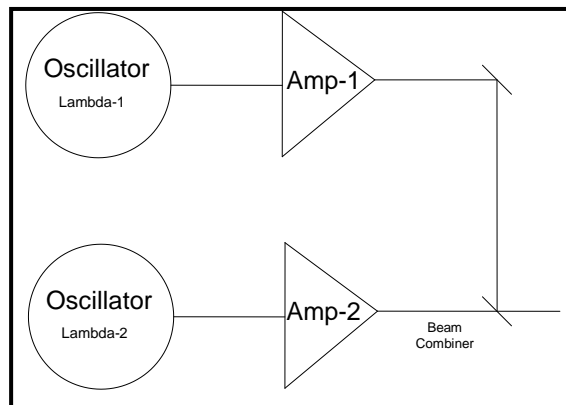


*Figure 5.23: Schematic of high power, dual-wavelength dye laser generation using external cavity beam combination (Individual Amplification scheme) (Amp-1: Amplifier-1, Amp-2: Amplifier-2, BRM: Beam Routing Mirror, C. Amp: Common Amplifier)*

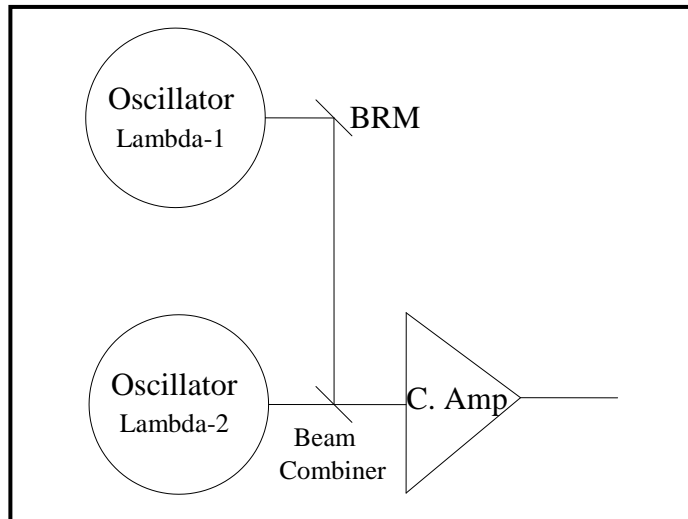


Figure 5.24: Schematic of high power, dual-wavelength dye laser generation using external cavity beam combination (Common Amplifier scheme)

(Amp-1: Amplifier-1, Amp-2: Amplifier-2, BRM: Beam Routing Mirror, C. Amp: Common Amplifier)

### 5.2.3.2 Experimental Study on DCM Dye Common Amplifier:

Both the oscillator beams ( $\lambda_1$  &  $\lambda_2$ ) were spatially overlapped using a broadband beam splitter based combiner. It was chosen due to the capability of handling closer wavelengths, the same polarization, and high average power laser beam. A relay lens of suitable focal length was used to match the spatial properties of both the laser beams at the common amplifier dye cell. The spatial overlap of two dye laser beams was confirmed by monitoring spot size overlaps at near and far distance more than 10 m. The DCM dye with a concentration of 1.5 mM in spectroscopic grade ethanol was chosen as the gain medium due to its favorable absorption of green beam and emission at the desired wavelength range. A transversely pumped common amplifier was set up using a green beam (510.6 nm) of CVL as shown in fig. 5.25.

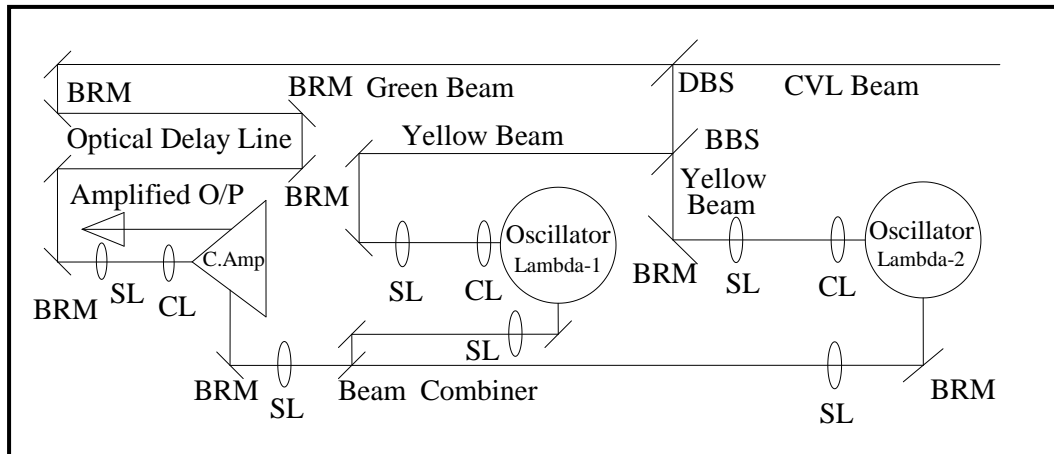


Figure 5.25: Optical layout of the experiment, (DBS: Dichroic Beam Splitter, BRM: Beam Routing Mirror, SL: Spherical Lens, CL: Cylindrical Lens)

A common convex lens of focal length 400 mm at a suitable distance from the common amplifier cell was used to focus the combined laser beam into the transversely pumped common amplifier dye cell. Temporal synchronization between the two dye signal wavelengths was achieved by providing suitable delays, which was ensured using a fast photodiode and oscilloscope (Agilent make, Model No.: MSO 7054 A). The relative output power ratio was measured by using a monochromator (Make: Applied Photophysics, Model: F/3.4) and photodiode based power meter for characterizing the common amplifier.

### 5.2.3.3 Characterization of Dual-wavelength Co-amplifier:

The common amplifier was characterized by varying input signal beam and pump power. The amplified output power of individually amplified beams and co-amplified composite beam were measured using Ophir make power meter (model: FL 250A, accuracy 3%). The characteristics of common amplifier are presented in the following manner i.e. amplifier characteristics of individual  $\lambda_1$ , individual  $\lambda_2$ , composite ( $\lambda_1 + \lambda_2$ ) input beam and their gain competition behavior. The co-amplified composite

output beam was separated using monochromator and power of separated laser beams ( $\lambda_1$  &  $\lambda_2$ ) were measured using a power meter for output characterization.

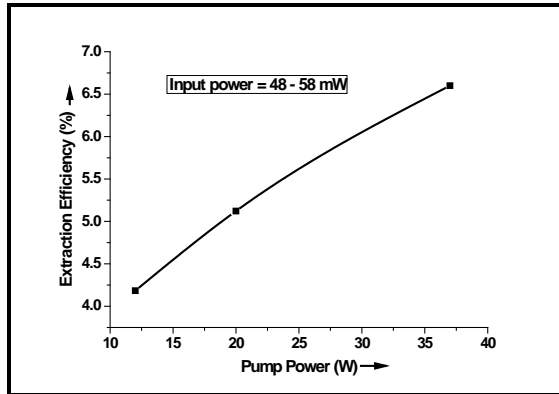


Figure 5.26: Pump power effect on amplifier extraction efficiency of individually amplified  $\lambda_1$  beam

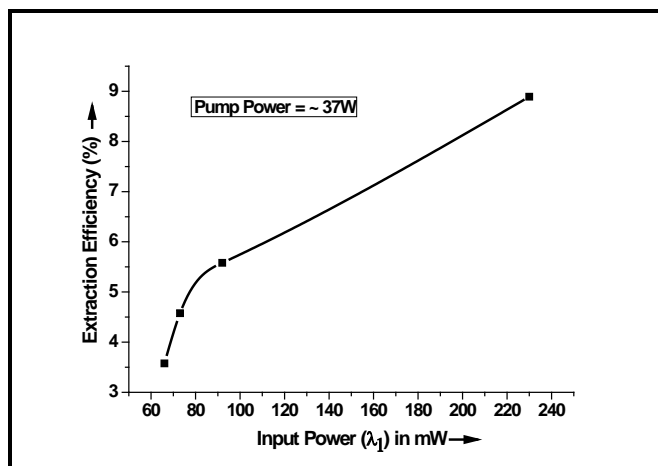


Figure 5.27: Input power effect amplifier extraction efficiency of individually amplified  $\lambda_1$  beam

Fig. 5.26 and fig. 5.27 depict the amplification characteristics of the individual  $\lambda_1$  beam and the extraction efficiency. It was found that the extraction efficiency increased from 4.18% to 6.6 % (fig. 5.26) with a pump power increment of 12 W to 37 W, while the input power was in the range of 48 – 58 mW. Extraction efficiency was increased from 3.5 % to 8.5% (fig. 5.27) when

## CHAPTER - 5

input power was increased from 60 mW to 240 mW at the fixed pump power of 37W.

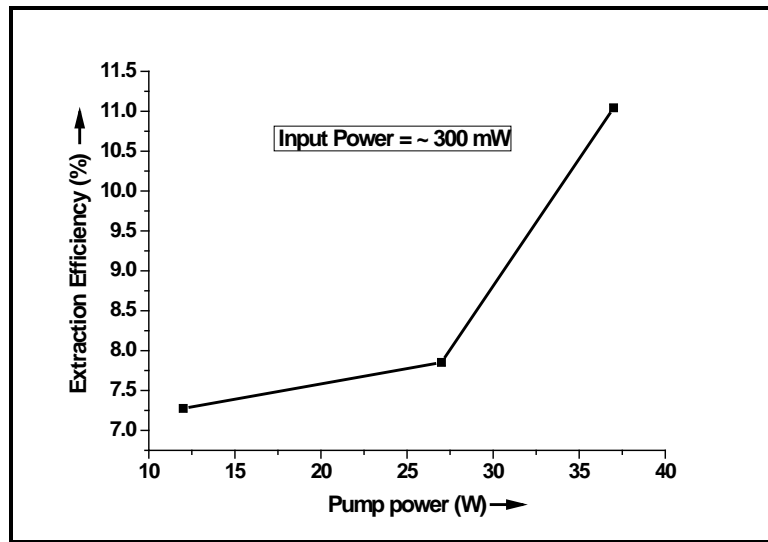


Figure 5.28: Amplifier extraction efficiency of individually amplified  $\lambda_2$  beam (Pump power effect)

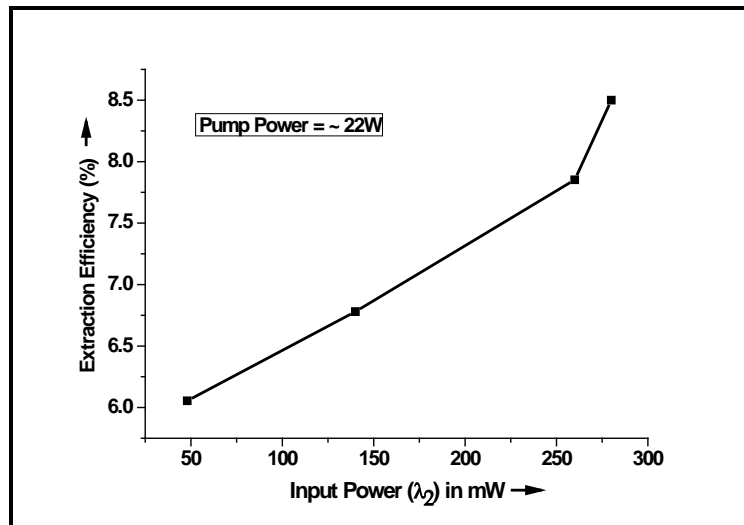
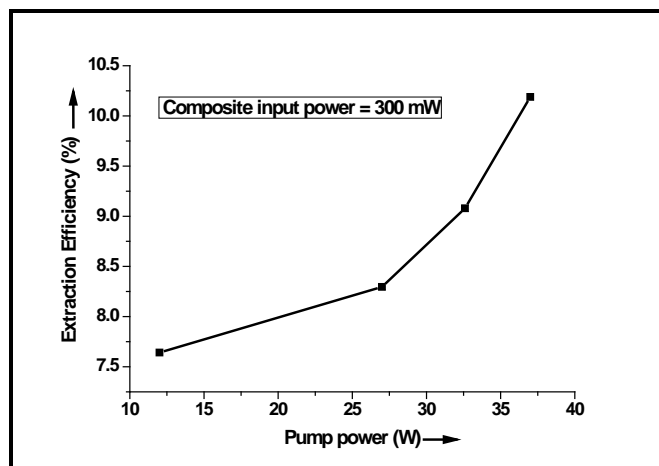


Figure 5.29: Amplifier extraction efficiency of individually amplified  $\lambda_2$  beam (Input power effect)

Figure 5.28 shows the characteristics of the individually amplified beam at the second ( $\lambda_2$ ) wavelength. Extraction efficiency increased from 7.27% to 11 % (as shown in fig. 5.28) with an increase of pump power from 12 W to 37W with the signal power of  $\lambda_2$  was nearly 300 mW. The extraction efficiency was

increased from 6.1 % to 8.5% (as shown in fig. 5.29) with increasing signal power from 48 mW to 280 mW with a fixed pump power of 22W. Higher efficiency for the second wavelength was attributed to higher input signal power as compared to the first wavelength.

The effect of input and pump power variation on the extraction efficiency for composite ( $\lambda_1$  &  $\lambda_2$ ) laser beam is shown in fig. 5.30 and 5.31. Increase in extraction efficiency from 8.85 % to 16.50% (as shown in fig. 5.30) was achieved when input signal power increased from 200 mW to 980 mW at the fixed pump power of 37W. Extraction efficiency increased from 7.6% to 10.5 % (as shown in fig. 5.31) when pump power was increased from 12 W to 37W while input composite signal power was 300 mW.



*Figure 5.30: Pump power effect on extraction efficiency of the common amplifier with the composite input beam*

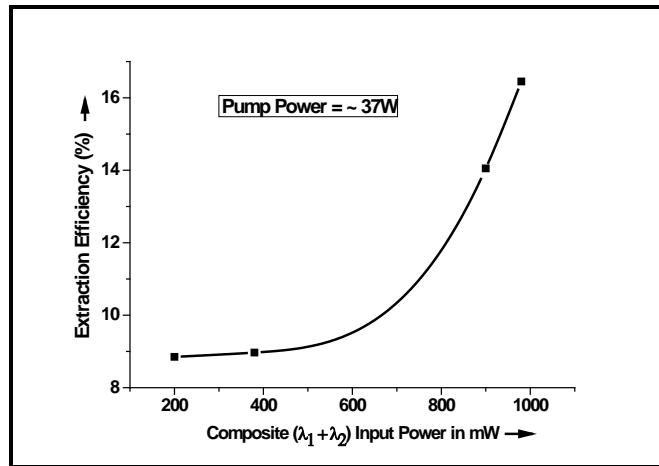


Figure 5.31: Input power effect on extraction efficiency of the common amplifier with the composite input beam

The input power ratio ( $P_{in}(\lambda_1) / P_{in}(\lambda_2)$ ) was varied from 1.92 to 0.08. Corresponding output power ratio in the case of individual amplification was found to vary from 0.96 to 0.52. The output power ratio variation reduced to 0.5 to 0.23 for the co-amplified configuration. This was due to the effect of gain competition among both the wavelengths which is discussed in the subsequent section.

#### 5.2.3.4 Gain Competition in Common Amplifier:

Gain competition in the homogenous gain profile depends significantly on input intensity, wavelength, location of wavelength in the gain profile of the dye gain medium used and polarization of input and pump beams [5.1]. The correlation in the input-output power ratio in two conditions was established. The first condition was amplification characteristics when no gain competition was present (individually amplified case) and in the second condition when the gain competition was present (co-amplification case).

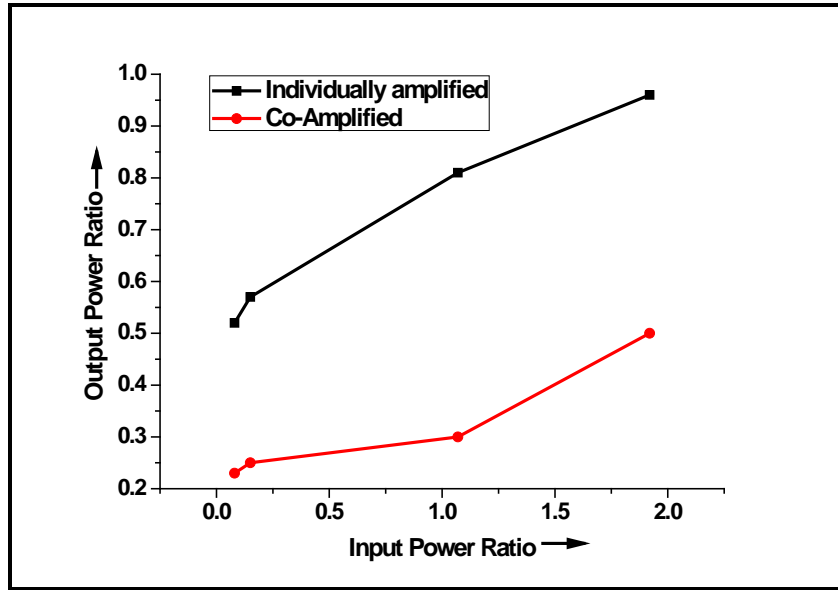


Figure 5.32: Input-output correlation of dual-wavelength common amplifier

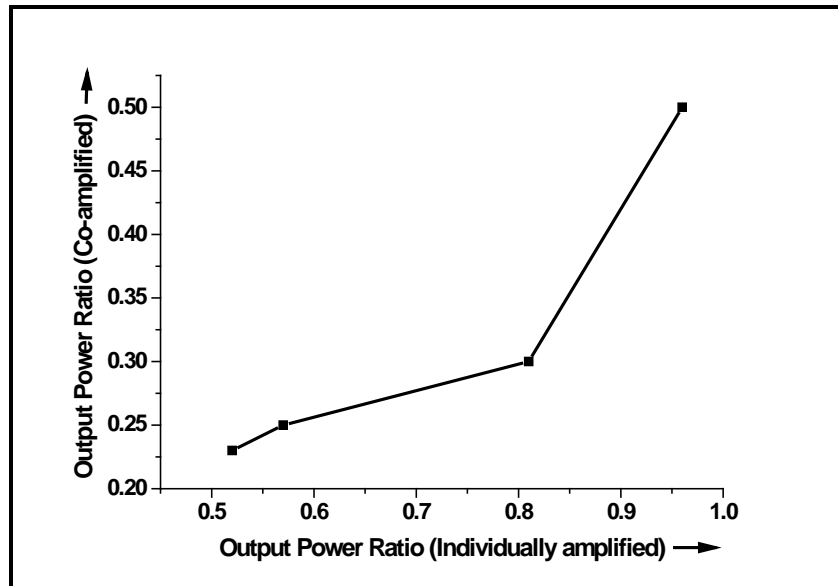


Figure 5.33: Output relation for the individual and co-amplified scheme in the common amplifier

Figure 5.32 depicts the behavior of output power ratio ( $P_{out}(\lambda_1)/P_{out}(\lambda_2)$ ) with an input power ratio ( $P_{in}(\lambda_1)/P_{in}(\lambda_2)$ ) in both the cases. It was observed that output power ratio in the case of  $\lambda_1$  and  $\lambda_2$  co-amplified (CA) follows the similar trend as that of  $\lambda_1$  &  $\lambda_2$  amplified individually (IA) but with a reduced competitive gain. The ratio of output power increased with an increase in the

## CHAPTER - 5

ratio of input signal power. It can be seen in figure 5.33 that, the ratio of co-amplified output power ( $P_O^{CA}$ ) increased with the individually amplified output power ratio ( $P_O^{IA}$ ). Data was recorded for three input power ratios i.e. equal input for both wavelengths (ratio ~ 1.08), the input of first wavelength was high (ratio~1.92) and input of second wavelength was high (ratio~0.08). These data points gave significant information about input-output correlation and gain competition behavior of the common amplifier configuration.

A gain competition coefficient (GCC) was defined by taking the ratio of output power when both the wavelengths were co-amplified ( $P_O^{CA}$ ) to the ratio of output powers when those wavelengths were individually amplified ( $P_O^{IA}$ ). GCC gives information about the gain competition behavior of the common amplifier by considering IA and CA together. Table -5.3 gives the quantitative behavior of GCC and input-output power ratio correlation.

*Table 5.3: Input-output power ratio correlation and Gain Competition*

*Coefficient (GCC)*

Input power ratio ( $P_{in}=P_1 / P_2$ )	Output power ratio for individually amplified beam ( $P_O^{IA}$ )	Output power ratio for co-amplified beam ( $P_O^{CA}$ )	Gain Competition Coefficient (GCC) ( $P_O^{CA} / P_O^{IA}$ ).
0.08	0.52	0.23	0.44
0.15	0.57	0.25	0.43
1.07	0.81	0.3	0.37
1.92	0.96	0.5	0.52

## CHAPTER - 5

---

Gain competition characteristics were analyzed for three cases of  $P_{in}$  being  $\sim 0$ ,  $\sim 1$  and  $\sim 2$ . GCC was 0.37 for the case of  $P_{in}$  of 1.07 and GCC increased to 0.44 and 0.52 when  $P_{in}$  reduced to 0.08 and increased to 1.92 respectively. Increment in the GCC indicates lower gain competition effect and higher individual dominance.  $P_1$  very low and  $P_2$  very high implies  $P_{in} \sim 0$ . In this case, the laser beam of the second wavelength saturates the gain medium earlier than the first wavelength and hence gets amplified more efficiently than the first wavelength and the second wavelength dominates this region of operation. In this zone of operation, even doubling of the input ratio from 0.08 to 0.15 has an insignificant effect on the output power ratio (0.52 to 0.57 for IA case and 0.23 to 0.25 for CA case) and GCC (0.44 at 0.08 and 0.43 at 0.15). It shows that in this case, the contribution of the first wavelength is only 23 to 25 % in the power of the second wavelength. Therefore it can be concluded that the gain competition, in this case, is in favor of the second wavelength and the first wavelength fails to compete.

In the case of equal input power ( $P_{in} = 1.07$ ), relative emission cross-section of the dye gain medium for first and second wavelength plays a significant role as compared to the input power effects. This shows an increase in the contribution of the first wavelength from 25 % to 30% of the power of the second wavelength in the CA case. In this zone of operation, competition for taking away the gain is higher. In the third case  $P_{in}$  was further increased to 1.92. As the contribution of the first wavelength in the input was increased, the output power of the first wavelength increased from 30% to 50% of the second wavelength in the CA case. The first wavelength starts competing with the second wavelength in utilizing the competitive gain. This zone of operation is

## CHAPTER - 5

---

dominated by power levels of the first wavelength. Therefore increment in the GCC from 0.37 to 0.52 shows decreased competition and dominance of the first wavelength in this zone of operation. This analysis shows that input power levels and their ratio play an important role in the gain competition effect. The input power ratio required to be adjusted depends on the gap of the wavelengths and location on the gain curve of the dye used. The various output power ratios have been successfully generating using this study for spectroscopic experiments. Spectroscopic studies required polarization of the constituent beams to be the same therefore polarization characterization of the dual-wavelength beam was carried out and results are tabulated in table-5.4. The pump laser beam was polarised using a cube polariser. The composite signal was ensured to be preferentially p-polarised. The common amplifier was pumped in three pump beam polarisation configurations i.e. s-polarised, p-polarised and un-polarised.

*Table 5.4: Effect of pump power polarisation on extraction efficiency*

Pump polarisation	Pump Power (W)	Dye input power	Dye output power	Extraction efficiency
s-polarised	13	430 mW	1220 mW	6.08%
p-polarised	17	430 mW	1650 mW	7.17%
un-polarised	34.4	430 mW	3450 mW	8.78%

It was found that there was no significant difference in amplification efficiencies when pump polarization was parallel to the dye signal as compared to the case when perpendicular to the dye signal. The effect of polarization on

gain competition would have been significant in the case of orthogonal polarization for  $\lambda_1$  &  $\lambda_2$  [5.14] in the input composite laser beam.

### **5.2.3.5 Performance of Spectral Beam Combination Scheme:**

Co-amplification (CA) based spectral beam combination of two laser beams, wavelength separated by only 5-7 nm was found to be very efficient in an oscillator-amplifier configuration. Table-5.4 contains the expected performance of the system with experimentally determined oscillator powers and amplifier efficiency for the case of an individually amplified case. Amplifier ( $\lambda_1$  and  $\lambda_2$ ) extraction efficiency (Eff) was determined at 18.5 W. Half of the common amplifier pump was taken as the same power will be available to pump two amplifiers for the case of individual amplification (IA). The splitting ratio of the available 30/70 beam splitter designed for 500-600 nm was tested and found to be 20/70 for  $\lambda_1$  and  $\lambda_2$  respectively. Comparison of the schemes as tabulated in the table-5.5 and 5.6, revealed that we could achieve 3.45 times more power in the case of common amplifier configuration. Higher efficiency in common amplifier configuration was achieved due to higher conversion efficiency of the amplifier at the higher pump power of 38.4 W (~16.5%) as compared to 18.5 W (7.25%) in the second case. This was the added advantage to the co-amplifier based scheme. Combination losses were observed to be reduced to 39% (0.759 W in CA case and 1.949 W in the IA case). A composite, dual-wavelength dye laser beam of 7.35 W was generated with a composite dye beam input power of 980 mW using a green beam pumped DCM dye common amplifier. The reduction of one amplifier stage resulted in reduced Fresnel losses and improved system compactness. This gives a fair comparison among both the schemes. Table-5.5 contains experimentally obtained values from the co-amplification experiment.

## CHAPTER - 5

*Table 5.5: Expected performance of the individually amplified scheme*

Scheme	Oscillator $\lambda_1$ Output ( Pump= 5.7 W )	Amplifier $\lambda_1$ Output ( Pump: 18.5W )	Oscillator $\lambda_2$ Output ( Pump= 25 W )	Amplifier $\lambda_2$ Output ( Pump= 18.5W )	Combiner losses for (20% $\lambda_1$ +70% $\lambda_2$ ) splitter	Total Output Power (Combined) W
I.A. Scheme	480 mW (Exp.)	1.45 W Eff=5.1% (Exp.)	1250 mW (Exp.)	2.63 W Eff=7.25% (Exp.)	1.16 (80% $\lambda_1$ ) + 0.789(30% $\lambda_2$ ) =1.949 (Cal.)	0.290 W +1.841W =2.13 W (Cal.)

*Table 5.6: Measured performance of the co-amplified scheme*

Scheme	Oscillator $\lambda_1$ Output ( Pump= 5.7 W )	Oscillator $\lambda_2$ Output ( Pump= 25 W )	Combiner losses for (20% $\lambda_1$ +70% $\lambda_2$ ) splitter	Common Amplifier Pump: 38.4 W	Total Output Power (Combined) W
C.A. scheme	480 mW (Measured)	1250 mW (Measured)	0.384 (80% $\lambda_1$ ) + 0.375(30% $\lambda_2$ ) = 0.759 W (Measured)	7.35 W Eff=16.5% (Measured)	7.35 W (Measured)

The composite output laser beam was having the same aspect ratio with reasonably good co-linearity observed over a distance of 15 meters. It was due to the essential amplification requirement of spatial overlap of constituent laser beams at the gain dimension of 500 micrometers. The necessary condition of temporal synchronization at the amplifier dye cell was ensured the output pulse synchronization for the CA case.

### **5.3 Conclusions:**

The external cavity beam combination is advantageous for individual optimization of the oscillators. Individual amplification and common amplification based schemes were studied under this category of spectral beam combination technique. Two oscillators were optimally setup operating at two wavelengths separated by less than 10 nm. Rh 101 dye in ethanol was finalized for the efficient oscillator operation in the red wavelengths. CVL and DPSSL pumped dye laser oscillators were characterized. CVL pumped dye laser was proved to be efficient than DPSSL pumped dye laser due to shorter rise time and narrower pulse width. Amplification of individual oscillator beams was carried out in yellow (CVL) pumped transverse amplifier using Rh 101 dye. Optimized concentration and pump power for this configuration were found to be at 0.825 mM and 10 W respectively. Beam splitter was used for the laser beam combination of individually amplified beams. The combination loss in this spectral beam combination scheme was concluded to be higher (more than 43%). Calculations of the co-amplification based combination scheme suggested improved efficiency, which was experimentally demonstrated by CVL pumped DCM dye co-amplification studies.

The common amplifier approach for combined dual-wavelength generation from CVL pumped dye laser oscillator amplifier chains with complete utilization of green and

yellow beams was investigated in detail. Combination losses ( $\sim 40\%$  that of the IA scheme) were significantly reduced in comparison to the general approach due to combination at lower power levels. Higher amplifier extraction efficiency at the added pump power in the case of co-amplification is adding to the efficiency of the overall dual-wavelength laser generation set-up. This efficient spectral beam combination technique was successfully tested with wavelength separation of 5-7 nm in between  $\lambda_1$  and  $\lambda_2$ . The input power ratio plays a significant role in closely separated wavelengths in the common amplifier. Beam splitter ratio can be changed to tune the input power ratio to generate the required output power ratio. This configuration is very efficient for dual-wavelength beam generation provided wavelengths falls in the dye emission range. Rh 101 dye in ethanol was found to be better than PM 650 for yellow beam pumped dye laser oscillator. Gain competition coefficient was defined and analyzed for studying the gain competition behavior in detail.

Co-amplification based dual-wavelength generation scheme can be used for high power generation due to high damage thresholds of a beam splitter based beam combiner. Individual amplification proved to be efficient for distant wavelengths, whereas co-amplification found to be most suited for closely separated wavelength beam combinations. This technique can handle the high power of the same polarization beams as well. The common amplifier approach of generating closely spaced dual-wavelength dye laser is an efficient, compact and versatile technique for generating higher powers in oscillator amplifier configuration. The wide spectral tuning of CVL pumped dye lasers can be obtained by simply changing the dye solution and keeping the same experimental set up to enhance the value and applicability of this work to many more such applications.

# Chapter: 6

## Multilayer Dielectric Coated Fabry Perot Beam Combiner for High Power, Pulsed Dye laser

---

### 6.1 Introduction:

Intra-cavity beam combination and co-amplification based beam combination schemes are efficient for spectral beam combination of closer wavelength ( $<10$  nm). However, both of these schemes limit their potential due to gain competition complexity. Therefore, a gain competition free spectral beam combination scheme for laser wavelengths needs to be studied. Multilayer dielectric coatings play a vital role in tailoring the properties of the optical devices used for various purposes in the laser systems and its spectral beam combination applications. Multilayer thin-film coated mirror, bandpass filter, edge filter, notch filter, and Fabry-Perot filter are few devices, which become an essential part of any laser beam combination system. Multilayer dielectric coated filters are used to either split the composite laser beam into its constituents or combine the individual laser beams to generate a multi-wavelength composite laser beam. The edge and bandpass filter based laser beam combiner has been used for high power laser systems due to ease of handling high power and wide tunability [6.1].

These laser beam combiners are used for combining the wavelengths separated more than 15 nm [6.2, 6.3]. These filters have higher damage threshold and ease of alignment due to flat reflection over the desired wavelength range and transmission region as demonstrated by M. Nand et.al. [6.4]. Combiner for closer wavelengths  $< 10$  nm is not available commercially, which motivated us to study this type of combiners

for spectral beam combination requirements. Sharper spectral transmission profile of the Fabry Perot (FP) etalon (filter) makes it applicable for such specific purposes. FP etalons are popular for its use in many laser resonators and diagnostic configurations like linewidth narrowing inside a resonator cavity and spectral quality assessment of the laser beam [6.5, 6.6]. Multilayer dielectric coated FP filter is frequently used in filtering out the unwanted wavelength photons from the incident beam in spectroscopy experiments. A. Zohbi et.al., has made an FP thin film optical filter for mid-IR spectroscopy applications [6.7]. FP filter has been used in wavelength division multiplexing by V.K.H. Ghasemi et.al. [6.8]. Application of FP filter for laser beam combination of closer wavelengths, narrow linewidth, high power laser beams has been not studied in detail in the published literature.

Intra-cavity beam combined multi-wavelength dye laser generates widely separated as well as closely separated wavelength simultaneously by tuning constituent sub-cavities to required wavelengths [6.9]. Multiple wavelength emission from a single cavity is advantageous for simultaneously sensing of more than one species at a time if their absorption band falls in the emission wavelength range of the dye or dye mixture to be used. High power, closely separated dual-wavelength laser beam can be generated by co-amplification of the combined laser beam in a common power amplifier stage [6.10]. This technique suffers from the gain competition among the wavelengths exploiting the same homogeneously broadened dye gain profile. Individual optimization of beam properties and intensities becomes difficult in the co-amplification technique. Spectral beam combination of individually optimized, narrow linewidth, high power, laser beams with closer wavelength needs a combining element capable of handling such stringent requirements. Individual optimization of beam properties can be done using a passive optical beam combining element. The above

environmental applications and diversity of the dye laser applications motivated to study the dual-wavelength dye laser generation using an FP filter based novel spectral beam combination approach for closely separated wavelengths.

In this chapter, The design, fabrication, and characteristics of a FP filter, employed for spectral beam combination of high power, tunable dye laser beams is discussed in detail. Novel observations on amplified spontaneous emission (ASE) filtering in the dye laser are discussed. A mechanism for handling tunability of the dye laser in FP based spectral beam combination (SBC) is described. The current study is categorized into three major parts. In the first part; the design and fabrication of an FP beam combiner is described. In the second section, the characterization of the indigenously fabricated thin-film FP beam combiner is discussed. Results pertaining to characteristics and testing of the spectral beam combination scheme with two high power dye laser beams using FP beam combiner are discussed in the last section. The generation of dye lasers utilized for this testing is described in the previous chapters of this thesis.

### **6.2 Designs of Multi-layer, Thin Film, Interference Filters for Closely Separated Wavelengths:**

Thin-film coated devices are versatile and can be designed in many ways to meet the stringent research and development requirements. It is needed to develop a device suitable for combing a closer wavelength separated by less than 10 nm. Therefore, an interference filter based combiner designs having the potential of combining closer wavelengths has been chosen and edge filter and FP filter based designs were finalized to take up the beam combiner development.

**6.2.1 Edge Filter Design for Widely Separated Wavelengths:**

Interference filter, which has high transmission either for longer wavelengths (high pass filter, HPF) or for lower wavelengths (low pass filter, LPF) were considered for the intended design near red wavelength (632.8 nm). Among both the type of designs, HPF was finalized due to lower ripples in the transmission spectrum. HPF filter design using  $\text{TiO}_2$  /  $\text{SiO}_2$  as high and low refractive index material was analyzed. The periodic multiple thin layers of high (H) and low (L) refractive index were arranged using the  $(0.5HL0.5H)^{19}$  stack formula in the design software (TF Calc and open filter). A total of 39 layers in the above sequence were finalized. Quarter-wave optical thickness was calculated at 604 nm as the reference wavelength. The first three and last three layer thicknesses were tailored in non-quarter wave thickness to achieve the desired transmission values at intended design wavelengths near 632.8 nm having 6 to 10 nm difference. The transmission spectrum analyzed using the above mentioned design is shown in fig. 6.1.

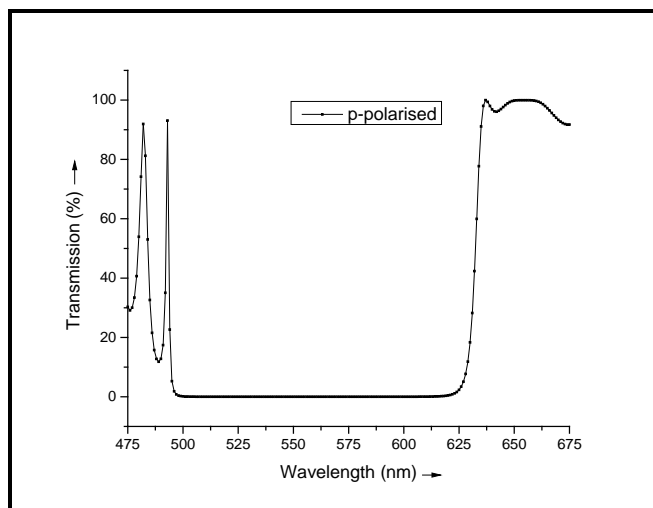


*Figure 6.1: Transmission spectrum of edge filter designed for closer wavelength*

Transmission at 637 and 622 nm wavelength having a difference of 15 nm was found to be 99.98 % and 1% respectively, whereas transmission of 90 % and 10% was achieved at wavelength difference of 7 nm (10% at 628 nm and 90% at 635 nm). This shows the transmission slope of 11 .5 % per nm. This design was observed to be suitable for closer wavelength combination but around 40 layers are required to be deposited. This design will be compared with FP interferometer based cavity designs in the subsequent sections.

### **6.2.2 Single Cavity Fabry Perot Beam Combiner Design:**

An FP based beam combiner was selected due to the intended closer wavelength beam combination. The FP beam combiner was designed with TiO<sub>2</sub> and SiO<sub>2</sub> as high and low refractive index materials respectively [6.11]. Layer sequence and thickness were designed for peak transmission in the red range (near 632.8 nm) at an angle of incidence (AOI) of 45<sup>0</sup>. The sequence of 19 layers with stack formula ((HL) <sup>4</sup> H 2L (HL) <sup>4</sup> H) optimized for 707 nm at normal incidence was finalized among various designs, compared using sensitivity analysis. The thickness of the high and low refractive index layers was determined using standard optimization techniques.

Analyzed transmission spectrum (p-polarised) of the FP filter design at normal incidence and incidence at 45 degrees is shown in fig. 6.2. It can be seen that the transmission peak is shifted from 707 to 644 nm by changing the normal incidence angle to 45 degrees (AOI). On the left side of the peak, transmission increased from 5 % to 95 % for a wavelength change of 634 nm to 644 nm. A similar change of 95 % to 5% in transmission for an increase in the wavelength from 644 to 654 nm was observed. The slope of the transmission curve was approximately 9 % per nm. This sharp transmission spectrum profile (5 to 95%

change for 10 nm) showed a possibility for an FP filter based beam combination for closely separated laser wavelengths (<10nm).

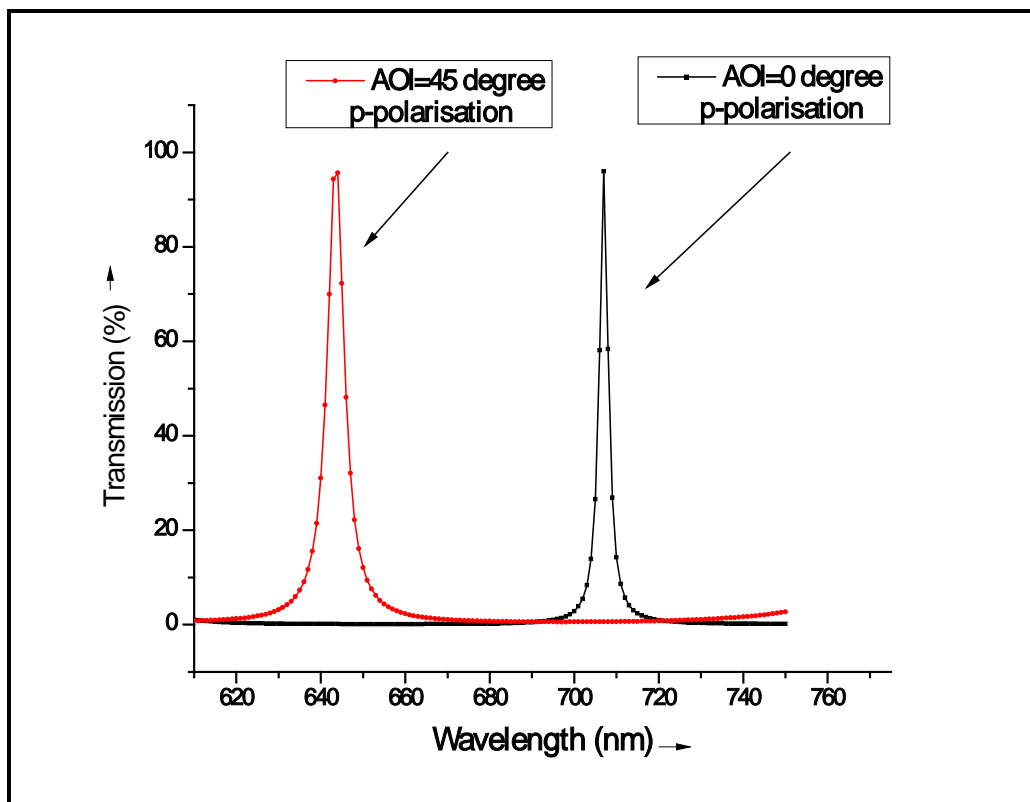


Figure 6.2: Transmission spectrum (p-polarised) of the designed FP beam combiner (at AOI of 0 and 45 degree)

Exploring this capability for a closer wavelength combination was one of the objectives of this study.

### 6.2.3 Dual Cavity Fabry Perot Beam Combiner Design:

Sharp slope, improved efficiency at closer wavelengths achievable using 19 layers in an FP filter design seems to be better as compared to 39 layers edge filter. Matching the steep transmission peak at the desired wavelength adds the complexity in implementation. Therefore, beam combiner using two cascaded FP cavities embedded in the single device was thought to be beneficial. A design using  $\text{TiO}_2$  and  $\text{SiO}_2$  as the high and low refractive index materials were numerically analyzed using  $(\text{HL})^4 \text{H} 2\text{L} (\text{HL})^4 \text{H} (\text{HL})^4 \text{H} 2\text{L}$

(HL)<sup>4</sup> H as the stack formula. A total of 37 quarter-wave thick layers were required to achieve the desired transmission spectrum. Quarter wave thickness was calculated using 815 nm as the reference wavelength. Device (10 mm thick, quartz glass substrate) was designed to work at a 45-degree angle of incidence. The calculated transmission spectrum of the dual cavity FP combiner is shown in fig. 6.3.

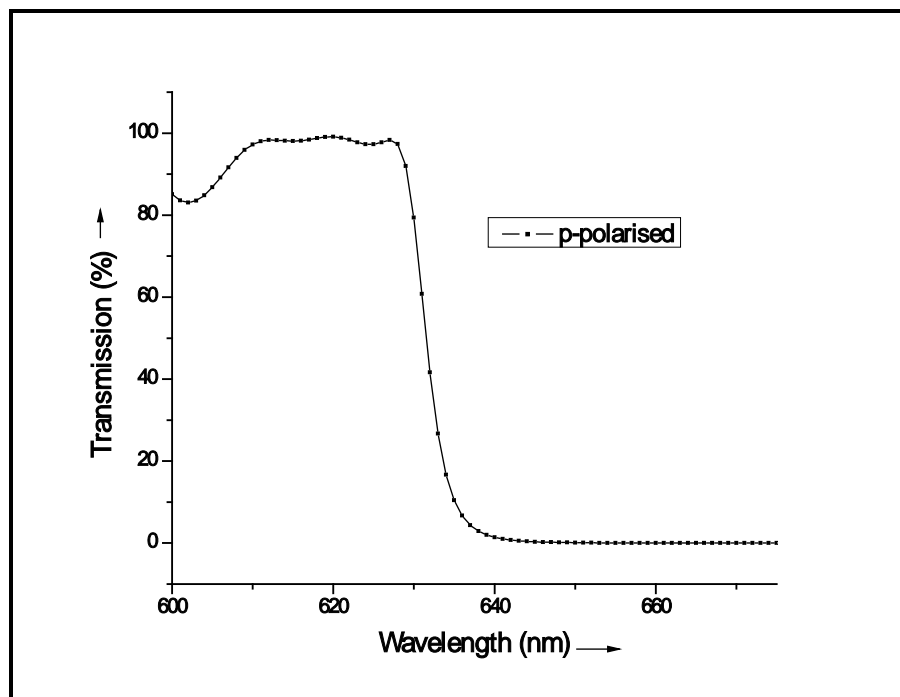


Figure 6.3: Designed transmission spectrum of the dual cavity FP combiner

It can be seen that the transmission profile became like an edge filter. The transmission slope was also sharp enough to combine the closer wavelengths. But the higher number of layers in dual cavity filter to meet the same sharpness as compared to 19 layers in a single cavity combiner was not preferred. In practical scenarios, the device with a lower number of layers is easy to fabricate. Therefore, the single cavity FP beam combiner was selected for fabrication and characterization for the high power dye lasers.

### 6.3 Fabrication of Single Cavity Fabry Perot Laser Beam Combiner:

To achieve the desired optical performance of the optical device, single or multilayer dielectric coating of alternate high and low refractive index layers in a specifically designed manner, are used. A multilayer thin film Fabry Perot (FP) interference filter design was chosen due to its sharp transmission profile as compared to edge filter or bandpass filter. This filter was designed for the p-polarized incident laser beam as described in earlier section (section 6.2.2).

A FP beam combiner based on the optimized design was fabricated for further studies. Electron beam evaporation was used for the deposition of the films on BK-7 glass and quartz substrates. Substrate preparation and cleaning before deposition plays a key role in the deposited film quality. The substrates were cleaned ultrasonically in alcohol/acetone and de-ionized water before the deposition. To get a uniform film, substrates were rotated at 5rpm during deposition. The film depositions were carried out in an automated ion-assisted electron beam evaporation system. The 99.99% pure TiO<sub>2</sub> tablets and SiO<sub>2</sub> granules (Cerac Inc.) were evaporated and deposited on the substrate. The vacuum chamber was pumped down below  $2 \times 10^{-7}$  mbar before deposition. The substrate temperature was maintained at  $150 \pm 1^\circ\text{C}$ , during the entire process of deposition. To find out the optimum deposition parameter, a series of experiments at different discharge voltages and currents were performed. Ion assisted deposition was carried out using a gridless end hall ion source (40 – 210 eV, 0 – 7 A, gases: O<sub>2</sub> & Ar) with the injection of high purity (99.995%) O<sub>2</sub> and Ar in the ion source and hollow cathode electron source respectively. The partial oxygen pressure during the deposition was kept different for different materials. The deposition rate for all the materials was  $0.5 \pm 0.01$  nm/s, controlled by quartz crystal monitor (Inficon, IC/5) providing feedback to the e-beam gun (e-Vap, MDC). The optical thicknesses of

the layers were also controlled by an optical thickness monitoring system (Intellevation, UK). On-line spectrophotometric techniques were used to precisely control film optical thickness and its optical constants (within 1% of the desired value) during the deposition of a multilayer structure. This is also coupled with in-situ physical thickness monitoring. The optical quality of the growing multilayer could be continuously compared to the expected behavior and deviations from the target might be detected at an early stage of the process, where a correction may be feasible without losing the coating batch. A feedback loop between process parameters and online monitoring helps in achieving high repeatability.

#### **6.4 Characterization of the Laser Beam Combiner Using Spectrophotometer:**

Characteristics of the combiner govern its effectiveness for the intended application. Transmission spectrum, laser-induced damage threshold, and surface morphology were required to be determined for using this combiner in high power laser beam combination application.

Characterization of coatings developed is essential before their use in lasers and other spectroscopic experiments. The spectral transmission spectrum of the FP beam combiner was characterized in the range 190 to 1200 nm using spectrophotometer (VARIAN CARY5000 & CARY50), variable angle spectroscopic ellipsometer for determination of film thickness and optical constants (SOPRA GES-5). Peak transmission (~83%) of the combiner at normal incidence for p-polarised light was found to be at 709.5 nm. Transmission of p-polarized beam reduced from 83% to 5 % for wavelength change from 709.5 nm to 714.5 nm respectively. The transmission slope of the fabricated combiner was approximately 15 % per nm. This sharpness in the transmission was found to be suitable for the intended spectral beam combination experiment of closer wavelengths. Maximum transmission (~55%) at 45<sup>0</sup>AOI was

found to be at 644 nm. This was determined by theoretically extrapolating the measured transmission value at normal incidence. The transmission spectrum of the FP beam combiner was recorded at normal incidence and the measured transmission spectrum is shown in fig. 6.4.

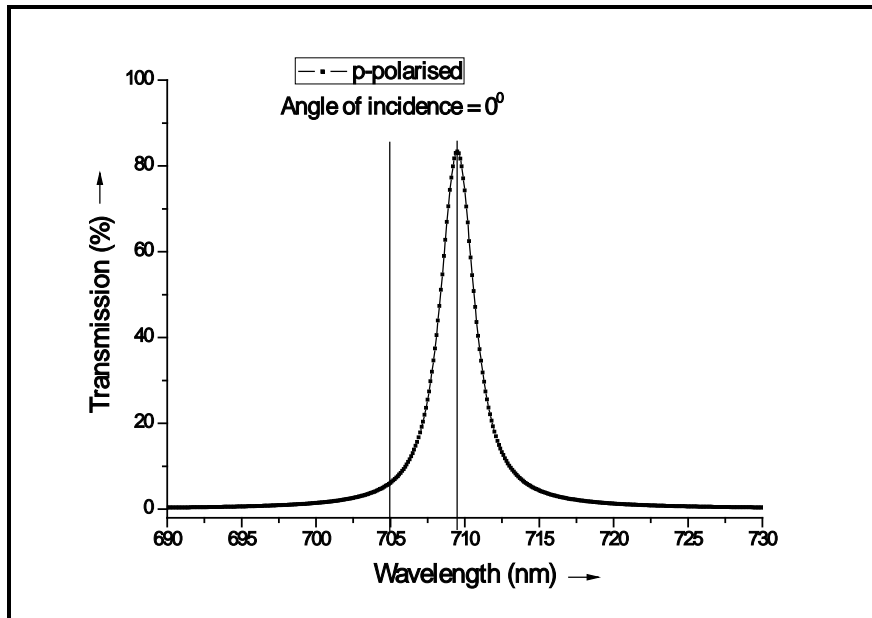


Figure 6.4: The measured transmission spectrum of the fabricated FP combiner

The difference in wavelength of peak transmission (707 nm, designed combiner, and 709.5 nm, fabricated combiner) was attributed due to film thickness errors during the deposition process.

### 6.5 Surface Morphology of the Laser Beam Combiner by Atomic Force Microscopy:

The surface morphology of the beam combiner was investigated by AFM in intermittent mode using a diamond-like carbon (DLC) tip having a radius of curvature ~1-3 nm. Roughness is generally used to assess the surface quality of an optical component but it only describes height variation and does not take the lateral distribution of height into account. Height-height correlation function (HHCF) is a second-order statistical parameter that takes both heights and their lateral variations into account. It renders more useful information about surface viz., roughness, grain

size, and fractals, etc. For quantitative analysis of surface in the present study, 1-D HHCF has been computed from AFM data using the following formulations [6.12,6.13]:

$$H(r_x) = \frac{1}{N(N-m)} \sum_{l=1}^N \sum_{n=1}^{N-m} (z_{n+m,l} - z_{n,l})^2 \quad \dots \quad (1)$$

Here  $m = r_x/\Delta x$ . In this way, HHCF can be evaluated in a discrete set of  $r_x$  values separated by sampling interval  $\Delta x$ . In the present case, scan data points have been taken equally in x and y-direction. HHCF prominently depicts grain structure in thin films. It increases steeply (linear) for lower 'r' values and then starts saturating for higher 'r' values. The lower value of HHCF means that two heights under consideration stand for better correlation. The starting point of saturation represents the correlation length. It depicts that heights with lateral distance more than correlation length are badly correlated. The slope of the linear region of HHCF gives roughness exponent which represents the high-frequency roughness or local morphology of the grain. Correlation length corresponds to geometrical grain size [6.14].

To get surface parameters, measured HHCF has been fitted with theoretical formulation for self-affine surfaces using Gaussian function as follows [6.15]:

$$H(r) = 2\sigma^2 \left[ 1 - \exp(-(r/\xi)^{2\alpha}) \right] \quad \dots(2)$$

Where  $\sigma$  is RMS roughness which describes the fluctuations of heights exponent ' $\alpha$ ' is roughness exponent which describes grain morphology depicting the wiggleness of the local slope on the surface. A higher value of  $\alpha$  ( $\leq 1$ ) implies the smoother line edge.  $\xi$  is the correlation length. Figure 6.5 shows HHCF for the surface of developed multilayer beam combiner. RMS roughness value computed from HHCF analysis is 2.9 nm. For optical wavelengths, such roughness value does not render substantial

## CHAPTER - 6

surface scattering which is good for intended experiment to conserve light intensity. The average surface grain size is 48 nm and the roughness exponent is 0.65 which is considered as low. As mentioned above, a lower value of ' $\alpha$ ' implies sharper or steeper edge at grain boundaries.

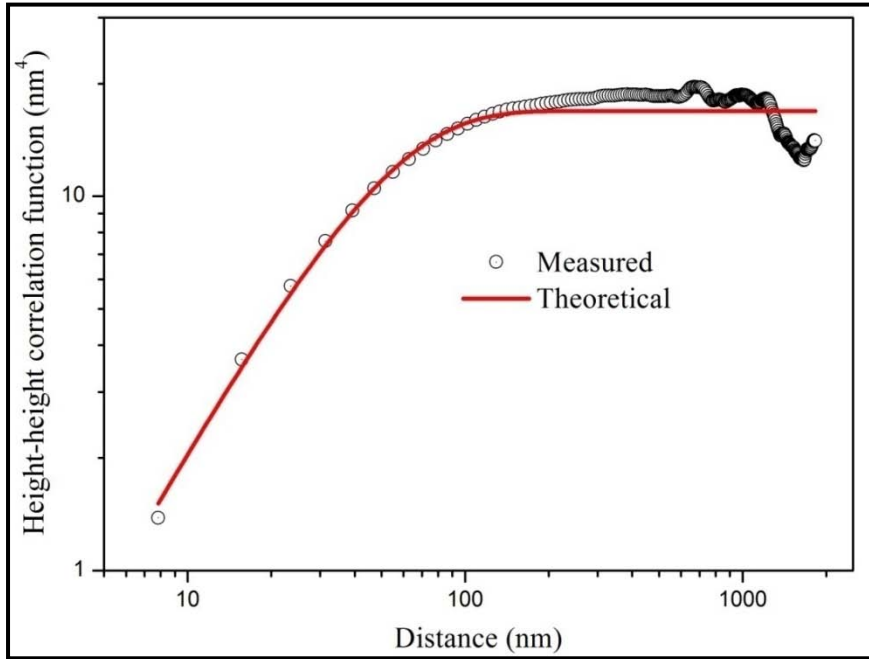
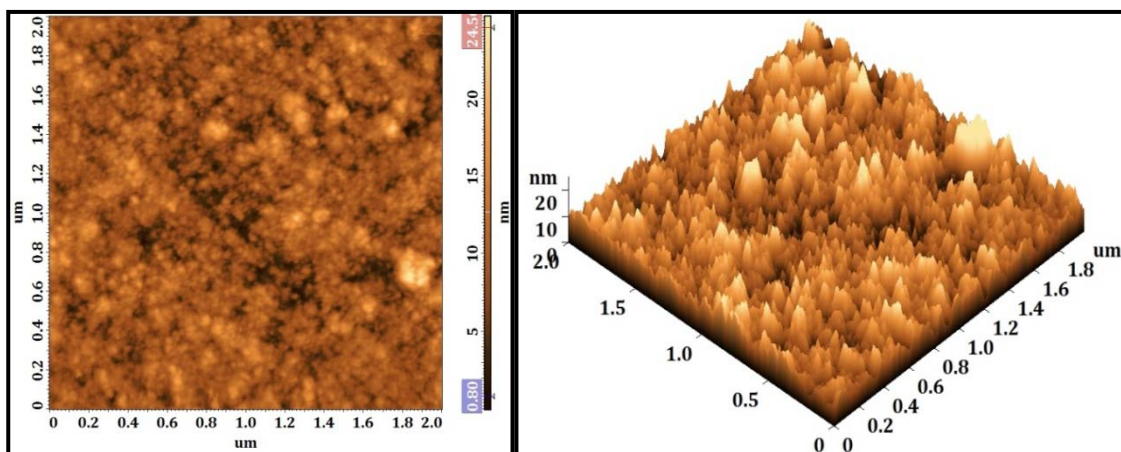


Figure 6.5: Height-height correlation function

Images of the FP beam combiner surface morphology captured by AFM are shown in fig. 6.6.



a) 2-D image of the surface

b) 3-D image of the surface

Figure 6.6: 2-D & 3-D AFM surface image of the beam combiner

2-D and 3-D AFM surface images are shown in fig. 6.6(a) and 6.6(b) also corroborate the low value of roughness exponent. The surface morphology of the ion-assisted e-beam evaporated beam combiner found to be suitable for the high power spectral beam combination application.

### **6.6 Laser-Induced Damage Threshold Determination of FP Beam Combiner:**

Damage threshold estimation of the device was essential for application in the high power lasers. Laser damage threshold was measured using 2<sup>nd</sup> harmonics of Nd: YAG laser of having pulse width: 8 ns, wavelength: 532 nm, repetition rate: 10 Hz. Second harmonic of Nd: YAG laser having a beam diameter of 5 mm was focussed using a spherical lens of focal length 300 mm on the designated location of the FP beam combiner. The sample was placed at a distance of 185 mm from the focusing lens. The energy of the laser was varied and point of interaction was monitored. A visible damage spot was observed on the sample at the laser energy of 25.5 mJ. The energy of 25.5 mJ at a distance of 185 mm (calculated laser spot diameter of 3.8 mm) resulted in an energy density of 0.22 J/cm<sup>2</sup>. Therefore, the damage threshold value of 0.22 J/cm<sup>2</sup> seems to be safe limit for the use of this combiner, beyond which damage might occur.

### **6.7 Spectral Beam Combination Using FP Beam Combiner:**

Spectral beam combination (SBC) using FP combiner for two wavelength ranges namely: closer wavelengths separated by less than 10 nm and distant wavelengths separated by more than 10 nm has been experimentally demonstrated. The schematic of the spectral beam combination experiment is shown in fig. 6.7. Two dye MOPA chains (fig. 6.7) were routed to the spectral beam combination module using suitable optical components.

High reflectivity mirrors were used to achieve the spatial overlap between both the laser beams at the beam combiner and its collinearity was ensured at a distance of

more than 15 m. The angle of incidence at the FP combiner was fixed for suitably combining the wavelength in appropriate ratios. The first laser beam ( $\lambda_1$ ) was transmitted through the combiner, whereas the second laser beam ( $\lambda_2$ ) was reflected from the combiner to obtain the spatial overlap as well as co-linearity in the combined laser beam.

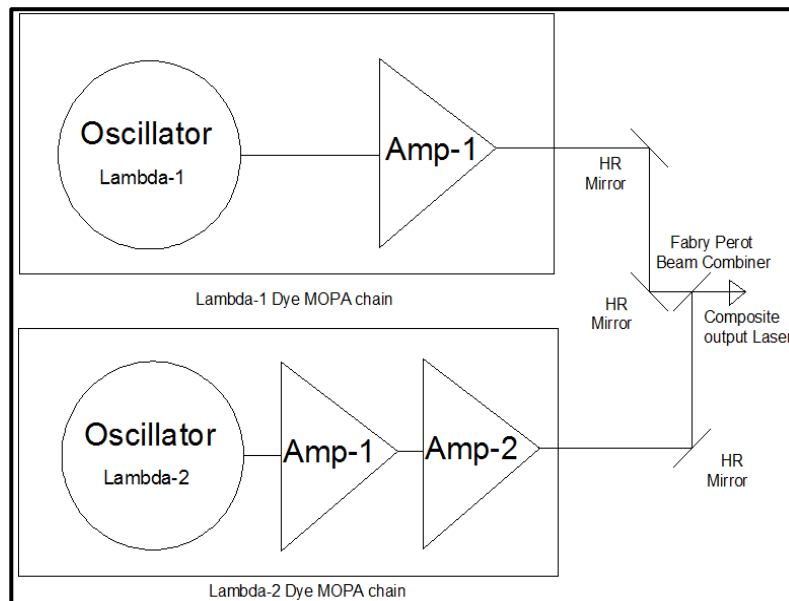


Figure 6.7: Schematic of spectral beam combination setup (HR: High Reflectivity, Amp-1: Yellow pumped amplifier, Amp-2: Green pumped additional amplifier)

Partially reflected beam of the first laser ( $\lambda_1$ ) and a transmitted beam of the second laser ( $\lambda_2$ ) was dumped on a beam dump. Characteristics of SBC for both the cases were studied and being presented.

### 6.7.1 SBC by FP Combiner for Closely Separated Wavelengths:

The first and second wavelengths of the dye laser were tuned to a difference of  $7 (\pm 3.5)$  nm around 632.8 nm. The second wavelength was nearly 7 nm higher than the first wavelength. The combination efficiency of transmitting a laser beam ( $\lambda_1$ ) and reflecting laser beam ( $\lambda_2$ ) was measured to be 47% and 92% respectively, with an overall combination efficiency of 72%. Total power of composite dye laser beam was 5.85 W in which  $\lambda_1$  was 1.25 W and  $\lambda_2$  was 4.6

W with total incident laser power of 8.15 W (2.65 W of  $\lambda_1$  & 5.5 W of  $\lambda_2$ ). For the comparison with the beam splitter (R: 70 ( $\lambda_2$ ); T: 30( $\lambda_1$ )) based beam combiner, the total power of composite laser beam was as 4.65 W (0.8 W of  $\lambda_1$  & 3.85 W of  $\lambda_2$ ) for the same incident laser power. The overall beam combination efficiency of the beam splitter based combiner was 57% while beam combination efficiency of FP beam combiner was 15% higher (72 % compared to 57%) than the beam splitter based combiner.

### **6.7.2 SBC by FP Combiner for Widely Separated Wavelengths:**

This FP combiner was tested for combining the wavelengths of a widely separated laser beam. To qualify this combiner for the higher power laser beam of widely separated dye laser wavelengths, two high power dye laser beams were utilized. This device was successfully tested for dye laser powers up to 12 W. The dye lasers were tuned to have a difference of 30 nm ( $\pm 15$ nm) around 632.8 nm. Transmission of first wavelength and reflection of the second wavelength was measured to be around 44 % and 95% respectively. Input laser power during this testing was 2.8 W for wavelength-1 ( $\lambda_1$ ) and 8W for wavelength ( $\lambda_2$ ) respectively for first and second dye laser beams. Output power after combination with FP beam combiner was measured to be 1.25 W and 7.7 W for the first  $\lambda_1$  and second laser  $\lambda_2$  beam respectively. A combination efficiency of approximately 84% was obtained. It would have been more than 98 % in the case of edge filter based beam combiner. Therefore, in the case of widely separated wavelengths, the efficiency of the FP beam combiner was lesser by approximately 15% as compared with the edge filter based beam combiner. This proved that the FP beam combiner is an

efficient device for SBC of closely separated wavelengths but not efficient for widely separated wavelengths.

### **6.7.3 Amplified Spontaneous Emission (ASE) Filtering Using FP Beam Combiner:**

High power generation in dye laser requires higher pump powers. Unwanted inline ASE is generated and amplified in the power amplifier modules of a dye laser MOPA chain operating at higher pump powers. It has been experimentally observed that the inline ASE in the dye laser depends on the lasing wavelength in the tuning range. The ASE is more in the laser output power as we deviate from its peak wavelength [6.16, 6.17]. It becomes unavoidable if the required wavelength is at the end of the tuning range. ASE filtering mechanisms are inserted in between amplifier stages to suppress ASE amplification in the MOPA chain. Insertion of these devices adds Fresnel losses and reduces the overall efficiency of the MOPA chain. We have observed ASE filtering from the transmitting laser beam at the stage of the laser beam combination stage itself, which prevented a separate ASE filtering mechanism in the dye laser MOPA chain. The experimental setup consists of a grating of 1800 lines per mm and a thermopile based power meter (Ophir make, Model FL 150A, accuracy 3%). The laser beam having the higher ASE (deliberately set for the first laser by tuning to the end of the tuning range) was made to incident for maximum transmission through the combiner. Laser beam incident on the grating diffracted in the two streams i.e. laser wavelength and ASE component. The percentage of ASE present in the laser beam was assessed by taking the ratio of measured average power in both the streams. ASE measurement setup is depicted in fig. 6.8.

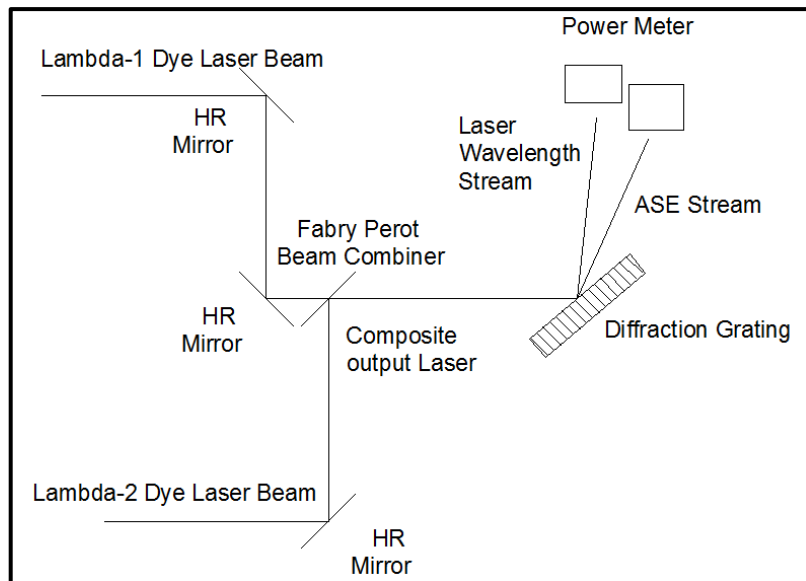


Figure 6.8: Experimental set up for ASE measurement

ASE content in the laser beam was measured without inserting the beam combiner in the path. Similarly, the ASE content in the transmitted beam through the FP beam combiner was measured by following the same method, at the same location. Reduction of ASE from 40% to < 5% was achieved using the FP filter as a spectral beam combiner. No ASE filtering effect was observed in the case of a beam splitter based beam combiner. On analyzing the transmission spectrum and tuning range of the transmitting laser, it was found that when dye laser is operating at the end of its wavelength tuning range, then the inline ASE is more in the output power of the dye laser. The inline ASE extracts more gain near the emission peak of the laser dye in comparison to either end of the lasing wavelength in the tuning range.

The calculated transmission spectrum at an optimized angle of incidence ( $48^\circ$  &  $43^\circ$  for closer and distant wavelength difference case) for the required wavelength (both cases) is shown in fig. 6.9. This spectrum explains the inherent genesis of the ASE filtering mechanism in FP characteristics for both the cases. FP filter has a sharp transmission peak optimized for laser

wavelength and highest reflection (lowest transmission) for the remaining part of the tuning range.

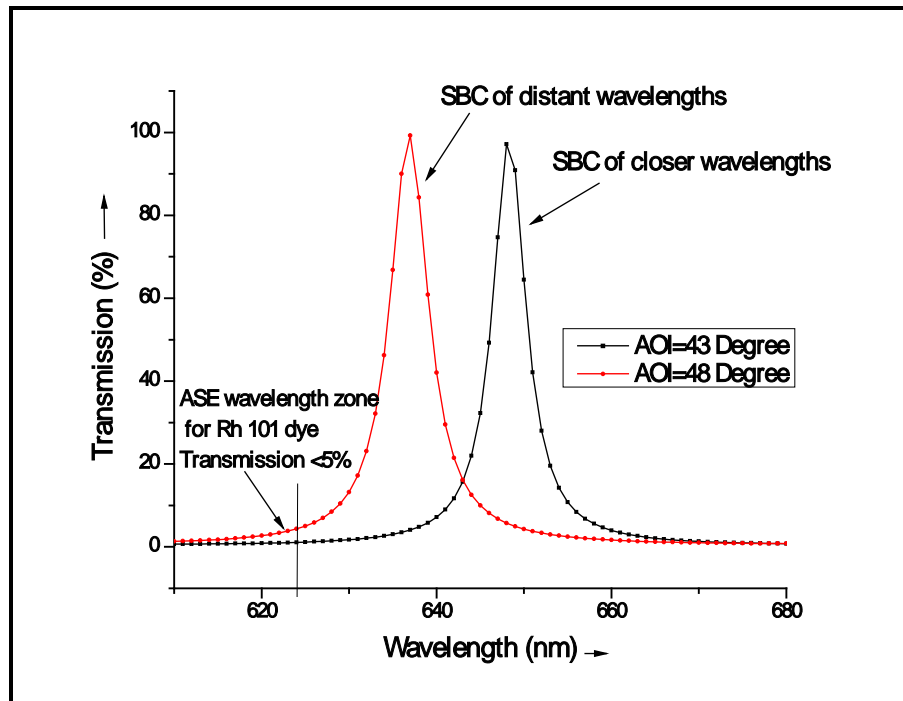


Figure 6.9: ASE filtering feature in the transmission spectrum of the FP filter (both cases)

ASE part of the incident laser beam falls in the spectral rejection band of the filter (combiner) as marked in fig. 6.9, and hence gets reflected out of the combined laser beam. This resulted in the filtering out of ASE from the transmitted beam at the combination stage. We have observed a significant advantage in the ASE filtering of the transmitted beam for dye laser operating at the end of the tuning ranges. This function became the added advantage of the FP beam combiner, in addition to an efficient beam combination of the closer wavelengths. This feature of the FP combiner was used during the alignment and optimization procedure of the dye laser MOPA chain for minimizing the inline ASE. It can be seen (fig. 6.9) that no ASE filtering is expected for reflected beam as this falls in the same region of reflection. It was

experimentally validated by measuring ASE in the second laser beam which was combined in the reflection mode by the beam combiner. Therefore, it can be concluded that ASE filtering using the FP combiner is most effective in the case of a transmitted laser beam operating at the end of the wavelength tuning range.

**6.7.4 FP Beam Combiner Implementation for Widely Tunable Lasers:**

Edge filter based beam combiner is easy to use in tunable lasers due to their flat reflection and transmission profile beyond the cut-off wavelength zone. Sharp transmission profile of FP combiner at one wavelength for one angle of incidence poses difficulty to implement this like a laser beam combiner for a widely tunable laser system. This has high transmission at a particular wavelength and transmission falls sharply with in few nanometres beyond its peak transmission wavelength.

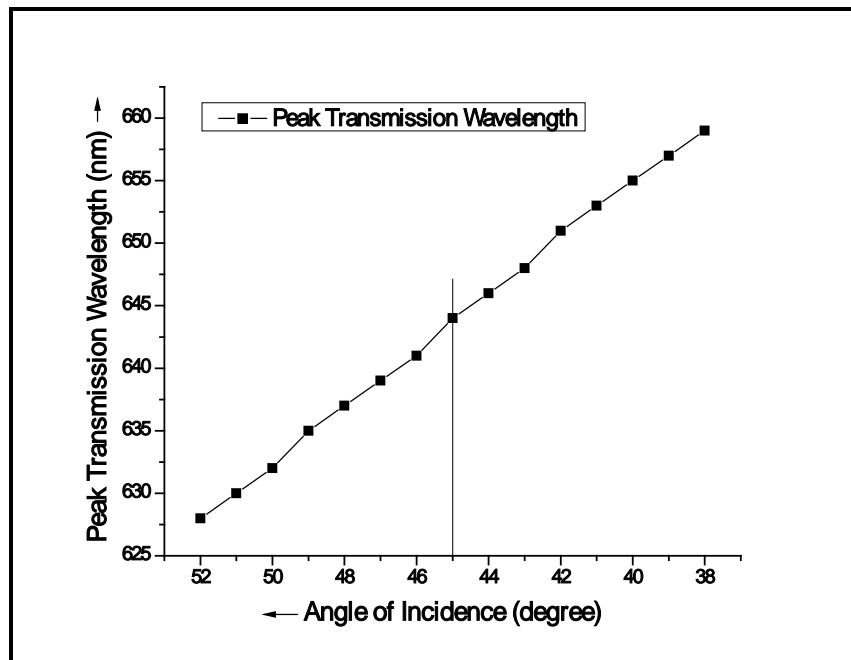
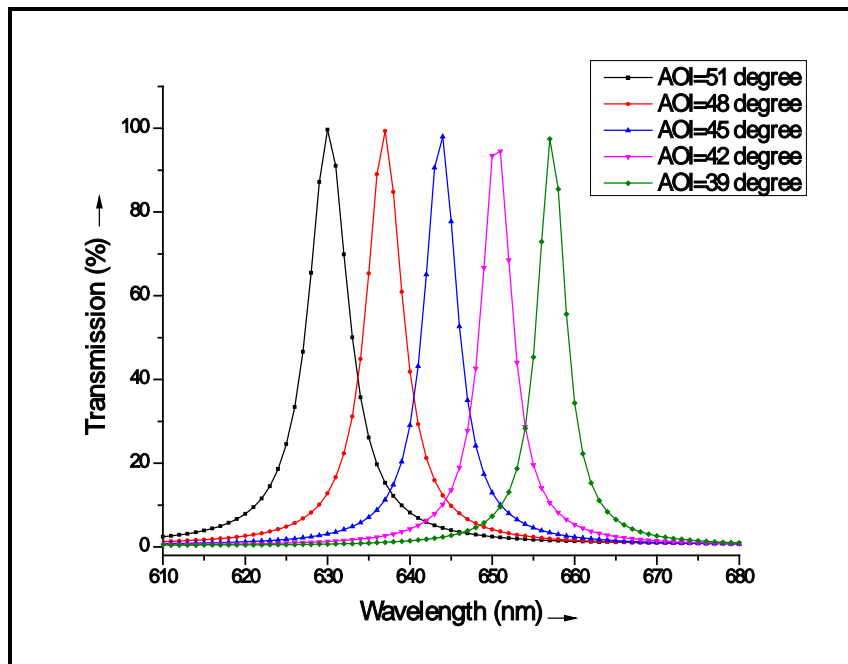


Figure 6.10: Shift in the transmission spectrum (calculated) due to change of AOI

The FP beam combiner was characterised for various wavelengths (wide tunability) using widely tunable dye laser. A new strategy has been chalked out for

its implementation to handle a wider tuning range using angle dependent transmission of FP combiner. Angle dependence of the transmission peak of the FP filter was analyzed, which is depicted in fig. 6.10. It was observed that a spectral shift of 2 nm per degree can be achieved by tuning the angle of incidence to the FP combiner. The transmitting wavelength can be changed from 628 nm to 658 nm while tuning the angle of incidence from 52 to 38 degrees respectively.



*Figure 6.11: Spectral variation with the change of AOI (calculated)*

Spectral variation with angle tuning is shown in fig.6.11 and has been observed that the wavelength of peak transmission shifts with a change in the angle of incidence, without a significant reduction in the transmission amplitude. Transmission is minimum beyond the peak transmission wavelength, which is used for the combination of laser beams operating at various wavelengths with that of other than peak wavelength. This effect was calculated for change of angle of incidence from 39 to 51 degrees. This feature was exploited for spectral beam combination of closely and widely separated wavelengths using the same FP

combiner aligned at a suitably adjusted angle of incidence as per wavelength requirement.

A novel combination of rotation and translation was employed to incorporate such angle tuning in the SBC scheme, which is depicted in fig. 6.12.

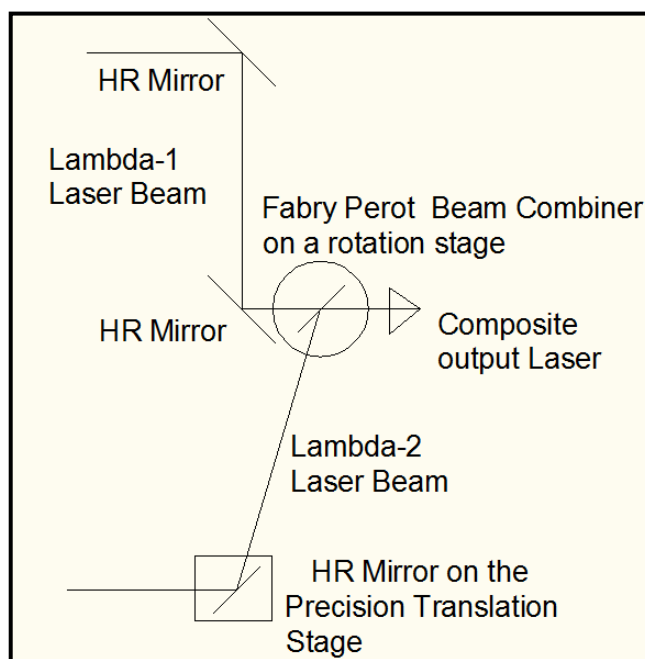


*Figure 6.12: Schematic of spectral beam combination of widely tunable lasers*

Figure 6.12 describes the schematic of the mechanism used for spectral beam combination of tunable lasers using FP combiner. The first wavelength laser beam was made to incident for maximum transmission whereas; second laser beam was reflected to achieve the spatial overlap and co-linearity. The high reflectivity mirror was used for manoeuvring the incidence angle of the second laser beam on the beam combiner. This manoeuvring mirror was mounted on a translation stage. Linear translation of the mirror changed the incidence angle direction of the second laser beam on the FP combiner while maintaining the spatial overlap.

FP combiner was mounted on the rotation stage to optimally tune the angle of incidence for transmitting wavelength. The necessary angle of incidence of the second wavelength was varied using the translation stage to spatially overlap and

maintain co-linearity of both the laser beams on the combiner. The co-linearity was established over a distance of more than 15 meters.

Shifting of the transmission peak by varying the angle of incidence was utilized for the spectral combination of various wavelengths. A combination of mirror translation for reflected beam ( $\lambda_2$ ) and rotation of FP beam combiner ( $\lambda_1$ ) was performed to tune the combiner along with tuning of the laser beams. It has been achieved and maintained the spatial overlap over a length of 15 m. This scheme was successfully tested for a closer (difference  $< 10\text{nm}$ ) as well as a distant wavelength (difference  $\sim 30\text{ nm}$ ) by changing the AOI of the combiner. This validates the applicability of this mechanism for a wider range of operating wavelengths. Spectrally beam combined by FP combiner generated the dual-wavelength dye laser beam, which has been used for spectroscopy experiments successfully.

### **6.8 Conclusions:**

The thin-film interference filter based beam combiners were studied. These types of spectral beam combiners are suitable for gain competition free combination of high power pulsed laser beams. Single cavity FP beam combiner was found to be most suitable with sharper transmission slope achievable by a lesser number of thin-film layers. However, it suffers from a stringent angle optimization requirement. This sharp transmission spectral profile was found to be advantageous for another functionality of ASE filtering. Optimized design of edge filter, single cavity FP and dual cavity FP beam combiner were analyzed. Multilayer dielectric coated Fabry Perot filter proved to be a special device for spectral beam combination of closer as well as distant wavelengths. It shows a dual character that is useful for combining high power laser beams as well as act as a filter for ASE. The observations on ASE filtering are

specifically for the combination of laser wavelengths away from the peak of the tuning range. It is expected to improve the efficiency of the dye MOPA chain by avoiding additional lossy ASE filtering mechanisms between the amplifying stages. The device coated with 19 layers of  $\text{TiO}_2$  and  $\text{SiO}_2$  proves to be efficient for the combination of closer wavelength as compared with beam splitter based beam combiners. This FP beam combiner have high damage threshold and good surface roughness values suitable for high power laser applications. Spectral shifting of the FP combiner by changing the angle of incidence was implemented for widely tunable laser systems. A combination of translation in the routing mirror and rotation of the FP filter is a successful strategy for handling the wide tunability of the lasers. This work is directly implementable for the tunable lasers required for DIAL based environmental applications. The applications of this FP combiner in CVL pumped high power, narrowband; broadly tunable dye lasers have been successfully demonstrated.



# Chapter: 7

## Summary and Future Scope

---

### **7.1 Introduction:**

Multi-wavelength, tunable dye lasers are suitable for DIAL based environmental exploration and many other such applications. Spectral beam combination techniques are utilized for generating multi-wavelength tunable dye lasers with desired properties. An elaborated study on spectral beam combination techniques for high power, high pulse repetition rate, pulsed, dye laser is presented in this thesis. Three laser beam combination techniques namely intra-cavity beam combination, co-amplification based external cavity beam combination and multilayer dielectric coated Fabry Perot (FP) beam combiner were studied in detail for combining the laser beams of closely separated wavelengths less than 10nm. Spectral beam combination using the FP beam combiner proved to be the most efficient technique among all three methods studied for this research work. Indigenously developed high repetition rate, high power copper vapor laser systems were utilized to pump the high power pulsed dye lasers. Efficient spectral beam combination of closer wavelengths with high power was the main objective of this thesis work. The important contributions from the entire research work described in the six major chapters of the thesis are being summarised here.

### **7.2 Summary of The Thesis: Contributions:**

- An indigenously developed copper vapor laser (CVL) system was characterized with plane-plane and positive branch un-stable resonator configurations. Divergence of the output CVL laser beam was measured using power in the bucket method and the Ophir make  $M^2$  meter.

Divergence in the case of the plane-plane resonator was found to be nearly 2 mrad, whereas the divergence was in the range of few mrad for unstable resonator configuration, which was dependent on the magnification of the resonator mirrors. The reduction of divergence to 0.37 mrad was achieved in the case of an unstable resonator with a magnification factor of 98. Optimized operational parameters namely output average power, divergence, green to yellow ratio, electrical input power, neon buffer gas pressure were found for this CVL system, which were determined as 40W, 0.4 mrad, 3:2, in the range of 5.8 to 6kW, 45mbar respectively.

- The CVL laser emits inherently dual wavelengths namely green at 510.6 nm and yellow at 578.2 nm. Dichroic filters are used to separate these wavelengths for pumping the dye lasers. The multi-layer thin film based optical components were theoretically designed to convert this dual-wavelength CVL laser into a single wavelength system. Two interference filter based mirrors, one for green emission (stack formula:  $(0.5L H 0.5L)^7$ ) and another for yellow emission (stack formula:  $(0.5H L 0.5H)^8$ ) were designed using  $TiO_2$  and  $SiO_2$  as high and low refractive index material respectively for plane-plane resonator configuration [7.1]. A multifunctional window (stack:  $(0.5L H 0.5L)^{18}$ ) was designed for polarized, single wavelength emission from a CVL laser system [7.2].
- The master oscillator power amplifier (MOPA) chain is utilized to boost the power of an individual CVL laser beam. A MOPA configuration of six modules was utilized to generate a high pump power beam of nearly 125 W. Power gain of an amplifier in the MOPA chain was experimentally determined at several input power levels. The power gain of 33, 30 and 26

W was determined with the input signal of 12, 30 and 42W respectively in the second amplifier unit. Total extractable power using four MOPA designs were evaluated based on the experimentally determined amplifier power gain. It was observed that net extractable power in a single long chain, splitted chain after an oscillator, splitted chain after amplifier; periodic power withdrawal configuration has the capability of delivering the power levels in the range of 136W, 161 W, 168 W, and 179 W respectively [7.3].

- The higher temperature of the discharge tube is required for the CVL operation to provide sufficient copper atom density. This results in the thermal lens effect, which reduces the output laser beam diameter to subsequent amplifier units. The effective focal length of the CVL amplifier due to the thermal lens was experimentally measured to be 50 m using the CVL oscillator as a probe beam. The effect of electrical input power and neon buffer gas pressure on the effective thermal lens focal length was determined. It was found that the effective thermal focal length decreased from 307 m to 50 m with increasing electrical input power from 3.5 kW to 6.2 kW at fixed buffer gas pressure, whereas it increased from 42 m to 70 m with increasing neon buffer gas pressure from 18 to 120 mbar for fixed electrical input power. Multilayer dielectric coated infrared reflector window design was carried out and its effect on the effective thermal lens focal length was estimated [7.4]. Four compensation techniques theoretically evaluated for a larger MOPA chain of 8 modules. These techniques are slightly divergent oscillator beam, single-stage re-collimation, double stage re-collimation, and re-collimation with beam

## CHAPTER - 7

---

diameter recovery (RBDR) for minimizing the thermal lens effect were theoretically analyzed using a ray-tracing approach. Total extractable power in the proposed eight module CVL MOPA chain with hybrid (slight divergent beam at one stage and RBDR at two stages) thermal lens compensation was calculated to be around 257 W, which is 2.2 times higher than the un-compensated MOPA chain (117W) of 8 modules [7.5].

- Laser dye chromophores cover a wide spectral range from 400 nm to 1100 nm. This can be further tailored using different solvent's environment by varying pH and their mixtures. Photo-physical properties of the dye were modified by changing the pH of the ethanol solvent, ethanol-water binary solvent, and methanol as a solvent. The redshift of 9-10 nm and 8 nm was achieved in the absorption and emission peak of the Rh 101 dye in ethanol respectively by changing the pH of the dye solution from 6.6 to 5.1. The pH of the solvent was modified by the addition of acetic acid in a suitable concentration [7.6]. Changing the solvent from ethanol to methanol resulted in the redshift of the tuning range by 13 nm in a yellow pumped Rh 101 dye laser. The use of water-ethanol binary solvent for yellow CVL beam pumped SRh101 dye was examined. It was found that the peak of the tuning range was red-shifted by 12 nm for water to ethanol volumetric ratio changed from 0 to 1. Improvement in the efficiency from 3.1% to 4.25% was achieved for the same change in the volumetric ratio of the binary solvent [7.7].
- A smaller thermo-optic coefficient of the dye solvents is desirable for obtaining a good quality laser beam in a high power dye laser system. Thermo-optic coefficient of ethanol, water, and their binary mixture was

measured using the Michelson interferometer based technique and the thermo-optic coefficient for these solvents was measured to be  $3.955 \times 10^{-4}$ ,  $0.9492 \times 10^{-4}$  and  $3.2629 \times 10^{-4}$  respectively [7.8].

- Binary dye mixture was utilized to extend the tuning range of a dye laser. The tuning range was extended from 40 nm to 82 nm in a three-wavelength dye laser using the optimized concentration of PM567 and DCM binary dye mixture. It was observed that the concentration of the constituent laser dyes in a binary dye mixture plays a significant role in tailoring the tuning range, which was experimentally tested [7.9].
- Three cavities namely linear, folded cavity with prism beam expander (PBE) and linear cascaded cavity without PBE were used to achieve narrowband multi-wavelength dye laser of more than three wavelengths. The linear cascaded grating cavity was selected for further experiments on simultaneous operation of a dye laser emitting four to five wavelengths. The second harmonic Nd: YAG laser was used as a pump source for Rh6G, DCM, PM567 dye lasers [7.10].
- CGIG and HCGIG based intra-cavity beam combined configurations were characterized in detail to determine simultaneous multi-wavelength operation. These techniques were found to be suitable for the generation of four to five, narrowband wavelengths in a single compact resonator cavity with several sub-cavities [7.11]. Zone of operation for simultaneous four wavelength generation was experimentally determined.
- Two external cavity beam combination configurations for high power, dual-wavelength CVL pumped dye laser were studied. In the first configuration (individual amplification, IA), dye laser oscillator beams

were amplified in the dye MOPA chain, followed by spectral beam combination using beam splitters. In another configuration, spectral beam combination at the dye laser oscillator beams was done, followed by co-amplification of the dual-wavelength composite dye laser beam in the common amplifier. Co-amplification based spectral beam combination technique for oscillator-amplifier configuration in case of closer wavelengths was found to be efficient. The beam combination losses were only 40% as compared to individual amplification configuration, whereas amplification efficiency of 16.45 % could be achieved in the common amplifier due to pumping with double pump power (38.5 W as compared to 19W). It was concluded that spectral beam combination after amplification is suitable for widely separated wavelengths, whereas co-amplification of the combined beam was proved to be more efficient for closely (<10 nm) separated wavelengths [7.12].

- Multilayer thin-film dielectric coated interference filter designs were carried out for a closer wavelength beam combination. Among edge filter, single cavity Fabry-Perot (FP) filter and dual cavity FP filter designs, the single cavity FP filter was selected. This filter was designed by considering 19 layers of  $\text{TiO}_2$  and  $\text{SiO}_2$  as high and low refractive index layers following the stack formula,  $((\text{HL})^4 \text{H} 2\text{L} (\text{HL})^4 \text{H})$ . This beam combiner was fabricated using an ion-assisted electron beam evaporation technique [7.13].
- It was characterized for transmission spectrum, surface morphology and damage threshold using a spectrophotometer, atomic force microscope

(AFM) and laser-induced damage threshold (LIDT) techniques respectively [7.14].

- This FP beam combiner was successfully tested for combining the laser wavelength separation by less than 10 nm, which was proved to be more efficient as compared to beam splitter based combiner. This FP combiner has added the advantage of reduced amplified spontaneous emission (ASE) for the transmitted laser beam operating at the end of its tuning range. A tuning mechanism for the FP beam combiner for widely tunable dye laser systems was successfully implemented for combining closely as well as the widely separated wavelength of dye laser beams [7.14].

### **7.3 Future Scope:**

In the future, remotely operable, optical fiber pumped, intra-cavity beam combined dual-wavelength laser system will be developed. Application of multi-wavelength dye laser in trace analysis and environmental application will be explored. Remote gas sensing based exploration will be an important work towards environmental monitoring and control.



# REFERENCES

---

## CHAPTER-1:

- [1.1]. O. Svelto, Principles of Lasers, Fifth Edition, Springer (2010).
- [1.2]. H. Jelinkova, Lasers for Medical Applications, *Wood Head Publishing* (2013).
- [1.3]. C.B. Moore, Chemical and Bio-chemical Applications of Lasers, Vol. 1, *Academic Press*, (1974).
- [1.4]. Qian Peng1, Asta Juzeniene, Jiyao Chen , Lars O Svaasand, Trond Warloe, Karl-Erik Giercksky, Johan Moan, Lasers in medicine, *Rep. Prog. Phys.* 71 056701 (28pp), (2008).
- [1.5]. Hong Jin Kong, Beam Combination Using Stimulated Brillion Scattering Phase Conjugate Mirror for Laser Fusion Driver, *Journal of the Korean Physical Society*, Vol. 49, pp.S39-S42 (2006).
- [1.6]. E. Yatsuka, T. Yamamoto, T. Hatae, K. Torimoto and K. Itami, Lossless Laser Beam Combiner Employing a High Speed Rotating Half-wave Plate, *Review of Scientific Instruments*, Vol. 88, 076107 (2017).
- [1.7]. R.K. Kirkwood et.al. Plasma-based Beam Combiner for Very High Fluence and Energy, *Nature Physics*, Vol. 14, pp 80-84 (2018).
- [1.8]. I. Balboa, B. Huang, G. Naylor, M. Walsh, A. Sirinelli, P. Parsons, J. Fessey, M. Townsend, M. Beurskens, N. Conway, J. Flanagan, M. Kempenaars and A. Kirk, Laser Beam Combiner for Thomson Scattering Core LIDAR, *Review of Scientific Instruments*, Vol. 81, 10D534 (2010).
- [1.9]. T.Y. Fan, Laser Beam Combining for High Power, High Radiance Source, *IEEE Journal of Selected Topics in Quantum Electronics*, Vol. 11(3), pp 567-577, (2005).
- [1.10].A.L. Jones Jr., R.J. De Young, Compact Solid-state Dye Polymer Laser for Ozone Lidar Applications, *Optical Engineering*, 41(11), pp 2951–2958, (2002).

## REFERENCES

---

- [1.11]. Takuya Nayuki, Kohji Marumoto, Development of a Differential-absorption Lidar System for Measurement of Atmospheric Atomic Mercury by Use of The Third Harmonic of an LDS-dye Laser, *Applied Optics*, Vol. 43(35), pp. 6487-6491, (2004).
- [1.12]. Takashi Fujii, Tetsuo Fukuchi, Dual Differential Absorption Lidar for the Measurement of Atmospheric SO<sub>2</sub> of the Order of Parts in 10<sup>9</sup>, *Applied Optics*, Vol. 40(6), pp. 949-956 (2001).
- [1.13]. S. Chudzyński A. Czyżewski, Multi-wavelength Lidar for Measurements of Atmospheric Aerosol, *Optics and Lasers in Engineering*, Vol. 37, pp 91-99 (2002).
- [1.14]. D.J. Gray, J. Anderson, Using a Multi-wavelength LiDAR for Improved Remote Sensing of Natural Waters, *Applied Optics*, Vol. 54(31), pp F232-F242 (2015).
- [1.15]. Y. Oki et.al., Multi-wavelength Distributed-feedback Dye Laser Array and its Application to Spectroscopy, *Optics Letters*, Vol. 27(14), pp. 1220-1222 (2002).
- [1.16]. Takuya Nayuki, Tetsuo Fukuchi, Sum-frequency-generation System for Differential Absorption Lidar Measurement of Atmospheric Nitrogen Dioxide, *Applied Optics*, Vol. 41(18), (2002).
- [1.17]. Takashi Fujii, Tetsuo Fukuchi, Trace Atmospheric SO<sub>2</sub> Measurement by Multi-wavelength Curve-fitting and Wavelength-optimized Dual Differential Absorption Lidar, *Applied Optics*, Vol. 41(3), pp. 524-531 (2002).
- [1.18]. N.D. Hung, P. Brechignac, Tunable Alternate Double-Wavelength Single Grating Dye Laser for DIAL Systems, *Applied Optics*, Vol. 27 (10), pp1906-1908, (1988).
- [1.19]. F.J. Duarte, L. Hillman, Dye Laser Principles, 1<sup>st</sup> Edition, *Academic Press*, (1990).
- [1.20]. F.J. Duarte, Tunable Laser Applications, 3<sup>rd</sup> Edition, *CRC, Press, Taylor & Francis* (1995).
- [1.21]. F.J. Duarte, Tunable Lasers Handbook, *Elsevier Science Publisher* (2003).
- [1.22]. L.G. Nair, Dye Lasers, *Progress in Quantum Electronics*, Vol. 7, pp 153-268 (1982).

## REFERENCES

---

- [1.23].F.P. Schafer, Dye Lasers, *Topics in Applied Physics*, Vol. 1, Springer-Verlag Berlin Heidelberg GmbH (1973).
- [1.24].Isaac L. Bass, Regina E. Bonanno, Richard P. Hackel, Peter R. Hammond, High-Average-power Dye Laser at Lawrence Livermore National Laboratory, *Applied Optics* Vol. 31(33), pp. 6993-7006 (1992).
- [1.25].Kiwamu Takehisa, Scaling up of a High Average Power Dye Laser Amplifier and its New Pumping Designs, *Applied Optics*, Vol. 36(3), pp. 584-592 (1997).
- [1.26].Paramjit Rana, G.Sridhar, K.G. Manohar, Characteristics of a Cascaded Grating Multi wavelength Dye Laser, *Optics and Laser Technology*, Vol. 86, 39-45, (2016).
- [1.27].Paramjit Rana, S.K. Mishra, D. Bhale, S.P. Sahoo, G. Sridhar, V.S. Rawat, Co-amplification: An Efficient Spectral Beam Combination Approach for High Power, Closely Separated Dual Wavelength Dye Laser Systems”, *Optics Communications*, Vol. 451, 367-373, (2019).
- [1.28].D. Haubrich, M. Dornseifer, and R. Wynands, Lossless beam combiners for nearly equal laser frequencies, *Review of Scientific Instruments*, Vol. 71, pp 338-342, (2000).
- [1.29].C. Lei, Y. Gu, Z. Chen, Z. Wang, P. Zhou, Y. MA, H. Xiao, J Leng, X. Wang, Jhou, X. Xu, J. Chen, Z. Liu, Incoherent Beam Combining of Fiber Lasers by an All-fiber  $7 \times 1$  Signal Combiner at a Power Level of 14 kW, *Optics Express*, Vol. 26(7), pp 10421-27, (2018).
- [1.30].Zel'dovich, B. Y. ; Popovichev, V. I. ; Ragulsky, V. V. & Faizullov, F. S. Connection Between the Wave fronts of the Reflected and Exciting Light in Stimulated Mandel'shtem-Brillouin Scattering, *Sov. Phys. JETP*, Vol. 15, 109, (1972).
- [1.31].Zel'dovich, B. Y.; Pilipetsky, N. F. & Shkunov, V. V. Principle of Phase Conjugation, *Springer-Verlag, Berlin, Heidelberg, New York and Tokyo*, (1985).

## REFERENCES

---

- [1.32]. Damzen, M. J., Vlad, V. I., Babin, V. & Mocofanescu A. Stimulated Brillouin Scattering, *Institute of Physics Publishing*, Bristol and Philadelphia, (2003).
- [1.33]. Brignon, A. & Huignard J.-P. Phase Conjugate Laser Optics, *John Wiley & Sons, Inc.*, New Jersey and Canada, (2004).
- [1.34]. T.H. Russell, S. M. Willis, M. B. Crookston, W. B. Roh, Stimulated Raman scattering in Multimode Fibers and its Application to Beam Cleanup and Combining, *J. Nonlinear Optical Physics Material*, Vol. 11(3), pp 303-316 (2002).
- [1.35]. Yu. G. Basov, Optical Designs of Two-frequency Dye Lasers (Review), *Journal of Applied Spectroscopy*, Vol. 49 (6), pp. 1209-1219, (1988).
- [1.36]. E.F. Zalewski, R.A. Keller, Tunable Multiple Wavelength Organic Dye Laser, *Applied Optics*, Vol. 10(12), pp 2773-2775 (1971).
- [1.37]. D.J Taylor, S.E. Harris, S.T.K. Nieh and T.W. Hasch, Electronic Tuning of a Dye Laser Using the Acousto-Optic Filter, *Applied Physics Letters*, Vol. 19 (8), pp 269 (1971).
- [1.38]. Hershel S. Pilloff; Simultaneous Two-wavelength Selection in the N<sub>2</sub> Laser Pumped Dye Laser, *Applied Physics Letters*, Vol. 21 (8), pp 339-340 (1972).
- [1.39]. C.Y. Wu., J.R. Lombardi, Simultaneous Two Frequency Oscillation in a Dye Laser System, *Optics Communications*, Vol. 7(3), pp 233-236 1973).
- [1.40]. A. A. Friesem, U. Ganiel, G. Neumann, Simultaneous Multiple Wavelength Operation of a Tunable Dye Laser, *Applied Physics Letter*, Vol. 23(5), pp 249-51(1973).
- [1.41]. R.C. Hilborn, H.C. Brayman, Simultaneous Two-wavelength Output from Multiple-Dye Pulsed Tunable Dye Lasers, *Journal of Applied Physics*, Vol. 45(11), pp 4912-1914 (1974).
- [1.42]. G. Marowsky, F. Zaraga, Dual Wavelength Operation of Two Coupled Dye Lasers, *Optics Communications*, Vol. 11(4), pp 343-345 (1974).

## REFERENCES

---

- [1.43]. C. Kittrell, R.A. Bernheim, Simultaneous Tunable Two Wavelength Operation of Flashlamp Pumped Dye Lasers, *Optics Communications*, Vol. 19(1), pp 5-6 (1976).
- [1.44]. A.J. Schmidt, Simultaneous Two Wavelength Output of N<sub>2</sub> pumped Dye Lasers, *Optics Communications*, Vol. 14(3), pp 294 - 295 (1975).
- [1.45]. Haim Lotem and R.T. Lynch, Double Wavelength Laser, *Applied Physics Letters*, Vol. 27, No. 6 pp 344 - 346 (1975).
- [1.46]. B.R. Marx, G. Holloway and L. Allen, Simultaneous Two Wavelength Narrow Band Output From a Pulsed Dye Laser, *Optics Communications*, Vol. 18(4), pp 437 - 438 (1976).
- [1.47]. H. Inomata, and A.I. Carswell, Simultaneous Tunable Two Wavelength Ultraviolet Dye Laser, *Optics Communications*, Vol. 22(3) pp 278 - 282 (1976)
- [1.48]. E. Winter, G. Veith, A.J. Schmidt, Two Polarized Wavelength Generated in a Nitrogen Laser Pumped Dye Laser, *Optics Communications*, Vol. 25(1), 1978.
- [1.49]. R. Dorsinville, Longitudinal Pumped Dual Wavelength Dye Laser, *Optics Communications*, Vol. 26 (3), pp 419-420 (1978).
- [1.50]. Y. Prior, Double Frequency Narrow-band Grazing Incidence Pulsed Dye Laser, *Review of Scientific Instruments*, Vol. 50(2), pp 259-260, (1979).
- [1.51]. L.G. Nair, A Double Wavelength Nitrogen Laser Pumped Dye Laser, *Applied Physics*, Vol. 20, pp 97-99 (1979).
- [1.52]. S. Chandra, A. Compaan, Double Frequency Dye Lasers With A Continuously Variable Power Ratio, *Optics Communications*, Vol. 31(1), pp 73-75 (1979).
- [1.53]. L.G. Nair, K. Dasgupta, Double Wavelength Operation of a Grazing Incidence Tunable Dye Laser, *IEEE Journal of Quantum Electronics*, Vol. QE-16(2), (1980).

## REFERENCES

---

- [1.54]. S.G. Dinev, I.G. Koprinkov, K.V. Stamenov, K.A. Stankov, C. Radzewicz, Two Wavelength Single Mode Grazing Incidence Dye Laser, *Optics Communications*, Vol. 32(2), pp 313-316, (1980).
- [1.55]. H.J. Kong, S.S. Lee, Dual Wavelength and Continuously Variable Polarization Dye Laser, *IEEE Journal of Quantum Electronics*, Vol. QE-17(4), pp 43-441, (1981).
- [1.56]. M.N. Nenchev, Y.H. Meyer, Two-Wavelength dye-Laser Operation Using a Reflecting Fizeau Interferometer, *Applied Physics*, Vol. 24, pp. 7-9 (1981).
- [1.57]. A. Nomura, Y. Shimomura, Y. Saito, T. Kano, Simple Tunable Dye Laser Using a Dielectric Multilayer Filter, *Review of Scientific Instruments*, Vol. 53 (4), pp 539-540, (1982).
- [1.58]. J.P. Sage, Y. Aubry, High Power Tunable Dual Frequency Laser System, *Optics Communications*, Vol. 42 (6), pp 428-430, (1982).
- [1.59]. I. Golub, G. Erez, R. Shuker, Simultaneous Operation of Distributed Feedback and Grating Tuned Dye Lasers, *Applied Physics B*, Vol. 31, pp75-78 (1983).
- [1.60]. S.W. Williams, D.W.O. Heddle, Simultaneous Two-Wavelength Tunable Dye Laser With No Mode Competition And With A Wavelength Separation of More than 200 nm, *Optics Communications*, Vol. 45(2), pp 112-114, (1983).
- [1.61]. M. Schutz, U. Heitmann, A. Hese, Development of a Dual-Wavelength Dye-Laser System for the UV and Its Application to Simultaneous Multi-element Detection, *Applied Physics B*, Vol. 61, pp 339-343 (1995).
- [1.62]. D.K. Ko, G. Lim, S.H. Kim, J. Lee, Dual-Wavelength Operation of a Self-seeded Dye Laser Oscillator, *Applied Optics*, Vol. 35(12), pp 1995-1998, (1996).
- [1.63]. S. Jelvani, B. Khodadoost, E. Mohajerni, R. Sadighi, Dual Wavelength Dye Laser Pumped by a Copper Vapor Laser, *Laser Physics*, Vol. 13(10), pp1275-1278, (2003).

## REFERENCES

---

- [1.64].S. Jelvani, B. Khodadoost, Gain Competition Effect in Dual-wavelength Dye Lasers, *Optics & Laser Technology*, Vol. 39(1), pp182-188 (2007).
- [1.65].R. Khare, S.R. Daulatabad, K.K. Sharangpani, R. Bhatnagar, An Independently Tunable, Collinear, Variable Delay, Two-wavelength Dye Laser, *Optics Communications*, Vol. 153(1–3), pp 68-72 (1998).
- [1.66].O.J. Zapata-Nava, P.R. Montero, M. DavidIturbe-Castilo, C.G.T. Palacios, Grating Cavity Dual Wavelength Dye Laser, *Optics Express*, Vol. 19(4), pp. 3483-3491, (2011)
- [1.67].M. Liu, Y. Liu, Z. Peng, S. Wang, Q. Wang, Q. Mu, Z.Cao, Li. Xuan, Organic Solid-State Tri-Wavelength Lasing from Holographic Polymer-Dispersed Liquid Crystal and a Distributed Feedback Laser with a Doped Laser Dye and a Semiconducting Polymer Film, *Materials*, Vol. 10 , 509, pp 1-10 (2017).
- [1.68].R. Khare, S.R. Daulatabad, H.S.Vora, R. Bhatnagar, A tunable Three Wavelength Copper Vapor Laser Pumped Dye Laser with Collinear Output, *Optics Communications*, Vol. 114 (3–4), pp 275-279 (1995).

### CHAPTER-2:

- [2.1] C. E Little, Ed., Metal Vapour Lasers- Physics, Engineering and Applications, *Wiley, New York*, (1999).
- [2.2] C.E. Little and N.V. Sabotinov, Pulsed Metal Vapor Laser, *NATO ASI Series; Kluwer Academic Pub.*, (1996).
- [2.3] J. J. Chang, B. E. Warner, C. D. Boley, and E. P. Dragon, High-power copper vapour lasers and applications, in Pulsed Metal Vapour Lasers- *Proceeding of the NATO Advanced Research Workshop on Pulsed Metal Vapour Lasers-Physics and Emerging Applications in Industry, Medicine and Science*, St. Andrews, U.K., Aug. 6–10, 1995, C. E. Little and N. V. Sabotinov, Eds., pp. 101–112, Kluwer Academic publishers, The

## REFERENCES

---

- Netherlands (1996). Kushner and B.E. Warner, *J. Appl. Phys.* 54(6), pp 2970-2982, (1983).
- [2.4] S V Kireev, S L Shnyrev, I. G. Simanovsky and S. V. Suganeev Using a Copper-Vapor Laser (578.2nm) in a New Method of Laser Fluorescence for Molecular Iodine Isotopes to Detect Gases in Real Time, *Laser Phys. Letter.*, Vol. 11, pp 095701 (2014).
- [2.5] Knowles M.R.H., Micro-ablation with High Power Pulsed Copper Vapor Lasers, *Optics Express*, Vol. 7(2), pp 50–55 (2000).
- [2.6] Peng Q, Juzeniene A, Chen J, Svaasand L O, Warloe T, Giercksky K-E and Moan J, Lasers in Medicine, *Rep. Prog. Phys.*, Vol. 71, 056701, pp 1-22 (2008).
- [2.7] Gubarev F. A., M. S. Klenovskii, A Long Pulse CuBr Vapor Oscillator for Laser Monitor Applications, *J. Phys. Conf. Ser.*, Vol. 671, pp 012019 (2016).
- [2.8] R. Mahakud, J. Kumar, O. Prakash, S. K. Dixit, S. V. Nakhe, FBG Inscription by a Biprism Interferometer: Analysis and Experiment, *Applied Physics B*, Vol. 121(3), pp 283–295 (2015).
- [2.9] E. Gu, C.W. Jeon, H.W. Choi, Grice, M.D. Dawson, E. Killy, M.R.H. Knowles, Micromachining and Dicing of Sapphire, Gallium Nitride and Micro LED Devices With UV Copper Vapour Laser, *Thin Solid Films*, Vol. 453–454, pp 462–466 (2004).
- [2.10] R Sadighi-Bonabi, K Pasandideh, M Zand and H Nazari Mahroo, Stable and Efficient Operation of a Large-bore Copper Vapor Laser with Funnel-shaped, Grooved Copper Electrodes, *Laser Physics*, vol. 27, 035001 pp 5; (2017).
- [2.11] W.T. Walter, N. Solimene, M. Piltch, G. Gould, Efficient Pulsed Gas Discharge Lasers, *IEEE J. Quantum Electron.*, Vol. 2(9), pp130, (1966).
- [2.12] M.J. Kushner and B.E. Warner, Large-bore Copper Vapor Lasers: Kinetics and Scaling Issues, *Journal of Applied Physics*, Vol. 54(6), pp 2970-2982, (1983).

## REFERENCES

---

- [2.13] V V Zubov, Nikolai A Lyabin and A D Chursin, Efficient Master-Oscillator-Amplifier System Utilizing Copper Vapor Laser Active Elements, *Sov. J. Quantum Electron.* Vol. 16(12), pp 1606-1610, (1986).
- [2.14] P. Liang, R. Hua, Q. Shen, Thermal lens and its Effects in Copper-Vapor Lasers, *Appl. Phys. B*, Vol. 60(6), pp 557-563 (1995).
- [2.15] M. J. Withford, D. J. W. Brown, R. J. Carman, and J. A. Piper, Enhanced Performance of Elemental Copper-Vapor Lasers by Use of H<sub>2</sub>-HCl-Ne Buffer-gas Mixtures, *Optics Letters*, Vol. 23(9), pp 706-708 (1998).
- [2.16] David W. Coutts and Daniel J. W. Brown, Formation of Output in Copper Vapor Lasers, *Applied Optics* Vol. 34(9), pp 1502-1512 (1995).
- [2.17] R. Bhatnagar, S.K. Dixit, J.K. Mittal, B. Singh, S.V. Nakhe, K.K. Sharangpani, A Copper Vapor Laser With a Positive Branch Self-filtering Unstable Resonator, *Optics Communications*, Vol.82 ( 5-6), pp 557-562 (1991).
- [2.18] S.K. Dixit, Filtering Resonators, *Nova Science Publishers Inc*, United States(2001)
- [2.19] Time Resolved Beam Divergence from a Copper Vapor Laser with Unstable resonator DW Coutts, *IEEE journal of quantum electronics*, Vol. 31 (2), pp 330-342 (1995).
- [2.20] David W. Coutts, Daniel J. W. Brown, and James A. Piper, Measurements of the Divergence Evolution of a Copper-vapor Laser Output by Using a Cylindrical Imaging Technique, *Applied Optics* Vol. 32(12), pp. 2058-2061 (1993).
- [2.21] Paramjit Rana, S.K. Mishra, Jaya Mukherjee, V.S. Rawat, Multilayer Dielectric Thin Film Optical Coating Design for Single Wavelength Operation of Inherently Dual Wavelength Copper Vapor Laser, *Proceeding of International Conference of Optics and Electro-Optics (ICOL)*, I.R.D.E. Dehradun (2019).

## REFERENCES

---

- [2.22] Paramjit Rana, R.B. Tokas, V.S. Rawat, S. Thakur, N.K. Sahoo, Design of Multifunctional Window for Polarized Green Copper Vapor Laser Oscillator Amplifier Chain, *Proceedings of DAE-BRNS National Laser Symposium-26*, (2016).
- [2.23] Prakash O, Gorakh N. Tiwari, Sudhir K. Dixit, and Rajiva Bhatnagar, Single-pulse time-resolved Comparative Study on the Performance of a Master Oscillator Power-Amplifier Copper Vapor Laser System with Generalized Diffraction Filtered and Unstable Resonators as Master Oscillators, *Applied Optics*, Vol. 42(18), pp 3538–45 (2003).
- [2.24] D.W. Coutts, Double-pass Copper Vapor Laser Master Oscillator Power Amplifier Systems: Generation of Flat-top Focused Beams for Fiber Coupling and Percussion Drilling, *IEEE Journal of Quantum Electronics*, Vol. 38(9), pp1217-24, (2002).
- [2.25] Daniel J. W. Brown, Michael J. Withford, and James A. Piper, High-Power, High-Brightness Master-Oscillator Power-Amplifier Copper Laser System Based on Kinetically Enhanced Active Elements, *IEEE Journal of Quantum Electronics*, Vol. 37(4), pp 518-524 (2001).
- [2.26] G.N. Tiwari, R K Mishra, R Khare, S V Nakhe, Development of Copper Bromide Laser Master Oscillator Power Amplifier System, *Pramana J. of Physics*, Vol. 82(2), pp 217-25, (2014).
- [2.27] Comparative study of Copper Vapour Laser Master Oscillator Power Amplifier Configurations, Paramjit Rana, S.K. Mishra, S.P. Sahoo, S.K. Agarwalla, G. Sridhar, V.S. Rawat, *Proceedings of DAE-BRNS National Laser Symposium-28*, (2018).
- [2.28] V.M. Zharikov, V.V. Zubov, M. A. Ležnĭnikov, Nikolai A Lyabin and A D Chursin Thermal Gas Lens in a Copper Vapor Laser, *Sov. J. Quantum Electron.* Vol. 14(5), pp 623-626, (1984).
- [2.29] H.K.V. Lotsch and W.C. Davis, The Lensing Effect of CO<sub>2</sub> Laser Plasma, *Applied Optics*, Vol. 9 (12), pp 2725-2728 (1970).

## REFERENCES

---

- [2.30] S. Sinha, K. Dasgupta, Self-defocusing of Light in Copper Vapour Laser. *Applied Physics B*, Vol. 64(6), pp 667-670 (1997).
- [2.31] R. Biswal, G.K. Mishra, Girija S Purbia, Pravin K Agrawal, Om Prakash, Sudhir K Dixit, Jeevan K Mittal, A Comparative Study on Thermal Lensing Characteristics of Low ( $\sim 500^\circ\text{C}$ ) and High ( $\sim 1500^\circ\text{C}$ ) Temperature Variants of Copper Vapor Laser, *Optical Engineering*, Vol. 50(8), pp 084202-1 (2011).
- [2.32] Sunita Singh, G. Sridhar, Study of Thermal Lensing Effects in a Copper Vapor Laser, *Optics & Laser Technology*, Vol. 32, 89-91 (2000).
- [2.33] Murthy MVRK. Lateral Shearing Interferometer in Optical Shop Testing 2<sup>nd</sup> ed.: editor: Malacara D, *New York: Wiley*, (1992).
- [2.34] Claude A. Klein, Optical Distortion Coefficients on Laser Windows, *Optical Engineering*, Vol. 29 (4), pp 343-350 (1990).
- [2.35] M. Amit, S. Lavi, G.Erez, E. Miron, Temporal and Spatial Properties of an Oscillator-Amplifier Copper Vapor Laser, *Optics Communication*. Vol. 62(2), 110-114 (1987).
- [2.36] Paramjit Rana, V.S. Rawat, Thin Film Design of IR Reflector Window for Reduced Thermal Lensing in Copper Vapor Laser, *AIP Conference Proceedings*, Vol. 2115(1), 030281, pp 1-4 (2019).
- [2.37] Stéphane Larouche and Ludvik Martinu, OpenFilters: Open-source Software for the Design, Optimization, and Synthesis of Optical Filters, *Applied Optics*, Vol. 47(13) pp C219-C230 (2008).
- [2.38] H. Angus Macleod, Thin Film Optical Filters, 4th edition, *CRC press*. (2010).

### CHAPTER-3

- [3.1]. Ulrich Blachmann, Lambdachrome Laser Dyes, 3<sup>rd</sup> Edition, *Lambda Physik*, (2000).
- [3.2]. F.J. Duarte, Tunable Lasers Handbook, *Elsevier Science Publisher* (2003).
- [3.3]. F.J. Duarte, JA Piper, Narrow Linewidth, High PRF Copper Laser Pumped Dye Laser

## REFERENCES

---

- Oscillators, *Applied Optics*, Vol. 23(9), pp. 1391-1394 (1984).
- [3.4]. F.J. Duarte, J.A. Piper, Prism Pre-expanded Grazing Incidence Grating Cavity for Pulsed Dye Lasers, *Applied Optics*, Vol. 20(12), pp. 2113-2116, (1981).
- [3.5]. J. Jorge, G.R. Castro, M.A.U. Martines, Comparison among Different pH Values of Rhodamine B Solution Impregnated into Mesoporous Silica, *Orbital*, Vol.5 (1),pp 23-29, (2013).
- [3.6]. A. Satpati , S. Senthilkumar, M. Kumbhakar, S.Nath, DK Maity, Pal H., Investigations of the Solvent Polarity Effect on the Photophysical Properties of Coumarin-7 dye, *Photochemistry and Photobiology*, Vol. 81(2), pp 270-8 ( 2005).
- [3.7]. A K Ray, S Sinha, S Kundu, S Sasikumar, S K S Nair, T Pal, K Dasgupta, High-Repetition-rate, Narrow-band Dye Lasers with Water as a Solvent for Dyes, *Applied Optics*, Vol. 41(9), pp. 1704-1713, 2002.
- [3.8]. C. V. Bindhu, S. S. Harilal, V.P.N. Nampoori and C. P. G. Vallabhan, Solvent Effect on Absolute Fluorescence Quantum Yield of Rhodamine 6G Determined Using Transient Thermal Lens Technique, *Modern Physics Letters B*, Vol. 13(16), pp 563–576 (1999)
- [3.9]. H El-Kashef, R Shalaby, Thermo-optical Properties of Polar Dielectric Laser Dye Solvents, *Optics and Laser Technology*, Vol. 44(1), pp71 – 73, (2012).
- [3.10]. V S Rawat, L M Gantayet, G Sridhar, S Singh, Design of the Dye Cell of a Dye Laser to Facilitate Repetitive Operation in the Single Longitudinal Mode, *Laser Physics*, Vol.23(3), pp 035001,(2013).
- [3.11]. R Ghazy, Thermo-optical Properties of Some Common Laser Dye Solvents, *Journal of Photochemistry and Photobiology A: Chemistry*, Vol.119 (1), pp 61-66, (1998).
- [3.12]. V S Rawat, L M Gantayet, G Sridhar, S Singh, A Computational Model for Transient Temperature Rise in a Dye Laser Gain Medium Pumped by a Copper Vapor Laser, *Laser Physics*, Vol. 24(2), pp 025005, 2014.

## REFERENCES

---

- [3.13]. P Brochard, V G Mazza, R Cabanel, Thermal Nonlinear Refraction in Dye Solutions: A Study of the Transient Regime, *Journal of Optical Society of America B*, Vol. 14 (2), pp 405 – 414, 1997.
- [3.14]. R Kita, S Wiegand, J L Strathmann, Sign change of the Soret Coefficient of Poly (ethylene oxide) in Water/ethanol Mixtures Observed by Thermal Diffusion Forced Rayleigh Scattering, *J. Chemical Physics*, Vol. 121, pp 3874 – 3883, (2004).
- [3.15]. M Daimon, A Masumura, Measurement of the refractive index of distilled water from the near-infrared region to the ultraviolet region, *Applied Optics*, Vol. 38(18), pp 3811 – 3820, (2007).
- [3.16]. K C Silva, O A Sakai, A Steimacher, F Padrochi, M L Baesso, A C Bento, A N Medina, S M Lima, R C Oliveira, J C S Moraes, K Yukimitu, E B Araujo, M Petrovich, D W Hewak, Temperature and Wavelength Dependence of the Thermo-optical Properties of Tellurite and Chalcogenide Glasses, *J Applied Physics*, Vol. 102, pp 073507, (2007).
- [3.17]. Rafed A. Ali, Oday Mazin Abdul-Munem, Ahmed Naji Abd, Study the Spectroscopic Characteristics of Rhodamine B Dye in Ethanol and Methanol Mixture and Calculation the Quantum Efficiency, *Baghdad Science Journal*, Vol.9(2), pp 352-360, (2012).
- [3.18]. Amit Nag, Debabrata, Goswami, Solvent Effect on Two-photon Absorption and Fluorescence of Rhodamine Dyes, *Journal of Photochemistry and Photobiology A: Chemistry*, Vol.206 (2–3), pp 188-197, (2009).
- [3.19]. S Sinha, A K Ray, S Kundu, S Sashikumar, K Dasgupta, Heavy-water-based Solutions of Rhodamine Dyes: Photophysical Properties and Laser Operation, *Applied, Physics B*, Vol. 75(1), pp 85 – 90, (2002).
- [3.20]. B.R. Gyathri, J.R.Mannekutla, S.R.Inamdar, Effect of Binary Solvent Mixtures (DMSO/water) on the Dipole Moment and Lifetime of Coumarin Dyes, *J. of Molecular Structure*, Vol. 889 (1-3), pp 383-393, (2008).

## REFERENCES

---

- [3.21]. A.K. Ray, S. Sinha, S. Kundu, S. Kumar, K. Dasgupta, A Binary Solvent of Water and Propanol for use in High Average Power Dye Lasers. *Applied Physics B*, Vol. 87, issue 3, pp 489-495, (2007).
- [3.22]. P. Burlamacchi, H.F. Ranea, Characteristics of a Multicolor Dye Laser, *Optics Communications*, Vol. 31(2 ), pp 185-188, (1979).
- [3.23]. Sucharita Sinha, Alok K Ray, Soumitra Kundu, Tamal B Pal, Sivagiriyal KS Nair, Kamalesh Dasgupta, Spectral Characteristics of a Binary Dye Mixture Laser, *Applied optics*, Vol. 41(33), 7006-7011 (2002).

### CHAPTER-4

- [4.1] R. khare, S.R. Daulatabad, H.S. Vora, R. Bhatnagar, A Tunable Three Wavelength Copper Vapor Laser Pumped Dye Laser with Collinear Output, *Optics Communications* Vol. 114 (3-4),pp 275-279 (1995).
- [4.2] Yasunori Saito, Tsukasa Teramura, Akio Nomura, Tetsuo Kano, Simultaneously Tunable Three Wavelength Dye Laser, *Applied Optics*, Vol. 24(16), pp2477-2478 (1985).
- [4.3] P. Burlamacchi, H.F.Ranea Sandoval, Characteristics of a Multicolor Dye Laser, *Optics Communications*, Vol. 31(2), 185-188 (1979).
- [4.4] I. Shoshan, N.N. Danon, U.P. Oppenheim; Narrowband Pperation of a Pulsed Dye Laser without Intracavity Beam Expansion, *Journal of Applied Physics*, Vol.48, pp4495 (1977).
- [4.5] M.G. Littman and H.J. Metcalf, Spectrally Narrow Pulsed Dye Laser without Beam Expander, *Applied Optics*, Vol.17 (14), pp . 2224-2227, (1978).
- [4.6] S. Saikan, Nitrogen Laser Pumped Single Mode Dye Laser, *Applied Physics*, Vol. 17(1), pp 41-44, (1978).
- [4.7] M.G. Littman, Single Mode Operation of Grazing Incidence Pulsed Dye Laser, *Optics Letters*, Vol. 3(4) pp. 138-140, (1978).

## REFERENCES

---

- [4.8] L.G. Nair and K. Dasgupta; Double Wavelength Operation of a Grazing Incidence Tunable Dye Laser, *IEEE Journal of Quantum Electronics*, Vol. QE-16(2), pp 111-112, (1980).
- [4.9] Y. Prior, Double Frequency Narrow Band Grazing Incidence Pulsed Dye Laser, *Review of Scientific Instruments*, Vol. 50(2), pp 259-260, (1979).
- [4.10] <http://www.avantes.com/products/spectrometers/sensline/item/327-avaspec-uls2048xl>
- [4.11] S. Jelvani, B. Khodadoodt; Gain Competition Effect in Dual Wavelength Dye Lasers, *Optics and Laser Technology*, Vol. 39(1), pp182-188 (2007).
- [4.12] S. Jelvani, B. Khodadoost, E. Mohajerani and R. Sadighi; Dual Wavelength Dye Laser Pumped by a Copper Vapor Laser, *Laser Physics*, Vol. 13(10), pp1275- 278 (2003).

### CHAPTER-5

- [5.1]. S. Jelvani, B. Khodadoodt; Gain Competition Effect in Dual Wavelength Dye Lasers, *Optics and Laser Technology*, Vol. 39(1), pp182-188 (2007).
- [5.2]. S. Jelvani, B. Khodadoost, E. Mohajerani and R. Sadighi; Dual Wavelength Dye Laser Pumped by a Copper Vapor Laser, *Laser Physics*, Vol. 13(10), pp1275- 278 (2003).
- [5.3]. Ulrich Blachmann, *Lambdachrome laser dyes*, 3<sup>rd</sup> Edition, Lambda Physik, (2000).
- [5.4]. I.L. Bass, Regina E. Bonanno, Richard P. Hackel, and Peter R. Hammond, High-average-power dye laser at Lawrence Livermore National Laboratory, *Applied Optics*, Vol. 31( 33), pp 6993-7006, (1992).
- [5.5]. L.G Nair, Dye Lasers, *Progress in Quantum Electronics*, Vol. 7 (3-4), pp 153-268 (1982).

### CHAPTER-6

- [6.1] Fan Chen, Jun Ma, Cong Wei, Rihong Zhu, Wenchao Zhou, Qun Yuan, Shaohua Pan, JianYun Zhang, Yize Wen, and Jiantai Dou, 10 kW-level Spectral Beam Combination of

## REFERENCES

---

- Two High Power Broad Linewidth Fiber Lasers by means of Edge Filters, *Optics Express*, Vol.25(26), pp 32783-32791 (2017).
- [6.2] <https://www.newport.com/p/DCM11>
- [6.3] <https://www.edmundoptics.com/f/dichroic-laser-beam-combiners-8f67c2b5/14451/>
- [6.4] Mangla Nand, Babita, S Jena, RB Tokas, P Rajput, C Mukharjee, S Thakur, SN Jha, NK Sahoo, Development of High Damage Threshold Multilayer Thin Film Beam Combiner for Laser Application, *AIP Conference Proceedings*, Vol. 1731 (1), 080051 (2016).
- [6.5] Francisco J. Duarte, *Tunable Laser Optics* (Academic Press), pp 115-155 (2003).
- [6.6] Junwen Xue, Wei Chen, Ying Pan, Jinqian Shi, Yujie Fang, Haijun Xie, Mingyuan Xie, Lu Sun, Binghua Su, Pulsed Laser Linewidth Measurement using Fabry-Pérot Scanning Interferometer, *Results in Physics*, Vol. 6, pp 698-703 (2016).
- [6.7] Ayman Zohbi, M.A. Hasan, Design And Fabrication Of Thin-Film Optical Filters For Mid-Infrared Spectroscopy Application, *International Journal of Scientific & Technology Research*, Vol. 3(10), pp 71-76, (2014).
- [6.8] Vahideh Khadem Hosseini Ghasemi, Design Tunable Optical Thin Film Fabry-Perot Filter In Dense Wavelength Division Multiplexer, *Majlesi Journal of Telecommunication Devices*, Vol. 2(1), pp 167-171, (2012).
- [6.9] Paramjit Rana, G.Sridhar, K.G. Manohar, Characteristics of a Cascaded Grating Multi-wavelength Dye Laser, *Optics and Laser Technology*, Vol. 86, pp 39-45, (2016).
- [6.10] Paramjit Rana, Mishra, S. K.; Sahoo, S. P.; Bhale, D.; Sridhar, G.; Rawat, V. S., Co-amplification: An Efficient Spectral Beam Combination Approach for High Power, Closely Separated Dual Wavelength Dye Laser Systems, *Optics Communications*, Vol. 451, pp 367-373 (2019).

## REFERENCES

---

- [6.11] B. Wang, G. Dai, H. Zhang, X Ni, Z Shen, J. Lu, Damage Performance of  $\text{TiO}_2/\text{SiO}_2$  Thin Film Components Induced by a Long-pulsed Laser, *Applied Surface Science*, Volume 257(23), pp 9977-9981 (2011).
- [6.12] J. Ferré-Borrull, Angela Duparré, Etienne Quesnel, Procedure to Characterize Microroughness of Optical Thin films: Application to Ion-beam-sputtered Vacuum-ultraviolet Coatings, *Applied Optics*, Vol. 40(13), pp 2190-2199(2001).
- [6.13] R.B. Tokas, S Jena, S Thakur, NK Sahoo., Effect of Angle of Deposition on Micro-roughness Parameters and Optical Properties of  $\text{HfO}_2$  Thin Films Deposited by Reactive Electron Beam Evaporation, *Thin Solid Films*, Vol. 609, pp 42-48(2016).
- [6.14] R.B. Tokas, S. Jena, J.S. Misal, K.D. Rao, S.R. Polaki, C. Pratap, D.V. Udupa, S.Thakur, S. Kumar, N.K. Sahoo, Study of  $\text{ZrO}_2$  Thin films Deposited at Glancing Angle by Radio Frequency Magnetron Sputtering under Varying Substrate Rotation, *Thin Solid Films*, Vol. 645 , pp 290-299, (2018).
- [6.15] C.H. Zhang, Liu, Z. -J.; Li, K. Y.; Shen, Y. G.; Luo, J. B., Microstructure, Surface Morphology, and Mechanical Properties of Nanocrystalline  $\text{TiN}/\text{Amorphous Si}_3\text{N}_4$  Composite Films Synthesized by Ion Beam Assisted Deposition, *Journal of Applied Physics*, Vol. 95(3), pp 1460-1467, (2004).
- [6.16] L.G. Nair, K. Dasgupta, Amplified Spontaneous Emission in Narrow Band Pulsed Dye Laser Oscillators - Theory and Experiment, *IEEE Journal of Quantum Electronics*, Vol. 21(11), pp 1782-1794 (1985).
- [6.17] V.S. Rawat, G Sridhar, S Singh, LM Gantayet, Operation of a CVL Pumped Dye Laser in the Single Longitudinal Mode and Its Parametric Characterization, *Optik*, Vol. 124(17), pp 2837-2843 (2013).

## REFERENCES

---

### CHAPTER-7

- [7.1] Multilayer Dielectric Thin Film Optical Coating Design for Single Wavelength Operation of Inherently Dual Wavelength Copper Vapor Laser, Paramjit Rana, S.K. Mishra, Jaya Mukherjee, V.S. Rawat, Proceeding of International Conference of Optics and Electro-Optics (ICOL) 2019, I.R.D.E. Dehradun.
- [7.2] Design of multifunctional window for polarized green copper vapor laser oscillator amplifier chain, Paramjit Rana, R.B. Tokas, V.S. Rawat, S. Thakur, N.K. Sahoo Proceedings of National Laser Symposium – 2016.
- [7.3] Comparative study of Copper Vapour Laser Master Oscillator Power Amplifier configurations, Paramjit Rana, S.K. Mishra, S.P. Sahoo, S.K. Agarwalla, G. Sridhar, V.S. Rawat, Proceedings of National Laser Symposium 2018.
- [7.4] Thin Film Design of IR Reflector Window for Reduced Thermal Lensing in Copper Vapor Laser”, Paramjit Rana, V. S. Rawat, AIP Conference Proceedings 2115, issue 1, 030281, pp 1-4 (2019).
- [7.5] Thermal Lensing in Copper Vapor Laser Oscillator-Amplifier Configuration: It’s Measurement, Role and Compensation, Paramjit Rana, S.K. Mishra, V.S. Rawat *Communicated (Optik)*.
- [7.6] pH modulated photophysical characteristics of Rh101 dye for CVL pumped dye lasers, Paramjit, S.K. Mishra, V.S. Rawat, S.P. Sahoo, S.K. Agarwalla, G.Sridhar, A.K. Ray, K.G. Manohar, Proceedings of National Laser Symposium 2015.
- [7.7] Characteristics of SulfoRhodamine 101 dye laser in ethanol-water binary solvent mixture, S.K. Mishra, Paramjit Rana, S.P. Sahoo, S.K. Agarwalla, G. Sridhar, V.S. Rawat, Proceedings of National Laser Symposium 2018.
- [7.8] Measurement of Thermo Optical Coefficient for Commonly used Dye solvents , S.K. Mishra, Paramjit Rana, S.P. Sahoo, S.K. Agarwalla, G.Sridhar, D. Bhale, N.O. Kawade,

## REFERENCES

---

- V.S. Rawat, *International Journal of Photonics and Optical Technology*, 2018, Vol. 4, Iss. 2, 12-16.
- [7.9] Spectral characteristics of three wavelength laser in dye mixture, Paramjit Rana, G. Sridhar; Proceedings of National Laser Symposium – 2015.
- [7.10] Multi wavelength narrowband dye laser, G.Sridhar, Paramjit Rana Proceedings of National Laser Symposium – 2016.
- [7.11] Characteristics of a cascaded grating multi wavelength dye laser”, Paramjit Rana, G.Sridhar, K.G. Manohar, *Optics and Laser Technology*, 2016, Vol. 86, 39-45.
- [7.12] Co-amplification: An Efficient Spectral Beam Combination Approach for High Power, Closely Separated Dual Wavelength Dye Laser Systems, Paramjit Rana, S.K. Mishra, D. Bhale, S.P. Sahoo, G. Sridhar, V.S. Rawat, *Optics Communications*, 2019, Vol. 451, 367-373.
- [7.13] Design optimization and deposition of laser beam combiner, C. Mukherjee, Rajiv Kamparath, A.S. Joshi, Paramjit Rana, V.S. Rawat, R.K. Rajawat, N.K. Sahoo and P.A. Naik, Proceedings of National Laser Symposium – 2017.
- [7.14] Multilayer Dielectric Coated Fabry Perot Spectral Beam Combiner for High Power, Tunable Laser Applications, Paramjit Rana, C. Mukherjee, S.K. Mishra, Rajiv Kamparath, S.P. Sahoo, Jaya Mukherjee, V.S. Rawat; Under review (*Optics & Laser Tech.*).  
“Characterization of dye cells for a high repetition rate pulsed dye laser by particle image velocimetry (PIV)”, S.K. Mishra, Paramjit Rana, Siba P. Sahoo, Nitin O Kawade, V.S. Rawat, *Laser Physics*, 2019, Vol.29, 065001; 1-8.
- [7.15] An efficient spectral beam combination technique for closely separated wavelengths for high power CVL pumped dye laser oscillator amplifier chains; Paramjit, S.K. Mishra, V.S. Rawat, S.P. Sahoo, S.K. Agarwalla, G. Sridhar, K.G. Manohar, Proceedings of National Laser Symposium – 2015.

## REFERENCES

---

- [7.16] Comparison of Hydraulic Resistance in Different Dye Cells Used in the High Repetition Rate Pulsed Dye Lasers, S K Mishra, Paramjit, V S Rawat, S P Sahoo, S K Agrawalla, G Sridhar, K G Manohar, Proceedings of National Laser Symposium – 2015.
- [7.17] Jitter tolerance studies on dye laser oscillator amplifier configuration, Paramjit Rana, S.K. Agarwalla, S.P. Sahoo, S.K. Mishra, D. Bhale, G. Sridhar, V.S. Rawat; Proceedings of National Laser Symposium – 2016.
- [7.18] Measurement of Thermo Optical Coefficient for Commonly Used Dye Solvents, S K Mishra, Paramjit, S P Sahoo, S K Agrawalla, G Sridhar, N Kawade, V S Rawat, Proceedings of National Laser Symposium – 2016.
- [7.19] Computationally Generated Dye Cell for High Repetition Rate Pulsed Dye Lasers, S K Mishra, Paramjit, S P Sahoo, S K Agrawalla, G Sridhar, V S Rawat, Proceedings of National Laser Symposium – 2017.